Application of human organoids in ion transport studies

Domenique Zomer-van Ommen

Committee:

Prof. dr. R.H.J. Houwen, chair

Prof. dr. L.J. Bont

Prof. dr. N.M. Wulffraat

Prof. dr. H. Tiddens

Prof. dr. I. Braakman

ISBN: 978-90-393-7002-5

Cover photo shows the lock 'Prins Bernhard' near Tiel, the Netherlands, for water navigation between 'de Waal' and 'Amsterdam Rijnkanaal'. Provided by Rijkswaterstaat / Joop van Houdt (https://beeldbank.rws.nl).

Layout done by Domenique. Printed by: Gildeprint, www.gildeprint.nl.

Application of human organoids in ion transport studies

Toepassing van humane organoïden in ion transport studies

(met een samenvatting in het Nederlands)

Proefschrift

ter verkrijging van de graad van doctor aan de Universiteit Utrecht op gezag van de rector magnificus, prof.dr. H.R.B.M. Kummeling, ingevolge het besluit van het college voor promoties in het openbaar te verdedigen op donderdag 12 juli 2018

des middags te 4.15 uur

door

Domenique Dieudonnée Zomer-van Ommen

geboren op 25 oktober 1988 te Tiel

Promotor: Prof.dr. C.K. van der Ent

Copromotor: Dr. J.M. Beekman

Dit proefschrift werd mede mogelijk gemaakt met financiële steun van de Nederlandse Cystic Fibrosis Stichting (NCFS), Vrienden Wilhelmina Kinderziekenhuis en ZonMw.

TABLE OF CONTENTS

CHAPTER 1

General introduction

CHAPTER 1

Human bodies are physically protected against the environment by sheets of connective cells that is called the epithelium [1]. Epithelial cells form the skin and surfaces of the body cavities, but also function as barriers between organs and other tissues [1].

In this thesis we develop new models to study epithelial ion transport and we study their use to better understand and potentially treat the diseases cystic fibrosis and cholera. Both these diseases are caused by malfunctioning of a protein called Cystic Fibrosis Transmembrane Conductance Regulator (CFTR) [2,3]. CFTR is an ion channel expressed in many epithelial tissues and plays a critical role in ion and fluid transport across the apical membrane [4,5]. In this chapter we describe the current knowhow concerning CFTR-dependent epithelial ion transport, and how new cellular models are needed to further improve our understanding and the treatment of ion channel diseases and dysregulations.

Epithelial ion transport

Epithelial cells can be derived from all three germ layers and their shape, organization and function are organ-dependent [6]. Epithelial cells have their apical surface faced to the lumen and the basolateral side attached to connective tissue [1]. They regulate apical ion and subsequent fluid homeostasis via various ion channels, transporters and exchangers, as well as the passive paracellular pathway. Apical secretion of e.g. chloride results in a negative loading of the lumen, which induces a driving force for paracellular sodium secretion. The secretion of chloride and sodium results in the osmotic driving force for secretion of water. [5]

The functioning of hollow organs, like the airways and the intestine, is dependent on ion and fluid homeostasis, and dysregulation leads to disease. [5] For example in cystic fibrosis (CF), reduced apical secretions by the pseudo-stratified epithelial cells in the airways impair the mucociliary clearance of microorganisms, resulting in infection, inflammation and airway obstruction [5,6]. Reduced biliary, pancreatic and intestinal epithelial secretions result in defective food digestion and nutrient uptake, as well as intestinal obstruction. [5,6] Malfunctioning of ion transport can also mediate disease severity of e.g. inflammatory bowel diseases and Crohn's disease [6]. Despite some of the key players underlying epithelial ion and fluid transport have been identified, many aspects of human ion transport remain poorly understood. [5]

Cystic fibrosis

Cystic fibrosis (CF) is the most common life-shortening genetic disease in Caucasians [7] affecting ~85,000 individuals worldwide and ~1,500 individuals in the Netherlands [8,9]. Newborns in the Netherlands are tested for CF and other severe congenital disorders using a heel prick blood spot screen since 2011 [10].

CF was recognized as a unique disease entity, based on its pancreatic pathology, by Dorothy Andersen in 1938. Paul DiSant'Agnese discovered that children with CF had very high amounts of salt in their sweat [11,12]. Then, in 1959, Gibson and Cooke established a sweat test to measure raised sweat electrolytes in people with CF. The principal of this test still forms the cornerstone of CF diagnosis. It was subsequently shown in the 1980s that CF was caused by defects in epithelial ion transport. [12]

CF manifests mainly in the airways, the pancreas, sweat glands, intestine, and male reproductive tract (**Fig. 1**) [13,14]. It is a progressive disease and several symptom-targeting therapies have been developed,

including pancreatic enzyme supplements, high-fat diets, antibiotics, mucolytics, and physical exercise programs [15]. People with CF have a limited life expectancy (currently 47 years on average for newborns, as announced during the North American Cystic Fibrosis Conference 2017) due to progressive loss of organ function. The most prevalent cause of death is respiratory failure due to impaired mucociliary clearance that leads to enhanced infection and inflammation and progressive lung damage [16]. Lung transplantation is currently the last option to extend the life span [17].

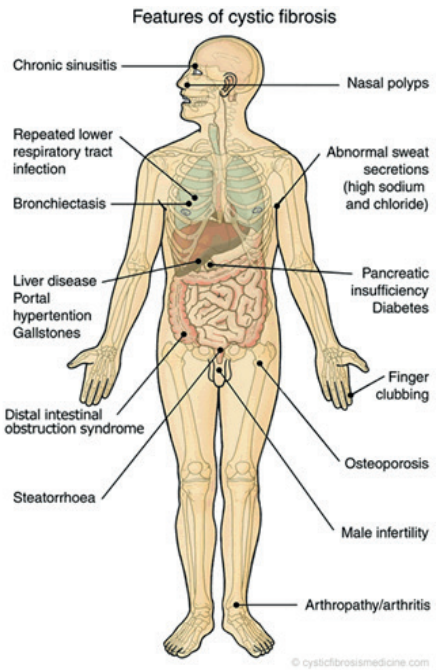

Figure 1. *Some of the most frequent impaired body functions due to cystic fibrosis. Via cysticfibrosismedicine.com, visited 13-Jan-2018.*

CFTR

The diagnosis became easier and more accurate since 1989 when the *CFTR* gene was identified as CF-causing due to loss-of-function mutations [2,18,19]. In 1991 it was shown that CFTR is not only a regulator but also an ion channel itself, mediating chloride transport in response to high intracellular cAMP and protein kinase A activity [20]. In the sweat glands, where protein kinase A and subsequently CFTR are continuously active, reabsorption of chloride into secreted sweat is reduced when CFTR is impaired. As a result, the sweat chloride concentration SCC is higher in people with CF. [4,11,17]

The aberrant channel function of CFTR can also be determined with intestinal current measurements (ICM) in *ex vivo* rectal biopsies [21–23] and *in vivo* measurements (nasal potential difference, NPD) that measure potential differences between the nasal epithelium and the skin [24]. In both tests, the stimulation of tissues with cAMP raising agents are central to detecting abnormalities in the electrochemical properties of the tissues. Both ICM and NPD are now important diagnostic assays for people with inconclusive symptoms and/or unknown *CFTR* genotypes [21–23,25,26].

The homeostasis of ion and fluid transport is also disrupted upon hyperactivation of CFTR that can result from interactions with intestinal pathogens. For example, the microorganism *Vibrio cholerae* induces severe secretory diarrhea, leading to severe dehydration and annually 95,000 deaths worldwide [3,27–29] *Vibrio cholerae* produces toxins that are internalized by enterocytes and lead to strong production of cAMP. The resulting hyperactivation of CFTR leads to hypersecretion of chloride and water. [3,27,28] This illustrates the central role that CFTR plays in maintaining epithelial ion and fluid functions, and indicates that CFTR-targeting by pharmacotherapy can have important therapeutic implications for multiple epithelial ion and fluid transport diseases.

CFTR and epithelial ion transport

Current literature indicate that cellular signaling cooperatively regulate CFTR and many other ion channels, transporters and exchangers to maintain ion and fluid homeostasis throughout the body [5,13] (**Fig. 2**). Intracellular cAMP plays a critical role to co-regulate apical and basolateral ion transport throughout various epithelial cells. As stated above, cAMP-PKA signaling plays a direct role in CFTR-gating and the secretion of chloride (Cl^-), bicarbonate (HCO_3^-) and other anions at the apical membrane [5,14]. Apical chloride channel SLC26A9, present in the airways and gastrointestinal tract, also secretes chloride in a cAMP-dependent manner, and might even interact with CFTR. [30,31] A second major chloride secretion pathway in epithelial cells is triggered by intracellular calcium. Apical chloride channels like TMEM16A, which is mainly present in the glands and airways, then secreted chloride [5,30,32–35]. The apical secretion of chloride is mainly regulated by the basolateral uptake of chloride. The basolateral Na^+-K^+-Cl^- cotransporter 1 (NKCC1) plays a major role in this process and allows basolateral entry of chloride, sodium and potassium [5]. Upon increased intracellular calcium or cAMP, both basolateral K^+ channels and ATP-dependent Na^+/K^+ pumps increase their K^+ conductance to establish an K^+ equilibrium [5]. As a result, a driving force is created towards apical anion secretion via hyperpolarization of the cell membranes. [36]

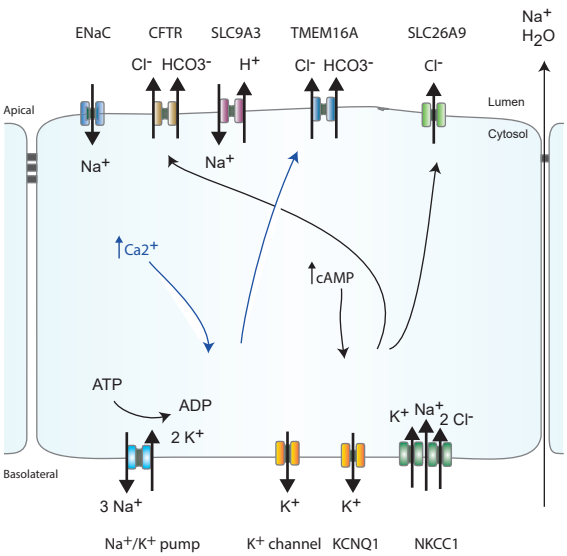

Figure 2. *Epithelial ion transport. cAMP- and calcium-dependent secretory pathways including the main ion channels, transporters, pumps, and two apical absorptive components* [5].

Apical absorption of sodium, via epithelial sodium channel ENaC and Na^+/H^+ exchanger NHE_3 (SLC9A3), decreases the secretion of cAMP-mediated anions like chloride [37]. The role of sodium increases when CFTR function is reduced, which makes this ion an important factor in CF, but the interactions between sodium and chloride still need to be unraveled. [14]

Modifying CFTR function

For CF, pharmacotherapies are being established that restore the basis of CF by targeting specifically the mutant CFTR protein. The first compound that entered the market was ivacaftor (Kalydeco™), a potentiator increasing the gating (open state) of CFTR (**Fig. 3**) [38,39]. Kalydeco is now registered in Europe for nine gating mutations and the residual CFTR function mutation p.Arg117His [40]. After the development of lumacaftor, a corrector which improved the trafficking of ER-localized mutant CFTR (**Fig. 3**) [41], the combination of ivacaftor/lumacaftor (Orkambi™) proved to be efficacious in people homozygous for p.Phe508del [42]. Ivacaftor with the investigational corrector tezacaftor has a more

beneficial safety profile, while retaining similar efficacy as compared to Orkambi [43,44]. Also, so-called next-generation CFTR modulators are being studied in clinical trials in combination with current drugs, for treating individuals with a single p.Phe508del mutation with profound effects. These encouraging results provide the hope that effective therapies will be developed in the coming decade for the majority of people with CF.

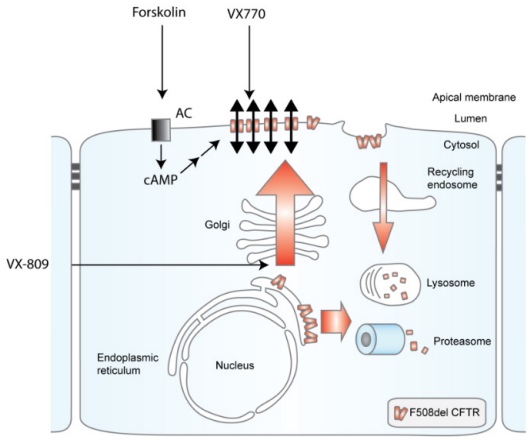

Figure 3. *Cellular CFTR pathophysiology and small molecule targeting. Schematic representation of the epithelial cell. F508del-mutated CFTR protein is mostly degraded when it leaves the endoplasmic reticulum. When treated with lumacaftor (VX-809), the folding and trafficking of CFTR is improved. When arrived at the apical plasma membrane, CFTR gating is improved by ivacaftor (VX-770) and chloride secretion can take place upon cAMP stimulation by e.g. forskolin.*

Alternatively, for diarrheal diseases like cholera, inhibition of CFTR or other cellular pathways might be beneficial to improve survival upon infection. Current therapies to treat cholera infection are partially and temporarily effective, including fluid replacement, rehydration therapy and oral cholera vaccines [5,46].

Alternative approaches may complement the fluid replacement strategies, to more effectively counterbalance the massive fluid loss upon cholera infection. To develop and explore such potential treatments, cellular models with translational opportunities would be needed to facilitate a quick identification of new drugs for this economically challenging treatment population [28,47].

CFTR modulator treatment heterogeneity

While the novel CFTR modulators highlight a paradigm shift by being the first so-called 'curative treatments' for CF, many people with CF still do not (sufficiently) benefit. People eligible for treatment show highly diverse responses, despite sharing identical *CFTR* mutations. It is also unclear whether the current CFTR modulators that are developed for the most abundant p.Phe508del mutation (present in approximately 90% of the individuals with CF [48,49]) are efficacious for other mutations. Currently, more than 2000 mutations, with often unknown impact, are described in Cystic Fibrosis Mutation Databases [48,50]. These mutations have been classified based on their functional defects (**Table 1**), however, many *CFTR* mutations remain uncharacterized in terms of treatment response [15,17]. Additionally, regarding very rare *CFTR* mutations, the potentially responsive mutations are simply not being identified, because of the low prevalence of these mutations and the resulting difficulties in designing clinical trials.

The heterogeneity in CF treatments points out that more effective treatments remain needed, even for people already receiving CFTR modulators. Additionally, stratification methods with greater precision than *CFTR* genotyping, that is currently used, could help to better identify the individuals that may respond to treatment.

Table 1. *Classification of CFTR mutations based on functional defect* [17].

Class #	Result	Class #	Result
I	Severely reduced or even absent protein production	IV	Reduced channel conductance
II	Impaired processing in the cell due to misfolding	V	Reduced protein levels
III	Impaired channel gating	VI	Decreased protein stability at the cell membrane

Bypass

An alternative approach of treating subjects with CF might be by the CFTR-independent restoration of chloride secretion and subsequent fluid homeostasis via targeting of other ion channels. As indicated above, TMEM16A and SLC26A9 represent epithelial ion channels that secrete chloride and might restore transport independent of CFTR. Their potential has been shown in preclinical transfection models as reviewed by Mall and Galietta [30]. However, targeting these ion channels might cause side-effects in other tissues, e.g. TMEM16A also appears to be able to induce bronchoconstriction via its presence on smooth muscle cells [51]. And if SLC26A9 interacts with CFTR, as mentioned above, the attainment of effectively targeting this ion channel might be dependent on the *CFTR* mutation.

Another option is to even bypass the impaired chloride secretion, and instead restore fluid secretion by blocking sodium and subsequent water absorption through manipulation of ENaC [30]. However, a recent trial with an ENaC inhibitor did not meet its primary end point [52]. As the precise function of alternative ion channels remain mostly unknown, more knowledge is needed to determine whether and how these alternative ion channels might become attractive therapeutic targets for CF and beyond [30].

Adult stem cell-based intestinal organoids

New stem cell culture technologies allow for long-term culturing of adult human epithelial tissue that self-organize into 3D structures, called organoids, which recapitulate organ key features on structure and function. [53] Starting with the discovery of Leucine-rich repeat-containing G-protein coupled receptor 5 (Lgr5) being an adult stem cell marker of intestinal epithelium in 2007 [54], mouse organoid culture protocols were developed, and quickly followed by long-term culture protocols of human-derived organoids [55,56]. These organoids can be stored in biobanks and are genetically stable during long-term *in vitro* culture in contrast to tumor-derived cell lines [57]. These cultures therefore facilitate long-term supply of annotated living human materials. The adult stem cell-derived organoids retain epigenetic information of their tissue-of-origin and are thus distinct from 3D organotypic cultures derived from (induced) pluripotent stem cells. Adult stem cell-derived organoids provide understanding of subject-specific self-renewal of the organ tissue in both physiologic and pathophysiologic conditions. [53]

The best established adult organoid culture model is the human intestinal organoid culture model. These organoids can be established from any part of the intestine and are formed with the apical side of the epithelial cells facing inwards towards the organoid lumen. They recapitulate the *in vivo* situation in having clearly defined regions with distinct cell types such as stem-cell containing crypts and differentiated cells, and grow as a single-layered epithelium. [55,58,59] Human intestinal organoids

allowed for the study of epithelial ion transport and disease [57]. Our lab developed a model to measure CFTR function using organoids derived from subjects with CF [58]. Intestinal organoids swell upon cAMP activation and subsequent CFTR-induced ion and fluid transport into their lumen. Impaired ion secretion due to *CFTR* mutations results in reduced organoid swelling. Quantifying organoid swelling turned out to be a measure for residual CFTR function [58]. This demonstrates that organoids can be used to model human epithelial diseases, and opens new potential uses of organoids for CFTR-dependent ion transport studies.

Other stem cell-based models

Since the development of protocols to culture intestinal organoids, other epithelial tissues from all three germ layers followed, like liver, pancreas, stomach, and brain organoids. [53] For airway tissue, only short-term culturing remains possible. Two groups demonstrated that short term airway spheroid cultures could be established with a pseudo-stratified organization and various cell types such as goblet and ciliated cells. Both methods lack the self-organizing capacity of organoids, since the primary cells needed to be either selected out or mixed with non-epithelial cells to obtain the spheres. [60,61]. Also, the long-term culturing of airway cells remain difficult.

Organoids as biomarker tools for therapy

Patient-derived organoids are an attractive tool to preclinically assess effective therapies in a personalized, yet cost-effective manner. [53] Intestinal organoids can be used to measure CFTR residual function [58,62] and these cultures can be used to determine individual and *CFTR*-dependent drug response with *in vivo* benefit [62,63]. However, additional explorative studies are needed into their value as drug screening platforms, and to validate their performance for predicting *in vivo* therapeutic response. Also, the use of intestinal or airway organoids may be essential to study genetic modifiers and additional ion channels that might affect CF disease or therapeutic responses.

Thesis aims and outline

In this thesis we aimed to validate and develop new stem cell-based *in vitro* models for epithelial ion transport studies.

In **chapter 2**, we explored whether intestinal CF organoids can be used to study drugs that repair premature termination codons. In **chapter 3**, we used intestinal organoids to screen for drugs with potential clinical benefit. A new electrophysiological assay using 2D cultured intestinal monolayers from 3D grown organoids, and relations between ion transport and organoid swelling were studied in **chapter 4**. In **chapter 5** we showed that we can establish long-term human primary airway organoid cultures and their application to human disease modeling. **Chapter 6** describes how primary human organoids derived from various tissue can be used to characterize ion transport modulators. We demonstrated that organoid swelling is also highly valuable to determine the potency of cholera toxin inhibitors in **chapter 7**.

References

1. Fleming T. *Epithelial Organization and Development*.; 1992.
2. Riordan JR, Rommens JM, Kerem B, et al. Identification of the cystic fibrosis gene: cloning and characterization of complementary DNA. *Science*. 1989;245(4922):1066-1073. http://www.ncbi.nlm.nih.gov/pubmed/2475911.
3. Sigman M, Luchette FA. Cholera: Something Old, Something New. *Surg Infect*. 2012;13(4):216-222. doi:10.1089/sur.2012.127.
4. Riordan JR. CFTR function and prospects for therapy. *Annu Rev Biochem*. 2008;77:701-726. doi:10.1146/annurev.biochem.75.103004.142532.
5. Frizzell RA, Hanrahan JW. Physiology of epithelial chloride and fluid secretion. *Cold Spring Harb Perspect Med*. 2012;2(6):a009563. doi:10.1101/cshperspect.a009563.
6. Shashikanth N, Yeruva S, Ong MLDM, Odenwald MA, Pavlyuk R, Turner JR. Epithelial Organization: The Gut and Beyond. *Compr Physiol*. 2017;7(October):1497-1518. doi:10.1002/cphy.c170003.
7. Sosnay PR, Siklosi KR, Van Goor F, et al. Defining the disease liability of variants in the cystic fibrosis transmembrane conductance regulator gene. *Nat Genet*. 2013;45(10):1160-1167. doi:10.1038/ng.2745.
8. Lopes-Pacheco M. CFTR modulators: Shedding light on precision medicine for cystic fibrosis. *Front Pharmacol*. 2016;7(SEP):1-20. doi:10.3389/fphar.2016.00275.
9. Registry DC. Dutch Cystic Fibrosis Registy Report 2016. 2017;(October). www.ncfs.nl.
10. RIVM. Heel prick. http://www.rivm.nl/en/Topics/H/Heel_prick#handout. Accessed January 4, 2018.
11. Davis PB. Cystic Fibrosis Since 1938. *Am J Respir Crit Care Med*. 2006;173(5):475-482. doi:10.1164/rccm.200505-840OE.
12. Littlewood JM. History of Cystic Fibrosis. In: *Cystic Fibrosis*. ; 2007.
13. Cutting GR. Cystic fibrosis genetics: from molecular understanding to clinical application. *Nat Rev Genet*. 2014;16(1):45-56. doi:10.1038/nrg3849.
14. Stoltz DA, Meyerholz DK, Welsh MJ. Origins of Cystic Fibrosis Lung Disease. *N Engl J Med*. 2015;372(4):351-362. doi:10.1056/NEJMra1300109.
15. Amaral MD. Novel personalized therapy for cystic fibrosis: treating the basic defect in all patients. *J Intern Med*. September 2014. doi:10.1111/joim.12314.
16. Elborn JS. Cystic fibrosis. *Lancet*. 2016;388(10059):2519-2531. doi:10.1016/S0140-6736(16)00576-6.
17. Bell SC, De Boeck K, Amaral MD. New pharmacological approaches for cystic fibrosis: Promises, progress, pitfalls. *Pharmacol Ther*. 2015;(145):19-34. doi:10.1016/j.pharmthera.2014.06.005.
18. Rommens JM, Iannuzzi MC, Kerem B, et al. Identification of the cystic fibrosis gene: chromosome walking and jumping. *Science*. 1989;245(4922):1059-1065. http://www.ncbi.nlm.nih.gov/pubmed/2772657. Accessed November 14, 2014.
19. Kerem B, Rommens JM, Buchanan JA, et al. Identification of the cystic fibrosis gene: genetic analysis. *Science*. 1989;245(4922):1073-1080. doi:10.1126/SCIENCE.2570460.
20. Anderson MP, Gregory RJ, Thompson S, et al. Demonstration that CFTR is a chloride channel by alteration of its anion selectivity. *Science*. 1991;253(5016):202-205. http://www.ncbi.nlm.nih.gov/pubmed/1712984. Accessed January 29, 2018.
21. Li H, Sheppard DN, Hug MJ. Transepithelial electrical measurements with the Ussing chamber. *J Cyst Fibros*. 2004;3(SUPPL. 2):123-126. doi:10.1016/j.jcf.2004.05.026.
22. De Jonge HR, Ballmann M, Veeze H, et al. Ex vivo CF diagnosis by intestinal current measurements (ICM) in small aperture, circulating Ussing chambers. *J Cyst Fibros*. 2004;3 Suppl 2:159-163. doi:10.1016/j.jcf.2004.05.034.
23. Derichs N, Sanz J, Von Kanel T, et al. Intestinal current measurement for diagnostic classification of patients with questionable cystic fibrosis: validation and reference data. *Thorax*. 2010;65(7):594-599. doi:10.1136/thx.2009.125088.
24. ECFS Diagnostic Network Working Group T. NPD ECFS SOP. https://www.ecfs.eu/ecfs_dnwg.
25. Wilschanski M, Famini H, Strauss-Liviatan N, et al. Nasal potential difference measurements in patients with atypical cystic fibrosis. *Eur Respir J*. 2001;17(6):1208-1215. http://www.ncbi.nlm.nih.gov/pubmed/11491166. Accessed January 29, 2018.

26. Farrell PM, White TB, Ren CL, et al. Diagnosis of Cystic Fibrosis: Consensus Guidelines from the Cystic Fibrosis Foundation. *J Pediatr*. 2017;181:S4-S15.e1. doi:10.1016/J.JPEDS.2016.09.064.
27. Petri Jr WA, Miller M, Binder HJ, Levine MM, Dillingham R, Guerrant RL. Review series Enteric infections, diarrhea, and their impact on function and development. *J Clin Invest*. 2008;118(4):1277-1290. doi:10.1172/JCI34005.tively.
28. Bijvelds MJC, Loos M, Bronsveld I, et al. Inhibition of Heat-Stable Toxin–Induced Intestinal Salt and Water Secretion by a Novel Class of Guanylyl Cyclase C Inhibitors. *J Infect Dis*. 2015;jiv300. doi:10.1093/infdis/jiv300.
29. Ali M, Nelson AR, Lopez AL, Sack DA. Updated global burden of cholera in endemic countries. *PLoS Negl Trop Dis*. 2015;9(6):1-13. doi:10.1371/journal.pntd.0003832.
30. Mall M a., Galietta LJ V. Targeting ion channels in cystic fibrosis. *J Cyst Fibros*. 2015;14(5):561-570. doi:10.1016/j.jcf.2015.06.002.
31. Bertrand C, Zhang R, Pilewski J, Frizzell R. SLC26A9 is a constitutively active, CFTR-regulated anion conductance in human bronchial epithelia. *J Gen Physiol*. 2009;133:421–38.
32. Yang Y, Cho H, Koo J, et al. TMEM16A confers receptor-activated calcium-dependent chloride conductance. *Nature*. 2008;455(30):1210-1215.
33. Schroeder B, Cheng T, Jan Y, Jan L. Expression cloning of TMEM16A as a calcium-activated chloride channel subunit. *Cell*. 2008;134:1019-1029.
34. Caputo A, Caci E, Ferrera L, et al. TMEM16A, a membrane protein associated with calcium-dependent chloride channel activity. *Science (80-)*. 2008;322:590-594.
35. Scudieri P, Caci E, Bruno S, et al. Association of TMEM16A chloride channel overexpression with airway goblet cell metaplasia. *J Physiol*. 2012;590:6141-6155.
36. Matos JE, Sausbier M, Beranek G, Sausbier U, Ruth P, Leipziger J. Role of cholinergic-activated KCa1.1 (BK), KCa3.1 (SK4) and KV7.1 (KCNQ1) channels in mouse colonic Cl- secretion. *Acta Physiol*. 2007;189(3):251-258. doi:10.1111/j.1748-1716.2006.01646.x.
37. Foulke-Abel J, In J, Yin J, et al. Human Enteroids as a Model of Upper Small Intestinal Ion Transport Physiology and Pathophysiology. *Gastroenterology*. 2015. doi:10.1053/j.gastro.2015.11.047.
38. Van Goor F, Hadida S, Grootenhuis PDJ, et al. Rescue of CF airway epithelial cell function in vitro by a CFTR potentiator, VX-770. *Proc Natl Acad Sci U S A*. 2009;106(44):18825-18830. doi:10.1073/pnas.0904709106.
39. Ramsey B, Davies JC, McElvaney N, et al. A CFTR Potentiator in Patients with Cystic Fibrosis and the G551D Mutation. 2011;365(18):1663-1672.
40. De Boeck K, Davies JC. Where are we with transformational therapies for patients with cystic fibrosis? *Curr Opin Pharmacol*. 2017;34:70-75. doi:10.1016/j.coph.2017.09.005.
41. Van Goor F, Hadida S, Grootenhuis PDJ, et al. Correction of the F508del-CFTR protein processing defect in vitro by the investigational drug VX-809. *Proc Natl Acad Sci U S A*. 2011;108(46):18843-18848. doi:10.1073/pnas.1105787108.
42. Wainwright CE, Elborn JS, Ramsey BW, et al. Lumacaftor-Ivacaftor in Patients with Cystic Fibrosis Homozygous for Phe508del CFTR. *N Engl J Med*. 2015:1-12. doi:10.1056/NEJMoa1409547.
43. Rowe SM, Daines C, Ringshausen FC, et al. Tezacaftor–Ivacaftor in Residual-Function Heterozygotes with Cystic Fibrosis. *N Engl J Med*. 2017:NEJMoa1709847. doi:10.1056/NEJMoa1709847.
44. Taylor-Cousar JL, Munck A, McKone EF, et al. Tezacaftor–Ivacaftor in Patients with Cystic Fibrosis Homozygous for Phe508del. *N Engl J Med*. 2017;377(21):NEJMoa1709846. doi:10.1056/NEJMoa1709846.
45. World Health Organization. Bacterial Agents of Enteric Diseases of Public Health Concern Salmonella serotype Typhi Shigella Vibrio cholerae. *Man Lab Identif Antimicrob susceptibility Test Bact Pathog public Heal importance Dev world*. 2003.
46. Bi Q, Ferreras E, Pezzoli L, et al. Protection against cholera from killed whole-cell oral cholera vaccines: a systematic review and meta-analysis. *Lancet Infect Dis*. 2017;17(10):1080-1088. doi:10.1016/S1473-3099(17)30359-6.
47. Fu O, Pukin A V., van Ufford HCQ, et al. Tetra- versus Pentavalent Inhibitors of Cholera Toxin. *ChemistryOpen*. 2015;4:471-477. doi:10.1002/open.201500006.
48. The Clinical and Functional TRanslation of CFTR. http://cftr2.org. Accessed September 8, 2017.
49. CFTR2. CFTR2 variant list. 2017.
50. Cystic Fibrosis Mutation Database. http://www.genet.sickkids.on.ca.

51. Huang F, Zhang H, Wu M, et al. Calcium-activated chloride channel TMEM16A modulates mucin secretion and airway smooth muscle contraction. *Proc Natl Acad Sci U S A*. 2012;109(40):16354-16359.
52. Vertex. Vertex Reports Third-Quarter 2017 Financial Results. Oct. https://www.businesswire.com/news/home/20171025006319/en/. Published 2017. Accessed January 29, 2018.
53. Clevers H. Modeling Development and Disease with Organoids. *Cell*. 2016;165(7):1586-1597. doi:10.1016/j.cell.2016.05.082.
54. Barker N, van Es JH, Kuipers J, et al. Identification of stem cells in small intestine and colon by marker gene Lgr5. *Nature*. 2007;449(7165):1003-1007. doi:10.1038/nature06196.
55. Sato T, Vries RG, Snippert HJ, et al. Single Lgr5 stem cells build crypt-villus structures in vitro without a mesenchymal niche. *Nature*. 2009;459(7244):262-265. doi:10.1038/nature07935.
56. Sato T, Stange DE, Ferrante M, et al. Long-term expansion of epithelial organoids from human colon, adenoma, adenocarcinoma, and Barrett's epithelium. *Gastroenterology*. 2011;141(5):1762-1772. doi:10.1053/j.gastro.2011.07.050.
57. Sato T, Clevers H. Growing self-organizing mini-guts from a single intestinal stem cell: mechanism and applications. *Science*. 2013;340(6137):1190-1194. doi:10.1126/science.1234852.
58. Dekkers JF, Wiegerinck CL, de Jonge HR, et al. A functional CFTR assay using primary cystic fibrosis intestinal organoids. *Nat Med*. 2013;19(7):939-945. doi:10.1038/nm.3201.
59. Dekkers JF, van der Ent CK, Beekman JM. Novel opportunities for CFTR-targeting drug development using organoids. *Rare Dis (Austin, Tex)*. 2013;1:e27112. doi:10.4161/rdis.27112.
60. Rock JR, Onaitis MW, Rawlins EL, et al. Basal cells as stem cells of the mouse trachea and human airway epithelium. *Proc Natl Acad Sci U S A*. 2009;106(31):12771-12775.
61. Tan Q, Choi KM, Sicard D, Tschumperlin DJ. Human airway organoid engineering as a step toward lung regeneration and disease modeling. *Biomaterials*. 2017;113:118-132. doi:10.1016/j.biomaterials.2016.10.046.
62. Dekkers JF, Berkers G, Kruisselbrink E, et al. Characterizing responses to CFTR-modulating drugs using rectal organoids derived from subjects with cystic fibrosis. *Sci Transl Med*. 2016;8(344):13. doi:10.1126/scitranslmed.aad8278.
63. Dekkers R, Vijftigschild LAW, Vonk AM, et al. A bioassay using intestinal organoids to measure CFTR modulators in human plasma. *J Cyst Fibros*. 2015;14(2):178-181. doi:10.1016/j.jcf.2014.10.007.

1

CHAPTER 2

Limited premature termination codon suppression by read-through agents in cystic fibrosis intestinal organoids

D.D. Zomer-van Ommen[a,1], L.A.W. Vijftigschild[a,1], E. Kruisselbrink[a], A.M. Vonk[a], J.F. Dekkers[a], H.M. Janssens[c], K.M. de Winter-de Groot[b], C.K. van der Ent[b], J.M. Beekman[a,b]

Journal of Cystic Fibrosis. Volume 15, Issue 2, March 2016, Pages 158-162.

a. Laboratory of Translational Immunology, UMC Utrecht, The Netherlands, b. Dept of Pediatric Pulmonology, Wilhelmina Children's Hospital, UMC Utrecht, The Netherlands, c. Dept of Pediatrics, Sophia Children's Hospital/ Erasmus MC-University Medical Center, Rotterdam, The Netherlands. 1. Authors contributed equally.

Short Communication. https://doi.org/10.1016/j.jcf.2015.07.007. Received 15 April 2015, Revised 26 June 2015, Accepted 19 July 2015, Available online 5 August 2015.

CHAPTER 2

Abstract

Premature termination codon read-through drugs offer opportunities for treatment of multiple rare genetic diseases including cystic fibrosis. We here analyzed the read-through efficacy of PTC124 and G418 using human cystic fibrosis intestinal organoids (E60X/4015delATTT, E60X/F508del, G542X/F508del, R1162X/F508del, W1282X/F508del and F508del/F508del). G418-mediated read-through induced only limited CFTR function, but functional restoration of CFTR by PTC124 could not be confirmed. These studies suggest that better read-through agents are needed for robust treatment of nonsense mutations in cystic fibrosis.

Keywords: Nonsense suppression, Intestinal organoids, G418, PTC124, Cystic fibrosis, Read-through

Introduction

Cystic fibrosis (CF) is caused by mutations in the cystic fibrosis transmembrane conductance regulator (*CFTR*) gene that encodes a cAMP-regulated anion channel (1). *CFTR* mutations associate with various functional defects and disease severities (2). CFTR-targeting drugs have been developed that improve *CFTR* mutation-specific defects, such as gating by VX-770 (3) and plasma membrane trafficking by VX-809 (4). These drugs are not effective as stand-alone treatment for nonsense mutations that are present in approximately 12% of CF subjects and lead to prematurely truncated, non-functional CFTR protein (5).

Aminoglycosides, like G418, have been found to induce read-through of premature termination codons (PTCs) (6), by interacting with the ribosome during translation, and attracting a near cognate aminoacyl-tRNA to the ribosomal A site, to continue translation (7). To bypass cell toxicity associated with aminoglycosides, PTC124 (Ataluren) was developed as a non-toxic suppressor of premature termination codons (8). Normal stop codons were not affected, although the mechanism for selectivity of PTC remains unclear (7,8). PTC124 activity for *CFTR* nonsense mutations has been demonstrated *in vitro* (9,10), but these data contrast with other studies that fail to demonstrate PTC124 read-through capacity (11–13). Clinical trials utilizing PTC124 have met inconsistent results, for cystic fibrosis as well as for nonsense-mutated Duchenne muscular dystrophy (14–19). A recent phase III clinical trial in CF did not find significant differences between PTC124 treatment and placebo, but retrospective data analysis suggested that aminoglycoside co-treatment prevented PTC124 activity (17). Collectively, these data indicate that the read-through activity of PTC124 remains unclear.

Here, we used a functional CFTR assay using human intestinal organoids to measure pharmacological induction of PTC read-through (20). Organoids are 3D spherical structures that consist of a polarized epithelial cell monolayer surrounding a single lumen, and are formed when adult stem cells from intestinal crypts are cultured in a culture matrix with appropriate growth media (21). Forskolin induces CFTR-dependent fluid secretion into the organoid lumen, causing rapid swelling of organoids (20). Here, we investigated organoids with various CFTR genotypes to study G418 and PTC124-mediated PTC read-through, and interactions with CFTR-targeting drugs.

Materials and methods

Collection of human organoids

Organoids were generated after intestinal current measurements in human rectal biopsies, obtained for diagnostic care. Informed consent was obtained according to the principles of the declaration of Helsinki.

Human organoid culture and functional CFTR measurements

Crypts were isolated from rectal biopsies of six subjects with cystic fibrosis (E60X/4015delATTT, E60X/F508del, G542X/F508del, R1162X/F508del, W1282X/F508del and F508del/F508del) as previously described (20). Briefly, after isolation, organoids were cultured for at least 3 weeks prior to CFTR function measurements by forskolin-induced swelling (20). We chose two concentrations of G418 and PTC124 via dosage titrations (data not shown) and as described in literature, respectively (8). Organoids were pre-incubated with G418 (100 and 200 μM), PTC124 (1 and 5 μM) and/or VX-809 (3 μM) 24 h prior

to forskolin stimulation, whereas VX-770 (1 μM) was added simultaneously with forskolin (5 μM). Luminal expansion and organoid swelling were monitored for 60 min using a Zeiss LSM 710 confocal microscope. In addition to organoid swelling, forskolin-induced luminal area at t = 60 min was analyzed blinded as percentage of total organoid surface area per well. Paired t-tests of treatment over non-treatment ratios are performed for statistical analysis.

Results

To investigate CFTR repair by PTC124 and G418, we measured swelling of human intestinal organoids compound heterozygous for a CFTR PTC allele and a frame shift allele (E60X/4015delATTT), lacking CFTR function as indicated by absence of forskolin-induced swelling (FIS) (20). G418 pretreatment induced very limited FIS indicating CFTR function, but no FIS was detected upon incubation with PTC124. Co-incubation of G418 with CFTR protein restoring drugs (VX-770 + VX-809) enhanced FIS (Fig. 1A). Induced swelling was very limited, therefore we analyzed the forskolin-induced luminal area (at t = 60 min, as percentage of total organoid area) to interpret the limited but differential swelling of the single compounds (Fig. 1B, C). We observed luminal area expansion by G418, whereas no effect was measured using PTC124 (Fig. 1C, D). G418 treatment did not increase luminal swelling of F508del homozygous organoids, demonstrating PTC specificity (Fig. 1C). These data confirmed the read-through activity of G418 but not of PTC124.

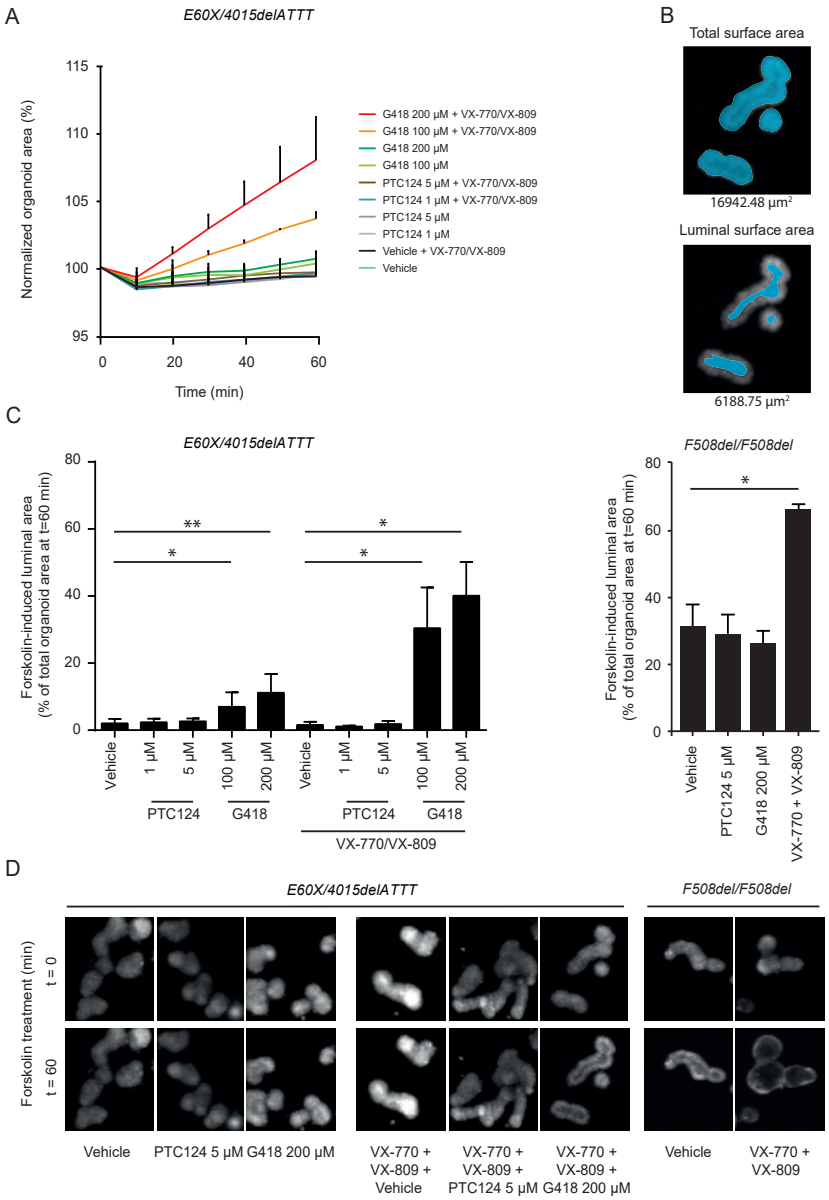

Fig. 1. *Correction of CFTR-PTC in intestinal organoids by G418 but not PTC124. Forskolin-induced swelling (FIS) of intestinal organoids (E60X/4015delATTT and F508del/F508del), incubated with either G418, PTC124 or DMSO (vehicle), w/o VX-809 for 24 h and stimulated with forskolin, w/o VX-770. Conditions were measured in triplicate at three independent time points for each patient. Concentrations were used as indicated. A) Normalized E60X/4015delATTT organoid area increase in 60 min of FIS (%, ± SD); B) representative images to determine total area and luminal area per well; C) luminal size (% of total organoid area) after 60 min of FIS (%, ± SD), *p < 0.05, **p < 0.01; D) representative confocal images, conditions as indicated.*

We next assessed read-through by G418 and PTC124 in organoids compound heterozygous for F508del and a nonsense mutation (E60X, G542X, R1162X and W1282X) (Fig. 2A). Subject genotype R1162X/F508del is a low responder, indicated by standard swelling assays performed in our laboratory (data not shown). G418 induced limited read-through in PTC-mutant organoids, which was significant when data from the four different patients was pooled, compared to non-treated organoids (Fig. 2B). Functional restoration was not observed using PTC124 for any of the donor organoids. Targeting the single CFTR-F508del allele by combined VX-770 and VX-809 treatment was most effective in all organoids. These data confirmed the read-through capacity of G418 for different PTCs, but the efficacy is limited compared to F508del-targeting drugs (Fig. 2).

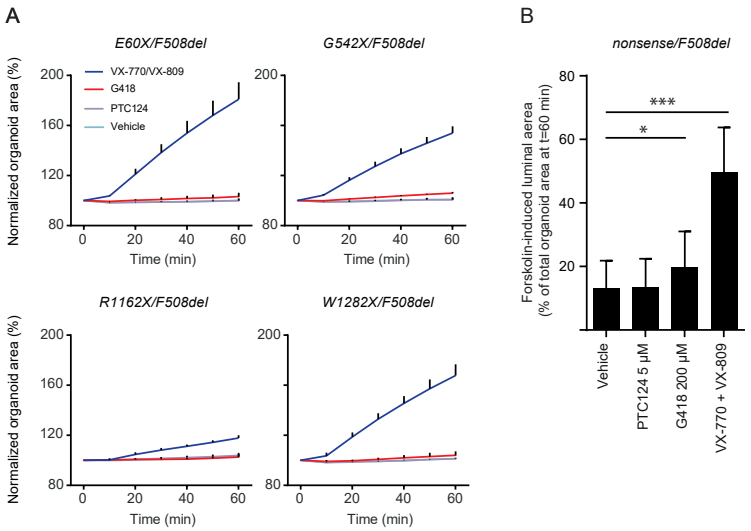

***Fig. 2**. Marginal effect of G418 and PTC124 compared to CFTR-protein targeting drugs. Forskolin-induced swelling (FIS) of nonsense/F508del intestinal organoids (E60X, G542X, R1162X and W1282X), incubated with either G418 (200 µM), PTC124 (5 µM) or DMSO (vehicle), w/o VX-809 (3 µM) for 24h. Forskolin-induced swelling (FIS) (5 µM, w/o VX-770 (1 µM)) was monitored for 60 min. Conditions were measured in triplicate and in three independent experiments for each patient. A) Normalized organoid area of PTC/F508del organoids (%, ± SD); B) Forskolin-induced luminal area as percentage of total organoid area at t = 60 min (± SD), pooled for all four genotypes of Fig. 2A, *p < 0.05, ***p < 0.001.*

Discussion

We investigated the efficacy of read-through agents to induce CFTR function in organoids with a PTC. Next to total organoid swelling, we analyzed the luminal expansion upon forskolin stimulation as percentage of total organoid area, which was found to be more sensitive than FIS (Fig. 1, 2). Forskolin-induced luminal expansion precedes organoid swelling, which allows analyzing compounds with limited efficacy. The dynamic range, however, is limited and quickly reaches a ceiling; when organoids expand to a greater extent, the ratio of luminal area and total organoid area will not change that much as illustrated by the limited effects of VX-809/VX-770 treatment in F508del homozygous organoids (Fig. 1).

G418 induced FIS and luminal expansion in a stop codon mutation-specific manner, demonstrating that read-through by pharmacological agents can be detected in organoids (Fig. 1, 2). The G418-induced CFTR function was further stimulated by CFTR-modifying drugs VX-770 and VX-809 in organoids lacking residual CFTR function (E60X/4015delATTT), confirming G418 induced full-length CFTR protein and confirming previous data (22) (Fig. 1A, C–D). It is very well possible that G418-induced full-length CFTR benefits from correction as some misfolding may occur upon integration of new amino acids by G418 but this was not specifically addressed. The efficacy of G418 + VX-770 + VX-809 was within the range associated with residual CFTR function of F508del homozygous organoids (Fig. 1C). These data indicated that E60X/4015delATTT intestinal organoids express sufficient CFTR nonsense mRNA levels for detection of read-through by pharmacological agents such as G418. The effect of G418-induced read-through on CFTR function in nonsense/F508del organoids was significant, yet very small compared to CFTR-targeting drugs (Fig. 2).

In contrast, PTC124 did not induce detectable read-through as standalone treatment or in combination with VX-770 and VX-809 (Figs. 1A, C, D, 2A). We tested two compound batches of PTC124, and included CFTR mutations that were previously associated with PTC124 read-through, such as G542X (c.1624G- > T) and W1282X (c.3846G- > A) (cftr2.org). Moreover, removal of antibiotics from the culture medium and inhibition of nonsense RNA-mediated decay by amlexanox pretreatment (10) did not increase G418-induced or PTC124-induced read-through (data not shown). We did not control for uptake of the read-through agents by organoids that might be limited due to specific culture conditions or selective activity of drug pumps. Despite our inability to detect PTC124 activity, it remains possible that some individuals may be identified who show response to PTC124. Also, the efficacy of PTC124 might be tissue- and/or species-specific, although PTC suppression by PTC124 was previously observed in mouse-intestine (9).

The inability to detect read-through by PTC124 in organoids is consistent with recently published *in vitro* data (11) and the lack of efficacy in phase 3 clinical trials in both CF (17) and Duchenne muscular dystrophy (18,19). However, data are conflicting with reports indicating subject-specific PTC124 activity in open-label phase 2 clinical trials as suggested from CFTR biomarker analysis (14–16), and the retrospective analysis of the phase 3 clinical trial data suggesting mild clinical efficacy of PTC124 in tobramycin-free subjects (17). Our data would support the development of more effective read-through compounds in combination with CFTR-protein restoring drugs.

Conflict of interest

JFD, CKE and JMB are inventors on a patent application related to these findings (PCT/IB2012/057497).

Acknowledgments

This work was part of the HIT-CF program, supported by grants of the Dutch Cystic Fibrosis Foundation (NCFS), the Wilhelmina Children's Hospital (WKZ) Foundation, and the Netherlands Organization for Health Research and Development (ZonMw) (Grant number 40-00812-98-14103). The funders had no role in study design, data collection and analysis, decision to publish or preparation of the manuscript.

References

[1] J.R. Riordan. CFTR function and prospects for therapy. Annu. Rev. Biochem. 77 (Jan 2 2008), pp. 701-726.

[2] P.R. Sosnay, K.R. Siklosi, F. Van Goor, K. Kaniecki, H. Yu, N. Sharma. Defining the disease liability of variants in the cystic fibrosis transmembrane conductance regulator gene. Nat. Genet., 45 (10) (Aug 25 2013), pp. 1160-1167.

[3] F. Van Goor, S. Hadida, P.D.J. Grootenhuis, B. Burton, D. Cao, T. Neuberger, et al. Rescue of CF airway epithelial cell function *in vitro* by a CFTR potentiator, VX-770. Proc. Natl. Acad. Sci. U. S. A., 106 (44) (Nov 3 2009), pp. 18825-18830.

[4] F. Van Goor, S. Hadida, P.D.J. Grootenhuis, B. Burton, J.H. Stack, K.S. Straley, et al. Correction of the F508del-CFTR protein processing defect *in vitro* by the investigational drug VX-809. Proc. Natl. Acad. Sci. U. S. A., 108 (46) (Nov 15 2011), pp. 18843-18848.

[5] K. De Boeck, A. Zolin, H. Cuppens, H.V. Olesen, L. Viviani. The relative frequency of CFTR mutation classes in European patients with cystic fibrosis. J. Cyst. Fibros., 13 (4) (Jan 15 2014), pp. 403-409.

[6] M. Howard, R.A. Frizzell, D.M. Bedwell. Aminoglycoside antibiotics restore CFTR function by overcoming premature stop mutations. Nat. Med., 2 (Apr 1996), pp. 467-469.

[7] K.M. Keeling, D. Wang, S.E. Conard, D.M. Bedwell. Suppression of premature termination codons as a therapeutic approach. Crit. Rev. Biochem. Mol. Biol., 47 (5) (2013), pp. 444-463.

[8] E.M. Welch, E.R. Barton, J. Zhuo, Y. Tomizawa, W.J. Friesen, P. Trifillis, et al. PTC124 targets genetic disorders caused by nonsense mutations. Nature, 447 (7140) (May 3 2007), pp. 87-91.

[9] M. Du, X. Liu, E.M. Welch, S. Hirawat, S.W. Peltz, D.M. Bedwell. PTC124 is an orally bioavailable compound that promotes suppression of the human CFTR-G542X nonsense allele in a CF mouse model. Proc. Natl. Acad. Sci. U. S. A., 105 (6) (Feb 12 2008), pp. 2064-2069.

[10] S. Gonzalez-Hilarion, T. Beghyn, J. Jia, N. Debreuck, G. Berte, K. Mamchaoui, et al. Rescue of nonsense mutations by amlexanox in human cells. Orphanet J Rare Dis, 7 (1) (Jan 2012), p. 58.

[11] S.P. McElroy, T. Nomura, L.S. Torrie, E. Warbrick, U. Gartner, G. Wood, et al. A lack of premature termination codon read-through efficacy of PTC124 (Ataluren) in a diverse array of reporter assays. PLoS Biol., 11 (6) (Jun 2013), p. e1001593.

[12] D.S. Auld, N. Thorne, W.F. Maguire, J. Inglese. Mechanism of PTC124 activity in cell-based luciferase assays of nonsense codon suppression. Proc. Natl. Acad. Sci. U. S. A., 106 (9) (Mar 3 2009), pp. 3585-3590.

[13] D.S. Auld, S. Lovell, N. Thorne, W.A. Lea, D.J. Maloney, M. Shen, et al. Molecular basis for the high-affinity binding and stabilization of firefly luciferase by PTC124. Proc. Natl. Acad. Sci. U. S. A., 107 (11) (Mar 16 2010), pp. 4878-4883.

[14] I. Sermet-Gaudelus, K. De Boeck, G.J. Casimir, F. Vermeulen, T. Leal, A. Mogenet, et al. Ataluren (PTC124) induces cystic fibrosis transmembrane conductance regulator protein expression and activity in children with nonsense mutation cystic fibrosis. Am. J. Respir. Crit. Care Med., 182 (10) (Nov 15 2010), pp. 1262-1272.

[15] E. Kerem, S. Hirawat, S. Armoni, Y. Yaakov, D. Shoseyov, M. Cohen, et al. Effectiveness of PTC124 treatment of cystic fibrosis caused by nonsense mutations: a prospective phase II trial. Lancet, 372 (9640) (Aug 30 2008), pp. 719-727.

[16] M. Wilschanski, L.L. Miller, D. Shoseyov, H. Blau, J. Rivlin, M. Aviram, et al. Chronic ataluren (PTC124) treatment of nonsense mutation cystic fibrosis. Eur. Respir. J., 38 (1) (Jul 2011), pp. 59-69.

[17] E. Kerem, M.W. Konstan, K. De Boeck, F.J. Accurso, I. Sermet-Gaudelus, M. Wilschanski, et al. Ataluren for the treatment of nonsense-mutation cystic fibrosis: a randomised, double-blind, placebo-controlled phase 3 trial. Lancet Respir. Med., 2 (7) (Jul 2014), pp. 539-547.

[18] R.S. Finkel, K.M. Flanigan, B. Wong, C. Bönnemann, J. Sampson, H.L. Sweeney, et al. Phase 2a study of ataluren-mediated dystrophin production in patients with nonsense mutation Duchenne muscular dystrophy. PLoS One, 8 (12) (Jan 2013), p. e81302.

[19] E.P. Hoffman, E.M. Connor. Orphan drug development in muscular dystrophy: update on two large clinical trials of dystrophin rescue therapies. Discov. Med., 16 (89) (Nov 2013), pp. 233-239.

[20] J.F. Dekkers, C.L. Wiegerinck, H.R. de Jonge, I. Bronsveld, H.M. Janssens, K.M. de Winter-de Groot, et al. A functional CFTR assay using primary cystic fibrosis intestinal organoids. Nat. Med., 19 (7) (Jul 2013), pp. 939-945.

[21] T. Sato, R.G. Vries, H.J. Snippert, M. van de Wetering, N. Barker, D.E. Stange, et al. Single Lgr5 stem cells build crypt-villus structures *in vitro* without a mesenchymal niche. Nature, 459 (7244) (May 14 2009), pp. 262-265.

[22] X. Xue, V. Mutyam, L. Tang, S. Biswas, M. Du, L.A. Jackson, et al. Synthetic Aminoglycosides Efficiently Suppress CFTR Nonsense Mutations and are Enhanced by Ivacaftor. Am. J. Respir. Cell Mol. Biol., 50 (Nov 19 2013), pp. 805-816.

Limited premature termination codon suppression by read-through agents in cystic fibrosis intestinal organoids

CHAPTER 3

β2-Adrenergic receptor agonists activate CFTR in intestinal organoids and subjects with cystic fibrosis

Lodewijk A.W. Vijftigschild[1,2,10], Gitte Berkers[1,10], Johanna F. Dekkers[1,2,11], Domenique D. Zomer-van Ommen[1,2,11], Elizabeth Matthes[3], Evelien Kruisselbrink[1,2], Annelotte Vonk[1,2], Chantal E. Hensen[1], Sabine Heida-Michel[1], Margot Geerdink[1], Hettie M. Janssens[4], Eduard A. van de Graaf[5], Inez Bronsveld[5], Karin M. de Winter-de Groot[1], Christof J. Majoor[6], Harry G.M. Heijerman[7], Hugo R. de Jonge[8], John W. Hanrahan[3], Cornelis K. van der Ent[1] and Jeffrey M. Beekman[1,9]

European Respiratory Journal 2016 48: 768-779; DOI: 10.1183/13993003.01661-2015.

[1]Dept of Pediatric Pulmonology, University Medical Center, Utrecht, The Netherlands. [2]Laboratory of Translational Immunology, University Medical Center, Utrecht, The Netherlands. [3]CF Translational Research Centre, Dept of Physiology, McGill University, Montréal, QC, Canada. [4]Dept of Pediatric Pulmonology, Erasmus Medical Center/ Sophia Children's Hospital, Rotterdam, The Netherlands. [5]Dept of Pulmonology, University Medical Center, Utrecht, The Netherlands. [6]Dept of Respiratory Medicine, Academic Medical Center, Amsterdam, The Netherlands. [7]Dept of Pulmonology and Cystic Fibrosis, Haga Teaching Hospital, The Hague, The Netherlands. [8]Dept of Gastroenterology and Hepatology, Erasmus University Medical Center, Rotterdam, The Netherlands. [9]Regenerative Medicine Center Utrecht, University Medical Center, Utrecht, The Netherlands. [10]These two authors contributed equally to this work. [11]These two authors contributed equally to this work.

Received October 8, 2015. Accepted May 11, 2016.

CHAPTER 3

Abstract

We hypothesized that people with cystic fibrosis (CF) who express CFTR (cystic fibrosis transmembrane conductance regulator) gene mutations associated with residual function may benefit from G-protein coupled receptor (GPCR)-targeting drugs that can activate and enhance CFTR function.

We used intestinal organoids to screen a GPCR-modulating compound library and identified β2-adrenergic receptor agonists as the most potent inducers of CFTR function.

β2-Agonist-induced organoid swelling correlated with the CFTR genotype, and could be induced in homozygous CFTR-F508del organoids and highly differentiated primary CF airway epithelial cells after rescue of CFTR trafficking by small molecules. The *in vivo* response to treatment with an oral or inhaled β2-agonist (salbutamol) in CF patients with residual CFTR function was evaluated in a pilot study. 10 subjects with a R117H or A455E mutation were included and showed changes in the nasal potential difference measurement after treatment with oral salbutamol, including a significant improvement of the baseline potential difference of the nasal mucosa (+6.35 mV, $p<0.05$), suggesting that this treatment might be effective *in vivo*. Furthermore, plasma that was collected after oral salbutamol treatment induced CFTR activation when administered *ex vivo* to organoids.

This proof-of-concept study suggests that organoids can be used to identify drugs that activate CFTR function *in vivo* and to select route of administration.

Introduction

The CFTR (cystic fibrosis transmembrane conductance regulator) gene encodes an apical anion channel and is mutated in subjects with cystic fibrosis (CF) [1]. Subjects with CF have an altered composition of many mucosal surface fluids, leading to dysfunction of the gastrointestinal and pulmonary systems as well as other organs. The most common mutation is a deletion of phenylalanine at position 508 (p.Phe508del; F508del) and is present in ~90% of subjects with CF, of which ~65% are F508del homozygotes (www.genet.sickkids.on.ca). CF disease expression is highly variable between subjects due to the complex relations between CFTR genotype, modifier genes and environmental factors, which are unique for each individual [2–6].

Approximately 2000 *CFTR* mutations have been described, which are divided into different classes according to their impact on CFTR expression and function [7]. Briefly, class I mutations result in no functional protein (e.g. stop codons and frameshifts), class II mutations severely affect apical trafficking (e.g. F508del), class III mutations disrupt channel regulation or gating (e.g. p.Gly551Asp; G551D), class IV mutations reduce channel conductance (e.g. p.Arg334Trp; R334W), class V mutations lead to reduced apical expression of normally functioning CFTR (e.g. p.Ala455Glu; A455E) and class VI mutations accelerate CFTR turnover at the plasma membrane. Whereas class I–III and VI mutations are generally associated with no or very limited residual function, some residual function is associated with class IV and V mutations and milder disease phenotype such as CFTR-A455E and CFTR-R117H (p.Arg117His; shared class III and IV) (www.cftr2.org).

Novel drugs are being developed to target mutation-specific CFTR defects. The potentiator VX-770 (ivacaftor) enhances the activity of apical CFTR and was shown to provide clinical benefit for patients with CFTR gating mutations [8–10]. Pharmacological repair of CFTR-F508del has proven more difficult, although encouraging phase III clinical trial results have been reported for CFTR-F508del homozygous subjects treated with a combination of ivacaftor and the corrector lumacaftor (VX-809) [11], which partly restores trafficking of CFTR-F508del to the apical membrane [12]. However, the therapeutic effects of these therapies are variable between subjects, and remain insufficient to fully restore CF and CFTR-related disease markers, indicating that more effective treatments are still required.

Individual CFTR function depends on endogenous signaling pathways that control its channel function. Various endogenous ligands have been identified which activate CFTR in a cAMP/protein kinase A-dependent fashion. Many of these ligands (e.g. vasoactive intestinal peptide, prostaglandins and β-adrenergic stimuli) signal by binding to G-protein coupled receptors (GPCRs), which release cytosolic G-proteins that activate adenylyl cyclase to generate cAMP [13–15]. While it is known that tissue-specific activity of CFTR is regulated by diverse ligands, the extent to which CFTR function is limited by cAMP production is not clear.

We hypothesised that cAMP-dependent signaling is a rate-limiting step for CFTR activation *in vivo* and that CF individuals who express alleles associated with residual function might benefit from existing drugs that stimulate cAMP. Therefore, we screened a small chemical compound library of GPCR modulators for their ability to stimulate (mutant) CFTR activity in primary rectal organoids from healthy control and CF subjects. Rectal organoids grow from intestinal stem cells and self-organise

into multicellular three-dimensional structures consisting of a single epithelial layer, with the apical membrane facing a closed central lumen [16–18]. Addition of forskolin, which raises cAMP, stimulates CFTR-dependent fluid secretion into the organoid lumen and induces rapid organoid swelling [19, 20]. Here, we provide proof-of-concept that intestinal organoids can be used as tool to identify potential drugs and route of administration for particular CF subgroups.

Materials and methods

Human participants

This study was approved by the Ethics Committee of the University Medical Centre Utrecht and the Erasmus Medical Center Rotterdam. Informed consent was obtained from all subjects. Organoids from healthy controls and CF subjects were generated from rectal biopsies after intestinal current measurements obtained 1) during standard CF care, 2) for diagnostic purposes or 3) during voluntary participation in studies.

Materials

The GPCR compound library, VX-809 and VX-770 were purchased from SelleckChem (Houston, TX, USA). Carvedilol, forskolin, salbutamol, salmeterol, terbutaline, epinephrine, ritodrine, dimethylsulphoxide (DMSO), N-acetylcysteine, nicotinamide and SB202190 were purchased from Sigma (St Louis, MO, USA). Formoterol was purchased from Santa Cruz Biotechnologies (Dallas, TX, USA). CFTRinh-172 was obtained from CFF Therapeutics (Chicago, IL, USA). Matrigel was purchased from BD (Franklin Lakes, NJ, USA). Calcein AM, supplements N-2 and B-27, Glutamax, advanced Dulbecco's modified Eagle medium/ Ham's F-12 (DMEM/F-12), penicillin/streptomycin, HEPES and murine epidermal growth factor (mEGF) were purchased from Life Technologies (Bleiswijk, The Netherlands). A83-01 was purchased from Tocris (Abingdon, UK). TOPflash and FOPflash were purchased from Millipore (Amsterdam, The Netherlands).

Human organoid cultures

Rectal crypt isolation and organoid expansion was performed with some adaptations of previously described methods [20, 21]. Briefly, rectal biopsies were thoroughly washed with PBS and incubated in 10 mM EDTA for 90 min at 4°C. The crypts were collected by centrifugation and suspended in 50% Matrigel and 50% complete culture medium (advanced DMEM/F-12 media supplemented with penicillin/streptomycin, HEPES, GlutaMax, nutrient supplements N-2 and B-27, N-acetylcysteine, nicotinamide, mEGF, A83-01, SB202190, and 50% Wnt3a, 20% Rspo-1 and 10% Noggin conditioned media) that was allowed to solidify at 37°C for 20 min in three droplets of 10 µL per well of a 24-well plate. The droplets were then immersed in pre-warmed complete culture medium and cultures were expanded for at least 3 weeks before assaying CFTR function. Complete culture medium was refreshed three times per week and organoids were passaged weekly. Quality of the conditioned media was assessed by dot blots, ELISA and luciferase reporter constructs (TOPflash and FOPflash) [22, 23].

GPCR compound library

The GPCR small-molecule compound library comprises 61 agonists and antagonists that target a wide range of GPCR families, including adrenergic, dopamine, opioid, serotonin, histamine and acetylcholine receptors. A complete list of chemicals in the library is given in online supplementary table S1.

CFTR function measurement in organoids

Organoids were reseeded 1 day before functional analysis in 96-well plates as described previously [20]. CFTR-F508del organoids were incubated with VX-809 (3 μM) for 24 h, as indicated in text and figure legends. Organoids were stained with Calcein green AM (2.5 μM) 1 h prior the addition of compound and each compound was tested at four different concentrations (10, 2, 0.4 and 0.08 μM). Forskolin (5 μM) and DMSO were used as positive and negative controls, respectively. Organoid swelling was monitored for 1 h using a Zeiss LSM 710 confocal microscope (Zeiss, Jena, Germany). The relative increase in surface area was calculated using Volocity (version 6.1.1; PerkinElmer, Waltham, MA, USA). The area under the curve was calculated as described previously [20]. Carvedilol (10 μM) was incubated for 30 min prior to stimulation and organoids were pre-treated with CFTRinh-172 (150 μM) for 4 h to inhibit CFTR-dependent responses.

Halide-sensitive YFP quenching in CFBE41o- cells

CFBE41o- cell lines overexpressing CFTR-F508del or CFTR-WT were grown in α-minimal essential medium containing 8% heat-inactivated fetal calf serum, penicillin and streptomycin at 37°C in a humidified 5% CO2 incubator as described [24, 25]. CFBE41o- cells were transduced with the ratiometric halide-sensitive pHAGFE2-YFP (46L-148Q-152L)-mKate sensor for measurement of CFTR activity as described previously [26]. Briefly, cells were incubated for 24 h with VX-809 (10 μM). After 20 min stimulation in a chloride-containing buffer, the cells were washed with iodide buffer and the decrease in fluorescence was monitored using a Zeiss LSM 710 microscope for 60 s. The rate of YFP (yellow fluorescent protein)/mKate quenching was calculated using Prism 6 (GraphPad, La Jolla, CA, USA).

Ussing chamber measurements in primary airway epithelial cells

Primary F508del/F508del human bronchial epithelial cells from the Primary Airway Cell Biobank of the CF Translational Research Centre at McGill University were cultured at the air/liquid interface for 3 weeks and pre-treated for 24 h with VX-809 (1 μM). Control monolayers from the same patients were handled similarly but exposed to vehicle (0.1% DMSO) during the pre-treatment period. For electrophysiological measurements, monolayers were mounted in Ussing chambers (EasyMount; Physiologic Instruments, San Diego, CA, USA) and voltage-clamped using a VCCMC6 multichannel current-voltage clamp (Physiologic Instruments, San Diego, CA, USA). The voltage clamp was connected to a PowerLab/8SP interface for data collection (ADInstruments, Colorado Springs, CO, USA) and analysis was performed using a PC as described previously [27]. Solutions were continuously gassed and stirred with 95% O2/5% CO2 and were maintained at 37°C by circulating water bath. Ag/AgCl reference electrodes were used to measure transepithelial voltage and pass current. Pulses (1 mV amplitude, 1 s duration) were delivered every 90 s to monitor resistance. A basolateral-to-apical Cl– gradient was imposed and amiloride (100 μM) was added on the apical side to inhibit the epithelial sodium channel (ENaC) current. Monolayers were exposed acutely to 10 μM forskolin or salbutamol or to the vehicle 0.1% DMSO. After the short circuit current (Isc) reached a plateau, a potentiator (either 50 μM genistein or 100 nM VX-770 as indicated) was added, followed by CFTRinh-172 to confirm that the current responses were dependent on CFTR. Salbutamol was also assayed after pre-treatment with the antagonist carvedilol (10 μM) for 30 min as a further test of receptor specificity.

Pilot study with inhaled and oral salbutamol

In this open-label phase II pilot study, 10 patients were randomly assigned to receive four times daily 200 µg salbutamol per inhalation or four times daily 4 mg salbutamol orally, for 3 consecutive days (www.trialregister.nl/trialreg/admin/rctview.asp?TC=4513). After a wash-out period of at least 4 days, patients received the opposite treatment. We included patients aged ≥18 years old with a CFTR-A455E or a CFTR-R117H mutation on at least one allele of whom rectal biopsies and organoid cultures showed residual CFTR function in previous studies [20]. Patients were excluded if they had an acute pulmonary exacerbation or an increased risk of side-effects of salbutamol. The primary outcome measures were changes in sweat chloride concentration (SCC) and changes in nasal potential difference (NPD) measurements, which are both *in vivo* biomarkers for CFTR function. The NPD and SCC measurements were performed according to the most recent version of the standard operating procedure of the European Cystic Fibrosis Society Clinical Trials Network (www.ecfs.eu/ctn). The results of these measurements before and after treatments with salbutamol were compared using a Wilcoxon signed-rank test. A secondary outcome measure was the CFTR-activating capacity of the patients' plasma in organoids. Therefore, whole blood was collected in sodium-heparin tubes before treatment and after the last dose of salbutamol, when the maximum concentration of salbutamol in the blood was expected (inhaled salbutamol after 30 min, oral salbutamol after 2 h; www.fk.cvz.nl). Plasma was isolated as described previously [28].

Patient plasma-induced organoid swelling

Patient plasma was collected before and after treatment with salbutamol and incubated (20% and 40% plasma) with organoids derived from subjects with CF with high residual CFTR function (R117H/F508del). Organoid swelling was monitored as described above. Reference values were generated by measurement of spiked salbutamol in 0%, 20% and 40% plasma.

Results

Screen for GPCR modulators of organoid swelling

To identify compounds that can activate CFTR, we assessed CFTR-dependent swelling of organoids in response to 61 GPCR-modulating compounds (figure 1) [20]. As observed previously, forskolin induced rapid swelling of CFTR-WT organoids and, to a lesser extent, of VX-809-treated homozygous CFTR-F508del organoids. As expected, DMSO did not induce swelling (figure 1a). Swelling was expressed as the area under the curve for each specific condition (figure 1a and b). Of the 61 compounds tested, dopamine, epinephrine, ritodrine and salbutamol dose-dependently induced swelling of CFTR-WT organoids, with highest potency for ritodrine and salbutamol, and lowest potency for dopamine (figure 1c and d). Epinephrine, ritodrine and salbutamol are ligands for β2-adrenergic receptors, and dopamine for the dopamine receptor. At the highest dose, the response to the four compounds was comparable to the forskolin-induced swelling (figure 1d). In VX-809-corrected F508del homozygous organoids, swelling was dose-dependently induced by epinephrine, salbutamol and ritodrine, but not by dopamine (figure 1c and e). The potency was highest for salbutamol and lowest for ritodrine. High levels of salbutamol induced swelling to a similar extent as forskolin (figure 1d). In conclusion, β2-adrenergic receptor stimulation can potently activate CFTR-WT and drug-corrected CFTR-F508del in organoids.

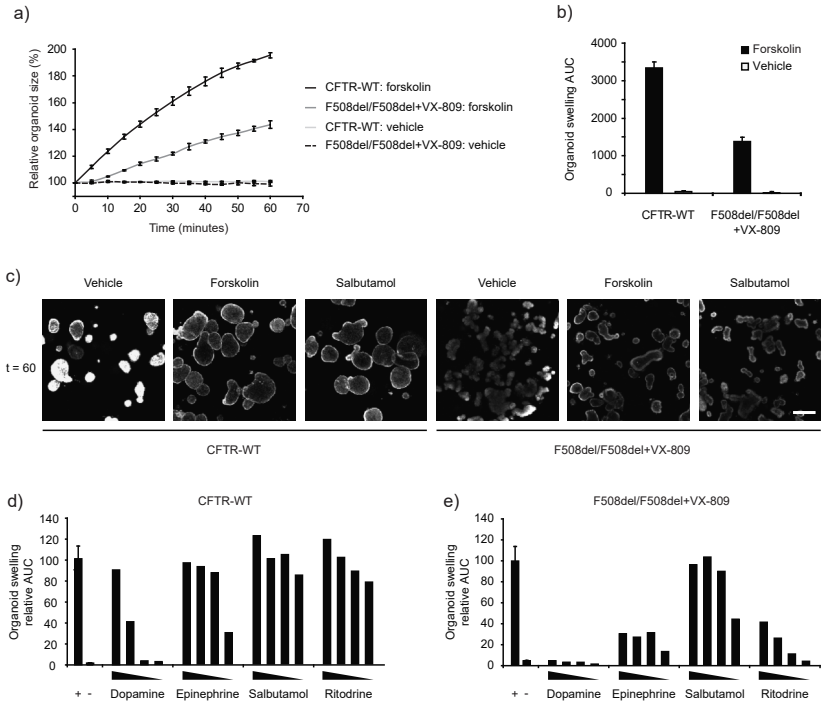

Figure 1. *G-protein coupled receptor (GPCR) modulator-induced swelling of healthy control and cystic fibrosis transmembrane conductance regulator (CFTR)-F508del organoids. a) CFTR wild-type (WT) and F508del homozygous organoids were stimulated with forskolin (5 μM) or dimethylsulphoxide (DMSO; vehicle, 0.05%) and the relative increase in size was monitored over 60 min. CFTR-F508del homozygous organoids were pre-incubated with VX-809 (3 μM) for 24 h. b) Quantification of the area under the curve (AUC) of a), baseline was set at 100%, t=60 min. c) Representative images of CFTR-WT and VX-809-corrected CFTR-F508del organoids after 60 min of stimulation with DMSO (vehicle), forskolin (5 μM) or salbutamol (10 μM). Scale bar: 200 μm. d) Positive compounds for induction of fluid secretion using CFTR-WT intestinal organoids after screening a GPCR modulator library (61 compounds). Forskolin (+) and DMSO (−) were used as positive and negative control, respectively. GPCR modulators were tested at 10, 2, 0.4 and 0.08 μM. Data are normalised to the forskolin response. e) Same compounds as in d), tested on VX-809 (3 μM)-treated F508del homozygous organoids.*

β2-Agonists robustly induce organoid swelling

Next, we assessed β2-adrenergic receptor stimulation by short- and long-acting agonists in organoids with various CFTR mutations (figure 2). First, salbutamol- and ritodrine-induced swelling was confirmed in organoids derived from three individual F508del homozygous patients (figure 2a). As expected, robust organoid swelling was only observed after treatment with the CFTR modulators VX-770 or VX-809, and was highest upon VX-770 and VX-809 combination treatment. In line with figure 1, ritodrine was somewhat less potent than salbutamol and forskolin, especially for VX-809-incubated organoids. Both short-acting (ritodrine, terbutaline and salbutamol) and long-acting (formoterol, salmeterol and isoproterenol) β2-agonists induced fluid secretion. Inhibition by CFTR-inh172 or carvedilol supported CFTR or β-adrenergic receptor specificity, respectively (figure 2b). Forskolin- and β2-adrenergic receptor-

induced swelling differed between organoids with distinct CFTR genotypes: we observed no swelling in organoids expressing two CFTR-null alleles (p.Glu60Ter and p.Ile1295fs; E60X and 4015delATTT), some swelling in CFTR-A455E or VX-809-corrected homozygous CFTR-F508del organoids and high swelling in CFTR-R117H expressing organoids (figure 2c). Dose-dependencies of β2-agonist-induced swelling were independent of the CFTR genotype or VX-809-rescued F508del, and indicated that long-acting β2-agonists were most potent, whereas forskolin was least potent (figure 2d). Representative examples of agonist-induced swelling are indicated in figure 2e. Together, these data demonstrate that various β2-agonists robustly induce CFTR function in a CFTR mutation-dependent manner.

Figure 2 (see next page). *β2-Agonists induce cystic fibrosis transmembrane conductance regulator (CFTR) activity. a) CFTR-F508del homozygous organoids were stimulated with ritodrine (10 μM), salbutamol (10 μM) or forskolin (5 μM). VX-809 (3 μM) was incubated for 24 h prior to stimulation. VX-770 (1 μM) was added simultaneously with the stimulus. AUC: area under the curve. Data were normalised to the combined VX-770+VX-809+forskolin response and organoids from three patients were measured at three independent time points in duplicate. Data are presented as mean±sem. b) VX-809 (3 μM) treated CFTR-F508del organoids were incubated with CFTRinh-172 or carvedilol before stimulation. β2-Agonists were used at 10 μM and forskolin at 5 μM. All data were normalised to forskolin and represent mean±sem of three independent measurements in duplicate. c) Organoids derived from patients with different CFTR genotypes were stimulated with β2-agonists (10 μM) or forskolin (5 μM). n: number of patients, measured at three independent time points in duplicate (mean±sem). d) Dose–response curves for different β2-agonists and forskolin in F508del/F508del, F508del/A455E and F508del/R117H organoids. All data were normalised to the highest concentration of stimulus and represent mean±sem of measurements at three independent time points. e) Representative images of organoids expressing CFTR-F508del and either CFTR-A455E or CFTR-R117H after 60 min of stimulation with dimethylsulphoxide (DMSO), forskolin (5 μM) or salbutamol (10 μM). Scale bar: 200 μm. Vehicle represents DMSO in all cases.*

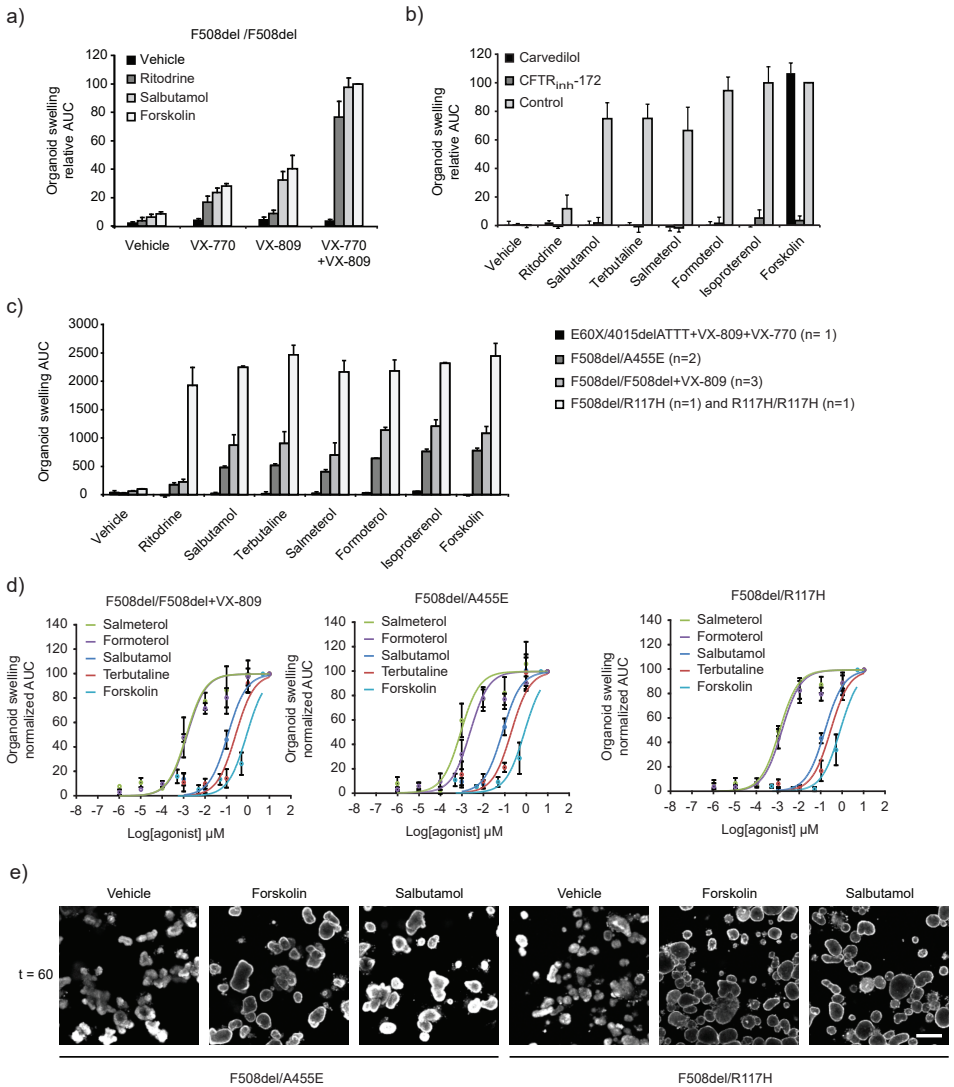

Salbutamol-mediated CFTR activation in bronchial epithelial cells

To confirm that intestinal organoid responses can be relevant for airway epithelial cells, CFTR activation by the β2-agonist salbutamol was studied in the CF airway cell line CFBE41o- (CFBE) and primary CF human bronchial epithelial cells. First, we studied CFTR-dependent iodide quenching rates in CFBE41o- cells that endogenously express CFTR-F508del and were previously transduced with CFTR-F508del (CFBE-F508del) or CFTR-WT (CFBE-CFTR-WT) cDNA [24]. To measure CFTR-dependent iodide influx, the cells were stably transduced with a YFP/mKate sensor, as described previously [26]. Quenching of the YFP signal by iodide (indicating CFTR activity) was induced by both forskolin and salbutamol in VX-809+VX-770-treated CFTR-F508del and CFTR-WT CFBE41o- cells (figure 3a). In addition, Ussing chamber experiments revealed that salbutamol and forskolin induced a CFTR-dependent short circuit current in

F508del homozygous human bronchial epithelial cells treated for 24 h with VX-809 and VX-770, but not in primary cultures without CFTR-repairing treatment (figure 3b–d). As expected, the acute response to forskolin and salbutamol was abolished by CFTRinh-172 and the salbutamol-induced response was inhibited by carvedilol (figure 3c and d). To conclude, activation of modulator-repaired CFTR-F508del by β2-agonists was recapitulated in respiratory cell lines and primary airway cultures.

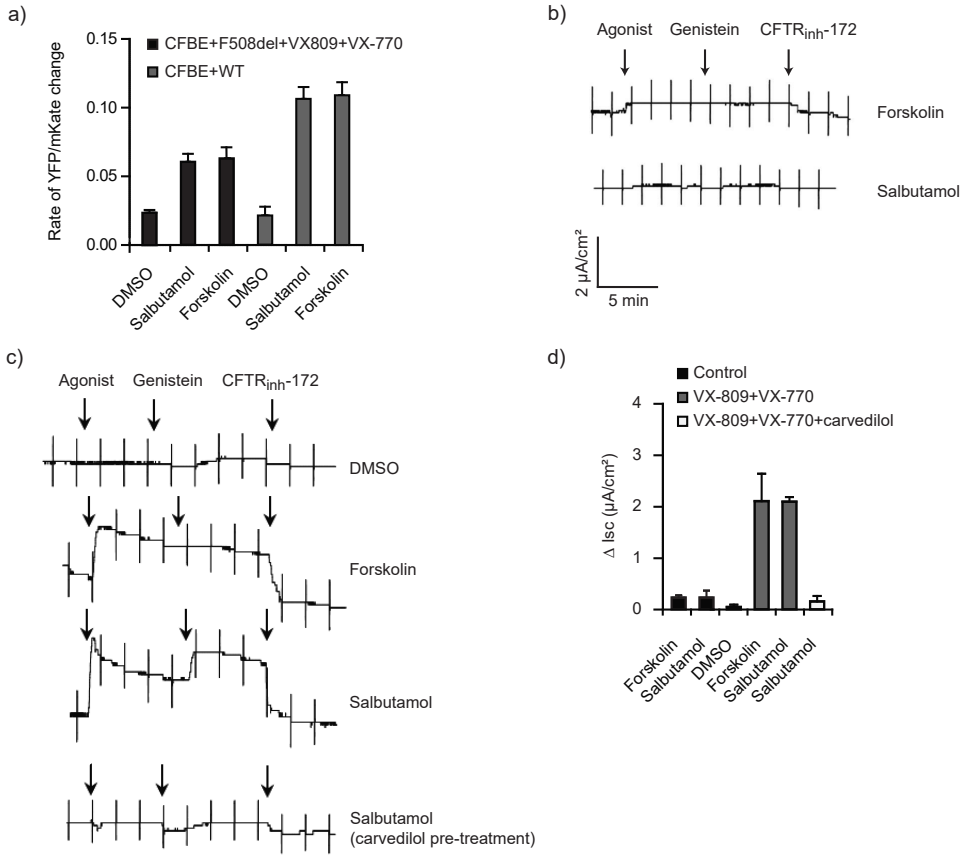

Figure 3. *β2-Agonist-induced cystic fibrosis transmembrane conductance regulator (CFTR) activation in bronchial epithelial cells. a) CFTR activity in CFBE41o- cells (CFBE) overexpressing CFTR-F508del or CFTR-WT, and stably expressing YFP (yellow fluorescent protein)/mKate, using a YFP quenching assay. CFBE41o- cells were pre-incubated for 24 h with VX-809 (10 µM), and stimulated with forskolin (25 µM) and VX-770 (10 µM) or salbutamol (10 µM) and VX-770 (10 µM) for 20 min prior to addition of iodide. Data are presented as mean±sem and are representative of three independent experiments. b) Highly differentiated primary CFTR-F508del bronchial epithelial cells cultured at the air/liquid interface were analysed in Ussing chamber experiments. Representative traces of primary CF cells untreated with CFTR modulator drugs and exposed acutely to forskolin or salbutamol. Constant current pulses used to monitor transepithelial resistance*

cause the vertical deflections. c) Representative Ussing chamber tracings for VX-809 (1 μM)- and VX-770 (100 nM)-treated primary CF bronchial epithelial cells, stimulated acutely with dimethylsulphoxide (DMSO), forskolin (10 μM) or salbutamol (10 μM). Scaling is identical to b). d) Quantification of b, c). Data are presented as mean±sem and are representative of three independent experiments.

Pilot study with inhaled and oral salbutamol

To evaluate if drugs identified by screens in rectal organoids can be used to modulate CFTR function *in vivo*, 10 CF patients were enrolled in a study, and treated with oral and inhaled salbutamol. One patient was only treated with oral salbutamol due to increased asthma symptoms during the wash-out period of salbutamol aerosol between both treatments. The baseline characteristics of the study population are shown in table 1.

Table 1. *Baseline characteristics of the 10 subjects enrolled in the pilot study. Data are presented as median (interquartile range) or n (%), unless otherwise stated. FEV1: forced expiratory volume in 1 s; CFTR: cystic fibrosis transmembrane conductance regulator.*

Age years	38.5 (31.5–49.0)
Male	4 (40)
Body mass index kg·m^{-2}	22.28 (20.38–28.16)
FEV1 % pred (range)	62.0 (44.8–84.8) (31–109)
***CFTR* genotype**	
F508del/A455E	9 (90)
F508del/R117H	1 (10)

To analyse the systemic delivery of salbutamol by inhalation or oral application, we stimulated F508del/R117H and F508del/A455E organoids with plasma collected before and after *in vivo* treatment. Plasma collected after oral salbutamol treatment significantly induced F508del/R117H organoid swelling compared with the plasma collected before treatment or after aerosol administration of salbutamol, indicating that plasma concentrations of salbutamol were highest after oral treatment (figure 4a and b). Spiking of pure salbutamol in pooled plasma of subjects before treatment indicated that active salbutamol levels were below detection levels upon aerosol treatment and detectable but low after oral treatment, amounting to ~5 nM (figure 4c). After correcting for 40% subject plasma samples, circulating salbutamol levels after oral treatment on average reached levels ~12.5 nM.

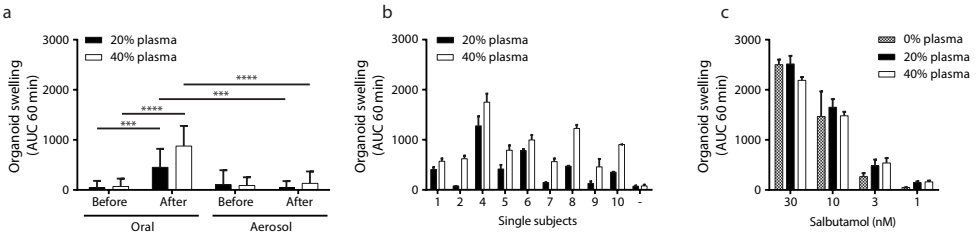

Figure 4. *Plasma-induced organoid swelling. a) Cystic fibrosis transmembrane conductance regulator (CFTR)-F508del/R117H organoids were stimulated with 20% and 40% plasma of each subject (n=9) both before and after treatment via both aerosol and oral administration of salbutamol. AUC: area under the curve (t=60 min). Outcomes of subjects were pooled to compare aerosol with oral administration. Data are presented as mean±sd. Paired t-tests were performed to determine significance. ***: p<0.001; ****: p<0.0001. b) Data from plasma samples after oral treatment of a) are presented per subject. Data are presented as mean±sd. -: pooled plasma of all donors before treatment. c) To quantify the concentrations of salbutamol in the plasma samples of the subjects, F508del/R117H organoids were stimulated with known concentrations of salbutamol spiked in 0%, 20% and 40% plasma.*

To monitor *in vivo* modulation of CFTR function, SCC and NPD measurements were performed before and after 3 days of treatment with salbutamol. An overview of the changes in the SCC and NPD values is given in tables 2 and 3. Consistent with the outcome of the salbutamol bioassay showing low (oral treatment) or undetectable (aerosol treatment) levels of salbutamol in the plasma (nanomolar range), the only significant change in NPD was seen upon oral (but not aerosol) treatment, i.e. the median baseline potential changed significantly (by 6.4 mV) in the direction of reduced sodium absorption, indicative of an improved CFTR function (table 2). However, we did not observe any significant changes in other NPD parameters nor in levels of sweat chloride (tables 2 and 3 and online supplementary tables S2 and S3).

Table 2. *Sweat chloride and nasal potential difference (NPD) responses to oral salbutamol. Data are presented as n or median (interquartile range), unless otherwise stated. #: p<0.05.*

Parameter	**Before oral treatment**	**After oral treatment**	**Change during oral treatment**	**p-value**
Subjects	10	10		
Sweat chloride mmol·L^{-1}	72.5 (66.8–82.3)	73.0 (67.3–77.0)	+0.5	0.359
NPD measurement mV				
Basal potential difference	−55.2 (−62.0–−43.4)	−48.8 (−57.5–−38.9)	+6.4	0.047#
Δamiloride	38.4 (26.6–44.8)	38.8 (27.8–45.1)	+0.4	0.878
ΔCl− free	−1.4 (−6.7–5.9)	−5.6 (−10.0–−1.2)	−4.2	0.203
Δisoproterenol	−1.4 (−2.9–2.9)	−0.1 (−2.9–1.7)	+1.3	0.646

Table 3. *Sweat chloride and nasal potential difference (NPD) responses to salbutamol aerosol. Data are presented as n or median (interquartile range), unless otherwise stated. #: n=8 for NPD measurement after aerosol treatment.*

Parameter	Before aerosol treatment	After aerosol treatment	Change during aerosol treatment	p-value
Subjects	9	9#		
Sweat chloride mmol·L^{-1}	67.0 (58.5–71.0)	70.0 (62.5–73.0)	+3.0	0.476
NPD measurement mV				
Basal potential difference	−47.3 (−54.4–−40.9)	−41.6 (−49.8–−37.4)	+5.7	0.123
Δamiloride	29.6 (23.4–41.7)	29.0 (19.8–36.6)	−0.6	0.208
ΔCl− free	−4.2 (−8.5–3.8)	−1.6 (−8.1–−0.2)	+2.6	0.401
Δisoproterenol	−2.4 (−4.6–−0.9)	−2.0 (−4.7–−0.7)	+0.4	0.878

Adverse events that were reported during treatment with salbutamol appeared higher for oral salbutamol and are summarised in table 4. The data of this pilot study tentatively indicate that oral, but not inhaled, treatment with β2-agonists may slightly improve residual CFTR function in nasal epithelium *in vivo*, but failed to further improve CFTR function in the sweat duct.

Table 4. *Adverse events during treatment with salbutamol. Data are presented as n times reported.*

Adverse event	During oral treatment	During aerosol treatment
Agitated feeling	1	
Palpitations	4	
Cough up more sputum	2	
Dry mouth	1	1
Tremor	5	1
Headache	1	1
Painful breathing		1

Discussion

The purpose of this study was to generate proof-of-concept that organoid-based measurements can be used to identify approved drugs that may modulate CFTR function *in vivo*. In this study, CFTR function measurements in organoids were applied to 1) prioritise potential drugs out of multiple candidates, 2) identify and verify subjects with potential responsive CFTR variants, and 3) study the optimal route of administration of the drug. As a whole, the results of the pre-clinical and clinical studies together indicate that organoid-based measurement can aid in designing clinical studies for subjects with CF.

We selected β2-agonists from 61 compounds that can modulate GPCR signaling, which are known activators of CFTR and anion transport. Surprisingly, the potency of β2-agonists to stimulate CFTR function was equal or greater than forskolin, which directly stimulates adenylyl cyclase downstream of GPCR, as observed in both primary intestinal and airway cells (figures 2 and 3) [13, 29]. The formation

of macromolecular complexes between β2-adrenergic receptors and CFTR may enable this efficient coupling of signals from β2-adrenergic receptors to CFTR [30]. The lack of CFTR activation by other compounds in this library most likely reflects the absence of their cognate receptors or their inability to induce sufficient CFTR-activating signals or coupling these to CFTR.

Measurement of *in vivo* CFTR function enhanced by exogenous activators such as β2-agonists requires a different approach as compared with direct CFTR protein restoring drugs such as VX-770 and VX-809. It relies on the ability of exogenous β2-agonists to phosphorylate and stimulate CFTR activity beyond levels associated with endogenous conditions. We anticipated that NPD could provide the most promising readout for an improvement of CFTR function, as intranasal infusion with the pan-β-agonist isoproterenol has been shown to further hyperpolarise the nasal epithelium in healthy controls *in vivo* by an average of 6.9 mV under low luminal chloride conditions [31, 32], suggesting that CFTR activity in this tissue is rate-limited by endogenous cAMP signaling. Whereas for diagnostic purposes and direct CFTR protein-restoring drugs, the combined change in NPD after addition of zero chloride solution and addition of isoproterenol is most informative, in patients treated with salbutamol we anticipated to find an enhanced response to low chloride but a reduced response to intranasally applied isoproterenol and no difference in the combined response to low chloride plus isoproterenol as both compounds activate endogenous cAMP. Although there was a tendency to an enhanced hyperpolarising response to zero chloride (−1.4→ −5.6 mV) and a decreased response to isoproterenol (−1.4→ −0.1 mV) upon oral (but not inhaled) treatment, this difference did not reach statistical significance. The baseline potential difference, which was clearly CF-like in both the A455E and the R117H patients (range −41.6– −55.2 mV; tables 2 and 3) showed a significant but limited increase towards non-CF baseline potential difference values (by 6.4 mV; table 2) in the orally treated patients, but this change was not paralleled by a reduced response to amiloride, an inhibitor of ENaC (table 2). Baseline potential appears to be predominated by ENaC-dependent Na+ absorption, which is enhanced in CF and modulated through direct CFTR protein-targeting drugs [33–35]. This lack of correlation seems to argue against an inhibitory effect of salbutamol treatment on ENaC activity, although the relatively low power of the pilot study and the large variation in potential difference responsiveness to ENaC does not entirely rule out such an effect. The latter interpretation would be in line with the tentative increase in zero chloride response discussed above and the known inhibitory effect of CFTR (through electrogenic or more complex coupling mechanisms) on ENaC activity in the airways. Alternatively, our data do not exclude the possibility that salbutamol inhibits other electrogenic ion transport pathways in the nasal epithelium, such as apical cation channels different from ENaC, e.g. acid-sensitive ion channels [36] or proton channels [37]. Taken together, the outcome of the NPD measurements suggests that oral salbutamol treatment slightly modifies the electrical properties of the nasal CF epithelium towards that of the non-CF nasal epithelium and could therefore be of (limited) benefit for the CF patients.

The lack of robust CFTR activation *in vivo*, in clear contrast with the potent stimulation of organoid swelling by submicromolar levels of salbutamol *in vitro* (figure 2d), is most likely due to the low levels of circulating β2-agonist observed upon *in vivo* treatment. In line with the findings in the NPD measurements, we only found a detectable CFTR-activating capacity in blood samples that were collected after treatment with oral, but not with inhaled salbutamol. The latter is consistent with a highly limited systemic delivery by β2-agonist inhalation [38] (figure 4a). However, even after treatment

with oral salbutamol, CFTR-activating levels in plasma were low (figure 4a and b), corresponding with pure salbutamol concentrations in the nanomolar range that can only marginally stimulate organoids (compare figure 4c and 2d). As such, only limited effects *in vivo* might have been expected, as we observed in only one of the NPD parameters. Although plasma levels are not similar to tissue levels, these data suggest that higher dosages may further improve efficacy of treatment, albeit that systemic side-effects of the treatment may limit the feasibility of increasing the dosage.

The lack of response in SCC is also indicative of a limited treatment response, albeit that this parameter needs to be interpreted with care. SCC is a highly sensitive CFTR function parameter, being capable of distinguishing between pancreas-sufficient and -insufficient groups, and pre-treatment SCC in our patient cohort clearly indicates that these patients have significant residual CFTR activity (table 3). Furthermore, in G551D patients this biomarker is also highly responsive to CFTR potentiator treatment [10]. However, isolated sweat glands from subjects also indicate that exogenous β-adrenergic stimuli can only stimulate ~40% of sweat ducts and later studies confirmed a high constitutive cAMP-dependent activation of CFTR in this tissue [39, 40]. This implies that only a limited window for exogenous β2-agonist stimulation likely exists *in vivo* in this tissue. The lack of treatment response in SCC we observed in this trial was therefore not completely unexpected considering the high constitutive CFTR activation in this tissue combined with the very low levels of circulating β2-agonists.

Additional clinical studies are required to further validate the effect of long-term treatment with oral β2-agonists on clinical outcome parameters (e.g. percentage predicted forced expiratory volume in 1 s, airway resistance, body mass index, quality of life) in CF patients, as this proof-of-concept study showed a minor but significant impact of treatment on the nasal mucosa, but no significant effect on Cl^- transport in the sweat ducts.

As expected, β2-agonists stimulate swelling of organoids in a CFTR mutation-dependent manner, based on residual function conferred by the CFTR genotype or by CFTR-modulating drugs (figure 2). Most subjects included in the study were compound heterozygous for A455E, and their organoids demonstrate residual CFTR function levels between the values seen with F508del and R117H/F508del compound heterozygotes [20]. This appears consistent with the SCC parameters measured in this study and with data from the CFTR2 database (www.cftr2.org). Our NPD data (tables 2 and 3 and online supplementary tables S2 and S3: response to chloride-free and isoproterenol) also showed evidence of residual CFTR function in the A455E patients, with a tendency to increase slightly but not significantly after oral salbutamol treatment. As the VX-770+VX-809-corrected CFTR-F508del function in organoids is higher than the level of residual function associated with CFTR-A455E [20], β2-agonists may also have added value for F508del homozygous subjects treated with CFTR-repairing drugs. In this context, cotreatments with β2-agonists may account for some of the pulmonary heterogeneity between patients that is observed in the response to CFTR modulator treatment [9, 11]. In addition, further stratification for CFTR genotypes with higher residual function (e.g. CFTR-R117H) may also enhance treatment effects with β2-agonists.

In conclusion, CFTR function measurements in intestinal organoids were used to screen for CFTR-activating drugs and subjects with CFTR variants that respond to these drugs *in vitro* were selected for *in*

vivo treatment. Oral treatment with salbutamol improved some CF characteristics of the nasal mucosa, but treatment efficacy was likely limited due to ineffective dosage, as apparent from measurements of plasma levels of salbutamol in our organoid-based bioassay. The study supports the concept that intestinal organoids are a valuable tool for selecting drugs and route of administration for CF clinical trials.

Acknowledgements

We thank M.C.J. Olling-de Kok (Dept of Pediatric Pulmonology, Wilhelmina Children's Hospital, University Medical Center, Utrecht, The Netherlands), E.M. Nieuwhof-Stoppelenburg and E.C. van der Wiel (Dept of Pediatric Pulmonology, Erasmus University Medical Center/Sophia Children's Hospital, Rotterdam, The Netherlands), N. Adriaens (Dept of Respiratory Medicine, Academic Medical Center, Amsterdam, The Netherlands), and M. Smink (Dept of Pulmonology and Cystic Fibrosis, Haga Teaching Hospital, The Hague, The Netherlands) for providing intestinal biopsies.

Footnotes

- Support statement: E. Matthes and J.W. Hanrahan were supported by the Canadian Institutes of Health Research. This work was supported by grants from the Dutch Cystic Fibrosis Foundation (NCFS) as part of the HIT-CF programme, the Wilhelmina Children's Hospital (WKZ) Foundation and the Dutch health organisation ZonMW, The Netherlands. Funding information for this article has been deposited with FundRef.

- Conflict of interest: Disclosures can be found alongside this article at erj.ersjournals.com

References

[1] Riordan JR. CFTR function and prospects for therapy. Annu Rev Biochem 2008; 77: 701–726.

[2] Weiler CA, Drumm ML. Genetic influences on cystic fibrosis lung disease severity. Front Pharmacol 2013; 4: 40.

[3] Vanscoy LL, Blackman SM, Collaco JM, et al. Heritability of lung disease severity in cystic fibrosis. Am J Respir Crit Care Med 2007; 175: 1036–1043.

[4] Sosnay PR, Siklosi KR, Van Goor F, et al. Defining the disease liability of variants in the cystic fibrosis transmembrane conductance regulator gene. Nat Genet 2013; 45: 1160–1167.

[5] Kerem E, Corey M, Kerem BS, et al. The relation between genotype and phenotype in cystic fibrosis – analysis of the most common mutation (delta F508). N Engl J Med 1990; 323: 1517–1522.

[6] Castellani C, Cuppens H, Macek M, et al. Consensus on the use and interpretation of cystic fibrosis mutation analysis in clinical practice. J Cyst Fibros 2008; 7: 179–196.

[7] Zielenski J. Genotype and phenotype in cystic fibrosis. Respiration 2000; 67: 117–133.

[8] Van Goor F, Hadida S, Grootenhuis PD, et al. Rescue of CF airway epithelial cell function *in vitro* by a CFTR potentiator, VX-770. Proc Natl Acad Sci USA 2009; 106: 18825–18830.

[9] Ramsey BW, Davies J, McElvaney NG, et al. A CFTR potentiator in patients with cystic fibrosis and the G551D mutation. N Engl J Med 2011; 365: 1663–1672.

[10] Accurso FJ, Rowe SM, Clancy JP, et al. Effect of VX-770 in persons with cystic fibrosis and the G551D-CFTR mutation. N Engl J Med 2010; 363: 1991–2003.

[11] Wainwright CE, Elborn JS, Ramsey BW, et al. Lumacaftor–ivacaftor in patients with cystic fibrosis homozygous for Phe508del CFTR. N Engl J Med 2015; 373: 220–231.

[12] Van Goor F, Hadida S, Grootenhuis PD, et al. Correction of the F508del-CFTR protein processing defect *in vitro* by the investigational drug VX-809. Proc Natl Acad Sci USA 2011; 108: 18843–18848.

[13] Chan HC, Fong SK, So SC, et al. Stimulation of anion secretion by beta-adrenoceptors in the mouse endometrial epithelium. J Physiol 1997; 501: 517–525.

[14] Smith JJ, Welsh MJ. cAMP stimulates bicarbonate secretion across normal, but not cystic fibrosis airway epithelia. J Clin Invest 1992; 89: 1148–1153.

[15] Waldman DB, Gardner JD, Zfass AM, et al. Effects of vasoactive intestinal peptide, secretin, and related peptides on rat colonic transport and adenylate cyclase activity. Gastroenterology 1977; 73: 518–523.

[16] Jung P, Sato T, Merlos-Suárez A, et al. Isolation and *in vitro* expansion of human colonic stem cells. Nat Med 2011; 17: 1225–1227.

[17] Sato T, Clevers H. Growing self-organizing mini-guts from a single intestinal stem cell: mechanism and applications. Science 2013; 340: 1190–1194.

[18] Sato T, Vries RG, Snippert HJ, et al. Single Lgr5 stem cells build crypt-villus structures *in vitro* without a mesenchymal niche. Nature 2009; 459: 262–265.

[19] Dekkers JF, van der Ent CK, Beekman JM. Novel opportunities for CFTR-targeting drug development using organoids. Rare Dis 2013; 1: e27112.

[20] Dekkers JF, Wiegerinck CL, de Jonge HR, et al. A functional CFTR assay using primary cystic fibrosis intestinal organoids. Nat Med 2013; 19: 939–945.

[21] Sato T, Stange DE, Ferrante M, et al. Long-term expansion of epithelial organoids from human colon, adenoma, adenocarcinoma, and Barrett's epithelium. Gastroenterology 2011; 141: 1762–1772.

[22] de Lau W, Barker N, Low TY, et al. Lgr5 homologues associate with Wnt receptors and mediate R-spondin signaling. Nature 2011; 476: 293–297.

[23] Korinek V, Barker N, Morin PJ, et al. Constitutive transcriptional activation by a beta-catenin–Tcf complex in APC–/– colon carcinoma. Science 1997; 275: 1784–1787.

[24] Bruscia E, Sangiuolo F, Sinibaldi P, et al. Isolation of CF cell lines corrected at DeltaF508-CFTR locus by SFHR-mediated targeting. Gene Ther 2002; 9: 683–685.

[25] Swiatecka-Urban A, Moreau-Marquis S, Maceachran DP, et al. Pseudomonas aeruginosa inhibits endocytic recycling of CFTR in polarized human airway epithelial cells. Am J Physiol Cell Physiol 2006; 290: C862–C872.

[26] Vijftigschild LA, van der Ent CK, Beekman JM. A novel fluorescent sensor for measurement of CFTR function by flow cytometry. Cytometry A 2013; 83: 576–584.

[27] Robert R, Carlile GW, Liao J, et al. Correction of the Delta phe508 cystic fibrosis transmembrane conductance regulator trafficking defect by the bioavailable compound glafenine. Mol Pharmacol 2010; 77: 922–930.

[28] Dekkers R, Vijftigschild LA, Vonk AM, et al. A bioassay using intestinal organoids to measure CFTR modulators in human plasma. J Cyst Fibros 2015; 14: 178–181.

[29] Walker LC, Venglarik CJ, Aubin G, et al. Relationship between airway ion transport and a mild pulmonary disease mutation in CFTR. Am J Respir Crit Care Med 1997; 155: 1684–1689.

[30] Naren AP, Cobb B, Li C, et al. A macromolecular complex of beta 2 adrenergic receptor, CFTR, and ezrin/radixin/moesin-binding phosphoprotein 50 is regulated by PKA. Proc Natl Acad Sci USA 2003; 100: 342–346.

[31] Knowles MR, Paradiso AM, Boucher RC. *In vivo* nasal potential difference: techniques and protocols for assessing efficacy of gene transfer in cystic fibrosis. Hum Gene Ther 1995; 6: 445–455.

[32] Boyle MP, Diener-West M, Milgram L, et al. A multicenter study of the effect of solution temperature on nasal potential difference measurements. Chest 2003; 124: 482–489.

[33] Rowe SM, Liu B, Hill A, et al. Optimizing nasal potential difference analysis for CFTR modulator development: assessment of ivacaftor in CF subjects with the G551D-CFTR mutation. PLoS One 2013; 8: e66955.

[34] Knowles M, Gatzy J, Boucher R. Relative ion permeability of normal and cystic fibrosis nasal epithelium. J Clin Invest 1983; 71: 1410–1417.

[35] Knowles MR, Stutts MJ, Spock A, et al. Abnormal ion permeation through cystic fibrosis respiratory epithelium. Science 1983; 221: 1067–1070.

[36] Qadri YJ, Rooj AK, Fuller CM. ENaCs and ASICs as therapeutic targets. Am J Physiol Cell Physiol 2012; 302: C943–C965.

[37] Iovannisci D, Illek B, Fischer H. Function of the HVCN1 proton channel in airway epithelia and a naturally occurring mutation, M91T. J Gen Physiol 2010; 136: 35–46.

[38] Halfhide C, Evans HJ, Couriel J. Inhaled bronchodilators for cystic fibrosis. Cochrane Database Syst Rev 2005; (4): CD003428.

[39] Reddy MM, Quinton PM. PKA mediates constitutive activation of CFTR in human sweat duct. J Membr Biol 2009; 231: 65–78.

[40] Reddy MM, Quinton PM. cAMP activation of CF-affected Cl– conductance in both cell membranes of an absorptive epithelium. J Membr Biol 1992; 130: 49–62.

Supplementary material

Supplementary table S1

ADL5859 HCl	850173-95-4
Granisetron HCl	107007-99-8
SB939	929016-96-6
Carvedilol	72956-09-3
Ketanserin (Vulketan Gel)	74050-98-9
Domperidone (Motilium)	57808-66-9
Maprotiline hydrochloride	10347-81-6
Dehydroepiandrosterone(DHEA)	53-43-0
JTC-801	244218-51-7
Bisoprolol	104344-23-2
Naftopidil Dihydrochloride	57149-08-3
AM-1241	444912-48-5
Dapoxetine hydrochloride (Priligy)	129938-20-1
Loperamide hydrochloride	34552-83-5
Naphazoline hydrochloride (Naphcon)	550-99-2
WAY-100635	162760-96-5
Fingolimod (FTY720)	162359-56-0
Agomelatine	138112-76-2
Alfuzosin hydrochloride(Uroxatral)	81403-68-1
Dapagliflozin	461432-26-8
Enalapril maleate (Vasotec)	76095-16-4
Amfebutamone (Bupropion)	31677-93-7
Olanzapine (Zyprexa)	132539-06-1
Epinephrine bitartrate (Adrenalinium)	51-42-3
LY310762	192927-92-7
LY404039	635318-11-5
Dimebon (Latrepirdine)	97657-92-6
Nebivolol (Bystolic)	152520-56-4
Benserazide	14919-77-8
Oxymetazoline hydrochloride	2315-02-8
Dopamine hydrochloride (Inotropin)	62-31-7
BRL-15572	193611-72-2
Amisulpride	71675-85-9
Sumatriptan succinate	103628-48-4
Silodosin (Rapaflo)	160970-54-7

Chlorpromazine (Sonazine)	69-09-0
Racecadotril (Acetorphan)	81110-73-8
Ritodrine hydrochloride (Yutopar)	23239-51-2
ADX-47273	851881-60-2
Asenapine	85650-56-2
Tianeptine sodium	30123-17-2
Risperidone (Risperdal)	106266-06-2
Clonidine hydrochloride (Catapres)	4205-91-8
Salbutamol sulfate (Albuterol)	51022-70-9
Clomipramine hydrochloride (Anafranil)	17321-77-6
BMY 7378	21102-95-4
Doxazosin mesylate	77883-43-3
Venlafaxine	99300-78-4
Quetiapine fumarate (Seroquel)	111974-72-2

Supplementary Table S2. Sweat Chloride and Nasal Potential Difference response to oral salbutamol per subject included in the pilot study.

	Sweat Chloride *(mmol/L)*		Nasal Potential Difference Measurement *(mV)*							
Subject	Before treatment	After treatment	Basal PD before treatment	Basal PD after treatment	Δ Amil before treatment	Δ Amil after treatment	Δ Cl^- free before treatment	Δ Cl^- free after treatment	Δ Iso before treatment	Δ Iso after treatment
1	72	65	-20	-25	15	17	-4	-4	0	7
2	82	87	-41	-41	31	30	4	8	-2	-4
3	83	77	-59	-50	43	46	-6	-7	-3	-1
4	53	45	-62	-55	34	42	5	-7	5	2
5	91	75	-45	-34	20	21	8	5	3	-1
6	75	76	-63	-59	47	45	1	-3	-2	2
7	67	71	-74	-65	55	48	9	-13	-3	-3
8	73	71	-52	-47	44	41	-12	-12	3	-3
9	72	68	-58	-57	43	37	-9	-4	-12	1
10	66	77	-44	-47	29	33	-4	-9	-1	1

Supplementary Table S3. Sweat Chloride and Nasal Potential Difference response to salbutamol aerosol per subject included in the pilot study.

Subject	Sweat Chloride *(mmol/L)*		Nasal Potential Difference Measurement *(mV)*							
	Before treatment	After treatment	Basal PD before treatment	Basal PD after treatment	Δ Amil before treatment	Δ Amil after treatment	Δ Cl^- free before treatment	Δ Cl^- free after treatment	Δ Iso before treatment	Δ Iso after treatment
1	67	75	-22	-20	13	16	-7	-1	5	-1
2	61	106	-44	-41	30	31	11	3	-1	-3
3	-	-	-	-	-	-	-	-	-	-
4	43	41	-38	-36	29	23	3	-5	-8	-1
5	67	70	-52	-42	18	19	5	0	-1	-4
6	79	71	-57	-52	48	37	-4	-3	-1	-1
7	74	69	-62	-71	45	44	-10	-9	-2	-5
8	68	70	-47	-44	39	34	-9	-13	-4	2
9	58	71	-51	-	30	-	-8	-	-3	-
10	59	56	-46	-41	32	27	-4	-1	-6	-5

β2-Adrenergic receptor agonists activate CFTR in intestinal organoids and subjects with cystic fibrosis

CHAPTER 4

Comparison of *ex vivo* and *in vitro* intestinal cystic fibrosis models to measure CFTR-dependent ion channel activity

Domenique D. Zomer-van Ommen[a, b], Eyleen de Poel[a, b], Evelien Kruisselbrink[a, b], Hugo Oppelaar[a, b], Annelotte M. Vonk[a, b], Hettie M. Janssens[c], Cornelis K. van der Ent[a], Marne C. Hagemeijer[a, b, 1], Jeffrey M. Beekman[a, b, *, 1]

J Cyst Fibros. 2018 Mar 13. pii: S1569-1993(18)30030-4. doi: 10.1016/j.jcf.2018.02.007. [Epub ahead of print]

a. Department of Pediatric Pulmonology, Wilhelmina Children's Hospital, University Medical Center Utrecht, Utrecht, The Netherlands, Regenerative Medicine Center Utrecht, University Medical Centre Utrecht, Utrecht, The Netherlands, b. Department of Pediatric Pulmonology, Erasmus Medical Centre, Sophia Children's Hospital, Rotterdam, The Netherlands, 1. Authors contributed equally.

* Corresponding author at: jbeekman@umcutrecht.nl, Uppsalalaan 8, 3584 CT, Utrecht, The Netherlands.

Abstract

BACKGROUND New functional assays using primary human intestinal adult stem cell cultures can be valuable tools to study epithelial defects in human diseases such as cystic fibrosis.

METHODS CFTR-mediated ion transport was measured in rectal organoid-derived monolayers grown from subjects with various CFTR mutations and compared to donor-matched intestinal current measurements (ICM) in rectal biopsies and forskolin-induced swelling of rectal organoids.

RESULTS Rectal organoid-derived monolayers were generated within four days. Ion transport measurements of CFTR function using these monolayers correlated with ICM and organoid swelling (r = 0.73 and 0.79 respectively). Culturing the monolayers under differentiation conditions enhanced the detection of mucus-secreting cells and was accompanied by reduced CFTR function.

CONCLUSIONS CFTR-dependent intestinal epithelial ion transport properties can be measured in rectal organoid-derived monolayers of subjects and correlate with donor-matched ICM and rectal organoid swelling.

Graphical abstract

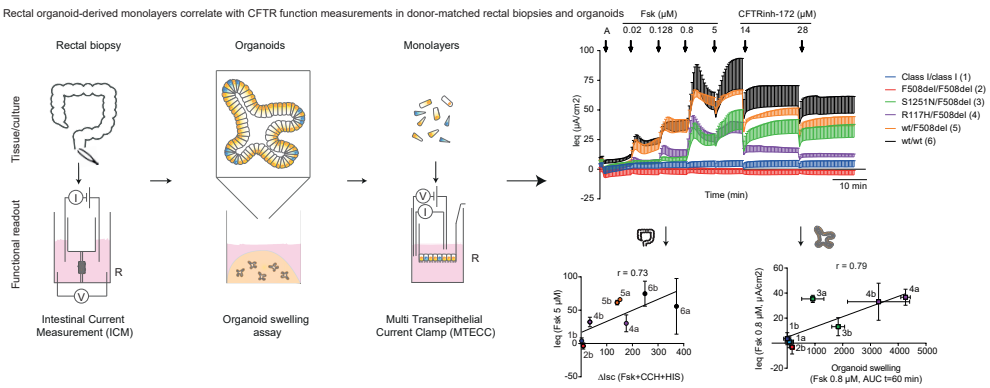

Abbreviations: A, amiloride; AUC, area-under-the-curve; cAMP, cyclic AMP; CCH, carbachol; CF, cystic fibrosis; CFTR, cystic fibrosis transmembrane conductance regulator; D, differentiation culture conditions; DMSO, dimethylsulfoxide; ENaC, epithelial sodium channel; FIS, forskolin-induced swelling; Fsk, forskolin; GAPDH, glyceraldehyde 3-phosphate dehydrogenase; HBE, human bronchial epithelial cells; HIS, histamine; IBMX, 3-isobutyl-1-methylxanthine; ICM, intestinal current measurements; Ieq, equivalent short-circuit current; Isc, short-circuit current; LGR5, Leucine-rich repeat-containing G-protein coupled receptor 5; MTECC, Multi Transepithelial Current Clamp; N, non-differentiation culture conditions; NKCC1, Na-K-Cl co-transporter 1; ns, not significant; PAS, periodic acid-Schiff; Rt, transepithelial resistance; RT-q, reverse transcription quantitative; wt, wild type

Keywords: Electrophysiology; CFTR; differentiation; donor-matched; organoids; monolayers; biopsies

Introduction

Human *ex vivo* tissues and *in vitro* cell culture models play a central role in drug development, and have received increasing attention lately as patient stratification and personalized medicine applications [1]. Recent adult stem cell culture technologies have enabled an unprecedented ability to expand primary human tissues *in vitro* [1]. These culture technologies allow for the quick establishment of clinically-annotated disease-specific biobanks which offer new opportunities for disease modeling [2].

One of these exciting opportunities is the 3D culturing of intestinal adult stem cells into organoids [3,4]. We developed a fluid secretion assay by quantitating the swelling of rectal organoids upon incubation with secretagogues [5]. Fluid secretion is driven by epithelial ion transport, but direct measurement of ion transport in organoids is difficult due to their enclosed luminal compartment. Nonetheless, this organoid swelling assay has been highly instrumental for disease modeling and determining preclinical and individual treatment responses in cystic fibrosis (CF) [6,7] and cholera-induced secretory diarrhea [8].

CF is a rare, genetic disease, caused by mutations in the CF Transmembrane Conductance Regulator (CFTR) gene that impairs functioning of the cyclic AMP (cAMP)-regulated CFTR ion channel. Reduced CFTR function leads to aberrant transport of anions and fluids across epithelial membranes and results in accumulation of viscous mucus, most notably in the lungs and gastro-intestinal tract, which leads to organ dysfunction. [9]. CFTR mutations are classified by CFTR expression and function: (I) defective synthesis, (II) reduced trafficking, (III) impaired gating of the channel, (IV) reduced conductance, (V) impaired synthesis and trafficking, and (VI) reduced cell membrane stability [10].

Electrophysiological readouts in Ussing chambers [11] are commonly used to study epithelial ion transport. Intestinal current measurements (ICM) of cAMP-regulated anion secretion can be used to measure residual CFTR function in rectal biopsies [12]. Drug development studies for CF have relied heavily on Ussing chamber studies using differentiated human bronchial epithelial (HBE) cell cultures to measure CFTR activity [13,14]. A major limitation of both approaches is the restricted cell availability due to invasive sampling procedures and limited *in vitro* cell expansion capability [15,16].

The development of assays to study ion transport properties of epithelia, using human stem cells as an unlimited source, are important for studying human diseases and drug development. Recently, intestinal epithelial monolayers from primary mouse and human tissue were successfully grown in Transwell permeable supports [17,18]. Here, our aims were to apply these protocols (i) to generate monolayers derived from rectal organoids with varying CFTR residual function, (ii) to measure CFTR-mediated ion transport in these monolayers with the Multi Transepithelial Current Clamp (MTECC) 24-well system [19,20], (iii) to compare the data with CFTR function measurements in donor-matched rectal biopsies and organoids using the established ICM an organoid swelling assays, respectively [5,12,15,21], and (iv) to modify cell composition and ion channel function by adapting culture conditions.

Methods and materials

Human rectal biopsies and CFTR genotypes

Rectal biopsies were obtained for standard care or participation in a study (approved by the ethics committees of University Medical Center Utrecht and Erasmus Medical Centre Rotterdam). Informed consent to perform CFTR function assays was obtained from all subjects. Twelve subjects were studied in total, including two subjects per mutation class I to IV: class I/class I - E60X/4015delATTT (c.178G > T/c.3883delATTT) and 1811 + 1G > C/1811 + 1G > C (c.1679 + 1G > C/ c.1679 + 1G > C), class II - two subjects F508del(p.Phe508del)/F508del, class III - two subjects S1251N (p.Ser1251Asn)/F508del, and class IV - two subjects R117H (p.Arg117His)/F508del. In addition, two carrier subjects (wt/F508del) and two wild type subjects (wt/wt) were studied. [22].

Intestinal current measurements (ICM)

ICM was performed for standard care, diagnostics or clinical studies as described previously [12] and according to Standard Operating Procedure ICM_EU001 (version 2.7, 2011). Short-circuit currents (Isc) were measured in an Ussing chamber system (Physiologic Instruments) using a voltage clamp (DVC-1000, World Precision Instruments). Tracings were recorded with PowerLab (8/30, AD Instruments) and analyzed using LabChart 6 software.

Rectal organoid culturing

Organoids were generated and cultured as previously described [5,6,21]. Growth medium was refreshed every 2-3 days and organoids were passaged every seven days.

Organoid swelling assay

The organoid swelling experiments were performed as previously published, with minor adaptations [5,21]. Experiments were performed with undifferentiated organoids or organoids cultured for five days with differentiation medium (organoid growth medium without Wnt3a-conditioned medium, nicotinamide and SB202190) [4]. Organoids were acutely stimulated with forskolin (Fsk, 0.8 and 5 µM), carbachol (CCH, 100 µM) or histamine (HIS, 500 µM).

Culturing of organoid-derived monolayers

Culturing of monolayers was performed using previously published protocols with slight modifications [18,23]. 24-wWell Transwell HTS plates (3378, Corning) were coated with PureCol (Advanced Biomatrix) diluted 1:100 in Dulbecco's Phosphate-Buffered Saline (PBS) supplemented with calcium and magnesium (Gibco) and incubated for 2 h at 37 °C/5% CO2 after which the PureCol solution was removed. Seven-day old organoid cultures were trypsinized (TrypLE, Thermo Fisher) for 2x × 2 min at 37 °C and mechanically disrupted after each incubation period. 250,000 cells were seeded per insert, with addition of 100 µl and 600 µl organoid growth medium supplemented with Y-27632 (10 µM, Selleck Chemicals), at the apical and basolateral sides respectively. Medium (without Y-27632) was refreshed every 1-–2 days. After four days the measured resistance values exceeded 100 Ω.·cm2, indicating confluent monolayers. Electrophysiological measurements were either performed directly or growth medium was replaced with organoid differentiation medium for another five days, until the resistances of the monolayers exceeded 800 Ω.·cm2.

Alcian blue/Periodic acid-Schiff stainings of monolayer sections

Monolayers were fixed in formaldehyde 4% (Klinipath) for 10 minutesmin at room temperature, washed three times and stored at 4 °C in PBS. After paraffin embedding, 5 µm sections were prepared, followed by combined alcian blue and periodic acid-Schiff (PAS) staining (reagents from Merck and Klinipath). Sections were imaged using an Olympus BX43 (40x× magnification) with cellSens Entry software 1.14.

RNA isolation and reverse transcription quantitative (RT-q) PCR

Total RNA was isolated from the monolayers using the RNeasy mini kit (Qiagen) including the DNase digestion step (RNAse-Free DNase Set, Qiagen) according to the manufacturer's instructions. The amount and purity of the RNA samples were determined using the Nanodrop ND-1000 spectrophotometer (Thermo Scientific). cDNA was generated using the iScriptTM™ cDNA Synthesis Kit (BioRad) using the supplier's protocol.

The optimal annealing temperature for each primer pair was determined by performing gradient PCR analysis. The cDNA samples were analyzed using a two-step RT-qPCR protocol using SYBR Green (Supermix, BioRad). Standard curves were included to determine the amplification efficiencies of the primers (primer sequences are depicted in Table S1). Gene expression was quantified with the Pfaffl method [24] using glyceraldehyde 3-phosphate dehydrogenase (GAPDH) and ß-actin as housekeeping genes.

Electrophysiological measurements in monolayers

The MTECC system (24-well format, EP-devices) was used to perform electrophysiological measurements in monolayers cultured under (non-)differentiation conditions. Organoid growth medium was replaced by 160 µl and 940 µl of adjusted Ringer's buffer (in mM: 120 NaCl, 20 Hepes, 1.2 CaCl2, 1.2 MgCl2, 0.8 KH2PO4, 0.8 K2HPO4, 5 glucose, pH 7.4) supplemented with indomethacin (10 µM, Sigma) at the apical and basolateral sides, respectively. After 30 minutesmin of calibration, open circuit potential (PD) and transepithelial resistance (Rt) were measured and equivalent short-circuit (Ieq) currents were calculated every 30 secondss. The following compounds were sequentially added to the apical (mucosal, M) and/or basolateral (serosal, S) side: amiloride (S), forskolin (concentrations indicated in Figfigure. 3, M + S), CFTRinh-172 (concentrations indicated in Figfigure. 3, M + S, Cystic Fibrosis Foundation Therapeutics), dimethylsulfoxide (DMSO) (M + S) and carbachol (S). Order of compound addition was as indicated in the figures. Chemicals were supplied by Sigma Aldrich unless stated otherwise.

Statistical analyses

To determine statistical differences between donor responses within one assay, we performed one-way ANOVA and Tukey's multiple comparisons test with a single pooled variance. For analysis of organoid swelling, we used row-matched ANOVA. Paired t-tests were performed for the resistance values and mRNA expression levels of the (non-)differentiated monolayers. Correlations between the assays were determined by the Pearson correlation coefficient (Pearson's r). All analyses were performed using GraphPad Prism 7. In the figures, statistical differences were summarized per dataset or per CFTR genotype/mutation class to the maximal significant p-value. All p-values are depicted in the Supplementary data.

Results

Human rectal biopsies and donor-matched organoids to functionally measure CFTR

To perform CFTR function studies in intestinal tissue, we included material of twelve subjects with CFTR function from absent to normal (two donors per CFTR genotype). After isolation, rectal biopsies were mounted in Ussing chambers to record ion currents of the native epithelium upon stimulation with forskolin (Fsk), carbachol (CCH) and histamine (HIS). Phosphodiesterase-inhibitor IBMX raises intracellular cAMP-levels [25]. Increased intracellular Ca2+-levels induced by carbachol and histamine leads to basolateral and subsequent apical hyperpolarization via basolateral potassium channel activation, thereby increasing the driving force for apical chloride secretion via CFTR [12,26]. A representative tracing is depicted in Fig. 1a. We calculated the total short-circuit current (Isc) upon fsk, IBMX, CCH and HIS stimulation and observed CFTR genotype-dependent activity. For three donors, we could not combine the currents upon these four chemicals due to different protocols. All CF and carrier rectal biopsies responded significantly lower compared to wild type (Fig. 1b, all p-values in Fig. S1a). When considering the Isc responses of Fsk + IBMX + CCH or Fsk + IBMX alone, ICM was less capable of distinguishing between the different CFTR genotypes (data not shown), suggesting suboptimal measurement of CFTR function using these stimulants.

Next, we measured CFTR function of organoids generated from the initial twelve rectal biopsies used in our ICM experiments. We performed agonist-induced swelling assays on the donor-matched organoids under (non-)differentiation conditions. Forskolin-induced swelling (FIS) of organoids from non-CF genotypes (wt/F508del and wt/wt) could not be compared to mutant CFTR organoids because of their pre-swollen state under non-differentiation conditions [6]. Representative images (Fig. 1c) demonstrated differential swelling over time from organoids of four donors, cultured under non-differentiation conditions, upon 0.8 μM forskolin stimulation. In accordance with previous data [5], forskolin-induced swelling of class I/class I and F508del/F508del organoids was different from both S1251N/F508del and R117H/F508del organoids at 5 μM forskolin stimulation and S1251N/F508del responses were lower than R117H/F508del at 0.8 μM, but not 5 μM forskolin. (Fig. 1d, all p-values in Fig. S1b) We also explored CFTR-dependent fluid secretion when organoids were cultured for five days using differentiation medium. FIS was strongly reduced in all donors, indicating limited CFTR function upon differentiation (Fig. 1d), consistent with a decreasing gradient of CFTR expression from the crypts towards the villi in intestinal epithelium [27,28]. Carbachol induced very limited swelling in the non-differentiated organoids, which was even further reduced when organoids were cultured under differentiation conditions (Fig. 1d). Histamine-induced swelling levels were very low under both culturing conditions (data not shown). These data indicated that differentiation of organoids resulted in loss of CFTR function, but did not enhance carbachol-induced swelling.

In summary, Isc (Fsk + IBMX + CCH + HIS) measurements by ICM and FIS in organoids are both CFTR-dependent readouts, and require different conditions to optimally discriminate between CFTR function of different patient samples.

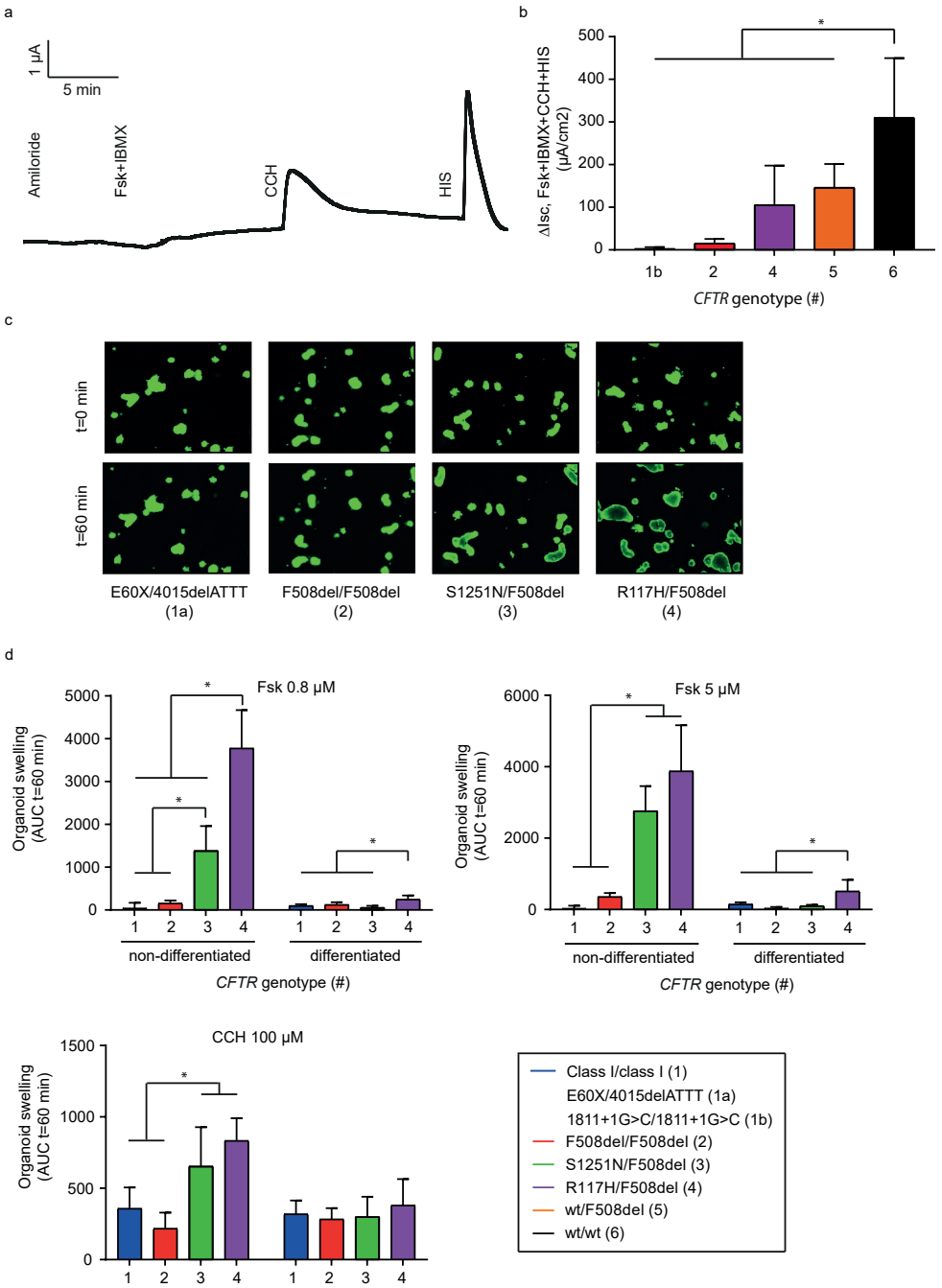
a
1 µA
5 min
Amiloride
Fsk+IBMX
CCH
HIS
b
ΔIsc, Fsk+IBMX+CCH+HIS (µA/cm2)
CFTR genotype (#)
1b
2
4
5
6
c
t=0 min
t=60 min
E60X/4015delATTT (1a)
F508del/F508del (2)
S1251N/F508del (3)
R117H/F508del (4)
d
Fsk 0.8 µM
Fsk 5 µM
Organoid swelling (AUC t=60 min)
non-differentiated
differentiated
CFTR genotype (#)
CCH 100 µM
Class I/class I (1)
E60X/4015delATTT (1a)
1811+1G>C/1811+1G>C (1b)
F508del/F508del (2)
S1251N/F508del (3)
R117H/F508del (4)
wt/F508del (5)
wt/wt (6)

Figure 1. *CFTR function measurements in donor-matched rectal biopsies and organoids. CFTR function measurements in rectal biopsies (intestinal current measurements, ICM) and rectal biopsy-derived organoids (organoid swelling) of twelve donors, two donors per CFTR genotype/mutation class. a) Representative tracing of ICM from a wild type rectal biopsy. b) Total changes in Isc (μA/cm2) after rectal biopsy stimulation with Fsk, IBMX, CCH and HIS. Each bar represents two donors except for 1b, genotypes are depicted in d. Data of three out of twelve donors could not be included due to a different protocol (E60X/4015delATTT (1a) and two S1251N/F508del (3)). c) Representative images of undifferentiated organoids stimulated with 0.8 μM forskolin. d) Forskolin-induced and carbachol-induced swelling of (non-)differentiated rectal organoids. Averages ± SD of three independent experiments. Each bar represents two donors, unless stated otherwise by addition of a or b to the corresponding number of CFTR mutation. Abbreviations: AUC, area-under-the-curve; CCH, carbachol; Fsk, forskolin; HIS, histamine; IBMX, 3-isobutyl-1-methylxanthine; ICM, intestinal current measurements; Isc, short-circuit currents; wt, wild type. * indicates p < 0.05. All p-values are presented in Fig. S1.*

Characterization of rectal organoid-derived monolayers

To determine whether we could use the Transwell monolayer culture model [18,23] as an additional model, we next generated monolayers from rectal organoids of the twelve donors used in the previous experiments (Fig. 1 and Section 3.1). We analyzed the morphology and mRNA expression levels of the organoid-derived monolayers cultured under non-differentiation conditions. Histological sections showed a single cell layer of the undifferentiated rectal cells (representative images of three donors are shown in Fig. S2a). Alcian blue/PAS staining of the monolayer sections showed occasionally a thin layer of PAS-positive polysaccharides at the apical side, indicating presence of some mucus, while no mucus-producing goblet cells were detected. Under non-differentiating conditions, ion channels CFTR (apical), Na-K-Cl co-transporter 1 (NKCC1, basolateral), and the adult intestinal stem cell marker LGR5 (Leucine-rich repeat-containing G-protein coupled receptor 5) were readily detectable by qRT-PCR and were not affected by the CFTR genotype (p-values > 0.05; Fig. S2b).

Five out of the twelve donors were used to characterize monolayers cultured under differentiation conditions. Alcian blue/PAS-stainings of these monolayers indicated that adjusting the culture conditions resulted in changes in cell composition and morphology including increased apical mucus, the presence of goblet cells and columnar cell shapes (Fig. 2a, three matched donor samples before and after differentiation are indicated). We also observed strong downregulation of CFTR, NKCC1 and LGR5 mRNA expression levels upon differentiation ($p < 0.05$ for CFTR and NKCC1, Fig. 2b). In summary, monolayers were formed already within four days after plating organoid-derived intestinal cells. The morphology and mucus properties of the monolayers could be modified upon five days of differentiation.

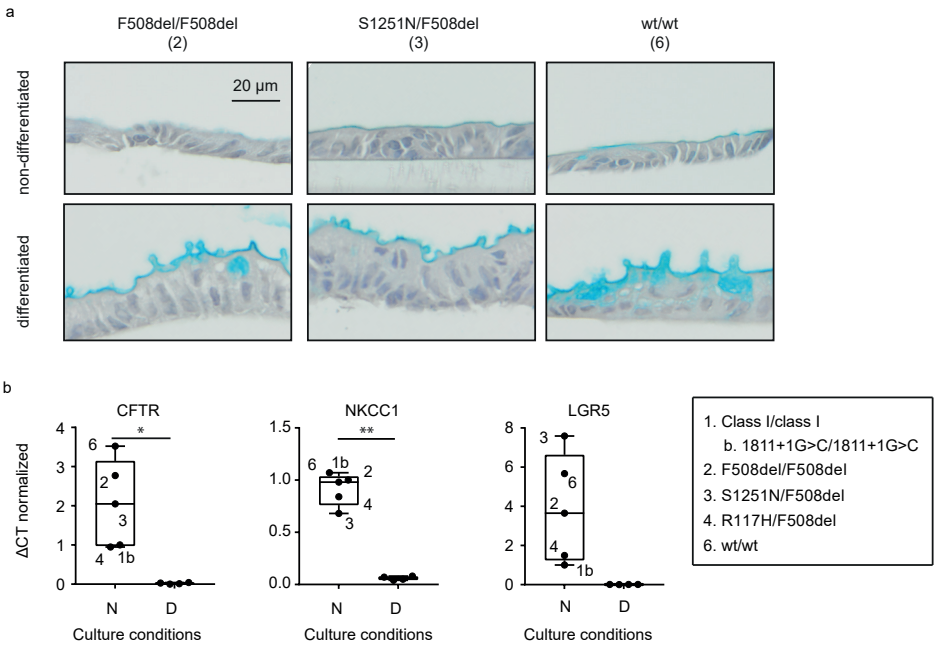

Figure 2. *Characterization of rectal organoid-derived monolayers. a) Representative histological sections of alcian Blue/PAS-stained F508del/F508del, S1251N/F508del and wild type monolayers cultured under both (non-)differentiation conditions. b) mRNA expression levels of CFTR, NKCC1 and LGR5 depicted as normalized delta (Δ) CT values. * indicates $p < 0.05$, ** means $p < 0.0021$. Abbreviations: CFTR, cystic fibrosis transmembrane conductance regulator; CT, threshold cycles; D, differentiation conditions; LGR5, Leucine-rich repeat-containing G-protein coupled receptor 5; N, non-differentiation conditions; NKCC1, Na-K-Cl co-transporter 1; wt, wild type.*

Electrophysiological properties of rectal organoid-derived monolayers

Having characterized the rectal organoid-derived monolayers we measured CFTR function in monolayers of the twelve donors using the MTECC system. This 24-well open-circuit system has mostly been used for electrophysiological drug screening purposes [19,20]. We assessed the electrophysiological properties by adding chemicals that modify ion channel activity. Amiloride addition transiently decreased the Ieq in all monolayers, indicating the presence of low functional levels of the epithelial sodium channel (ENaC) (Fig. 3a). The amiloride-sensitive sodium currents were similar between the donors (Figs. 3a, S3a) but were lower as compared to amiloride-sensitive currents in rectal biopsies (ΔIeq −6.04 ± 3.17 and ΔIsc −13.3 ± 5.7, respectively). Addition of forskolin induced currents in the monolayers, which were dependent on forskolin dosage and the CFTR genotype (Fig. 3a). Wild type (wt/wt) and carrier (wt/F508del) monolayers demonstrated approximately two times higher responses than those of R117H/F508del and S1251N/F508del monolayers. The forskolin-induced currents were CFTR-dependent, as no responses were detected in the monolayers derived from subjects with severe CFTR mutations (F508del/F508del and class I/class I). Indeed, all monolayers with two CF-causing mutations demonstrated significant lower currents compared to carriers and wild types at all forskolin concentrations ($p < 0.05$; Fig. S3a, p-values depicted in Fig. S3b). At 0.8 and 5 µM forskolin, class I/class

I and F508del/F508del monolayers demonstrated lower currents than S1251N/F508del and R117H/F508del. However, we could not distinguish S1251N/F508del monolayer responses from R117H/F508del at all forskolin concentrations tested. CFTR inhibitor CFTRinh-172 incubation partially abolished forskolin-induced currents (Fig. 3a).

Figure 3 (see next page). *Electrophysiological CFTR function measurements in rectal monolayers correlate with donor-matched outcomes of ICM and the organoid swelling assay. a) Ieq responses of monolayers cultured under non-differentiation conditions from twelve donors. Monolayers were incubated at the indicated time points with 100 μM amiloride (A) and forskolin and CFTRinh-172 with final concentrations as depicted. Each line represents means of three independent experiments of two donors (two experiments for wt/F508del donors). Statistical differences between the CFTR mutation groups are depicted here for 5 μM Fsk, all p-values can be found in Fig. S3. b-–d) Monolayers of five donors (one per CFTR genotype) cultured under (non-)differentiation conditions. b) Measured resistance values per culture condition. c) Ieq responses of the monolayers to indicated chemicals ± SD. Concentrations (in μM): A 100, Fsk 10, CCH 100, CFTRinh-172 20. d) Delta (Δ) changes in Ieq peak responses upon additions of amiloride, forskolin or carbachol to the monolayers for both culturing conditions, calculated from c. e + f) Donor-matched correlations of electrophysiological measurements in monolayers [Fsk stimulation (Ieq, μA/cm2)] with ICM of rectal biopsies [Fsk, CCH and HIS stimulation (Isc, μA/cm2)](e) and with organoid swelling upon stimulation with 0.8 μM Fsk (f). Addition of a or b to the corresponding number of CFTR mutation represents the two different donors per group. Abbreviations: A, amiloride; AUC, area-under-the-curve; CCH, carbachol; D, differentiation conditions; DMSO, dimethylsulfoxide; Fsk, forskolin; HIS, histamine; Ieq, equivalent short-circuit currents; Isc, short-circuit currents; N, non-differentiation conditions; RT, transepithelial resistance; wt, wild type. * = $p < 0.05$, **** = $p < 0.0001$.*

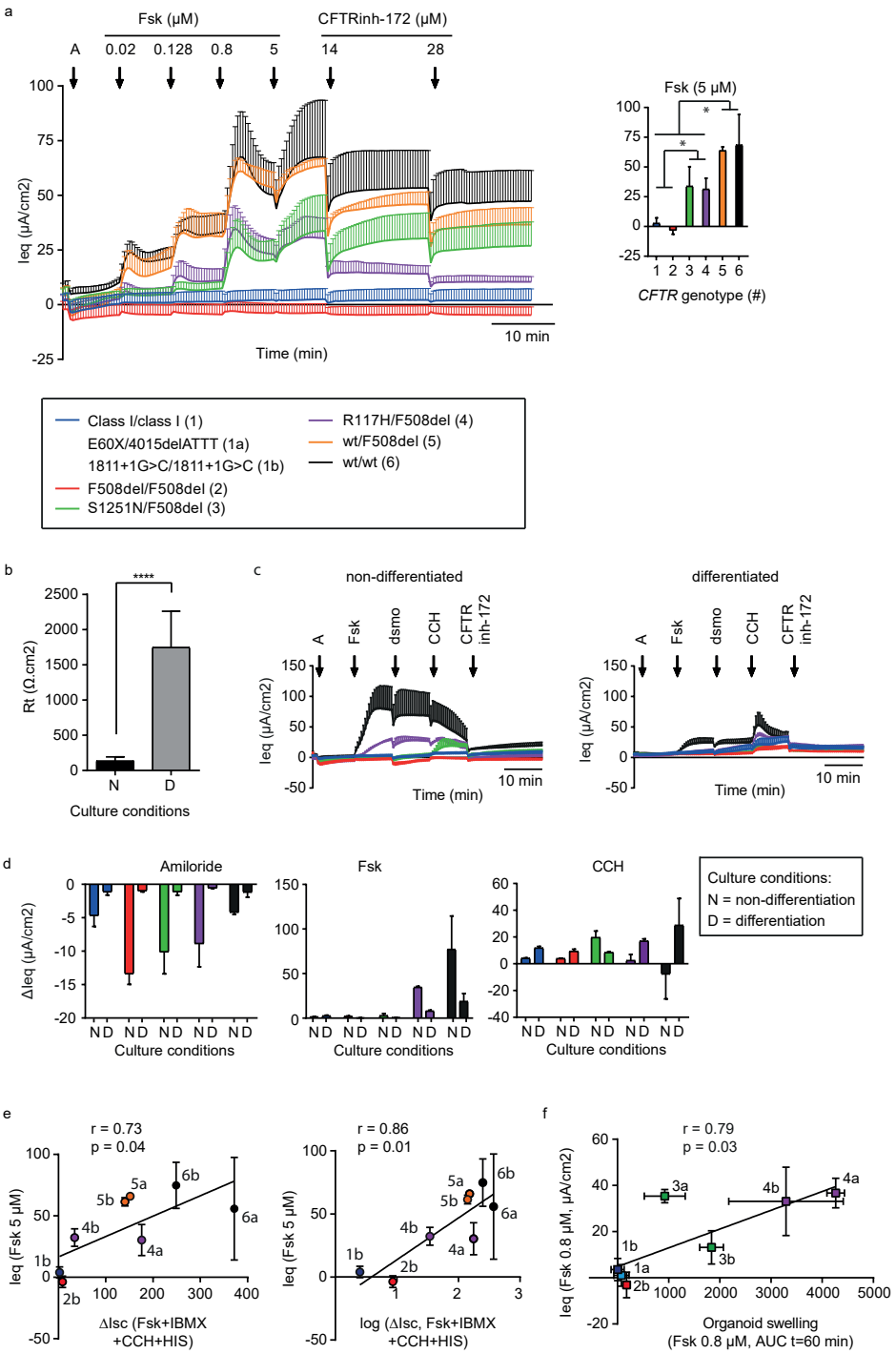
a
Fsk (μM)
CFTRinh-172 (μM)
A
0.02
0.128
0.8
5
14
28
Ieq (μA/cm2)
Time (min)
10 min
Fsk (5 μM)
CFTR genotype (#)
Class I/class I (1)
E60X/4015delATTT (1a)
1811+1G>C/1811+1G>C (1b)
F508del/F508del (2)
S1251N/F508del (3)
R117H/F508del (4)
wt/F508del (5)
wt/wt (6)
b
Rt (Ω.cm2)
****
N
D
Culture conditions
c
non-differentiated
differentiated
A
Fsk
dsmo
CCH
CFTR inh-172
Ieq (μA/cm2)
Time (min)
10 min
d
Amiloride
Fsk
CCH
ΔIeq (μA/cm2)
ND
Culture conditions
Culture conditions:
N = non-differentiation
D = differentiation
e
r = 0.73
p = 0.04
Ieq (Fsk 5 μM)
ΔIsc (Fsk+IBMX +CCH+HIS)
r = 0.86
p = 0.01
log (ΔIsc, Fsk+IBMX +CCH+HIS)
f
r = 0.79
p = 0.03
Ieq (Fsk 0.8 μM, μA/cm2)
Organoid swelling (Fsk 0.8 μM, AUC t=60 min)

We next compared how culture conditions modified ion channel activity using monolayers of five donors (one per CFTR genotype). Culturing the monolayers under differentiation conditions strongly increased the transepithelial electrical resistance, suggesting increased tight junctions and barrier formations ($p < 0.001$, Fig. 3b). Additionally, amiloride-sensitive and forskolin-induced currents were greatly reduced upon differentiation, indicating loss of ENaC and CFTR function (Fig. 3c-d). Differentiation culture conditions induced a small but consistent carbachol-induced current in all monolayers, which was strongest in wild type, but also consistently present in class I/class I monolayers (Fig. 3c-d). This indicated that the carbachol-induced current is partially CFTR-dependent under these differentiation conditions. Together, these results indicated that culture conditions can have a profound impact on the electrophysiological properties of the monolayers, with clear impact on epithelial resistance and cAMP- and calcium-mediated ion transport.

As a next step, MTECC measurements from organoid-derived monolayers were compared with ICM of donor-matched rectal biopsies. Short-circuit currents (Fsk + IBMX + CCH + HIS) of rectal biopsies showed a strong positive correlation with the 5 µM forskolin-induced currents of rectal monolayers cultured under non-differentiation conditions (Pearson's $r = 0.73$, $p = 0.04$; Fig. 3e). Upon log transformation of the currents of the biopsies, a stronger correlation with the monolayers responses was observed ($r = 0.86$, $p = 0.01$), indicating a non-linear correlation between both assays (Fig. 3e). Short-circuit currents of Fsk + IBMX + CCH or Fsk + IBMX demonstrated lower correlations with the organoid-derived monolayers (data not shown). Finally, we investigated whether forskolin-induced swelling of rectal CF organoids correlated with forskolin-induced currents of rectal monolayers cultured under non-differentiation conditions. Despite having fewer samples due to the lack of swelling measurements in healthy control organoids, the organoid responses demonstrated a strong correlation with the donor-matched monolayers Ieq at 0.8 µM forskolin (Pearson's $r = 0.79$, $p = 0.03$; Fig. 3f) and 5 µM forskolin stimulation (Pearson's $r = 0.76$, $p = 0.046$, data not shown).

In conclusion, the observed correlation of CFTR function measurements between either excised native rectal tissue or organoids with donor-matched monolayers demonstrates that this *in vitro* model system recapitulates key characteristics of the *in vivo* tissue. Furthermore, these data indicated that intestinal CFTR-dependent ion transport and fluid secretion are tightly coupled.

Discussion

We here developed an assay to characterize CFTR-dependent ion transport in monolayers of human primary intestinal epithelium derived from 3D cultured rectal organoids. This proof-of-concept study showed clear correlations between CFTR function measurements in undifferentiated monolayers with donor-matched ICM on *ex vivo* biopsies and fluid secretion assays by measurement of organoid swelling. Since rectal organoids provide a virtually unlimited resource of patient-derived cells [4], and biorepositories are currently being established (e.g. hub4organoids.eu), we anticipate that the electrophysiological monolayer assay will help to support intestinal epithelial ion transport studies in the context of CF or other diseases.

The correlations between the *ex vivo* tissue (rectal biopsies) and *in vitro* models (organoids and monolayers) relied on specific stimulatory conditions for each model. Since cAMP is the main cellular

activator of CFTR, we favored to compare data from the different assays using forskolin as primary stimulant. Although the number of patient samples was limited in this proof-of-concept study, the overall forskolin-induced responses were similar for both *in vitro* models. The outcomes were also in agreement with the disease liability of the studied CFTR genotypes in public registries [22,29]. Forskolin-induced currents from the S1251N/F508del monolayers were somewhat higher than anticipated based on public registries [22] and the donor-matched intestinal organoids responses. This may have resulted from technical variability and/or patient-specific biological factors that disconnect fluid secretion and ion transport. Organoid fluid transport is driven by sustained ion transport over the course of an hour, while the monolayer assay might be more suited to identify transient ion transport in epithelia due to the continuous ion transport measurements. The correlation between functional measurements in organoids and monolayers supports that CFTR-dependent fluid secretion in intestinal organoids is largely reflective of CFTR-dependent ion transport, as we published previously [5]. In depth studies are required to further evaluate the relationship between fluid secretion and ion transport, and whether potential differences thereof may help to understand individual disease features.

Previous work demonstrated that discrimination between CF and non-CF by ICM was optimal when currents evoked by multiple agonists (carbachol, forskolin and histamine) were added together [30–32]. Using identical stimulants but in a slightly different order, our data also showed the best discrimination between CFTR genotypes was when forskolin, carbachol and histamine were combined to induce currents, which resulted in the best correlations with both *in vitro* models.

The studies in rectal monolayers can further help to understand the epithelial properties of the native intestinal tissue. Rectal biopsies contain a mix of crypt-based stem cells, transient amplifying cells and differentiated cells. By adapting culture conditions, we could start to better study the properties of these cell populations independently. Previous studies in rectal biopsies showed that carbachol enhances apical chloride secretion via CFTR [12], which is consistent with the data we observed under differentiation conditions. Undifferentiated monolayers showed large forskolin-induced currents and little impact of carbachol on top of forskolin. This phenotype prevailed even in CF monolayers, suggesting that the calcium-dependent chloride secretion was not active or played only a limited role in the secretion of chloride. This may involve the high expression of basolateral NKCC1 in undifferentiated conditions and may interplay with other basolateral channels and transporters [33]. The upregulation of carbachol-induced currents in differentiated class I/class I monolayers indicated that under differentiating conditions carbachol also upregulated a CFTR-independent, calcium-mediated chloride secretory pathway.

The main cause of death for subjects with CF is pulmonary failure. As such HBE cells are widely used to study electrophysiology of CFTR [34]. However, the protocols for culturing and differentiating HBE cells into pseudo-stratified, CFTR-expressing airway epithelium, are difficult and time-consuming [16]. The various intestinal models used in this study have several advantages and limitations, and their suitability will depend on specific experimental questions and settings. Rectal biopsies allow the measurements of CFTR-dependent functions in near native tissue in only a couple of hours after isolation, but have limited throughput and are difficult to manipulate by CFTR modulators. The *in vitro* 3D intestinal organoid cultures offer the advantages of long term genetically-stable culturing, biobanking and large scale CFTR-

dependent function in relatively high throughput. With organoid-derived monolayers, ion transport properties can be directly assessed in undifferentiated intestinal epithelium in just four days after plating, followed by an additional five days of differentiation. We used a 24-well MTECC system which provides significant throughput when compared to conventional Ussing chambers, but our protocols might need further refinement to facilitate a better delivery of reagents as suggested from the limited activity of CFTRinh-172 as well as partial transient currents elicited by forskolin.

In this study, we used human primary rectal stem cells to generate monolayers for electrophysiological measurements. The CFTR-induced ion transport in undifferentiated monolayers with different CFTR genotypes correlated with donor-matched organoid swelling and native rectal biopsy current measurements. This electrophysiological assay might be useful (i) to functionally measure CFTR and alternative ion channel activity, (ii) to reduce or induce functional ion channel expression via differentiation culture conditions, and (iii) to assist in diagnosis or personalized drug testing. Next to electrophysiological measurements, the monolayer culture system provide opportunities to develop assays to study host/pathogen interactions or mucus properties and manipulation thereof [17,18] in primary intestinal cell cultures.

Acknowledgements

We thank S. Michel, G. Berkers and I. Bronsveld from University Medical Centre Utrecht (UMCU) for obtaining the rectal biopsies. Our thanks go out to W. van Driessche (EP-Devices, Belgium) and M. Gees (Galapagos, Belgium) for their assistance with the MTECC. We acknowledge J. van Rijn and S. Middendorp (UMCU) for providing us the LGR5 primer pair and K. Pateras (UMCU) for the assistance on statistical testing. We thank H.R. de Jonge from Erasmus Medical Centre Rotterdam for his electrophysiological expertise.

Funding

This work was supported by grants of the Dutch Cystic Fibrosis Foundation (NCFS, HIT-CF grant) and Netherlands Organization for Health Research and Development (ZonMw, grant number 40-00812-98-14103). Funding sources had no involvement in study design, collection, analysis, interpretation or writing.

References

[1] H Clevers, Modeling development and disease with organoids, Cell 165, 2016, 1586–1597, https://doi.org/10.1016/j.cell.2016.05.082.

[2] AL Bredenoord, H Clevers and JA Knoblich, Human tissues in a dish: the research and ethical implications of organoid technology, Science 355, 2017, , eaaf9414https://doi.org/10.1126/science.aaf9414, [80-].

[3] T Sato, RG Vries, HJ Snippert, M van de Wetering, N Barker, DE Stange, et al., Single Lgr5 stem cells build crypt-villus structures *in vitro* without a mesenchymal niche, Nature 459, 2009, 262–265, https://doi.org/10.1038/nature07935.

[4] T Sato, DE Stange, M Ferrante, RGJ Vries, JH Van Es, S Van Den Brink, et al., Long-term expansion of epithelial organoids from human colon, adenoma, adenocarcinoma, and Barrett's epithelium, Gastroenterology 141, 2011, 1762–1772, https://doi.org/10.1053/j.gastro.2011.07.050.

[5] JF Dekkers, CL Wiegerinck, HR de Jonge, I Bronsveld, HM Janssens, KM de Winter-de Groot, et al., A functional CFTR assay using primary cystic fibrosis intestinal organoids, Nat Med 19, 2013, 939–945, https://doi.org/10.1038/nm.3201.

[6] JF Dekkers, G Berkers, E Kruisselbrink, A Vonk, HR De Jonge, HM Janssens, et al., Characterizing responses to CFTR-modulating drugs using rectal organoids derived from subjects with cystic fibrosis, Sci Transl Med 8, 2016, , 13https://doi.org/10.1126/scitranslmed.aad8278.

[7] LAW Vijftigschild, G Berkers, JF Dekkers, DD Zomer-Van Ommen, E Matthes, E Kruisselbrink, et al., B2-Adrenergic receptor agonists activate CFTR in intestinal organoids and subjects with cystic fibrosis, Eur Respir J 48, 2016, 768–779, https://doi.org/10.1183/13993003.01661-2015.

[8] DD Zomer-Van Ommen, AV Pukin, O Fu, LHC Quarles Van Ufford, HM Janssens, JM Beekman, et al., Functional characterization of cholera toxin inhibitors using human intestinal organoids, J Med Chem 59, 2016, 6968–6972, https://doi.org/10.1021/acs.jmedchem.6b00770.

[9] JR Riordan, JM Rommens, B Kerem, N Alon, R Rozmahel, Z Grzelczak, et al., Identification of the cystic fibrosis gene: cloning and characterization of complementary DNA, Science 245, 1989, 1066–1073.

[10] J Zielenski, Genotype and phenotype in cystic fibrosis, 8, 2000, 117–133.

[11] H Li, DN Sheppard and MJ Hug, Transepithelial electrical measurements with the Ussing chamber, J Cyst Fibros 3, 2004, 123–126, https://doi.org/10.1016/j.jcf.2004.05.026.

[12] HR De Jonge, M Ballmann, H Veeze, I Bronsveld, F Stanke, B Tümmler, et al., Ex vivo CF diagnosis by intestinal current measurements (ICM) in small aperture, circulating Ussing chambers, J Cyst Fibros 3 (Suppl. 2), 2004, 159–163, https://doi.org/10.1016/j.jcf.2004.05.034.

[13] F Van Goor, S Hadida, PDJ Grootenhuis, B Burton, D Cao, T Neuberger, et al., Rescue of CF airway epithelial cell function *in vitro* by a CFTR potentiator, VX-770, Proc Natl Acad Sci U S A 106, 2009, 18825–18830, https://doi.org/10.1073/pnas.0904709106.

[14] F Van Goor, S Hadida, PDJ Grootenhuis, B Burton, JH Stack, KS Straley, et al., Correction of the F508del-CFTR protein processing defect *in vitro* by the investigational drug VX-809, Proc Natl Acad Sci U S A 108, 2011, 18843–18848, https://doi.org/10.1073/pnas.1105787108.

[15] PT Ikpa, MJC Bijvelds and HR de Jonge, Cystic fibrosis: toward personalized therapies, Int J Biochem Cell Biol 2014, https://doi.org/10.1016/j.biocel.2014.02.008.

[16] T Neuberger, B Burton, H Clark and F Van Goor, Use of Primary Cultures of Human Bronchial Epithelial Cells Isolated from Cystic Fibrosis Patients for the Pre-clinical Testing of CFTR Modulators, 742, 2011, 39–54, https://doi.org/10.1007/978-1-61779-120-8.

[17] C Moon, KL VanDussen, H Miyoshi and TS Stappenbeck, Development of a primary mouse intestinal epithelial cell monolayer culture system to evaluate factors that modulate IgA transcytosis, Mucosal Immunol 7, 2014, 818–828, https://doi.org/10.1038/mi.2013.98.

[18] KL VanDussen, JM Marinshaw, N Shaikh, H Miyoshi, C Moon, PI Tarr, et al., Development of an enhanced human gastrointestinal epithelial culture system to facilitate patient-based assays, Gut 2014, https://doi.org/10.1136/gutjnl-2013-306651.

[19] V Mutyam, M Du, X Xue, KM Keeling, E Lucile White, JRobert Bostwick, et al., Discovery of clinically approved agents that promote suppression of cystic fibrosis transmembrane conductance regulator nonsense mutations, Am J Respir Crit Care Med 194, 2016, 1092–1103, https://doi.org/10.1164/rccm.201601-0154OC.

[20] CB Vu, RJ Bridges, C Pena-Rasgado, AE Lacerda, C Bordwell, A Sewell, et al., Fatty acid cysteamine conjugates as novel and potent autophagy activators that enhance the correction of misfolded f508del-cystic fibrosis transmembrane conductance regulator (CFTR), J Med Chem 60, 2017, 458–473, https://doi.org/10.1021/acs.jmedchem.6b01539.

[21] SF Boj, AM Vonk, M Statia, J Su, RRG Vries, JM Beekman, et al., Forskolin-induced swelling in intestinal organoids: an *in vitro* assay for assessing drug response in cystic fibrosis patients, J Vis Exp 2017, 1–12, https://doi.org/10.3791/55159.

[22] The Clinical and Functional TRanslation of CFTR, [n.d.]http://cftr2.org, Accessed 8 September 2017.

[23] GF Vogel, JM Van Rijn, IM Krainer, AR Janecke, C Posovzsky, M Cohen, et al., Disrupted apical exocytosis of cargo vesicles causes enteropathy in FHL5 patients with Munc18-2 mutations, JCI Insight 2, 2017, 551–565, https://doi.org/10.1172/JCI.INSIGHT.94564.

[24] MW Pfaffl, A new mathematical model for relative quantification in real-time RT-PCR, Nucleic Acids Res 29, 2001, , e45https://doi.org/10.1093/nar/29.9.e45.

[25] TJ Kelly, L Al-Nakkash, CU Cotton and ML Drumm, Activation of endogenous D-F508 cystic fibrosis transmembrane conductance regulator by phosphodiesterase inhibition, J Clin Invest 98, 1996, 513–520.

[26] JE Matos, M Sausbier, GBeranek, U. Sausbier, P Ruth and J Leipziger, Role of cholinergic-activated KCa1.1 (BK), KCa3.1 (SK4) and KV7.1 (KCNQ1) channels in mouse colonic Cl- secretion, Acta Physiol 189, 2007, 251–258, https://doi.org/10.1111/j.1748-1716.2006.01646.x.

[27] I Crawford, PC Maloney, PL Zeitlin, WB Guggino, SC Hyde, H Turley, et al., Immunocytochemical localization of the cystic fibrosis gene product CFTR, Proc Natl Acad Sci U S A 88, 1991, 9262–9266.

[28] AEO Trezise and M Buchwald, *In vivo* cell-specific expression of the cystic fibrossis transmembrane conductance receptor, Lett Nat 353, 1991, 434–437.

[29] PR Sosnay, KR Siklosi, F Van Goor, K Kaniecki, H Yu, N Sharma, et al., Defining the disease liability of variants in the cystic fibrosis transmembrane conductance regulator gene, Nat Genet 45, 2013, 1160–1167, https://doi.org/10.1038/ng.2745.

[30] N Derichs, J Sanz, T Von Kanel, C Stolpe, A Zapf, B Tümmler, et al., Intestinal current measurement for diagnostic classification of patients with questionable cystic fibrosis: validation and reference data, Thorax 65, 2010, 594–599, https://doi.org/10.1136/thx.2009.125088.

[31] M Wilschanski, Y Yaakov, I Omari, M Zaman, CR Martin, M Cohen-Cymberknoh, et al., Comparison of nasal potential difference and intestinal current measurements as surrogate markers for CFTR function, J Pediatr Gastroenterol Nutr 63, 2016, 92–97, https://doi.org/10.1097/MPG.0000000000001366.

[32] M Cohen-Cymberknoh, Y Yaakov, D Shoseyov, E Shteyer, E Schachar, J Rivlin, et al., Evaluation of the intestinal current measurement method as a diagnostic test for cystic fibrosis, Pediatr Pulmonol 48, 2013, 229–235, https://doi.org/10.1002/ppul.22586.

[33] RA Frizzell and JW Hanrahan, Physiology of epithelial chloride and fluid secretion, Cold Spring Harb Perspect Med 2, 2012, , a009563https://doi.org/10.1101/cshperspect.a009563.

[34] SC Bell, K De Boeck and MD Amaral, New pharmacological approaches for cystic fibrosis: Promises, progress, pitfalls, Pharmacol Ther 2015, 19–34, https://doi.org/10.1016/j.pharmthera.2014.06.005.

Supplementary information

Gene	Forward primer (5'-3')	Reverse primer (5'-3')	Temperature (°C)
CFTR	CAACATCTAGTGAGCAGTCAGG	CCCAGGTAAGGGATGTATTGTG	62.5
NKCC1	TGGGTCAAGCTGGAATAGGTC	ACCAAATTCTGGCCCTAGACTT	64
LGR5	GAATCCCCTGCCCAGTCTC	ATTGAAGGCTTCGCAAATTCT	62
GAPDH	TGCACCACCAACTGCTTAGC	GGCATGGACTGTGGTCATGAG	62.5
ß-actin	CTGGAACGGTGAAGGTGACA	AAGGGACTTCCTGTAACAATGCA	64

Table S1. Primers used in RT-qPCR. Abbreviations: CFTR, Cystic Fibrosis Transmembrane Conductance Regulator; NKCC1, Na-K-Cl co-transporter 1; LGR5, Leucine-rich repeat-containing G-protein coupled receptor 5; GAPDH, Glyceraldehyde 3-phosphate dehydrogenase.

a

ICM fsk+IBMX+CCH+HIS		
Tukey's multiple comparisons test	Summary	Adjusted P Value
1b vs. 2	ns	0,9994
1b vs. 4	ns	0,3279
1b vs. 5	ns	0,1064
1b vs. 6	****	<0,0001
2 vs. 4	ns	0,2915
2 vs. 5	ns	0,0777
2 vs. 6	****	<0,0001
4 vs. 5	ns	0,904
4 vs. 6	***	0,0005
5 vs. 6	*	0,0128

1. Class I/class I
   a. E60X/4015delATTT
   b. 1811+1G>C/1811+1G>C
2. F508del/F508del
3. S1251N/F508del
4. R117H/F508del
5. wt/F508del
6. wt/wt

b

Fsk 0.8 µM					
Undifferentiated			Differentiated		
Tukey's multiple comparisons test	Summary	Adjusted P Value	Tukey's multiple comparisons test	Summary	Adjusted P Value
1 vs. 2	ns	0,9821	1 vs. 2	ns	0,9224
1 vs. 3	**	0,0017	1 vs. 3	ns	0,5825
1 vs. 4	****	<0,0001	1 vs. 4	**	0,0029
2 vs. 3	**	0,004	2 vs. 3	ns	0,2549
2 vs. 4	****	<0,0001	2 vs. 4	*	0,0119
3 vs. 4	****	<0,0001	3 vs. 4	***	0,0002

Fsk 5 µM					
Undifferentiated			Differentiated		
Tukey's multiple comparisons test	Summary	Adjusted P Value	Tukey's multiple comparisons test	Summary	Adjusted P Value
1 vs. 2	ns	0,8651	1 vs. 2	ns	0,6348
1 vs. 3	****	<0,0001	1 vs. 3	ns	0,942
1 vs. 4	****	<0,0001	1 vs. 4	**	0,0056
2 vs. 3	****	<0,0001	2 vs. 3	ns	0,9192
2 vs. 4	****	<0,0001	2 vs. 4	***	0,0004
3 vs. 4	ns	0,0678	3 vs. 4	**	0,0016

CCH 100 µM					
Undifferentiated			Differentiated		
Tukey's multiple comparisons test	Summary	Adjusted P Value	Tukey's multiple comparisons test	Summary	Adjusted P Value
1 vs. 2	ns	0,5575	1 vs. 2	ns	0,9613
1 vs. 3	*	0,0497	1 vs. 3	ns	0,9937
1 vs. 4	**	0,0012	1 vs. 4	ns	0,8544
2 vs. 3	**	0,0027	2 vs. 3	ns	0,9958
2 vs. 4	****	<0,0001	2 vs. 4	ns	0,583
3 vs. 4	ns	0,3526	3 vs. 4	ns	0,7183

Figure S1. P-values of one-way ANOVA multiple comparisons tests from Figure 1. a) Overview of all p-values from Fig. 1b. b) All p-values from Fig. 1d. Abbreviations: CCH, carbachol; Fsk, forskolin; HIS, histamine.

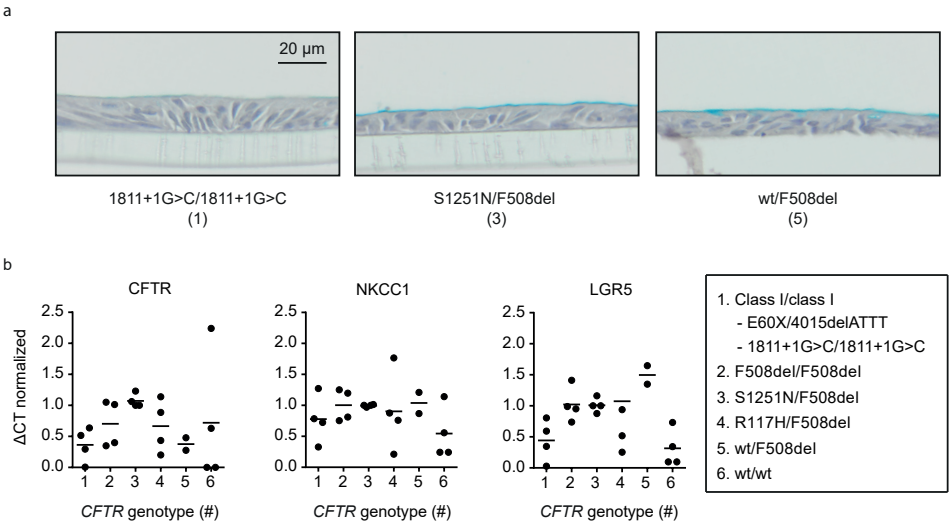

Figure S2. Characterization of rectal organoid-derived monolayers cultured under non-differentiating conditions. a) Representative histological sections of alcian Blue/PAS-stained monolayers from one carrier and two subjects with CF (*CFTR* genotypes as indicated). b) mRNA expression levels of ion channels CFTR (apical) and NKCC1 (basolateral), and cellular marker LGR5 as quantified by RT-qPCR in two independent experiments for twelve donors (two per *CFTR* genotype). The lines indicate the average value within a *CFTR* genotype/mutation class from two donors and two independent experiments (which are depicted as dots). Abbreviations: CFTR, cystic fibrosis transmembrane conductance regulator; LGR5, Leucine-rich repeat-containing G-protein coupled receptor 5; NKCC1, Na-K-Cl co-transporter 1; wt, wild type.

a

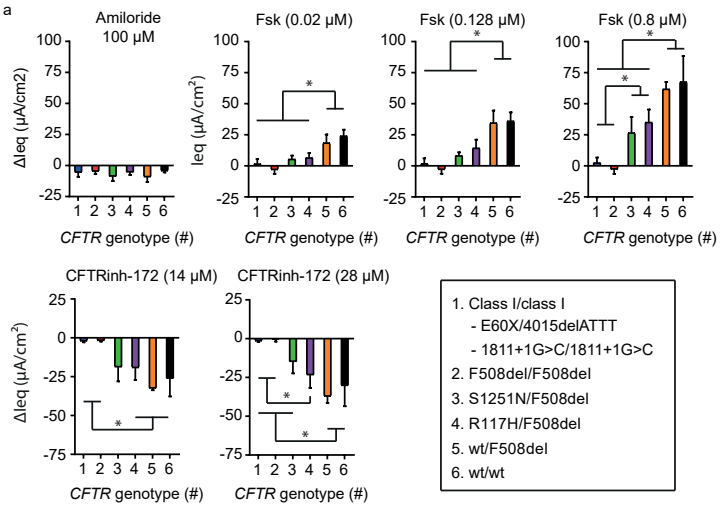

b

Fsk 0.02 µM			Fsk 0.128 µM			Fsk 0.8 µM		
Tukey's multiple comparisons test	Summary	Adjusted P Value	Tukey's multiple comparisons test	Summary	Adjusted P Value	Tukey's multiple comparisons test	Summary	Adjusted P Value
1 vs. 5	****	<0,0001	1 vs. 4	*	0,0148	1 vs. 3	*	0,021
1 vs. 6	****	<0,0001	1 vs. 5	****	<0,0001	1 vs. 4	***	0,0006
2 vs. 3	*	0,0474	1 vs. 6	****	<0,0001	1 vs. 5	****	<0,0001
2 vs. 4	*	0,0118	2 vs. 4	***	0,0005	1 vs. 6	****	<0,0001
2 vs. 5	****	<0,0001	2 vs. 5	****	<0,0001	2 vs. 3	**	0,0037
2 vs. 6	****	<0,0001	2 vs. 6	****	<0,0001	2 vs. 4	****	<0,0001
3 vs. 5	**	0,0018	3 vs. 5	****	<0,0001	2 vs. 5	****	<0,0001
3 vs. 6	****	<0,0001	3 vs. 6	****	<0,0001	2 vs. 6	****	<0,0001
4 vs. 5	**	0,0032	4 vs. 5	***	0,0002	3 vs. 5	**	0,0014
4 vs. 6	****	<0,0001	4 vs. 6	****	<0,0001	3 vs. 6	****	<0,0001
						4 vs. 5	*	0,0152
						4 vs. 6	***	0,0005

Fsk 5 µM			CFTRinh-172 14 µM			CFTRinh-172 28 µM		
Tukey's multiple comparisons test	Summary	Adjusted P Value	Tukey's multiple comparisons test	Summary	Adjusted P Value	Tukey's multiple comparisons test	Summary	Adjusted P Value
1 vs. 3	**	0,0093	1 vs. 3	**	0,0078	1 vs. 4	***	0,0005
1 vs. 4	*	0,0128	1 vs. 4	**	0,0036	1 vs. 5	****	<0,0001
1 vs. 5	****	<0,0001	1 vs. 5	****	<0,0001	1 vs. 6	****	<0,0001
1 vs. 6	****	<0,0001	1 vs. 6	****	<0,0001	2 vs. 3	*	0,0458
2 vs. 3	**	0,0016	2 vs. 3	**	0,0066	2 vs. 4	***	0,0002
2 vs. 4	**	0,0021	2 vs. 4	**	0,003	2 vs. 5	****	<0,0001
2 vs. 5	****	<0,0001	2 vs. 5	****	<0,0001	2 vs. 6	****	<0,0001
2 vs. 6	****	<0,0001	2 vs. 6	****	<0,0001	3 vs. 5	**	0,0021
3 vs. 5	*	0,0313				3 vs. 6	*	0,0262
3 vs. 6	**	0,0031						
4 vs. 5	*	0,0118						
4 vs. 6	***	0,0008						

Figure S3. Statistical analysis of electrophysiological measurements in undifferentiated rectal organoid-derived monolayers. a) (Change in) Ieq peak response upon amiloride, forskolin or CFTRinh-172 incubation calculated from Figure 3a. Each bar represents six means ±SD (means of two monolayers per donor: two donors per *CFTR* genotype and three independent experiments in total). The change in Ieq upon amiloride is relative to baseline, the change in Ieq upon CFTRinh-172 addition is relative to 5 µM forskolin stimulation. * indicating p<0.05. b) Overview of all p-values per *CFTR* genotype from a. Abbreviations: Fsk, forskolin; Ieq, equivalent short-circuit currents.

Comparison of *ex vivo* and *in vitro* intestinal cystic fibrosis models to measure CFTR-dependent ion channel activity

4

CHAPTER 5

Long-term expanding human airway organoids for disease modeling

Norman Sachs [1], Domenique D. Zomer-van Ommen [2], Angelos Papaspyropoulos [1], Inha Heo [1], Lena Böttinger [1], Dymph Klay [3], Fleur Weeber [4], Guizela Huelsz-Prince [5], Nino Iakobachvili [6], Marco C. Viveen [7], Anna Lyubimova [1], Luc Teeven [1], Sepideh Derakhshan [2], Jeroen Korving [1], Harry Begthel [1], Kuldeep Kumawat [2], Emilio Ramos [8], Matthijs F.M. van Oosterhout [3], Eduardo P. Olimpio [5], Joep de Ligt [7], Krijn K. Dijkstra [4], Egbert F. Smit [4], Maarten van der Linden [2], Emile E. Voest [4], Coline H.M. van Moorsel [3], Cornelis K. van der Ent [2], Edwin Cuppen [7], Alexander van Oudenaarden [1], Frank E. Coenjaerts [7], Linde Meyaard [2], Louis J. Bont [2], Peter J. Peters [6], Sander J. Tans [5], Jeroen S. van Zon [5], Sylvia F. Boj [8], Robert G. Vries [8], Jeffrey M. Beekman [2], Hans Clevers [1].

Submission in revision at Nature Biotechnology

Affiliations: 1. Hubrecht Institute-KNAW and UMC Utrecht, Netherlands; 2. Wilhelmina Children's Hospital and UMC Utrecht, Netherlands; 3. St. Antonius Hospital Nieuwegein, Netherlands; 4. Netherlands Cancer Institute, Amsterdam, Netherlands; 5. FOM Institute AMOLF, Amsterdam, Netherlands; 6. Maastricht University, Maastricht, Netherlands; 7. UMC Utrecht, Netherlands; 8. Hubrecht Organoid Technology, Utrecht, Netherlands

Materials and correspondence: h.clevers@hubrecht.eu

Abstract

Organoids are self-organizing 3D structures grown from stem cells that recapitulate essential aspects of organ structure and function. Here we describe a method to establish long-term-expanding human airway organoids from broncho-alveolar biopsies or lavage material. The pseudostratified airway organoid epithelium consists of basal cells, functional multi-ciliated cells, mucus-producing goblet cells, and CC10-secreting club cells. Airway organoids derived from cystic fibrosis (CF) patients allow assessment of CFTR function in an organoid swelling assay. Organoid culture conditions also allow gene editing as well as the derivation of various types of lung cancer organoids. Respiratory syncytial virus (RSV) infection recapitulated central disease features and dramatically increases organoid cell motility, found to be driven by the non-structural viral NS2 protein. We conclude that human airway organoids represent versatile models for the *in vitro* study of hereditary, malignant, and infectious pulmonary disease.

Introduction

To date, several approaches have been explored to generate mammalian airway organoids[1]. In 1993 Puchelle and colleagues described the first self-organizing 3D structures of adult human airway epithelium in collagen[2]. A first description of the generation of lung organoids from human iPS (induced pluripotent stem) cells was given by Rossant et al. and included the use of *CFTR*-mutant iPS cells as a proof of concept for modeling CF[3]. Snoeck and colleagues designed an improved four-stage protocol[4], while Spence and colleagues[5] followed a modified trajectory to generate mature lung organoids, containing basal, ciliated, and club cells. These cultures were stable for up to several months and resembled proximal airways. Hogan and colleagues reported the first adult stem cell-based murine bronchiolar lung organoid culture protocol, involving Matrigel supplemented with EGF[6]. Single basal cells isolated from the trachea grew into *tracheospheres* consisting of a pseudostratified epithelium with basal and ciliated luminal cells. These organoids could be passaged at least twice. No mature club, neuroendocrine, or mucus-producing cells were observed[6]. In a later study, this clonal 3D organoid assay was used to demonstrate that IL-6 treatment resulted in the formation of ciliated cells at the expense of secretory and basal cells[7]. Tschumperlin and colleagues combined human adult primary bronchial epithelial cells, lung fibroblasts, and lung microvascular endothelial cells in 3D to generate airway organoids[8]. Under these conditions, randomly-seeded mixed cell populations underwent rapid condensation to self-organize into discrete epithelial and endothelial structures that were stable up to four weeks of culture[8]. Hild and Jaffe have described a protocol for the culture of *bronchospheres* from primary human airway basal cells. Mature *bronchospheres* are composed of functional multi-ciliated cells, mucin-producing goblet cells, and airway basal cells[9]. Finally, Snoeck and colleagues generated lung bud organoids from human pluripotent stem cells that recapitulate fetal lung development[10]. However, none of these approaches allows continued, long-term expansion of airway epithelium *in vitro* limiting their practical use. We therefore set out to establish long-term culture conditions of human airway epithelial organoids that contain all major cell populations and allow personalized human disease modeling.

Results

Generation and characterization of human airway organoids

We collected macroscopically inconspicuous lung tissue from non-small-cell lung cancer (NSCLC) patients undergoing medically indicated surgery and isolated epithelial cells through mechanical and enzymatic tissue disruption (see Methods). Following our experience with generating organoids from other adult human tissues[11-15], we embedded isolated cells in basement membrane extract (BME) and activated/blocked signaling pathways important for airway epithelium (Supplementary Table 1). Under optimized conditions, 3D organoids formed within several days (94% success rate, n=18) and could be passaged by mechanical disruption at 1:2 to 1:4 ratios every other week for at least one year. Accordingly, they proliferated at comparable rates regardless of passage number (Extended Data Fig. 1a).

Since organoids were composed of a polarized, pseudostratified airway epithelium containing basal, secretory, brush, and multi-ciliated cells (Fig. 1a, b, Supplementary Video 1), we termed them airway organoids (AOs). Within the organoids, cells that stained positive for basal cell marker Keratin-14

(KRT14), club cell marker secretoglobin family 1A member 1 (SCGB1A1), cilia marker acetylated α-tubulin, or goblet cell marker mucin 5AC (MUC5AC) localized to their corresponding *in vivo* positions (Fig. 1c, Extended Data Fig. 1b). Secretory cells as well as cilia were functional as evidenced by immunofluorescence analysis capturing secretion of SCGB1A1-positive mucus into the organoid lumen (Fig. 1c) and time lapse microscopy showing cilia whirling around secreted mucus (Supplementary Video 2, 3).

We next compared expression levels of selected genes in ten independently established AO lines vs whole lung tissue by quantitative PCR (qPCR) (Extended Data Fig. 1c). While equally expressing the general lung marker NKX2-1 and several airway specific markers, AOs expressed virtually no HOXA5 (a bona fide lung mesenchyme gene) or alveolar transcripts emphasizing their airway epithelial composition. To identify global AO gene expression and verify maintenance of airway identity upon extended culturing, we sequenced RNA of three high-passage AO lines and three small intestinal organoid (SIO) lines. Upon comparative transcriptome ranking, we performed gene set enrichment analyses (GSEA) using gene lists for specific lung cell types (see Supplementary Table 2 and Methods)[16-19]. Basal cell, club cell, and cilia signatures were strongly enriched in AOs (Fig. 1d), whereas alveolar and secretory cell signatures were not, the latter due to the presence of secretory cells in both AOs and SIOs (Extended Data Fig. 1c, d). Bulk lung as well as small airway epithelial signatures strongly correlated with AOs (Fig. 1e). Hallmark lung genes encoding for secretoglobins, cytochromes, p63, SOX2, and others were consistently among the highest AO enriched genes (Fig. 1f). High levels of WNT3A transcripts explained why AOs – in contrast to SIOs – did not require the addition of exogenous WNT3A to the culture media. Maximum WNT pathway activation caused upregulation of the proposed lung stem cell gene LGR6, while WNT pathway inhibition caused loss of LGR6 as well as of the generic epithelial stem cell marker LGR5 (Extended Data Fig. 1e)[20,21]. Taken together, our culture conditions allow long term expansion of AOs that retain major characteristics of the *in vivo* epithelium.

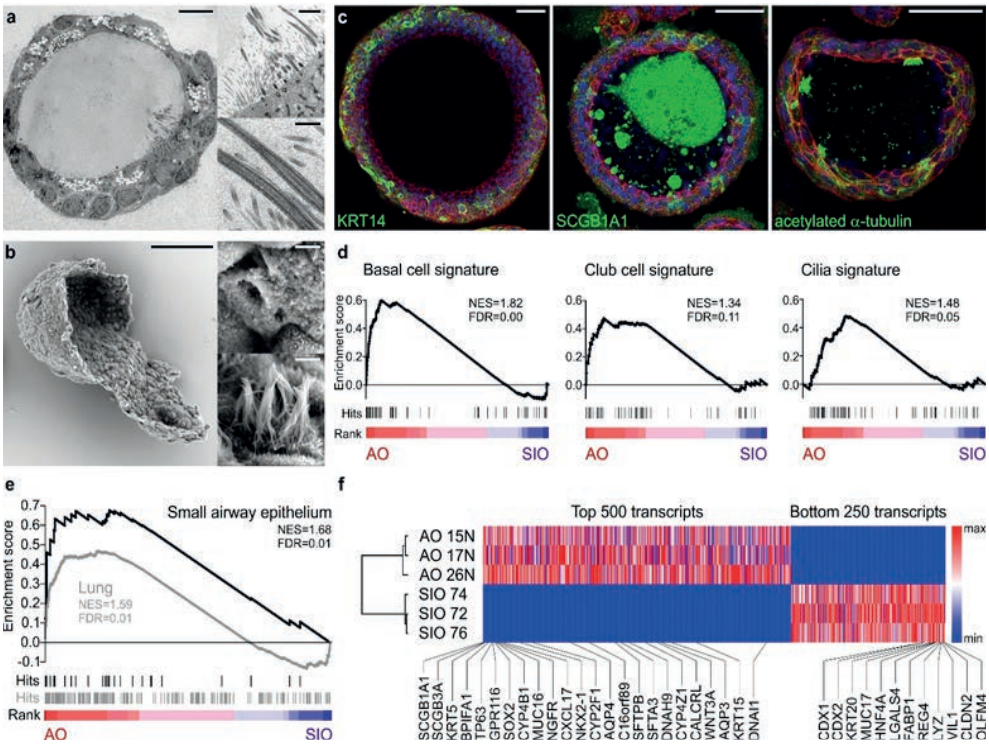

Figure 1. *Characterization of airway organoids.* ***a****, Transmission electron micrograph of an AO cross-section showing the polarized, pseudostratified epithelium containing basal, secretory, brush, and multi-ciliated cells. Details display apical microvilli and cilia with their characteristic microtubule structure. Scale bars equal 10 µm, 2 µm, and 500 nm. See also Supplementary Videos 1-3.* ***b****, Scanning electron micrograph of a partially opened AO visualizing its 3D architecture, as well as basal and apical ultrastructure. Details display apical surfaces of secretory and multi-ciliated cells. Scale bars equal 50 µm (overview) and 2 µm (details).* ***c****, Immunofluorescent mid-sections of AOs showing markers for basal cells (KRT14), club cells (SCGB1A1), and cilia (acetylated α-tubulin). KRT14 is present exclusively in basally localized cells, SCGB1A1 stains luminal cells and multiple luminally secreted mucus clouds, and cilia cluster apically on luminal cells. Counterstained are the actin cytoskeleton (red) and nuclei (blue). Scale bars equal 50 µm.* ***d****,* ***e****, Gene set enrichment analysis plots showing strong enrichment of indicated gene signatures in transcriptomes of three AO lines compared to three small intestinal organoid (SIO) lines. NES = normalized enrichment score, FDR = false discovery rate. See Supplementary Table 2 for signatures and leading-edge genes.* ***f****, Hierarchical clustering of the indicated AO and SIO lines. Analysis is based on the top 500 and bottom 250 expressed genes in averaged AO vs SIO transcripts (full list in Supplementary Table 2). Gradients depict the relative maximum and minimum values per transcript. Names and ranks of signature lung and intestinal genes are indicated.*

Airway organoids from patients with cystic fibrosis recapitulate central disease features and swell upon modulation of CFTR as well as activation of TMEM16A

Rectal organoids are being successfully used as functional model for cystic fibrosis (CF)[22], a multi-organ disease with extensive phenotypic variability caused by mutations in the CF transmembrane conductance regulator gene (CFTR)[23]. Following opening of the CFTR channel by cAMP-inducing agents (e.g. forskolin), anions and fluid are transported to the organoid lumen resulting in rapid organoid

swelling[24], allowing personalized *in vitro* drug screenings[25]. Modeling of the primarily affected CF lung epithelium has relied on air-liquid interface cultures and is complicated by limited cell expansion and lengthy differentiation protocols[26]. To assess the AO approach for CF disease modeling, we applied forskolin and observed a dose-dependent swelling response that was largely, but not entirely, abrogated upon chemical inhibition of CFTR (Fig. 2a, Extended Data Fig. 2a), indicating the presence of additional ion channels. Indeed, AOs – but not rectal organoids – swell upon addition of E_{act} (Fig. 2b, Extended Data Fig. 2a) an activator of the chloride channel TMEM16A[27,28]. We next established five AO lines from fresh or cryopreserved broncho-alveolar lavage fluid of independent CF patients (62% success rate, n=8). CF AOs presented a much thicker layer of apical mucus compared to patient matched rectal organoids and wild-type AOs (Fig. 2c, Extended Data Fig. 2b), recapitulating the *in vivo* CF phenotype. Forskolin-induced swelling was dramatically reduced in CF compared to wild-type AOs, correlated with severity of tested CFTR genotypes[29], and could be augmented with the CFTR modulators VX-770 and VX-809 (Fig. 2d, Extended Data Fig. 2c) in agreement with clinical data[30]. E_{act}-stimulation caused a swelling response similar to stimulation with forskolin ± VX-770 and VX-809 (Fig. 2d, Extended Data Fig. 2c). Taken together, these experiments establish that AO lines derived from small amounts of patient material can recapitulate central features of CF, a classic example of monogenic diseases.

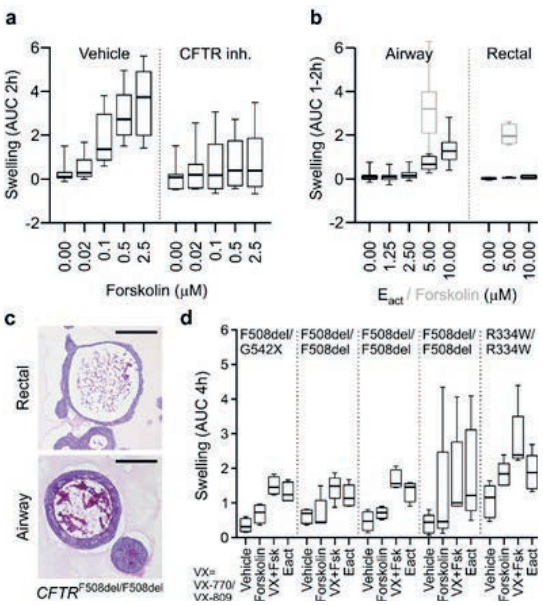

Figure 2. *Airway organoids to study cystic fibrosis.* ***a****, Box-and-Whisker plot showing concentration-dependent forskolin-induced swelling of AOs in the absence and presence of CFTR inhibitors CFTRinh-172 and GlyH101. Upon CFTR inhibition, swelling is noticeably decreased but not absent. Shown are pooled data from three different AO lines used in each of three independent experiments. AUC = area under the curve.* ***b****, Box-and-Whisker plot showing concentration-dependent E_{act}-induced swelling of AOs, but not rectal organoids (black outlines). Forskolin causes swelling in both organoid types (grey outlines). Shown are pooled data from three different AO and two different rectal organoid lines used in three to four independent experiments. Swelling was linear for 2h for AOs, but only 1h for rectal organoids. See Extended Data Fig. 2a for respective time course plots.* ***c****, Representative histological sections of periodic acid–Schiff (PAS) stained organoids from a CF patient with $CFTR^{F508del/F508del}$ mutation. Note the thick layer of PAS-positive polysaccharides apically lining the airway epithelium. Rectal organoids were generated from rectal biopsies, AOs were generated from broncho-alveolar lavages (BALs). Scale bars equal 50 µm. See Extended Data Fig. 2b for PAS-stained wild-type and $CFTR^{R334W/R334W}$ organoid sections.* ***d****, Box-and-Whisker plot showing swelling assays of several CF patient AO lines carrying the indicated CFTR mutations. Forskolin-induced swelling rarely exceeds vehicle controls in CF AOs, but increases in the presence of the CFTR-mutant modulating drugs VX-770 and VX-809. E_{act}-induced swelling exceeds forskolin-induced swelling to a similar extend as pre-treatment with VX-770 and VX-809 in four out of five CF AO lines. Shown are pooled data of four to five independent experiments. See Extended Data Fig. 2c for*

selected time course plots.

Generation of TP53 mutant airway organoids and selective expansion of tumoroids from primary and metastatic lung cancer.

We next tested if AOs can be used to model lung cancer, a global respiratory disease burden[31,32]. We have previously observed that remnants of normal epithelium in carcinoma samples will rapidly overgrow tumor tissue[13,15]. While we successfully generated organoid lines in the majority of cases (88% success rate, n=16), we could not selectively expand lung tumoroids by removing a single medium component (such as Wnt3A in colon tumoroids[15]), due to the diversity of mutated signaling pathways in lung cancer[31]. We reasoned Nutlin-3a[33] could drive *TP53* wild-type AOs into senescence or apoptosis and allow outgrowth of tumoroids with mutant p53, present in a large proportion of NSCLCs[34]. As proof of concept, we generated frameshift mutations in *TP53* of wild-type AOs with CRISPR-Cas9, causing Nutlin-3a resistance in selected sub-clones (Fig. 3a, Extended Data Fig. 3) due to lost p53 protein (Fig. 3b). Using Nutlin-3a selection, we indeed generated pure lung tumoroid lines from several NSCLC subtypes (including adenocarcinoma and large cell carcinoma) recapitulating fundamental histological characteristics of the respective primary tumors (Fig. 3c). In addition, we established pure tumoroid lines from needle biopsies of metastatic NSCLCs circumventing the need for Nutlin-3 selection (Fig. 3c, d) due to the absence of normal lung tissue (28% success rate, n=18). Hotspot DNA sequencing of selected cancer genes in tumoroids revealed loss- (e.g. *STK11*, *TP53*) and gain-of-function mutations (e.g. *KRAS*, *ERBB2*) (Fig. 3d, Supplementary Table 3). In conclusion, we show that AOs are amenable to subcloning and gene editing and we provide basic protocols for the selective outgrowth of p53 mutant TAOs from primary and metastatic NSCLCs.

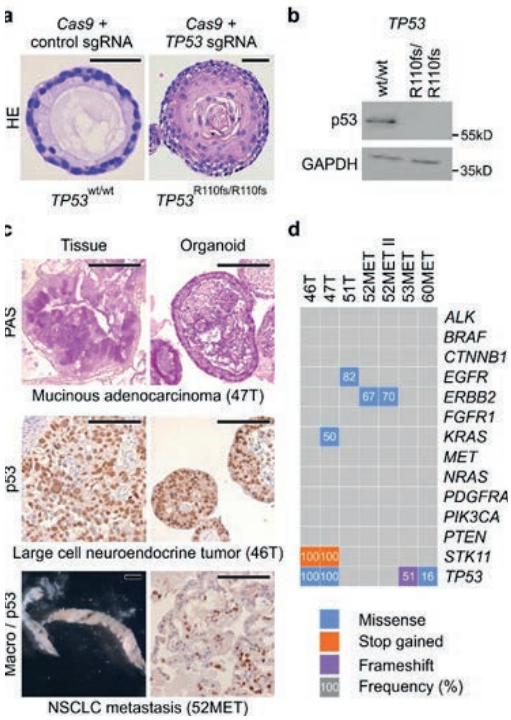

Figure 3. *Modeling lung cancer using airway organoids.* ***a****, Histology of representative control and engineered* $TP53^{R110fs/R110fs}$ *AO clones. Scale bars equal 100 µm.* ***b****, Western blot analysis of* $TP53^{wt}$ *and* $TP53^{R110fs/R110fs}$ *AOs show absence of p53 in the latter.* ***c****, Examples of TAOs derived from different resected primary lung cancer types (top and middle) as well as from a biopsy of metastatic NSCLC (bottom). Note the preservation of histological features between tissue-organoid pairs including PAS-positive mucus deposits, nuclear and cellular size abnormalities, and p53 immunolabelling. Scale bars equal 200 µm (histology) and 2 mm (macro).* ***d****, Mutation status of selected lung cancer genes in several TAO lines derived from primary as well as metastatic lung cancer. See Supplementary Table 3 for details. Note the preservation of mutant ERBB2 frequencies in 52MET and 52MET II TAOs, which have been derived from independent biopsies of the same cancer three months apart.*

RSV infection causes dramatic epithelial remodeling in airway organoids

Respiratory infections pose an even bigger global disease burden than genetic lung diseases[32]. RSV infections alone cause millions of annual hospital admissions and hundreds of thousands of deaths among young children[35] due to bronchiolitis, oedema, and abnormalities of the airway epithelium (necrosis, sloughing)[36]. Since disease pathology is incompletely understood, we tested if AOs can serve as *in vitro* model for RSV infection. RSV replicated readily in multiple AO lines (Fig. 4a, Supplementary Video 4) but failed to do so after pre-incubation with commercial palivizumab (an antibody against the RSV F-glycoprotein that prevents RSV-cell fusion) indicating specific virus-host interaction (Fig. 4b)[37]. Morphological analysis of RSV-infected AOs revealed massive epithelial abnormalities (Fig. 4c) that recapitulated *in vivo* phenomena including cytoskeletal rearrangements, apical extrusion of infected cells, and syncytia formation (Fig. 4c, d). We used time-lapse microscopy to visualize the underlying dynamics and surprisingly found RSV-infected AOs to rotate and move through BME to fuse with neighbouring AOs (Fig. 4e, Supplementary Video 4). Organoid motility was caused by increased motilities of all cells within RSV-infected AOs (Fig. 4f, Supplementary Videos 5-6). Mathematical modeling and simulation suggested organoid rotation to be the macroscopic manifestation of coordinated cell motilities (Extended Data Fig. 4, Supplementary Video 7). RNA-sequencing of RSV- vs mock-infected AOs showed strong enrichment for genes involved in interferon α/β signaling (particularly cytokines), which correlated with enrichment of migratory as well as of antiviral response genes (Fig. 4g, h, Supplementary Table 4). Enzyme-linked immunosorbent assays confirmed the secretion of significant quantities of cytokines such as IP-10 and RANTES from RSV-infected AOs (Fig. 4i). To test

whether secreted cytokines attract neutrophils (known to accumulate at RSV-infection sites *in vivo*[38]), we co-cultured RSV-infected AOs with freshly isolated primary human neutrophils. Time-lapse microscopy indeed showed preferential neutrophil recruitment to RSV-infected AOs compared to mock controls (Fig. 4j, Supplementary Videos 8 and 9) allowing experimental dissection of immune cell interaction with RSV-infected airway epithelium *ex vivo*. Mechanistically, the non-structural protein NS2 has been shown to induce the shedding of dead cells *in vivo*, leading to airway obstructions as well as to be required for efficient propagation of the virus *in vivo*[39,40]. RSV$^{\Delta NS2}$ indeed replicated less efficiently than RSV^{wt} in AOs (Fig. 4k, Supplementary Video 10), while inducible overexpression of NS2 alone in non-infected AOs induced motility and fusion of RSV-infected AOs, underlining the crucial role of the protein in the modification of the behaviour of the infected cell (Fig. 4l, Extended Data Fig. 5, Supplementary Video 11). Taken together, RSV-infected AOs recapitulate central disease features and reveal their underlying highly dynamic epithelial remodeling.

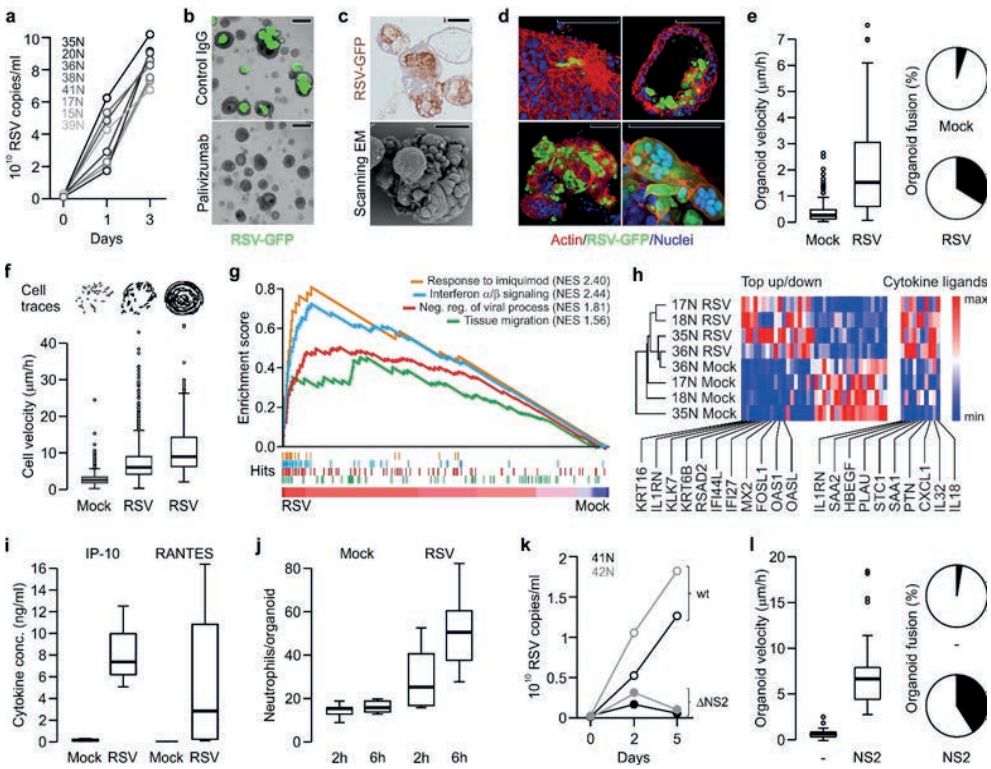

Figure 4. *Modeling RSV infection with airway organoids.* ***a,*** *Quantitative PCR showing RSV replication kinetics in the indicated AO lines. b, Representative phase contrast/GFP overlays of RSV-infected AOs (5d post infection). GFP signal is absent following pre-incubation with palivizumab (fusion blocking antibody) but not control IgG. Scale bars equal 100 µm.* ***c****, Immunohistochemical RSV-staining (top) and scanning electron micrograph (bottom) of RSV-infected AOs (5d post infection) show organoid fusion and blebbing. Scale bars equal 50 µm.* ***d****, 3D reconstructions of immunolabeled*

AOs 3d after RSV-infection showing (clockwise) cytoskeletal rearrangements, apical extrusion of infected cells, syncytia formation, and organoid fusion. Scale bars equal 50 µm. ***e****, RSV infection causes increased organoid velocity (Box-and-Whisker plot) and organoid fusion (pie chart). See also Supplementary Video 4.* ***f****, Cells within RSV-infected organoids are more motile than cells in control organoids irrespective of induced organoid rotation. Cell traces above individual Box-and-Whisker plots are from representative organoids. See also Extended Data Fig. 4 and Supplementary Videos 5-6.* ***g****, GSEA plots showing strong enrichment of indicated gene signatures in transcriptomes of four independently RSV- vs Mock-infected AO lines. NES = normalized enrichment score. See Supplementary Table 4 for signatures and leading-edge genes.* ***h****, Hierarchical clustering of the indicated AO lines displaying the 36 most differentially expressed genes of RSV- vs Mock-infected AO transcripts as well as selected cytokines (see Supplementary Table 4). Gradients depict the relative maximum and minimum values per transcript. Names and ranks of selected genes involved in migration (KRT16, KRT6B), interferon signaling (IL1RN, IFI44L), and viral response (MX2, OAS1) are indicated.* ***i****, ELISA-based quantification of cytokines secreted by Mock- vs RSV-infected AOs.* ***j****, Box-and-Whisker plot showing increased numbers of primary human neutrophils populating RSV- compared to Mock-infected AOs. See also Supplementary Videos 8 and 9.* ***k****, Quantitative PCR showing replication kinetics of wild-type (wt) and mutant RSV lacking NS2 (ΔNS2) in the indicated AO lines. See also Supplementary Video 10. l, Inducible overexpression of NS2 causes increased organoid velocity (Box-and-Whisker plot) and fusion (pie chart). See Extended Data Fig. 5, Supplementary Video 11.*

Discussion

Here we describe a versatile approach to establishing adult human airway epithelial organoids, containing all major cellular elements. We show the relative ease with which these can be grown from small amounts of routinely obtained patient material and provide evidence that the technology allows long-term expansion of such organoids from healthy individuals, but also from patients with a hereditary (CF) or malignant lung disease (NSCLC). We exploit the potential to derive sub-clones from AOs to demonstrate the feasibility of CRISPR gene editing. Finally, we show that AOs readily allow modeling of viral infections such as RSV and for the first time demonstrate the possibility to study neutrophil-epithelium interaction in an organoid model. Taken together, we anticipate that human AOs will find broad applications in the study of adult human airway epithelium in health and disease.

Methods

Procurement of human material and informed consent

The collection of patient data and tissue for the generation and distribution of airway organoids has been performed according to the guidelines of the European Network of Research Ethics Committees (EUREC) following European, national, and local law [1]. In the Netherlands, the responsible accredited ethical committees reviewed and approved the studies in accordance with the *'Wet medisch-wetenschappelijk onderzoek met mensen'* (medical research involving human subjects act)[2]. The medical ethical committee UMC Utrecht (METC UMCU) approved protocols 07-125/C (isolation and research use of neutrophils from healthy donors), TCBio 15-159 (isolation and research use of broncho-alveolar lavage fluid of CF patients), and TCBio 14-008 (generation of organoids from rectal biopsies of CF patients). The *'Verenigde Commissies Mensgebonden Onderzoek'* of the St. Antonius Hospital Nieuwegein approved protocol Z-12.55 (collection of blood, generation of normal and tumor organoids from resected surplus lung tissue of NSCLC patients). The Medical Ethics Committees of the Netherlands

Cancer Institute Amsterdam approved PTC14.0929/M14HUP (collection of blood, generation of normal and tumor organoids from resected surplus lung tissue of NSCLC patients), and PTC14.0928/M14HUM (generation of tumor organoids from biopsies of metastatic NSCLC). All patients participating in this study signed informed consent forms approved by the responsible authority. In all cases, patients can withdraw their consent at any time, leading to the prompt disposal of their tissue and any derived material. AOs established under protocols Z-12.55, PTC14.0929/M14HUP, and PTC14.0928/M14HUM were biobanked through Hubrecht Organoid Technology (HUB, www.hub4organoids.nl). Future distribution of organoids to any third (academic or commercial) party will have to be authorized by the METC UMCU/TCBio at request of the HUB in order to ensure compliance with the Dutch medical research involving human subjects' act.

Tissue processing

Solid lung tissue was minced, washed with 10 ml AdDF+++ (Advanced DMEM/F12 containing 1x Glutamax, 10 mM HEPES, and antibiotics) and digested in 10 ml airway organoid medium (Supplementary Table 1) containing 1-2 mg·ml^{-1} collagenase (Sigma-C9407) on an orbital shaker at 37°C for 1-2 h. The digested tissue suspension was sequentially sheared using 10 ml and 5 ml plastic and flamed glass Pasteur pipettes. After every shearing step the suspension was strained over a 100 µm filter with retained tissue pieces entering a subsequent shearing step with ~10 ml AdDF+++. 2% FCS was added to the strained suspension before centrifugation at 400 rcf. The pellet was resuspended in 10ml AdDF+++ and centrifuged again at 400 rcf. In case of a visible red pellet, erythrocytes were lysed in 2 ml red blood cell lysis buffer (Roche-11814389001) for 5 min at room temperature before the addition of 10 ml AdDF+++ and centrifugation at 400 rcf. Broncho-alveolar lavage fluid was collected and incubated with 10 ml airway organoid medium containing 0.5 mg·ml^{-1} collagenase (Sigma-C9407), 0.5% (w·v^{-1}) Sputolysin (Boehringer Ingelheim-SPUT0001), 250 ng·ml^{-1} amphotericin B, and 10 µg·ml^{-1} gentamicin on an orbital shaker at 37°C for 10-30 min. Next, the suspension was mildly sheared using a 1 ml pipet tip and strained over a 100 µm filter. 2% FCS was added to the strained suspension before centrifugation at 400 rcf. The pellet was resuspended in 10ml AdDF+++ and centrifuged again at 400 rcf.

Organoid culture

Lung cell pellets were resuspended in 10 mg·ml^{-1} cold Cultrex growth factor reduced BME type 2 (Trevigen-3533-010-02) and 40 µl drops of BME-cell suspension were allowed to solidify on prewarmed 24-well suspension culture plates (Greiner- M9312) at 37°C for 10-20 min. Upon completed gelation, 400 µl of AO medium were added to each well and plates transferred to humidified 37°C / 5% CO_2 incubators at ambient O_2. Medium was changed every 4 days and organoids were passaged every 2 weeks: cystic organoids were resuspended in 2 ml cold AdDF+++ and mechanically sheared through flamed glass Pasteur pipettes. Dense (organoids were dissociated by resuspension in 2 ml TrypLE Express (Invitrogen-12605036), incubation for 1-5 min at room temperature, and mechanical shearing through flamed glass Pasteur pipettes. Following the addition of 10 ml AdDF+++ and centrifugation at 300 rcf or 400 rcf respectively, organoid fragments were resuspended in cold BME and reseeded as above at ratios (1:1 – 1:6) allowing the formation of new organoids. Single cell suspensions were initially seeded at high density and reseeded at a lower density after ~1 week. NSCLC organoids could be distinguished from normal regular cystic organoids by morphology (size, irregular shape, thick organoid walls, dense)

as well as histology. Separation from normal AOs was achieved by manual separation and in case of *TP53* mutations by the addition of 5 µM Nutlin-3 (Cayman Chemicals-10004372) to the culture medium. Intestinal organoids were cultured as previously described [3].

Luminescent viability assay

Single cell suspensions from AOs were generated as described and counted. $3{\cdot}10^3$ cells per replicate were plated in BME and incubated in AO medium as described. At the indicated time points, the medium was removed and organoids were lysed in CellTiter Glo 3D (Promega) according to the manufacturer's instructions. Luminescence was measured using a microplate luminometer (Berthold Technologies).

Electron microscopy

For transmission EM, organoids were placed in BME on 3 mm diameter and 200 µm depth standard flat carriers for high pressure freezing and immediately cryoimmobilized using a Leica EM high-pressure freezer (equivalent to the HPM10), and stored in liquid nitrogen until further use. They were freeze-substituted in anhydrous acetone containing 2% osmium tetroxide and 0.1% uranyl acetate at –90°C for 72 hours and warmed to room temperature at 5ºC per hour (EM AFS-2, Leica). The samples were kept for 2 h at 4ºC and 2 h at room temperature. After several acetone rinses (4x 15 min), samples were infiltrated with Epon resin during 2 days (acetone: resin 3:1 3 h; 2:2 – 3 h; 1:3 – overnight; pure resin- 6 h + overnight + 6 h + overnight + 3 h). Resin was polymerised at 60ºC during 48 hours. Ultrathin sections from the resin blocks were obtained using an UC6 ultramicrotome (Leica) and mounted on Formvar-coated copper grids. Grids were stained with 2% uranyl acetate in water and lead citrate. Sections were observed in a Tecnai T12 Spirit electron microscope equipped with an Eagle 4kx4k camera (FEI Company) and large EM overviews were collected using the principles and software described earlier [4]. For scanning EM, organoids were removed from BME, washed with excess AdDF+++, fixed for 15 min with 1% (v/v) glutaraldehyde (Sigma) in phosphate buffered saline (PBS) at room temperature, and transferred onto 12 mm poly-L-lysine coated coverslips (Corning). Samples were subsequently serially dehydrated by consecutive 10 min incubations in 2 ml of 10% (v/v), 25% (v/v) and 50% (v/v) ethanol-PBS, 75% (v/v) and 90% (v/v) ethanol-H_2O, and 100% ethanol (2x), followed by 50% (v/v) ethanol-hexamethyldisilazane (HMDS) and 100% HMDS (Sigma). Coverslips were removed from the 100% HMDS and air-dried overnight at room temperature. Organoids were manipulated with 0.5 mm tungsten needles using an Olympus SZX9 light microscope and mounted onto 12 mm specimen stubs (Agar Scientific). Following gold-coating to 1 nm using a Q150R sputter coater (Quorum Technologies) at 20 mA, samples were examined with a Phenom PRO table-top scanning electron microscope (Phenom-World).

Time-lapse microscopy

Bright-field AO time-lapse movies were recorded at 37°C and 5% CO_2 on an AF7000 microscope equipped with a DFC420C camera using LAS AF software (all Leica). Bright-field cilia movement was recorded using the same set-up equipped with a Hamamatsu C9300-221 high speed CCD camera (Hamamatsu Photonics) at 150 frames per second using Hokawo 2.1 imaging software (Hamamatsu Photonics). Confocal imaging was performed using the following microscopes at 37°C and 5% CO_2: SP8X

(Leica), LSM710, LSM800 (both Zeiss), and Ultraview VoX spinning disk (Perkin Elmer).

Fixed immunofluorescence microscopy and immunohistochemistry

Organoids were removed from BME, washed with excess AdDF+++, fixed for 15 min in 4% paraformaldehyde, permeabilized for 20 min in 0.2% Triton X-100 (Sigma), and blocked for 45 min in 1% BSA. Organoids were incubated with primary antibodies over night at 4°C (anti-Keratin 14, Biolegend 905301; anti-SCGB1A1, Santa Cruz sc-9773; anti-acetylated α-tubulin Santa Cruz sc-23950; anti-Mucin 5AC, Santa Cruz sc-21701), washed three times with PBS, incubated with secondary antibodies (Invitrogen) over night at 4°C, washed two times with PBS, incubated with indicated additional stains (DAPI, life technologies D1306, phalloidin-atto 647, Sigma 65906), washed two times with PBS, and mounted in VECTASHIELD hard-set antifade mounting medium (Vectorlabs). Samples were imaged on SP5 and SP8X confocal microscopes using LAS X software (all Leica) and processed using ImageJ. For histological analysis, tissue and organoids were fixed in 4% paraformaldehyde followed by dehydration, paraffin embedding, sectioning, and standard HE and PAS stainings. Immunohistochemistry was performed using antibody against P53 (Santa Cruz, sc-126), GFP (Life technologies, A11122), and RSV (Abcam, ab35958). Images were acquired on a Leica Eclipse E600 microscope and processed using the Adobe Creative Cloud software package.

RNA sequencing

AOs derived from three independent human donors were collected 6 days after splitting (at passage 16, 18 and 19, respectively). Small intestinal organoids were also derived from three different human donors and collected 2 days after splitting (passage 7). Total RNA was isolated from the collected organoids using RNeasy kit (QIAGEN) according to manufacturer's protocol including DNaseI treatment. Quality and quantity of isolated RNA was checked and measured with Bioanalyzer2100 RNA Nano 6000 chips (Agilent, Cat. 5067-1511). Library preparation was started with 500ng of total RNA using the Truseq Stranded Total RNA kit with Ribo-Zero Human/Mouse/Rat set A and B by Illumina (Cat. RS-122-2201 and RS-122-2202). After preparation, libraries were checked with Bioanalyzer2100 DNA High Sensitivity chips (Cat. 5067-4626) as well as Qubit (Qubit® dsDNA HS Assay Kit, Cat. Q32854), all samples had a RIN value of 10. Libraries were equimolarly pooled to 2 nM and sequenced on the Illumina Nextseq, 2x75bp high output (loaded 1.0-1.4 pM of library pools). Samples were sequenced to an average depth of 9.4 million mapped reads (SD 2.6 million). After sequencing, quality control, mapping and counting analyses were performed using our in-house RNA analysis pipeline v2.1.0 (https://github.com/CuppenResearch/RNASeq), based on best practices guidelines (https://software.broadinstitute.org/gatk/guide/article?id=3891). In short, sequence reads were checked for quality by FastQC (v0.11.4) after which reads were aligned to GRCh37 using STAR (v2.4.2a) and add read groups using Picard perform quality control on generated BAM files using Picard (v1.141). Samples passing QC were then processed to count reads in features using HTSeq-count (v0.6.1). Read counting for genes (ENSEMBL definitions GRCh37, release 74) resulted in a 12 sample count matrix with Ensembl gene identifiers. DeSeq (v1.18.0) was used for read normalisation and differential expression analysis. Gene set enrichment analysis (GSEA) was performed using signature gene lists for airway basal cells [5], club cells [6], cilia [5], small airway epithelial cells [7], and lung [8] against normalized RNA-seq reads of three AO and three SIO lines using GSEA software v3.0 beta2 [9,10]. Normalized RNA-seq reads were averaged per organoid type and sorted by the

log_2 transformed ratio of AO over SIO. The 500 highest and 250 lowest transcripts were plotted using Morpheus (https://software.broadinstitute.org/morpheus) and CorelDraw X7.

RNA preparation and qRT-PCR

Total RNA was isolated from three independent lung organoid stains after 6, 12, 24, and 48 hrs upon either Wnt activation or Wnt inhibition by using RNeasy kit (QIAGEN). To inhibit Wnt signaling, 6 days after splitting the culture media of lung organoids was changed to media lacking R-spondin and included IWP2 (3 μM, Stemgent). To activate Wnt signaling, Chir (3 μM) was added to the culture media 6 days after splitting. cDNA was synthesized from 1 μg of total RNA using GoScript (Promega). Quantitative PCR was performed in triplicate using the indicated primers, SYBR green, and BioRad systems. Gene expression was quantified using the ΔΔCt method and normalized by HPRT.

Target	Forward Sequence (5'- 3')	Reverse Sequence (5'- 3')
HPRT	AAGAGCTATTGTAATGACCAGT	CAAAGTCTGCATTGTTTTGC
NKX2-1	ACCAAGCGCATCCAATCTCA	CAGAGCCATGTCAGCACAGA
HOXA5	CGAGCCACAAATCAAGCACA	GAATTGCTCGCTCACGGAAC
CDH1	TTACTGCCCCCAGAGGATGA	TGCAACGTCGTTACGAGTCA
CLDN1	CTGTCATTGGGGGTGCGATA	CTGGCATTGACTGGGGTCAT
KRT5	GCATCACCGTTCCTGGGTAA	GACACACTTGACTGGCGAGA
SCGB1A1	TCCTCCACCATGAAACTCGC	AGGAGGGTTTCGATGACACG
DNAH5	AGAGGCCATTCGCAAACGTA	CCCGGAAAATGGGCAAACTG
NPHP1	CAGAGCCACATGGCAACCTA	ACCCAGCCACAGCTTAACTC
AGR2	TCAGAAGCTTGGACCGCATC	AGTGTAGGAGAGGGCCACAA
UCHL1	GACGAATGCCTTTTCCGGTG	AGAAGCGGACTTCTCCTTGC
ID2	GCAGCACGTCATCGACTACA	TTCAGAAGCCTGCAAGGACA
ABCA3	CACCAGGGGCTCTCTAGACT	ACAGCCATCGTCTTGCTGAA
SFTPA1	CAGACGGGACCCCTGTAAAC	CCTGTCATTCCACTGCCCAT
SFTPC	ATGGATGTGGGCAGCAAAGA	CAGCAGGGAATGCCAAATCG
LGR5	CACCGCTCTCAGTCACTGGATAAGC	AAACGCTTATCCAGTGACTGAGAGC
LGR6	CCAAGGACAGTTTCCCAAAA	GACTCCTCATCATCAAGGTGAA
AXIN2	AGCTTACATGAGTAATGGGG	AATTCCATCTACACTGCTGTC
TROY	TGATGAAAGTAGGCAGGGCTGTGT	TCTCCAGCCAGTGTTTGTCCTTGA

Functional organoid swelling assay

Organoid swelling assays were performed as previously described [11]. Intestinal organoids were cultured for 7 days, collected, and disrupted. Smallest fragments were selected and seeded for swelling assays. AOs were sheared, passed through a 70 μm strainer and cultured for 4 days. Organoids were harvested and seeded for swelling assays in 96-well plates (Greiner). We seeded 50-100 organoids in 5 μl drops (50% BME) per well overlaid with 100 μl culture medium after gel solidification. Cultures were incubated for 24 h with or without CFTR-targeting drugs VX-809 and VX-770 (3 μM and 1 μM, respectively, Selleck Chemicals). The next day, cultures were pre-incubated for 3 h with CFTR-inhibitors (150 μM CFTRinh-172 and 150 μM GlyH101, Cystic Fibrosis Foundation Therapeutics) as indicated. Calcein green (3 μM,

Invitrogen) was added 1 h prior to stimulation with forskolin (Selleck Chemicals), E_{act} (Calbiochem), or DMSO (Sigma) at the indicated concentrations. Organoids were imaged per well (every 10 min, for 60-120 min in total or every 30 min, for 270 min in total) using confocal live cell microscopy (Zeiss LSM710 and LSM800) at 37°C and 5% CO_2. Data was analyzed using Volocity 6.1.1 (Perkin Elmer), Zen Blue (Zeiss) and Prism 5 and 6 (GraphPad).

TP53 editing

The organoid lipofection protocol was followed as previously described [12,13] with a few adaptations. Briefly, AOs grown in full organoid media were trypsinized for 20 min at 37°C and sheared with a glass pipette to produce single cells. After dissociation, cells were resuspended in 450 µl growth medium and plated in 48-well plates at a confluency of >90%. For each transfection, a total of 1.5 µg of plasmid DNA (sgRNA, Cas9) in 50 µl of serum-free medium (Opti-MEM; Gibco) were mixed with 4 µl of Lipofectamine 2000 (Invitrogen) in 50 µl of serum-free medium making up a total volume of 100 µl, which was then added to the cells. The plate was centrifuged at 600g at 32°C for 1 h and incubated for 4-5 h at 37°C before the cells were embedded in Basement Membrane Extract (BME;Amsbio) in full organoid medium. 10 µM of Nutlin-1 (Cayman Chemicals) were added to the cultures 1 day after transfection and maintained for 16-20 days for mutant *P53* selection. For clonal expansion, single organoids were picked. At least two human AO lines were used for engineering mutant *P53* organoids. For sequencing, genomic DNA was isolated using Viagen Direct PCR (Viagen). Primers for PCR amplification using GoTaq Flexi DNA polymerase (Promega) were: *P53*_for, 5′-CAGGAAGCCAAAGGGTGAAGA-3′, *P53*_rev, 5′-CCCATCTACAGTCCCCCTTG-3′. PCR products were purified using the QIAquick PCR purification kit (Qiagen) and cloned into pGEM-T Easy vector system I (Promega), followed by sequencing using the T7 primer. The sgRNA *P53* sequence was specifically designed to target exon 3 of the *P53* gene and was: 5′-GGGCAGCTACGGTTTCCGTCGUUUUA-3

Western blotting

Samples were lysed using SDS lysis buffer (50 mM Tris HCl pH 6.8, 2% SDS) supplemented with Complete Protease Inhibitors (Roche). Protein concentration was determined using Nanodrop Lite (Thermo Scientific) and equal amounts of protein were loaded on SDS-PAGE gels before transferring on PVDF membranes (Millipore). Membranes were blocked in 5% milk (diluted in 0.01% PBS-Tween) and incubated overnight with antibodies against: P53 (Santa Cruz, sc-126) and GAPDH (Abcam, ab-9485).

Hot-spot sequencing

AO gDNA was isolated using the DNeasy blood & tissue kit (Qiagen). A minimum of 100ng gDNA was submitted for sequencing cancer hotspots of Ion AmpliSeq™ Cancer Hotspot Panel v2Plus at the NGS Core of the UMC Utrecht. The following exons were (partially) covered:

Gene	ENST-nr.	Covered Exons															
ABL1	ENST00000318560.5	4	5	6	7												
AKT1	ENST00000349310.3	3	6														
ALK	ENST00000389048.3	22	23	24													

APC	ENST00000257430.4	14															
ARAF	ENST00000377045	6															
ATM	ENST00000278616.4	8	9	12	17	26	34	35	36	39	50	54	55	56	59	61	63
BRAF	ENST00000288602.6	11	15														
CALR	ENST00000316448	9															
CDH1	ENST00000261769.4	3	8	9													
CDKN2A	ENST00000304494.5	2															
CRAF (RAF1)	ENST00000251849	6															
CSF1R	ENST00000286301.3	7	22														
CTNNB1	ENST00000349496.5	3															
EGFR	ENST00000275493.2	3	7	15	18	19	20	21									
ERBB2	ENST00000269571.4	19	20	21	22	23	24										
ERBB4	ENST00000342788.4	3	4	6	7	8	9	15	23								
EZH2	ENST00000320356.2	16															
FBXW7	ENST00000281708.3	5	8	9	10	11											
FGFR1	ENST00000425967.3	4	7														
FGFR2	ENST00000457416.2	5	7	10													
FGFR3	ENST00000440486.2	7	9	14	16	18											
FLT3	ENST00000241453.7	11	14	16	20												
GNA11	ENST00000078429.4	5															
GNAQ	ENST00000286548.4	5															
GNAS	ENST00000371095.3	8	9														
HNF1A	ENST00000257555.4	3	4														
HRAS	ENST00000311189.7	2	3														
IDH1	ENST00000345146.2	4															
IDH2	ENST00000330062.3	4															
JAK2	ENST00000381652.3	14															
JAK3	ENST00000458235.1	4	13	16													
KDR	ENST00000263923.4	6	7	11	19	21	26	27	30								
KIT	ENST00000288135.5	2	9	10	11	13	14	15	17	18							
KRAS	ENST00000311936.3	2	3	4													
MDM2	ENST00000462284.1	6	7	8	9												

MET	ENST00000397752.3	2	11	14	16	19											
MLH1	ENST00000231790.2	12															
MPL	ENST00000372470.3	10															
MYD88	ENST00000396334	5															
NOTCH1	ENST00000277541.6	25	27	37													
NPM1	ENST00000296930.5	11															
NRAS	ENST00000369535.4	2	3	4													
PDGFRA	ENST00000257290.5	12	14	15	18												
PIK3CA	ENST00000263967.3	2	5	7	8	10	14	19	21								
PTEN	ENST00000371953.3	1	3	5	6	7	8										
PTPN11	ENST00000351677.2	3	13														
RB1	ENST00000267163.4	4	6	10	11	14	17										
RET	ENST00000355710.3	10	11	13	15	16											
SMAD4	ENST00000342988.3	3	4	5	6	8	9	10	11	12							
SMAR-CB1	ENST00000263121.7	3	4	5	9												
SMO	ENST00000249373.3	3	5	6	9	11											
SRC	ENST00000373578.2	14															
TP53	ENST00000420246.2	2	4	5	6	7	8	10									
VHL	ENST00000256474.2	1	2	3													

RSV infection of AOs

rgRSV224 (GFP version), rrRSV (RFP version), rgRSV P-eGFP-M (RSV^{wt}), and rgRSVΔNS2 13A ΔNS2 6120 P-eGFP-M ($RSV^{\Delta NS2}$) were produced as previously described [14-16]. For infection, AOs were washed in cold AdDF+++ and sheared with a flamed Pasteur pipette. Per infection, 2 µl virus (~$5{\cdot}10^7$ pfu·ml^{-1}) was placed in a U-bottom suspension 96-well and 50µl of sheared organoids (~500000 cells) in AdDF+++ were added. Empty wells were filled with PBS to prevent dehydration. Plates were incubated for 5 h at 37°C and 5% CO_2. Afterwards, contents of the wells was taken up in AdDF+++ and washed three times with excess AdDF+++. Organoids were seeded as described before. Alternatively, individual AOs were microinjected with ~250 nl virus in AdDF+++ (~$5{\cdot}10^7$ pfu·ml^1) using a micromanipulator and -injector (Narishige, M-152 and IM-5B) under a stereomicroscope (Leica, MZ75).

Single-cell tracking

Cells were manually tracked by following the center of mass of their nuclei using custom written image analysis software. Random cells were selected on the initial time frame so that they uniformly covered the organoid surface. In infected organoids, particularly when rotating rapidly, a small fraction of cells could not be identified between some consecutive time frames due to their fast movement, limiting

our ability to track the fastest-moving cells. In Fig. 4f and Extended Data Fig. 4b, three outliers were beyond the limits of the plot, reaching a maximum value of 117 μm·h^{-1}. Due to the difficulty of tracking fast-moving cells, outliers above 50 μm·h^{-1} are likely underrepresented. For each cell at each time point, RFP intensity was calculated by summing the pixel intensities within a disk of a radius of 5 pixels, corresponding to 3.22 μm, on the XY plane around the center of mass of the nucleus. To distinguish between RFP$^-$ and RFP$^+$ cells, an intensity threshold was manually chosen so that all nuclei in non-infected organoids were categorized as RFP$^-$.

Mathematical modeling of collective cell motility

To understand how local interactions between individual cells could give rise to collective rotational movement on the level of the organoid, we built a mathematical model of cells migrating within the constraints of the tissue they are embedded in. In our model, cells move on the surface of a sphere to mimic the organoid geometry. Each cell has a polarity vector $\bar{p}_i$ that represents the direction of migratory force production. However, cells are constrained by adhesive connections to neighboring cells. In our model, these connections are modeled by harmonic springs. In general, due to these adhesive constraints the total force $\bar{f}_i$ acting on each cell has a different orientation than the intrinsic polarity $\bar{p}_i$. We assume that cells change their internal polarity over time to align with the direction of $\bar{f}_i$. Crucially, this interaction causes neighboring cells to align their movement. To reproduce the random motility observed in non-infected cells, we assume the polarity direction also fluctuates in a stochastic manner. This effect perturbs synchronization of movement between neighboring cells. Cells are initially distributed uniformly over the surface of sphere, with random orientation for their polarity vectors. The force on cell *i* is given by the sum of the propulsive force in the direction of the polarity $\bar{p}_i$ and the spring forces $\bar{F}^{ij}$ due to the neighboring cells *j*:

$$\bar{F}_i = f_0 \bar{p}_i + \sum_j \bar{F}^{ij} \qquad (1)$$

The spring force between a pair of cells at positions $\bar{r}_i$ and $\bar{r}_j$ is given by:

$$\bar{F}^{ij} = -k(2\sigma - \|\bar{r}_j - \bar{r}_i\|)\frac{\bar{r}_j - \bar{r}_i}{\|\bar{r}_j - \bar{r}_i\|} \qquad (2)$$

where *k* is the spring constant. Here, σ corresponds approximately to the radius of the cell and, hence, the spring force is attractive when it is extended beyond its natural length 2σ and repulsive when compressed. The model is then described fully by two sets of ordinary differential equations, for the cell positions $\bar{r}_i$ and the cell polarities $\bar{p}_i$:

$$\frac{1}{\mu}\frac{d\bar{r}_i}{dt} = \bar{f}_i \qquad (3)$$

$$\frac{d\bar{p}_i}{dt} = [J\delta_i + \eta\xi(t)](\hat{e}_r^i \times \bar{p}_i) \qquad (4)$$

Here, cell movement is assumed to be overdamped, with μ the mobility. $\bar{f}_i$ is the projection of the total

force $\vec{F}_i$ in the local plane of cell *i*, i.e. $\vec{f}_i = \vec{F}_i - (\vec{F}_i \cdot \hat{e}_r^i) \cdot \hat{e}_r^i$, with $\hat{e}_r^i$ the unit vector orthogonal to the surface of the sphere at $\vec{r}_i$. The polarity vector $\vec{p}_i$ has length $\|\vec{p}_i\|=1$ and rotates with fixed angular velocity *J* in the direction that aligns it with $\vec{f}_i$. This direction is given by $\delta_i = \cos\theta_i/|\cos\theta_i|$, where θ_i is the angle between $\vec{p}_i$ and $\vec{f}_i$ and $\cos\theta_i = \left(\vec{p}_i \times \vec{f}_i/|\vec{f}_i|\right) \cdot \hat{e}_r^i$. In addition, we incorporate intrinsic stochastic fluctuations to the direction of cell polarity by the noise term $\xi(t)$, with noise strength η. In the absence of cell-cell communication, i.e. for *J*=0, the polarity vector $\vec{p}_i(t)$ will undergo a random walk that causes the polarity to deviate from its original polarity over time. Specifically, the correlation in polarity direction decreases in time as $\langle \vec{p}_i(0) \cdot \vec{p}_i(t) \rangle = e^{-t/\tau}$, where $\tau = \frac{2}{\eta^2}$ is the polarity persistence time.

Simulation of the mathematical model

To generate random initial configurations of *N* particles distributed approximately equidistantly on a sphere with radius $\frac{\rho}{\sigma} = \sqrt{\frac{N}{4\phi}}$, where ϕ is the cellular packing faction, particles were first placed at random positions on the sphere and then propagated using the spring force in Eq. (2) between nearest neighbors until global mechanical equilibrium was attained. At the start of the simulation, we assigned each particle *i* a polarity vector $\vec{p}_i$ with a random orientation in the tangent plane of the sphere at position $\vec{r}_i$ and determined the identity of the neighboring particles connected by a spring to particle *i* using Delauney triangulation. Equations (3) and (4) were integrated using the Euler-Maruyama method, with time-step $\mu k \cdot \Delta t = 5 \cdot 10^{-3}$. To ensure that the position $\vec{r}_i$ and polarity vector $\vec{p}_i$ remain well-defined throughout the simulation, after each time step we projected $\vec{p}_i(t+\Delta t)$ onto the tangent plane of the sphere at the new position $\vec{r}_i(t+\Delta t)$ and normalized the position and polarity so that $\|\vec{r}_i(t+\Delta t)\|=1$ and $\|\vec{p}_i(t+\Delta t)\|=1$. Simulations were performed with *N* =100, ϕ =1 and $\frac{f_0}{\sigma k}=1$, while we varied the parameters $\frac{J}{\mu k}$ and $\frac{\eta}{\mu k}$. While we use dimensionless parameters here, in the main text we use, without any loss of generality, parameters values for $\mu, k, \sigma = 1$.

Multiplex Immunoassays

AOs were infected with/without RSV as described. 3d after infection equal numbers of AOs were released from Matrigel using Cell Recovery Solution (Corning), washed, and replated overnight in 30µl AO medium as hanging drops. The next morning supernatants were collected and selected cytokines measured using an in-house developed and validated multiplex immunoassay (Laboratory of Translational Immunology, UMC Utrecht) based on Luminex technology (xMAP, Luminex Austin TX USA). The assay was performed as described previously[17]. Acquisition was performed with the Biorad FlexMAP3D (Biorad laboratories, Hercules USA) in combination with xPONENT software version 4.2 (Luminex). Data was analyzed by 5-parametric curve fitting using Bio-Plex Manager software, version 6.1.1 (Biorad).

Neutrophil isolation and co-culture with AOs

Human neutrophils were isolated from sodium-heparin anticoagulated venous blood of healthy donors by density gradient centrifugation with and Ficoll (Amersham Biosciences). Erythrocytes were lysed in ammonium chloride buffer (155 mM NH4Cl; 10 mM KHCO3; 0.1 mM EDTA in double-distilled H2O; pH = 7.2) and neutrophils were resuspended in RPMI 1640 (Life Technologies, Paisley, UK) supplemented with 10% (v/v) HI FBS (Biowest, Nuaillé, France) and 50 U/ml Penicillin-Streptomycin (Thermo Fisher Scientific,

Waltham, MA, USA). Purity of isolated neutrophils was analyzed using the CELL-DYN Emerald (Abbott Diagnostics, Illinois, USA). 100,000 freshly isolated neutrophils were co-seeded in BME with AOs that had been infected with/without RSV 3d earlier. Immediately after BME solidification, drops were overlaid with AO medium and live imaged as described. For quantification, neutrophils were labeled with 1µM Hoechst33342 prior to imaging with 3D confocal microscopy and the number of neutrophils attached to AOs with/without RSV counted 2h and 6h post cell-organoid-mixing.

Generation of inducible dTomato and RSV-NS2/dTomato overexpressing AO lines

The following sequence comprising humanized NS1, GS linker, FLAG tag, HA tag, P2A sequence, humanized NS2, GS linker, V5 tag, 6xHis tag, and T2A sequence flanked by EcoRI restriction sites was synthesized by Integrated DNA Technologies (Leuven, Belgium) and cloned into IDT Vector Amp Blunt:

gaattcgccaccATGGGCAGCAACTCCCTGAGCATGATCAAAGTGCGGCTGCAGAACCTGTTCGACAACGAC-
GAAGTCGCACTGCTCAAGATCACATGCTACACCGACAAGCTCATCCACCTGACCAACGCCCTGGCAAAGGCAGT-
GATCCACACTATCAAACTGAACGGTATCGTGTTCGTGCACGTCATCACCAGCAGCGACATCTGCCCTAACAA-
CAACATCGTCGTCAAGTCCAACTTCACAACAATGCCCGTGCTGCAGAACGGCGGCTACATCTGGGAGATGAT-
GGAGCTCACACACTGCTCCCAGCCCAACGGACTGATCGACGACAACTGCGAGATCAAGTTCTCCAAGAAGCT-
GAGCGACTCCACCATGACCAACTACATGAACCAGCTCTCCGAGCTGCTGGGATTCGACCTCAACCCTggcggcg-
gcggctcgggaggaggaggaagcgactacaaggacgacgatgacaagTACCCCTACGACGTGCCCGACTACGCCggaagcg-
gaGCTACTAACTTCAGCCTGCTGAAGCAGGCTGGAGACGTGGAGGAGAACCCTGGACCTATGGACACCACCCA-
CAACGACACCACTCCACAGCGGCTGATGATCACCGACATGCGGCCACTGTCCCTGGAGACCACCATCACCTCCCT-
GACCCGCGACATCATCACCCACCGGTTCATCTACCTGATCAACCACGAGTGCATCGTGCGGAAGCTGGACGAG-
CGGCAGGCCACCTTCACCTTCCTGGTGAACTACGAGATGAAGCTGCTGCACAAAGTCGGCAGCACCAAGTA-
CAAGAAGTACACTGAGTACAACACCAAATACGGCACCTTCCCAATGCCCATCTTCATCAACCACGACGGCTTCCT-
GGAGTGCATCGGCATCAAGCCCACAAAGCACACTCCCATCATCTACAAATACGACCTCAACCCTggtggtggtg-
gttcaggaggaggatcgGGTAAGCCTATCCCTAACCCTCTCCTCGGTCTCGATTCTACGCATCATCACCATCACCACg-
gaagcggaGAGGGCAGAGGAAGTCTGCTAACATGCGGTGACGTCGAGGAGAATCCTGGACCTgaattc. Humanized RSV-NS sequences were from Lo et al.[18], 2A sequences from Kim et al.[19]. EcoRI-tdTomato-NotI was amplified from pCSCMV:tdTomato using primers aagaattcatggtgagcaagggcgagg and ctgcggccgcttacttg-tacagctcgtccat and cloned into pLVX-TetOne™-Puro (Clontech) yielding an inducible dTomato lentiviral overexpression plasmid. EcoRI-hNS2-GS-V5-His-T2A-EcoRI was amplified from the IDT Vector using primers taccctcgtaaagaattcgccaccATGGACACCACCCACAACG and cttgctcaccatgaattcAGGTCCAGGATTCT and cloned into pLVX-TetOne-Puro-tdTomato yielding an inducible hNS2/dTomato lentiviral overexpression plasmid. Virus was generated and organoids infected as previously described[20]. Infected organoids were selected with 1 µg·ml^{-1} puromycin (Sigma). Expression was induced with 5 µM doxycycline (Sigma).

References for Methods

1 Lanzerath, D. *EUREC - Information - Germany*, <http://www.eurecnet.org/information/germany.html > (2011).

2 Borst-Eilers, E. S., W. *Wet medisch-wetenschappelijk onderzoek met mensen*, <http://wetten.overheid.nl/BWBR0009408/2016-08-01> (1998).

3 Sato, T. *et al.* Long-term expansion of epithelial organoids from human colon, adenoma, adenocarcinoma, and Barrett's epithelium. *Gastroenterology* **141**, 1762-1772, doi:10.1053/j.gastro.2011.07.050 (2011).

4 Faas, F. G. *et al.* Virtual nanoscopy: generation of ultra-large high resolution electron microscopy maps. *J Cell Biol* **198**, 457-469, doi:10.1083/jcb.201201140 (2012).

5 Dvorak, A., Tilley, A. E., Shaykhiev, R., Wang, R. & Crystal, R. G. Do airway epithelium air-liquid cultures represent the *in vivo* airway epithelium transcriptome? *Am J Respir Cell Mol Biol* **44**, 465-473, doi:10.1165/rcmb.2009-0453OC (2011).

6 Treutlein, B. *et al.* Reconstructing lineage hierarchies of the distal lung epithelium using single-cell RNA-seq. *Nature* **509**, 371-375, doi:10.1038/nature13173 (2014).

7 Hackett, N. R. *et al.* RNA-Seq quantification of the human small airway epithelium transcriptome. *BMC Genomics* **13**, 82, doi:10.1186/1471-2164-13-82 (2012).

8 Lindskog, C. *et al.* The lung-specific proteome defined by integration of transcriptomics and antibody-based profiling. *FASEB J* **28**, 5184-5196, doi:10.1096/fj.14-254862 (2014).

9 Mootha, V. K. *et al.* PGC-1alpha-responsive genes involved in oxidative phosphorylation are coordinately downregulated in human diabetes. *Nat Genet* **34**, 267-273, doi:10.1038/ng1180 (2003).

10 Subramanian, A. *et al.* Gene set enrichment analysis: a knowledge-based approach for interpreting genome-wide expression profiles. *Proc Natl Acad Sci U S A* **102**, 15545-15550, doi:10.1073/pnas.0506580102 (2005).

11 Dekkers, J. F. *et al.* A functional CFTR assay using primary cystic fibrosis intestinal organoids. *Nat Med* **19**, 939-945, doi:10.1038/nm.3201 (2013).

12 Schwank, G. *et al.* Functional repair of CFTR by CRISPR/Cas9 in intestinal stem cell organoids of cystic fibrosis patients. *Cell stem cell* **13**, 653-658, doi:10.1016/j.stem.2013.11.002 (2013).

13 Drost, J. *et al.* Sequential cancer mutations in cultured human intestinal stem cells. *Nature* **521**, 43-47, doi:10.1038/nature14415 (2015).

14 Guerrero-Plata, A. *et al.* Differential response of dendritic cells to human metapneumovirus and respiratory syncytial virus. *Am J Respir Cell Mol Biol* **34**, 320-329, doi:10.1165/rcmb.2005-0287OC (2006).

15 Hallak, L. K., Collins, P. L., Knudson, W. & Peeples, M. E. Iduronic acid-containing glycosaminoglycans on target cells are required for efficient respiratory syncytial virus infection. *Virology* **271**, 264-275, doi:10.1006/viro.2000.0293 (2000).

16 Liesman, R. M. *et al.* RSV-encoded NS2 promotes epithelial cell shedding and distal airway obstruction. *J Clin Invest* **124**, 2219-2233, doi:10.1172/JCI72948 (2014).

17 de Jager, W., te Velthuis, H., Prakken, B. J., Kuis, W. & Rijkers, G. T. Simultaneous detection of 15 human cytokines in a single sample of stimulated peripheral blood mononuclear cells. *Clin Diagn Lab Immunol* **10**, 133-139 (2003).

18 Lo, M. S., Brazas, R. M. & Holtzman, M. J. Respiratory syncytial virus nonstructural proteins NS1 and NS2 mediate inhibition of Stat2 expression and alpha/beta interferon responsiveness. *J Virol* **79**, 9315-9319, doi:10.1128/JVI.79.14.9315-9319.2005 (2005).

19 Kim, J. H. *et al.* High cleavage efficiency of a 2A peptide derived from porcine teschovirus-1 in human cell lines, zebrafish and mice. *PLoS One* **6**, e18556, doi:10.1371/journal.pone.0018556 (2011).

20 Koo, B. K. *et al.* Controlled gene expression in primary Lgr5 organoid cultures. *Nat Methods* **9**, 81-83, doi:10.1038/nmeth.1802 (2011).

References for main text

1 Barkauskas, C. E. *et al.* Lung organoids: current uses and future promise. *Development* **144**, 986-997, doi:10.1242/dev.140103 (2017).

2 Benali, R. *et al.* Tubule formation by human surface respiratory epithelial cells cultured in a three-dimensional collagen lattice. *Am J Physiol* **264**, L183-192 (1993).

3 Wong, A. P. *et al.* Directed differentiation of human pluripotent stem cells into mature airway epithelia expressing functional CFTR protein. *Nat Biotechnol* **30**, 876-882, doi:10.1038/nbt.2328 (2012).

4 Huang, S. X. *et al.* Efficient generation of lung and airway epithelial cells from human pluripotent stem cells. *Nat Biotechnol* **32**, 84-91, doi:10.1038/nbt.2754 (2014).

5 Dye, B. R. *et al. In vitro* generation of human pluripotent stem cell derived lung organoids. *Elife* **4**, doi:10.7554/eLife.05098 (2015).

6 Rock, J. R. *et al.* Basal cells as stem cells of the mouse trachea and human airway epithelium. *Proc Natl Acad Sci U S A* **106**, 12771-12775, doi:10.1073/pnas.0906850106 (2009).

7 Tadokoro, T. *et al.* IL-6/STAT3 promotes regeneration of airway ciliated cells from basal stem cells. *Proc Natl Acad Sci U S A* **111**, E3641-3649, doi:10.1073/pnas.1409781111 (2014).

8 Tan, Q., Choi, K. M., Sicard, D. & Tschumperlin, D. J. Human airway organoid engineering as a step toward lung regeneration and disease modeling. *Biomaterials* **113**, 118-132, doi:10.1016/j.biomaterials.2016.10.046 (2017).

9 Hild, M. & Jaffe, A. B. Production of 3-D Airway Organoids From Primary Human Airway Basal Cells and Their Use in High-Throughput Screening. *Curr Protoc Stem Cell Biol* **37**, IE 9 1-IE 9 15, doi:10.1002/cpsc.1 (2016).

10 Chen, Y. W. *et al.* A three-dimensional model of human lung development and disease from pluripotent stem cells. *Nat Cell Biol* **19**, 542-549, doi:10.1038/ncb3510 (2017).

11 Boj, S. F. *et al.* Organoid models of human and mouse ductal pancreatic cancer. *Cell* **160**, 324-338, doi:10.1016/j.cell.2014.12.021 (2015).

12 Huch, M. *et al.* Long-term culture of genome-stable bipotent stem cells from adult human liver. *Cell* **160**, 299-312, doi:10.1016/j.cell.2014.11.050 (2015).

13 Karthaus, W. R. *et al.* Identification of multipotent luminal progenitor cells in human prostate organoid cultures. *Cell* **159**, 163-175, doi:10.1016/j.cell.2014.08.017 (2014).

14 Sato, T. *et al.* Long-term expansion of epithelial organoids from human colon, adenoma, adenocarcinoma, and Barrett's epithelium. *Gastroenterology* **141**, 1762-1772, doi:10.1053/j.gastro.2011.07.050 (2011).

15 van de Wetering, M. *et al.* Prospective derivation of a living organoid biobank of colorectal cancer patients. *Cell* **161**, 933-945, doi:10.1016/j.cell.2015.03.053 (2015).

16 Dvorak, A., Tilley, A. E., Shaykhiev, R., Wang, R. & Crystal, R. G. Do airway epithelium air-liquid cultures represent the *in vivo* airway epithelium transcriptome? *Am J Respir Cell Mol Biol* **44**, 465-473, doi:10.1165/rcmb.2009-0453OC (2011).

17 Hackett, N. R. *et al.* RNA-Seq quantification of the human small airway epithelium transcriptome. *BMC Genomics* **13**, 82, doi:10.1186/1471-2164-13-82 (2012).

18 Lindskog, C. *et al.* The lung-specific proteome defined by integration of transcriptomics and antibody-based profiling. *FASEB J* **28**, 5184-5196, doi:10.1096/fj.14-254862 (2014).

19 Treutlein, B. *et al.* Reconstructing lineage hierarchies of the distal lung epithelium using single-cell RNA-seq. *Nature* **509**, 371-375, doi:10.1038/nature13173 (2014).

20 de Lau, W., Peng, W. C., Gros, P. & Clevers, H. The R-spondin/Lgr5/Rnf43 module: regulator of Wnt signal strength. *Genes Dev* **28**, 305-316, doi:10.1101/gad.235473.113 (2014).

21 Oeztuerk-Winder, F. & Ventura, J. J. The many faces of p38 mitogen-activated protein kinase in progenitor/stem cell differentiation. *Biochem J* **445**, 1-10, doi:10.1042/BJ20120401 (2012).

22 Noordhoek, J., Gulmans, V., van der Ent, K. & Beekman, J. M. Intestinal organoids and personalized medicine in cystic fibrosis: a successful patient-oriented research collaboration. *Curr Opin Pulm Med* **22**, 610-616, doi:10.1097/MCP.0000000000000315 (2016).

23 Ratjen, F. *et al.* Cystic fibrosis. *Nat Rev Dis Primers* **1**, 15010, doi:10.1038/nrdp.2015.10 (2015).

24 Dekkers, J. F. *et al.* A functional CFTR assay using primary cystic fibrosis intestinal organoids. *Nat Med* **19**, 939-945, doi:10.1038/nm.3201 (2013).

25 Dekkers, J. F. *et al.* Characterizing responses to CFTR-modulating drugs using rectal organoids derived from subjects with cystic fibrosis. *Sci Transl Med* **8**, 344ra384, doi:10.1126/scitranslmed.aad8278 (2016).

26 Fulcher, M. L., Gabriel, S., Burns, K. A., Yankaskas, J. R. & Randell, S. H. Well-differentiated human airway epithelial cell cultures. *Methods Mol Med* **107**, 183-206 (2005).

27 Namkung, W., Yao, Z., Finkbeiner, W. E. & Verkman, A. S. Small-molecule activators of TMEM16A, a calcium-activated chloride channel, stimulate epithelial chloride secretion and intestinal contraction. *FASEB J* **25**, 4048-4062, doi:10.1096/fj.11-191627 (2011).

28 Sondo, E., Caci, E. & Galietta, L. J. The TMEM16A chloride channel as an alternative therapeutic target in cystic fibrosis. *Int J Biochem Cell Biol* **52**, 73-76, doi:10.1016/j.biocel.2014.03.022 (2014).

29 Sosnay, P. R. *et al.* Defining the disease liability of variants in the cystic fibrosis transmembrane conductance regulator gene. *Nat Genet* **45**, 1160-1167, doi:10.1038/ng.2745 (2013).

30 Kuk, K. & Taylor-Cousar, J. L. Lumacaftor and ivacaftor in the management of patients with cystic fibrosis: current evidence and future prospects. *Ther Adv Respir Dis* **9**, 313-326, doi:10.1177/1753465815601934 (2015).

31 Chen, Z., Fillmore, C. M., Hammerman, P. S., Kim, C. F. & Wong, K. K. Non-small-cell lung cancers: a heterogeneous set of diseases. *Nat Rev Cancer* **14**, 535-546, doi:10.1038/nrc3775 (2014).

32 Ferkol, T. & Schraufnagel, D. The global burden of respiratory disease. *Ann Am Thorac Soc* **11**, 404-406, doi:10.1513/AnnalsATS.201311-405PS (2014).

33 Vassilev, L. T. *et al. In vivo* activation of the p53 pathway by small-molecule antagonists of MDM2. *Science* **303**, 844-848, doi:10.1126/science.1092472 (2004).

34 Deben, C., Deschoolmeester, V., Lardon, F., Rolfo, C. & Pauwels, P. TP53 and MDM2 genetic alterations in non-small cell lung cancer: Evaluating their prognostic and predictive value. *Crit Rev Oncol Hematol* **99**, 63-73, doi:10.1016/j.critrevonc.2015.11.019 (2016).

35 Nair, H. *et al.* Global burden of acute lower respiratory infections due to respiratory syncytial virus in young children: a systematic review and meta-analysis. *Lancet* **375**, 1545-1555, doi:10.1016/S0140-6736(10)60206-1 (2010).

36 Borchers, A. T., Chang, C., Gershwin, M. E. & Gershwin, L. J. Respiratory syncytial virus--a comprehensive review. *Clin Rev Allergy Immunol* **45**, 331-379, doi:10.1007/s12016-013-8368-9 (2013).

37 Huang, K., Incognito, L., Cheng, X., Ulbrandt, N. D. & Wu, H. Respiratory syncytial virus-neutralizing monoclonal antibodies motavizumab and palivizumab inhibit fusion. *J Virol* **84**, 8132-8140, doi:10.1128/JVI.02699-09 (2010).

38 Geerdink, R. J., Pillay, J., Meyaard, L. & Bont, L. Neutrophils in respiratory syncytial virus infection: A target for asthma prevention. *J Allergy Clin Immunol* **136**, 838-847, doi:10.1016/j.jaci.2015.06.034 (2015).

39 Liesman, R. M. *et al.* RSV-encoded NS2 promotes epithelial cell shedding and distal airway obstruction. *J Clin Invest* **124**, 2219-2233, doi:10.1172/JCI72948 (2014).

40 Teng, M. N. & Collins, P. L. Altered growth characteristics of recombinant respiratory syncytial viruses which do not produce NS2 protein. *J Virol* **73**, 466-473 (1999).

Acknowledgements

We would like to acknowledge Carmen Lopez-Iglesias for supporting high pressure freezing and freeze substitution. We thank Raimond Ravelli for providing transmission EM overview software and Antoni P.A. Hendrickx for help with scanning EM. We acknowledge Anko de Graaff and the Hubrecht Imaging Center for supporting light microscopy. We thank Inez Bronsveld for obtaining intestinal biopsies. We thank the WKZ Pediatric Pulmonology Department for obtaining lavage fluid. We are grateful to Stieneke van der Brink and Nilofar Ehsani for preparing media. Genetically modified RSV variants were generously provided by Peter Collins, Mark E. Peeples, and Ulla Buchholz. We thank the Multiplex Core facility of the LTI UMC Utrecht for developing, validating, and performing immunoassays.

Work at the Hubrecht Institute was supported by MKMD and VENI grants from the Dutch Organization of Scientific Research NWO (ZonMw 114021012 and 916.15.182), a Stand Up to Cancer International Translational Cancer Research Grant (a program of the Entertainment Industry Foundation administered by the AACR) and an Alpe d'Huze/KWF program grant (2014-7006). The spinning disk microscope is funded by NWO equipment grant 834.11.002. Work in the laboratory of S.J.T. is part of the research program of the Foundation for Fundamental Research on Matter (FOM), as part of NWO. The work of G.H. and J.S.Z. was supported by a NWO VIDI grant (680-47-529) and a HFSP Career Development Award (CDA00076/2014-C). Work at the St. Antonius Hospital was supported by the Prof. Dr. Jaap Swierenga Foundation (development of human lung organoids). J.M.B., D.Z., and C.K.E. were supported by a grant from The Netherlands Organisation for Health Research and Development (ZonMW 40-00812-98-14103) and the Dutch Cystic Fibrosis Society (HIT-CF program).

Author contributions

N.S. designed, performed, and analysed experiments and wrote the manuscript. N.S. and D.D.Z. designed, performed, and analysed swelling experiments. A.P. generated and analysed *TP53* mutant organoids. N.S., I.H., A.L., J.L., and A.O. performed and analysed RNA sequencing experiments. L.B. performed and analysed viability assays. N.S., D.K., F.W., M.F.M.O., K.K.D., E.F.S., E.E.V., C.H.M.M., C.K.E., S.F.B., R.G.V., and J.M.B. organized lung tissue collection. G.H.P., E.P.O, S.J.T., and J.S.Z. tracked and modelled single cell migration in RSV-infected organoids. N.S., L.T., and S.D. performed RSV infection experiments. J.K. and H.B. performed histology. M.F.M.O. classified lung tumors and evaluated organoid histology. K.K. and S.D. produced virus stocks. N.I. and P.J.P. performed transmission electron microscopy. M.C.V. quantified RSV replication. N.S. and E.R. generated organoid lines. M.L. isolated neutrophils. H.C. supervised the study.

Conflict of interest

N.S., H.C., J.M.B. and C.K.E. are inventors on patents/patent applications related to organoid technology.

Supplementary information

Extended Data Fig. 1

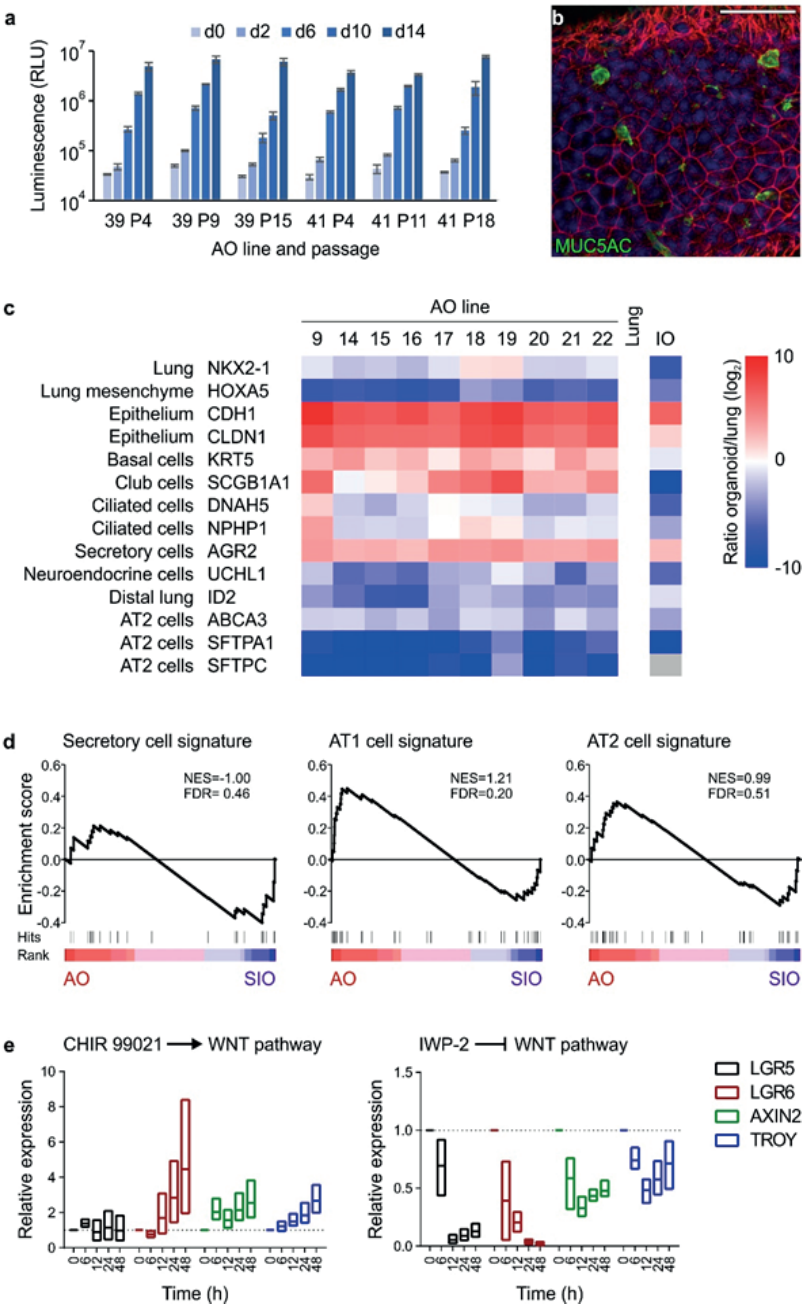

Extended Data Figure 1. *Further characterization of airway organoids.* ***a****, Luminescent cell viability assay comparing proliferative capacity of two independently generated AO lines at early, mid, and late passage numbers. Per group, 3000 cells were seeded and their expansion was measured at the indicated time points. Error bars represent standard deviations of technical triplicates.* ***b,*** *Immunofluorescent bottom-section of an AO showing secretory cell marker MUC5AC (green). Counterstained are the actin cytoskeleton (red) and nuclei (blue). Scale bar equals 50 µm.* ***c,*** *Heat map showing qPCR results of marker gene expression in ten individual AO lines compared to whole lung and one intestinal organoid line. Data are shown as log_2-transformed ratio of sample over whole lung. AOs express lung cell marker NKX2-1 at comparable levels to whole lung (pale blue to pale red), while being negative for lung mesenchymal marker gene HOXA5 (dark blue) and strongly positive for general epithelial markers CDH1 and CLDN1 (dark red). AOs furthermore express relatively more KRT5 (basal cell marker), SCGB1A1 (club cell marker), and AGR2 (secretory cell marker). Ciliated cell markers DNAH5 and NPHP1 are expressed at similar levels in AOs and whole lung (pale blue to pale red). AOs express less of neuroendocrine marker UCHL1, distal lung marker ID2, and AT2 markers ABCA3, SFTPA1, and SFTPC (white to dark blue). The intestinal organoid line is positive for epithelial, basal, and secretory cell markers (pale red to red), and negative for general lung, lung mesenchyme, club cell, ciliated cell, neuroendocrine cell, distal lung, and AT2 cell markers (pale blue to dark blue).* ***d,*** *Gene set enrichment analysis plots showing no enrichment of the indicated gene signatures in transcriptomes of three AO lines compared to three small intestinal organoid (SIO) lines. NES = normalized enrichment score, FDR = false discovery rate. See auxiliary data table S1 for signatures and leading-edge genes.* ***e,*** *Box plots showing changes in the expression of stem cell marker and WNT target genes over time following manipulation of the WNT pathway. Upon strong activation of the WNT pathway using GSK-3 inhibitor CHIR 99021, LGR5 expression remains unaltered, while expression of AXIN2 and TROY is moderately and expression of LGR6 is strongly increased. Upon blocking the WNT pathway with porcupine inhibitor IWP-2, LGR5 and LGR6 expression drops sharply, while AXIN2 and TROY expression is decreased moderately. Analysis is based on three independent experiments using AO lines 15, 17, and 26.*

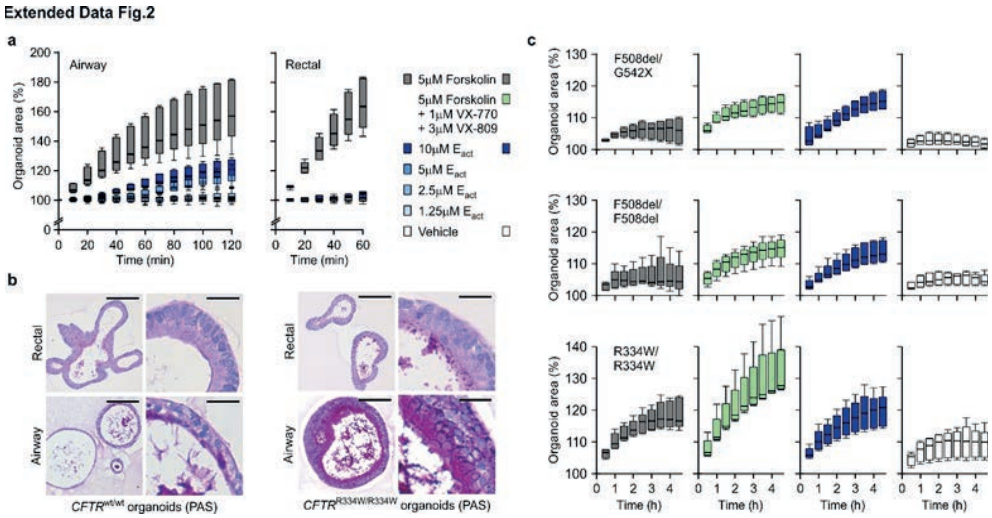

Extended Data Figure 2. *Additional data of airway organoids to study cystic fibrosis.* ***a****, Box-and-Whisker plots showing organoid swelling over time following stimulation with forskolin or* E_{act}*. While forskolin causes swelling in both organoid types (grey boxes),* E_{act} *causes concentration-dependent swelling only of AOs (blue hued boxes). Shown are pooled data from three different AO and two different rectal organoid lines used in three to four independent experiments. See Figure 2a, b for the respective AUC plots.* ***b****, Representative histological sections of PAS-stained wild-type organoids (unmatched, left panel) and organoids from a CF patient with* $CFTR^{R334W/R334W}$ *mutation (right panel). PAS-positive mucus is occasionally present within wild-type AOs but not rectal wild-type organoids, while the CF patient AOs regularly show thick layers of PAS-positive mucus. Rectal organoids from the same CF patient display only occasional regions with PAS-positive mucus. Rectal organoids were generated from rectal biopsies, AOs were generated from lung resection (wild-type) or BAL-fluid (CF patient). Scale bars equal 50 µm (overviews) and 10 µm (details). See Figure 2c for PAS-stained* $CFTR^{F508del/F508del}$ *organoid sections.* ***c****, Box-and-Whisker plots showing CF patient AO swelling over time following addition of the indicated stimuli. The respective CFTR mutations are given atop every row of plots. Forskolin-induced swelling (grey boxes) does not exceed vehicle controls in AOs with* $CFTR^{F508del/G542X}$ *and* $CFTR^{F508del/F508del}$ *genotypes, but increases in the presence of VX-770 and VX-809 (green boxes). In the same organoids,* E_{act}*-induced swelling (blue boxes) exceeds forskolin-induced swelling to a similar extend. AOs with the milder* $CFTR^{R334W/R334W}$ *genotype bottom row) show moderate forskolin-induced swelling that is increased in the presence of VX-770 and VX-809 and paralleled by* E_{act}*-induced swelling. Shown are pooled data of four to five independent experiments. See Figure 2d for the corresponding AUC-plots.*

Extended Data Fig. 3

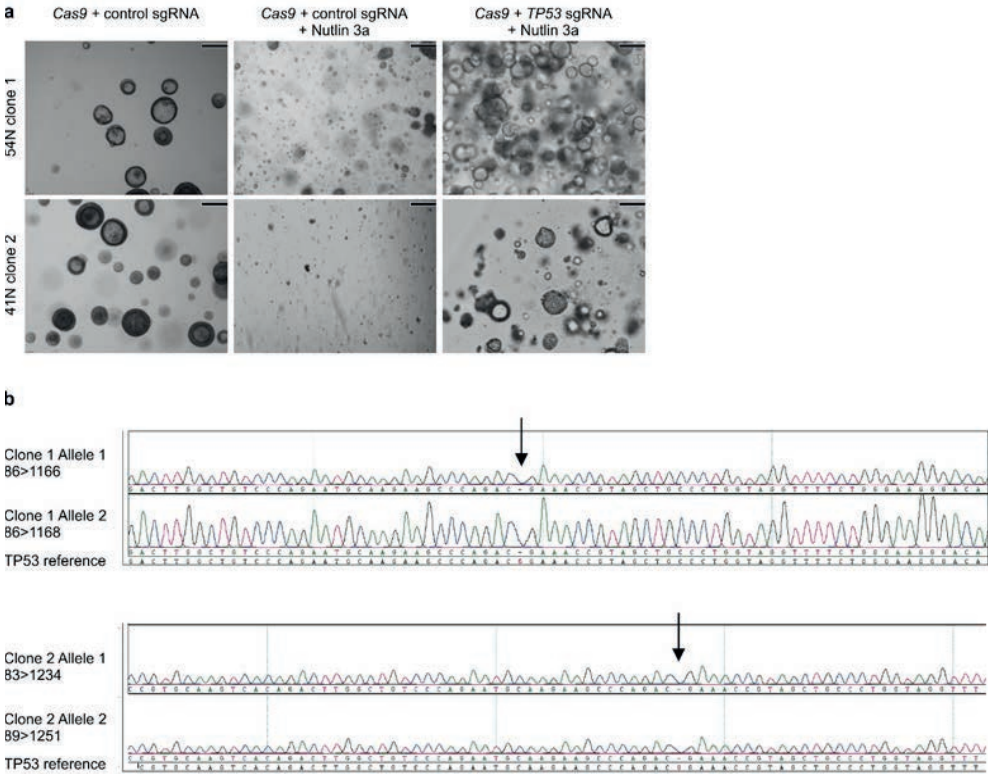

Extended Data Figure 3. *Additional data of TP53 edited AOs.* ***a****, Bright field images showing the effect of Nutlin 3a selection on two independently TP53 gene edited AO clones. While control AOs do not expand under selection (middle column), TP53 edited AO clones do (right column). Scale bars equal 100 µm.* ***b****, Sequencing chromatograms of TP53 edited AO clones showing bi-allelic generation of TP53 frame shifts.*

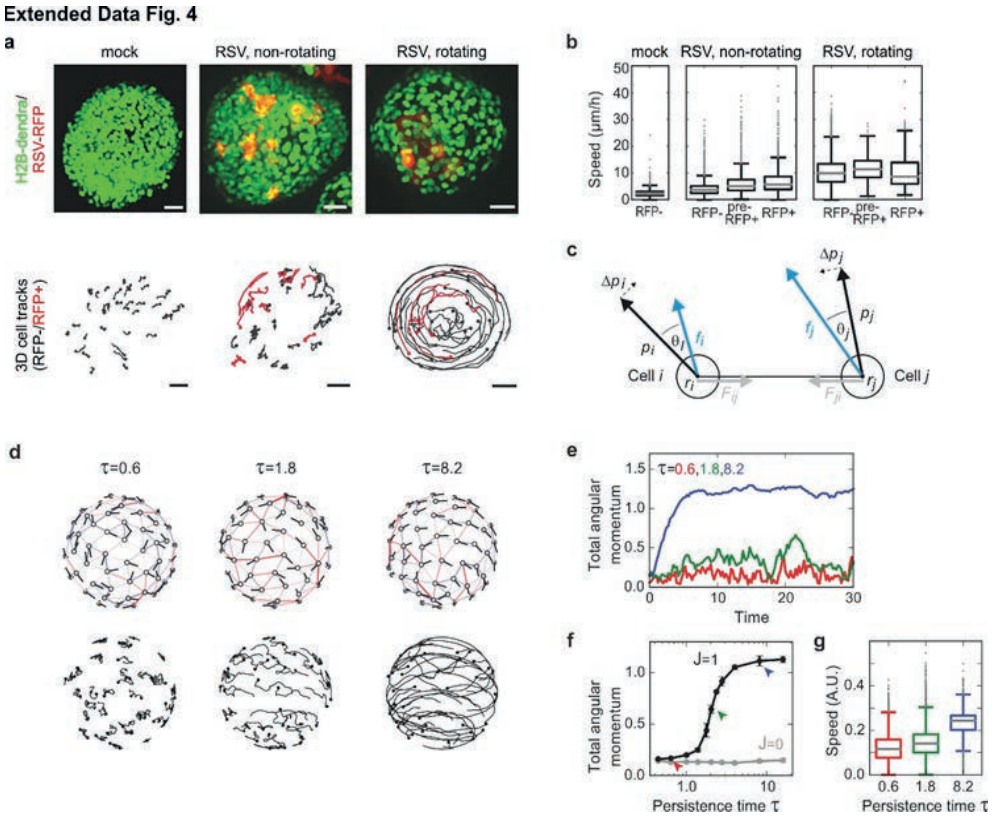

Extended Data Figure 4. *Single cell velocities of RSV-infected AOs and mathematical modeling of organoid rotation.* ***a****, Examples of non-infected (left), RSV-infected and non-rotating (middle), and RSV-infected and rotating (right) organoids with the corresponding tracks of randomly selected nuclei (n=41, 33, 35 respectively). Track durations are 14 h. Circles indicate the starting position of each track, and line color stands for either RPF- (black) or RFP+ (red) cells. Scale bars represent 25μm.* ***b****, Box plots of the speed distribution of every tracked nucleus at each time point for non-infected (n=3), infected but non-rotating (n=6) and infected and rotating (n=3) organoids, where 15-45 individual nuclei were tracked per organoid. For the infected organoids, nuclei were classified as RFP- when they showed no RFP signal for the duration of the track, pre-RFP+ when the nuclei showed no RFP signal yet but became RFP+ later, and RFP+ for nuclei that showed RFP signal.* ***c****, Vector schematic depicting the modeled relation between cells migrating within the constraints of an organoid sphere. See methods for details.* ***d****, Snapshots of the cell configuration (left) and cell tracks (right) for simulations with n=100 cells and increasing persistence time t=0.6, 1.8 and 8.2. The persistence time indicates the mean time over which the cell maintains its direction of polarization, in the absence of cell-cell interactions. White markers represent cell centers, with black lines showing the direction of the polarization vector. Adjacent cells are connected by springs, which are shown as colored lines. Springs are red when stretched and blue when compressed. Cell tracks are shown for the same time period for all three simulations, with black circles indicating the starting position of each track. See also Supplementary Video 7.* ***e****, Total angular momentum of the cell configuration as a function of time for simulations starting with random initial distribution of polarity vectors. For sufficiently high persistence time (=8.2, blue line), the cells rapidly establish rotational motion.* ***f****, Total steady state angular momentum as function of the persistence time , for simulations*

with cell-cell communication (black, =1) and without (grey, =0). Colored arrows indicate the persistence times corresponding to the simulations in panel e. ***g****, Box plots of the distribution of cell speed for the different persistence times in panel e. The distribution is calculated from n=5 independent simulations.*

Extended Data Fig. 5

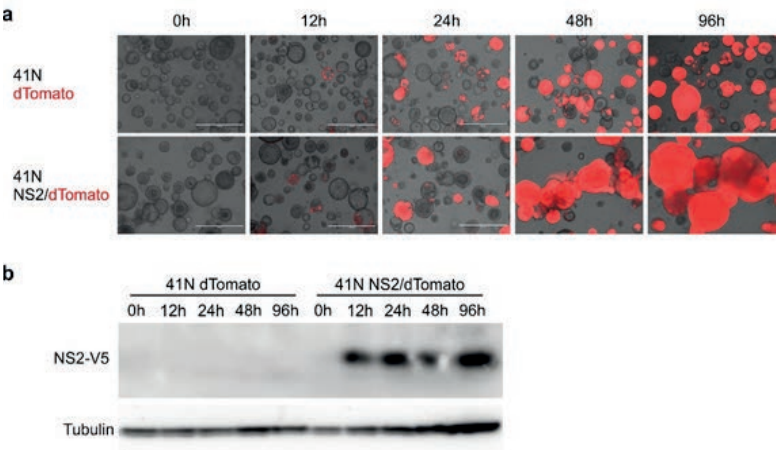

Extended Data Figure 5. *Inducible expression of NS2 in AOs.* ***a****, Brightfield/fluorescent micrographs of AOs inducibly overexpressing dTomato (top) or NS2 and dTomato (bottom) taken at the indicated time points following stimulation with doxycycline. While red signal increases in both lines, organoid fusion exclusively takes place in AOs expressing NS2. See Supplementary Video 11. Scale bars equal 400 µm.* ***b****, Western blots of protein lysates from the indicated AOs taken at the indicated time points following stimulation with doxycycline. NS2 protein is robustly detectable after 12h of stimulation.*

Supplementary Table 1 – Airway organoid media recipe

Media component	Signaling pathway		Supplier	Catalogue number	Final concentration
	activation	block			
R-Spondin 1	Wnt/b-catenin signaling		Peprotech	120-38	500 ng·ml^{-1}
FGF 7	FGFR2b signaling		Peprotech	100-19	25 ng·ml^{-1}
FGF 10	FGFR2b signaling		Peprotech	100-26	100 ng·ml^{-1}
Noggin	TGF-b signaling		Peprotech	120-10C	100 ng·ml^{-1}
A83-01	TGF-b signaling		Tocris	2939	500 nM
Y-27632	ROCK signaling		Abmole	Y-27632	5 mM
SB202190	p38 MAPK signaling		Sigma	S7067	500 nM
B27 supplement	a.o. insulin signaling		Gibco	17504-44	1x
N-Acetylcysteine	Antioxidant		Sigma	A9165-5g	1.25 mM
Nicotinamide	Co-enzyme precursor		Sigma	N0636	5 mM
GlutaMax 100x	Nutrient		Invitrogen	12634-034	1x
Hepes	Buffer		Invitrogen	15630-056	10 mM
Penicillin / Strepto-mycin	Antibiotics		Invitrogen	15140-122	100 U·ml^{-1} / 100 mg·ml^{-1}
Primocin	Antibiotic/antimycotic		Invivogen	Ant-pm-1	50 mg·ml^{-1}
Advanced DMEM/F12	Base medium		Invitrogen	12634-034	1x

Supplementary Tables 2, 3 and 4 are too extensive to present in this thesis:

Supplementary Table 2 – Transcriptome analysis AO vs SIO.

Supplementary Table 3 – Hotspot cancer gene sequencing of tumoroids

Supplementary Table 4 – Transcriptome analysis mock vs RSV-infected AOs.

Supplementary Videos are also part of this manuscript

CHAPTER 6

Human primary organoid cultures reveal off-target effects of TMEM16A inhibitor

D.D. Zomer-van Ommen[1,2], N. Sachs[3], B. Ponsioen[4], A.M. Vonk[1,2], E. Kruisselbrink[1,2], C.K. van der Ent[1], M.C. Hagemeijer[1,2], J.M. Beekman[1,2]

1. Pediatric Department, Wilhelmina Children's Hospital, University Medical Centre, Utrecht, the Netherlands, 2. Regenerative Medicine Centre, University Medical Centre, Utrecht, the Netherlands, 3. Clevers group, Hubrecht Institute, Utrecht the Netherlands, 4. Department of Medical Genetics, University Medical Centre, Utrecht, the Netherlands

Abstract

BACKGROUND Ion channel activators and inhibitors are widely used to functionally study epithelial ion transport. The ion channel Cystic Fibrosis Transmembrane Conductance Regulator (CFTR) plays a major role in ion and fluid homeostasis. Mutations in the *CFTR* gene can result in severely impaired chloride transport, leading to the disease cystic fibrosis. Transmembrane member 16A (TMEM16A) is currently being studied as alternative bypass channel for chloride secretion.

METHOD To determine functional activity of TMEM16A, we performed intestinal and airway organoid swelling assays upon CFTR and TMEM16A activation. We also tested a TMEM16A inhibitor T16Ainh-A01. Activity of T16AinhA01 was also measured in a fluorescence resonance energy transfer (FRET) assay.

RESULTS We measured dose-dependent swelling of both rectal and airway organoids upon incubation with TMEM16A inhibitor T16Ainh-A01, indicating cyclic AMP (cAMP) activation. This off-target effect of T16Ainh-A01 was confirmed in a FRET assay using non-primary HEK-293 cells.

CONCLUSIONS T16Ainh-A01 induced cAMP activation in both human primary organoids and a non-primary cell culture, which may lead to misinterpretation of functional data obtained using this inhibitor.

Introduction

Functional assays to study transepithelial ion secretion and fluid transport rely for a major part on chemical activators and inhibitors of ion channels, transporters and exchangers. In our laboratory, we study ion and fluid transport diseases, including cystic fibrosis (CF), in human primary rectal and airway epithelial organoids [1–3]. These 3D cultures have the ability to increase in size upon ion and subsequent fluid secretion into their lumen, and are therefore highly useful to quantitatively measure fluid secretion and ion channel function [1] (paper under review). Forskolin-induced swelling of the rectal organoids is solely dependent on the cystic fibrosis transmembrane conductance regulator (CFTR) protein, an epithelial anion channel activated via the cyclic adenosine monophosphate (cAMP) pathway [1] (paper under review). Airway organoids, however, possess other ion channels in addition to CFTR, including calcium-activated chloride channel and transmembrane member 16A (TMEM16A, anoctamin-1) (paper under review). TMEM16A is expressed on epithelial goblet cells and smooth muscle cells [4,5] and is being studied as potential therapeutic bypass channel to secrete chloride independent of the *CFTR* mutation [6,7]. To study the functional activity of TMEM16A, we applied TMEM16A activator E_{act} and inhibitor T16Ainh-A01 (Tocris) to organoid cultures [8]. Unexpectedly, we observed swelling, i.e. ion and fluid secretion, of both rectal and airway organoids upon incubation with the inhibitor. This observation was confirmed by fluorescence resonance energy transfer (FRET) experiments [9] in human embryonic kidney (HEK)-293 cells. These findings indicate that T16Ainh-A01 induced an off-target effect by activation cAMP, which may lead to misinterpretation of data.

Methods and materials

Generation and culturing of human primary intestinal and airway organoids

The generation of organoids from healthy lung tissue of non-small cell lung cancer patients obtained via resection was approved by the ethics committee of St. Antonius Hospital Nieuwegein (protocol Z-12.55). The medical ethical committee of the University Medical Center Utrecht (UMCU) approved the use of broncho-alveolar lavage fluid isolations and the generation of organoids from rectal biopsies (TCBio 15-159 and TCBio 14-008, respectively) in these studies. All participants from which primary cultures were used in this study signed an informed consent agreement. Rectal and airway organoids were generated and cultured as previously described [1,10] (paper under review).

Organoid swelling assay

Organoid swelling assays were performed as previously described [10] (paper under review). Organoids were pre-incubated for 3h with T16Ainh-A01 (various concentrations, Tocris) followed by stimulation with 2.5 µM forskolin, 10 µM TMEM16A activator E_{act} (a N-aroylaminothiazole) or DMSO (all purchased from Sigma). Three independent experiments were performed in triplicate. The average rectal organoid surface area per well (μm^2) was calculated at t=0 (after 3h of incubation with T16Ainh-A01 prior to stimulation). Organoid swelling induced by T16Ainh-A01 (purchased from Tocris and Sigma) was measured at t=0 and t=3h.

Fluorescence resonance energy transfer (FRET) assay

Exchange protein directly activated by cAMP 1 (Epac1). HEK-293 cells were grown on Willco dishes

(WillCo Wells) and transfected with the fourth-generation exchange protein directly activated by cAMP 1 (Epac1)-based FRET sensor for cAMP [9,11]. The cells were imaged on a Leica SP8-X inverted laser scanning confocal microscope (CLSM) using a 63x oil objective (NA 1.4). Donor fluorophores (mTurquoise2, mTurq2) were excited using Argon 458 nm laser light and emission of donor and acceptor fluorophores were collected at bandwidths of 462-505 and 515-600 nm, respectively. Time intervals were set at 10 seconds to accurately monitor FRET kinetics while working under non-phototoxic conditions. Compound addition (E_{act} or T16Ainh-A01) was preceded by mock-stimulation to control for pipetting artifacts and followed by 25 μM forskolin stimulation as a positive control. Post-acquisition image analysis was performed in custom-made macro scripts using ImageJ/Fiji, providing YFP/mTurq2 ratio traces for individually tracked cells. Three independent experiments were performed with at least in quadruple conditions. Changes in YFP/mTurq2 ratios upon were normalized to t=0 (0%) and forskolin ratio (100%).

Statistical analyses

Row-matched one-way ANOVA was performed to determine statistical differences in average organoid sizes. Paired t-tests were performed to determine statistical differences between FRET results of the baseline versus the compound tested (10 μM E_{act} or 100 μM T16Ainh-A01).

Results

Treatment for CF is improved by developing drugs that target the mutated ion channel CFTR and thereby improve chloride secretion [7]. TMEM16A is being explored as an alternative drug target to restore reduced chloride secretion in CF [6,7]. CFTR-mediated chloride and subsequent fluid secretion can be quantitatively studied in human primary organoids [1–3]. Little is known about the role of TMEM16A in rectal and airway organoids.

As such, to determine functional activity of TMEM16A in organoids, we assessed airway and rectal organoid swelling in absence or presence of an activator and inhibitor of this channel. The TMEM16A activator E_{act} induced swelling of airway organoids, which could be dose-dependently inhibited by T16Ainh-A01 pre-incubation (**Fig. 1a**). Maximal inhibition by inhibitor T16Ainh-A01 (Tocris) was achieved at 63 μM. As a control, we included forskolin, a cAMP activator known to maximally induce CFTR-mediated swelling [1]. Surprisingly, forskolin-induced swelling was also dose-dependently inhibited by T16Ainh-A01 in both airway and rectal organoids (Fig. 1a-b). E_{act} did not induce swelling in rectal organoids (**Fig. 1b**) confirming the absence of functional TMEM16A (paper under review). During the analysis of the raw image files of the organoids at t=0, we phenotypically observed pre-swollen organoids upon incubation with T16Ainh-A01 (representative images of rectal organoids in **Fig. 1c**). We quantitated the average surface area (in short 'size') of organoids after 3h of incubation with the inhibitor (**Fig. 1d-e**). The average size of airway organoids increased significantly upon incubation with 4 and 10 μM of T16Ainh-A01 (**Fig. 1d**, all p-values in **Table S1**). Rectal organoid sizes were increased significantly in size at 25 μM T16Ainh-A01 compared to the control and 4 μM T16Ainh-A01 conditions (**Fig. 1e**, p-values depicted in **Table S2**). These findings indicated that T16Ainh-A01 dose-dependently induced luminal fluid secretion, which impaired subsequent measurement of forskolin- and E_{act}-induced organoid swelling.

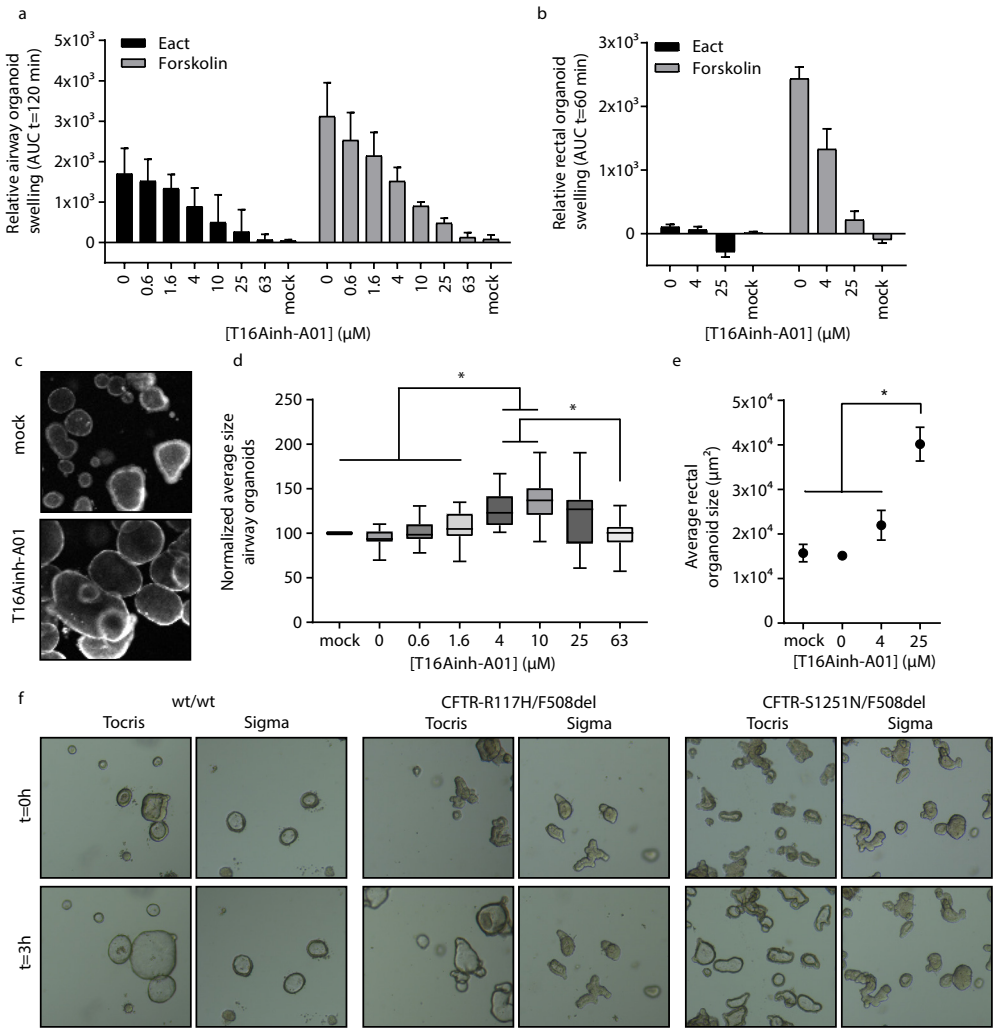

Figure 1. *Organoid swelling induced by T16Ainh-A01. a-b) Airway (a, three cultures) and rectal (b, one culture) organoids pre-incubated with T16Ainh-A01 (Tocris) with indicated concentrations for 3h prior to stimulation with 10 μM Eact or 2.5 μM forskolin. Swelling of organoids was monitored for 120 (a) and 60 min (b), and depicted as means of the area-under-the-curve (AUC) ± SD of three independent experiments performed in triplicate. c) Representative images of rectal organoids after 3h incubation with or without 25 μM T16Ainh-A01. d-e) Average size of airway (d, normalized to the mock condition) and rectal (e) organoids after 3h incubation with T16Ainh-A01, prior to compound stimulation. * means p-value <0.05 calculated via row-matched one-way ANOVA of three independent experiments. P-values per condition are depicted in supplementary tables. f) Representative images of wild type and cystic fibrosis rectal organoids before and after 3h incubation with 100 μM T16Ainh-A01 supplied by either Tocris or Sigma. 'mock' means no chemical added.*

To determine whether T16Ainh-A01-induced luminal secretion was supplier-dependent, we compared T16Ainh-A01 from Tocris with Sigma-Aldrich using rectal organoids of healthy subjects (**Fig. 1f**). We

imaged the organoids prior to and 3h after incubation with these inhibitors. Organoid swelling induced byT16Ainh-A01 from Sigma-Aldrich was very limited compared to T16Ainh-A01 from Tocris, which indicates both a supplier-dependent and -independent effect. We also assessed the effects of the inhibitors on rectal organoids from subjects with CF, to determine whether the swelling induced by T16Ainh-A01 was CFTR-dependent (**Fig. 1f**). Organoid swelling induced by T16Ainh-A01 (Tocris) was strongly reduced in *CFTR*-mutated rectal organoids, suggesting that the off-target effect of T16Ainh-A01 is CFTR-dependent.

We therefore hypothesized that T16Ainh-A01 was able to activate the cAMP pathway, resulting in the observed CFTR-dependent swelling. To test this hypothesis, we assessed with a FRET assay whether T16Ainh-A01 induced cAMP activity in HEK-293 cells transfected with YFP-Epac1-mTurq2, as previously reported [9,11]. The conformational change in Epac1 upon direct cAMP binding is visualized by the two light-sensitive molecules. We monitored the ability of T16Ainh-A01 and Eact to induce cAMP activity, followed by forskolin addition. Forskolin is a direct activator of adenylate cyclase and therefore a positive control in this assay. T16Ainh-A01 incubation significantly increased the distances between donor mTurq2 and acceptor YFP, while E_{act} did not ($p = 0.032$, **Fig. 2**). These data suggested that T16Ainh-A01 induced conformational Epac1 changes, which confirms the findings in human primary organoid that the inhibitor induced cAMP activity.

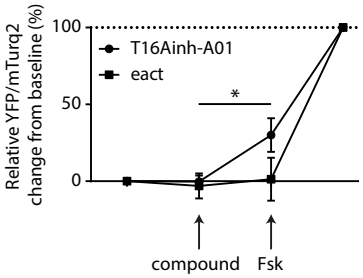

Figure 2. *cAMP activation in HEK-293 cells by T16Ainh-A01. cAMP activation upon E_{act} (10 μM) or T16Ainh-A01 (100 μM) and additional forskolin (25 μM) stimulation. Results of a fluorescence resonance energy transfer (FRET) assay using HEK-293 cells transfected with a cAMP sensor (YFP and mTurqoise2). Intracellular cAMP elevation induced conformational changes in YFP/mTurq2 ratio. Data are presented as relative to start (0%) and forskolin (100%) ± SD of three independent experiments performed in at least quadruplicates. * means p-value=0.032 for change in baseline upon T16Ainh-A01 addition.*

Discussion

Here, we showed that an inhibitor of TMEM16A (T16Ainh-A01), was able to induce swelling of airway and rectal organoids in a CFTR-dependent manner. Studies using a cAMP-regulated FRET sensor further suggested that the CFTR-dependent effects of T16Ainh-A01 in organoids acted via induction of intracellular cAMP. These findings suggest that T16Ainh-A01 supplied by Tocris has serious off-target effects, which might lead to misinterpretation of data when this inhibitor is used to study epithelial ion and fluid transport.

The T16Ainh-A01 inhibitor has been used in various ion transport studies of TMEM16A in epithelial and vascular tissue [8,12,13]. In a study by Davis et al it was concluded that T16Ainh-A01 was a very potent inhibitor of TMEM16A[12]. However, Boedtjker et al already questioned the selectivity of T16Ainh-A01 and other inhibitors as they showed that T16Ainh-A01 acted independent of chloride in smooth muscle cells, while T16Ainh-A01 was supposed to inhibit the chloride secretion mediated by TMEM16A [13]. Using T16Ainh-A01, it was concluded by Namkung et al that TMEM16A plays a minor part in calcium-activated chloride conductance in epithelial cells, since it only showed a partial effect [14]. Since in none of these studies cAMP activity was measured, it might be that the suggestive inhibition of calcium-activated chloride conductance is a result of induced cAMP-mediated chloride conductance. Given the fact that the mechanism of the inhibitor is still unknown, as already stated by Sondo et al [6], this needs more investigation.

We measured variation throughout the airway organoid cultures in the concentrations T16AinhA01 which induced maximal swelling. Since our data indicates that the off-target effect of T16Ainh-A01 is aimed at cAMP activation, it might be that the variation in amount of cAMP between the different donors is causing the biggest variation in response to the inhibitor. We observed reduced rectal organoid swelling when using T16Ainh-A01 from Sigma-Aldrich instead of Tocris. An explanation might be that the different stock concentrations (100 and 10 mM according to Tocris and Sigma, respectively) play an important role in the potency of the off-target effects of the inhibitor. Inhibitor of phosphodiestareses 3-Isobutyl-1-methylxanthin (IBMX) induced organoid swelling, but to a lesser extent than forskolin (unpublished data). T16Ainh-A01 was also not as effective as forskolin in inducing organoid swelling or cAMP activation in HEK-293 cells. A proposed mechanism of action might be that T16Ainh-A01 is less potent in stimulating adenylate cyclase or that the inhibitor also inhibits phosphodiesterases.

As already briefly mentioned, the mechanism of action of the T16Ainh-A01 inhibitor is still unknown[6]. Our results highlight the importance of validating chemicals using other batches and other suppliers. Incorporation of proper negative controls in experiments is also essential as the off-target effects of T16Ainh-A01 would have been undetected if we had not included the rectal organoids in this study. Testing the inhibitor on tissue lacking the protein TMEM16A was suggested previously by Boedtjker et al [13]. Furthermore, also the T16Ainh-A01-induced inhibition of forskolin-induced swelling of airway organoids indicated an additional mechanism of the inhibitor.

In conclusion, we report a cAMP-induced off-target effect of the chemical inhibitor T16Ainh-A01. This dose-dependent effect was observed by cAMP-dependent swelling of human primary rectal and airway organoids. We here share these findings to emphasize the importance of including proper negative controls in such experiments and to establish whether differences between batches and suppliers of chemical activators and inhibitors exist before initiating functional studies. Also, our data clearly indicate that human primary cell cultures are valuable models to identify ion channel activity upon addition of chemicals.

Acknowledgements

We thank G. Berkers and S. Michel for arranging and obtaining the rectal biopsies.

References

1. Dekkers JF, Wiegerinck CL, de Jonge HR, et al. A functional CFTR assay using primary cystic fibrosis intestinal organoids. *Nat Med*. 2013;19(7):939-945. doi:10.1038/nm.3201.
2. Dekkers JF, Berkers G, Kruisselbrink E, et al. Characterizing responses to CFTR-modulating drugs using rectal organoids derived from subjects with cystic fibrosis. *Sci Transl Med*. 2016;8(344):13. doi:10.1126/scitranslmed.aad8278.
3. Vijftigschild LAW, Berkers G, Dekkers JF, et al. B2-Adrenergic receptor agonists activate CFTR in intestinal organoids and subjects with cystic fibrosis. *Eur Respir J*. 2016;48(3):768-779. doi:10.1183/13993003.01661-2015.
4. Scudieri P, Caci E, Bruno S, et al. Association of TMEM16A chloride channel overexpression with airway goblet cell metaplasia. *J Physiol*. 2012;590:6141-6155.
5. Huang F, Zhang H, Wu M, et al. Calcium-activated chloride channel TMEM16A modulates mucin secretion and airway smooth muscle contraction. *Proc Natl Acad Sci U S A*. 2012;109(40):16354-16359.
6. Sondo E, Caci E, Galietta LJ V. The TMEM16A chloride channel as an alternative therapeutic target in cystic fibrosis. *Int J Biochem Cell Biol*. 2014;52:73-76. doi:10.1016/j.biocel.2014.03.022.
7. Mall M a., Galietta LJ V. Targeting ion channels in cystic fibrosis. *J Cyst Fibros*. 2015;14(5):561-570. doi:10.1016/j.jcf.2015.06.002.
8. Namkung W, Yao Z, Finkbeiner WE, Verkman AS. Small-molecule activators of TMEM16A, a calcium-activated chloride channel, stimulate epithelial chloride secretion and intestinal contraction. *FASEB J*. 2011;25(11):4048-4062. doi:10.1096/fj.11-191627.
9. Ponsioen B, Zhao J, Riedl J, et al. Detecting cAMP-induced Epac activation by fluorescence resonance energy transfer: Epac as a novel cAMP indicator. *EMBO Rep*. 2004;5(12):1176-1180. doi:10.1038/sj.embor.7400290.
10. Boj SF, Vonk AM, Statia M, et al. Forskolin-induced Swelling in Intestinal Organoids: An *In Vitro* Assay for Assessing Drug Response in Cystic Fibrosis Patients. *J Vis Exp*. 2017;(120):1-12. doi:10.3791/55159.
11. Klarenbeek J, Goedhart J, Van Batenburg A, Groenewald D, Jalink K. Fourth-Generation Epac-Based FRET Sensors for cAMP Feature Exceptional Brightness, Photostability and Dynamic Range: Characterization of Dedicated Sensors for FLIM, for Ratiometry and with High Affinity. doi:10.1371/journal.pone.0122513.
12. Davis AJ, Shi J, Pritchard H a T, et al. Potent vasorelaxant activity of the TMEM16A inhibitor T16A inh-A01. *Br J Pharmacol*. 2013;168(3):773-784. doi:10.1111/j.1476-5381.2012.02199.x.
13. Boedtkjer DMB, Kim S, Jensen AB, Matchkov VM, Andersson KE. New selective inhibitors of calcium-activated chloride channels - T16Ainh -A01, CaCCinh -A01 and MONNA - what do they inhibit? *Br J Pharmacol*. 2015;172(16):4158-4172. doi:10.1111/bph.13201.
14. Namkung W, Phuan PW, Verkman a. S. TMEM16A inhibitors reveal TMEM16A as a minor component of calcium-activated chloride channel conductance in airway and intestinal epithelial cells. *J Biol Chem*. 2011;286(3):2365-2374. doi:10.1074/jbc.M110.175109.

Supplementary data

Table S1

Airway organoid sizes					
Tukey's multiple comparisons test			Tukey's multiple comparisons test		
Comparison	Summary	Adjusted P Value	Compariso	Summary	Adjusted P Value
- vs. 0	ns	0,5886	0,6 vs. 4	**	0,0042
- vs. 0,6	ns	0,9999	0,6 vs. 10	**	0,0015
- vs. 1,6	ns	0,7902	0,6 vs. 25	ns	0,5117
- vs. 4	*	0,0184	0,6 vs. 63	ns	0,9532
- vs. 10	**	0,0053	1,6 vs. 4	**	0,0013
- vs. 25	ns	0,5665	1,6 vs. 10	**	0,0034
- vs. 63	ns	0,9991	1,6 vs. 25	ns	0,8498
0 vs. 0,6	*	0,0339	1,6 vs. 63	ns	0,4571
0 vs. 1,6	*	0,029	4 vs. 10	ns	0,6237
0 vs. 4	***	0,0007	4 vs. 25	ns	0,9093
0 vs. 10	***	0,0003	4 vs. 63	**	0,0078
0 vs. 25	ns	0,1486	10 vs. 25	ns	0,1717
0 vs. 63	ns	0,9867	10 vs. 63	****	<0,0001
0,6 vs. 1,6	ns	0,5677	25 vs. 63	ns	0,1055

Table S2

Rectal organoid sizes		
Tukey's multiple comparisons test		
Comparison	Summary	Adjusted P Value
- vs. 0	ns	0,9826
- vs. 4	ns	0,3278
- vs. 25	*	0,0302
0 vs. 4	ns	0,1799
0 vs. 25	*	0,0214
4 vs. 25	***	0,0007

Table S1+S2. p-values per concentration T16Ainh-A01 tested for airway organoid sizes (S1) and rectal organoid sizes (S2).

CHAPTER 7

Functional Characterization of Cholera Toxin Inhibitors Using Human Intestinal Organoids

Domenique D. Zomer-van Ommen‡, Aliaksei V. Pukin§, Ou Fu§, Linda H.C. Quarles van Ufford§, Hettie M. Janssens‖, Jeffrey M. Beekman‡, and Roland J. Pieters*§

J. Med. Chem., 2016, 59 (14), pp 6968–6972.

‡ Department of Pediatric Pulmonology, University Medical Centre Utrecht, Lundlaan 6, 3508 GA Utrecht, The Netherlands, § Department of Chemical Biology & Drug Discovery, Utrecht Institute for Pharmaceutical Sciences, Utrecht University, P.O. Box 80082, 3508 TB Utrecht, The Netherlands, ‖ Department of Pediatric Pulmonology, Erasmus Medical Center/Sophia Children's Hospital, Wytemaweg 80, 3015 CN Rotterdam, The Netherlands. *Phone: +31 (0)6 20293387. E-mail: r.j.pieters@uu.nl.

Brief Article. DOI: 10.1021/acs.jmedchem.6b00770. Publication Date (Web): June 27, 2016.

CHAPTER 7

Abstract

Preclinical drug testing in primary human cell models that recapitulate disease can significantly reduce animal experimentation and time-to-the-clinic. We used intestinal organoids to quantitatively study the potency of multivalent cholera toxin inhibitors. The method enabled the determination of IC50 values over a wide range of potencies (15 pM to 9 mM). The results indicate for the first time that an organoid-based swelling assay is a useful preclinical method to evaluate inhibitor potencies of drugs that target pathogen-derived toxins.

Graphical abstract

Abbreviations Used

CFTR, cystic fibrosis transmembrane conductance regulator; GM1os, GM1 oligosaccharides.

Introduction

Cholera toxin induces secretory diarrhea, resulting in severe dehydration(1, 2) and affecting 1.4–4.3 million individuals worldwide, of which 28000–143000 die each year.(3) Current protection consists of two vaccines, Shanchol and Dukoral, which are widely used but not very promising for children under six years of age, the most vulnerable group.(4) Inhibitory potency of bioactive compounds against cholera is typically evaluated in the rabbit ileal loop assay. However, this method is excessively stressful for the animals, time-consuming, and difficult to standardize.(5)

We recently described a simple and robust fluid secretion assay in a model of primary human intestinal organoids.(6, 7) Chemical induction of cAMP induces a rapid accumulation of fluid in the central lumen, and the resulting organoid swelling can be simply quantified. Using unmodified cells, this assay offers a drug testing platform for disease conditions involving fluid secretion, such as cystic fibrosis(6) or secretory diarrhea. For the latter condition, this remains to be demonstrated.

Here we use the organoid swelling assay to characterize pharmacological inhibitors of cholera toxin. Cholera toxin consists of the core region part A and the outer pentameric part B that binds to the pentasaccharide part of GM1-gangliosides. The binding is required for cell internalization, where cholera toxin A1 subunit is released into the cytosol (Figure 1).(1, 2) A1 triggers cAMP-dependent intestinal fluid hypersecretion via ion channels and transporters. The main channel is the cystic fibrosis transmembrane conductance regulator (CFTR), which secretes chloride and bicarbonate.(1, 2, 8) Hypersecretion is followed by paracellular hypersecretion of sodium and water.(1)

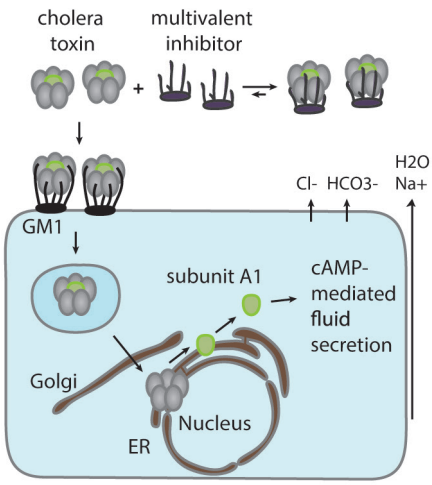

Figure 1. *Proposed mechanism and effect of inhibitors on the pathway of cholera toxin.*

Numerous inhibitors for cholera toxin have been developed over the years. Many of these are monovalent inhibitors derived from structure-based design,(9) however, high potency inhibitors so far were all based on multivalent designs(10-14) which contain several copies of the ligand attached to a single molecular scaffold such as a dendrimer.(15) Such inhibitors likely bridge several of the binding sites, which greatly enhances the potency, possibly in combination with aggregation mechanisms.(16) Cholera toxin inhibitors that are based on GM1os have shown the highest inhibitory potency so far.(10, 15, 17, 18) Recently, pentavalent versus tetravalent GM1os-based inhibitors were synthesized, compared, and shown to be of similar subnanomolar potency in an ELISA assay, and they exhibited similar aggregation behavior of the toxin.(19)

Most studies have reported the potency of the compounds using the same ELISA assay involving immobilized GM1 and HRP-conjugated CTB5. While this assay works well and is reproducible, a more biorelevant assay is needed. The mentioned rabbit ileal loop assay does function,(20) but practical and

ethical issues make it less suitable. We hypothesized that the swelling assay using human intestinal organoids could functionally assess the potency of cholera toxin inhibitors, thereby providing an additive method to current animal models. We used a series of inhibitors with a large range of potencies to also evaluate the dynamic range of the assay.

Results and Discussion

For comparison with the organoid assay, ELISA data were used (Table 1). We used the data from the recently reported tetravalent and pentavalent GM1os compounds 1 and 2 (Figure 2),(19) which are potent inhibitors in the picomolar range. Subsequently, the hydrophilic monovalent GM1os derivative 3 was used, which showed an IC50 of 110 nM. It is relevant to mention the word hydrophilic GM1 derivative. This derivative does not aggregate and behaves like a single molecule. This in contrast to GM1 derivatives with lipophilic tails that form aggregates and can vary widely in their ability to inhibit cholera toxin. To mention two examples, GM1 with two lipophilic tails (i.e., native GM1 ganglioside), which forms large micelles,(21) inhibits in the low nanomolar range (IC50 2.5 nM measured by us using the ELISA, and similar values are obtained by others(22)). GM1 with one lipohilic tail leads to relatively poor micromolar inhibition through an apparent counterproductive aggregation. It seems the polar derivative 3 is in between the two.(15, 17) Next, the nonspanning(23) GM1os dimer 4 with a short spacer was included in the panel. Its IC50 of 8 nM was ca. 1 order of magnitude better than the monovalent 3, which may be due to statistical rebinding effects, secondary binding effects of the second ligand, or even the bridging of pentamers. Finally, free galactose (5) was included as a weak millimolar inhibitor.

Table 1. *Inhibitory Potency of Cholera Toxin Inhibitors as IC50 (nM).* [a] *Inhibition of CTB5-HRP (40 ng/mL) binding to GM1 coated plates.* [b] *Inhibition of the swelling of intestinal organoids due to the action of cholera toxin (10 ng/mL).*

compd	ELISA assay[a]	organoid assay[b]
1	0.160 (ref 19)	0.034
2	0.260 (ref 19)	0.015
3	110	424
4	8	18
5 (galactose)	2.4×10^8 (ref 24)	9.1×10^6

To develop the organoid assay, intestinal organoids were stimulated dose dependently with cholera toxin to select a nonsaturating concentration for inhibitor testing while retaining maximal assay sensitivity (Figure 3). Stimulating organoids for 4 h with 10 ng/mL cholera toxin induced similar levels of swelling as saturating doses but with suboptimal kinetics. A lag phase of approximately 60–100 min was observed before cholera toxin induced swelling, consistent with the uptake and processing of the toxin (Figure 3). For comparison, amounts of cholera toxin detected in diarrhea has been detected as high as 1 μg/mL.(25)

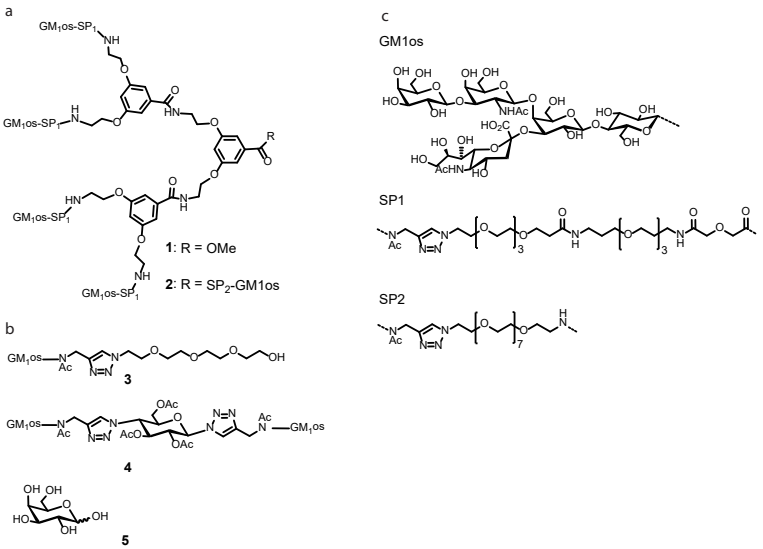

Figure 2. *Structures of (multivalent) cholera toxin inhibitors. (a) Structures of cholera toxin inhibitors 1 and 2. (b) Structures of inhibitors 3–5. (c) Additional structure elements GM1os, SP1, and SP2.*

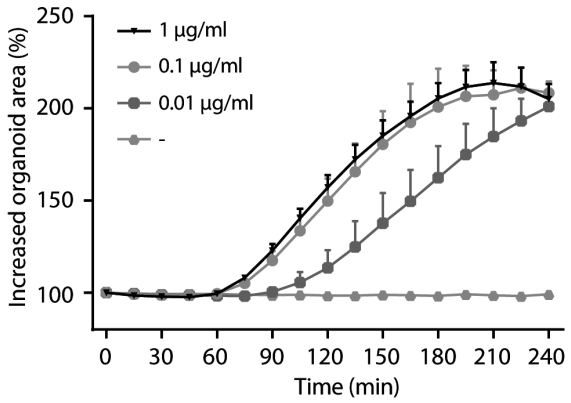

Figure 3. *Organoids were stimulated with cholera toxin as indicated (µg/mL), and organoid swelling was measured by relative area increase in time (t = 0 min: 100%), n = 1 triplicate ± SD.*

We next assessed dose-dependent inhibition of cholera toxin-mediated swelling of the four GM1os-based structures that differ in valency for binding cholera toxin B subunit (Figure 2). Free galactose (5) was again measured as a weak reference inhibitor. Organoids were stimulated with cholera toxin, with or without inhibitors. We found that tetravalent and pentavalent GM1os compounds 1 and 2 were most potent in inhibiting cholera toxin-induced swelling, with IC50 values in the picomolar range (IC50 of 34 and 15 pM, respectively) (Figure 4a, Table 1). Monovalent and bivalent GM1os compounds 3 and 4 were less potent (IC50 of 424 and 18 nM, respectively) but still effective. The monovalent compound 3 cannot take advantage of bridging binding sites within a toxin, while the bivalency of 4 seems to help here by a factor of ~20-fold. Monovalent galactose was the least potent (IC50 9.1 mM), as expected.(10) Also, for the highest dosages of inhibitors tested, organoids were additionally stimulated with forskolin, an adenyl cyclase activator, to control for toxicity of the inhibitors on the CFTR channel. Forskolin-stimulated organoid swelling was observed for all the conditions tested, indicating that the cholera toxin inhibitors do not inhibit CFTR chloride secretion by acting on CFTR directly (Figure 4b). Representative images are depicted in Figure 5.

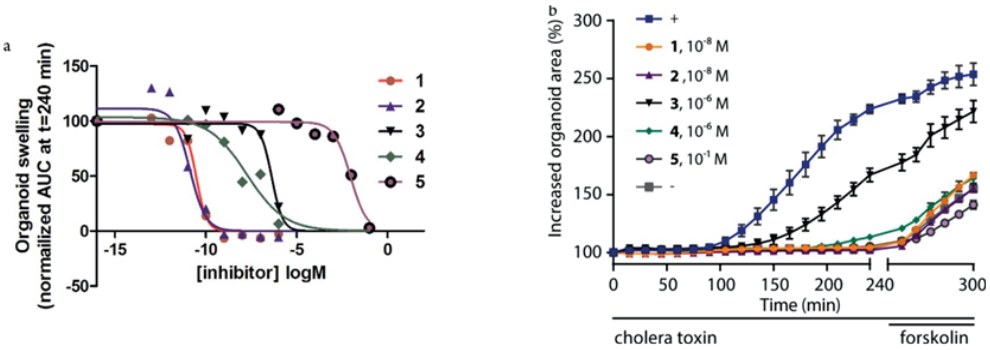

Figure 4. *Inhibitory potency of cholera toxin inhibitors indicated by intestinal organoid swelling. (a) Dose-dependent inhibition of cholera toxin-induced swelling, monitored for 4 h. Data represent three independent experiments (conditions in triplicate). (b) Organoid swelling curves after stimulation with cholera toxin (0.01 µg/mL), preincubated with the most effective dose of cholera toxin inhibitors (concentrations as indicated) and subsequent stimulation with 0.1 µM forskolin, n = 1 triplicate ± SD.*

The data indicate for the first time that multivalent GM1os-based compounds are highly effective in limiting cholera toxin-induced fluid secretion in human intestinal primary cells (Figure 4a). The organoid assay exhibited a very large dynamic range by clearly showing inhibition from the pico- to the millimolar range. The values correlated well with those obtained from the GM1-based ELISA type assay. Nevertheless, the best inhibitors 1 and 2 showed even lower values with the organoids. This can be explained by the fact that the organoid assay requires less cholera toxin (i.e., 10 ng/mL) to give a clearly observable phenomenon than the ELISA assay. Because we are talking IC50 values, 50% of the present CT molecules represents ca. 58 pM, a value close to the observed IC50 values for 1 and 2. The inhibition seems to be almost one to one in terms of stoichiometry, irrespective of whether at these concentrations aggregation phenomena(16) play a role, which is remarkable.

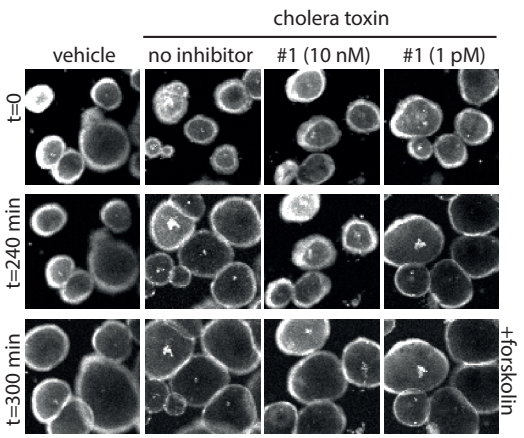

Figure 5. *Representative images of organoids upon cholera toxin stimulation, with or without inhibitor 1, conditions and time points as indicated.*

The organoid assay now makes it possible to do a biorelevant assay while avoiding animal experiments using rabbit intestines and while quantitatively showing the functional impact of inhibitors with large differences in potency (Figure 4a). However, with the use of organoids, the toxins are likely to bind basolateral to the epithelial cells instead of luminal, which could have resulted in an overestimation of the potencies. Furthermore, we did not take into account the adhesion of the bacterium itself.

The data suggest that the cholera toxin inhibitors could be used as prophylactic or acute drugs to inhibit cholera toxins to bind to cells. When the toxins are already bound to epithelial cells and internalized, other approaches are needed such as reducing Cl– hypersecretion or stimulating Na+ absorption via cyclase inhibitors or NHE3 activators, respectively.(8, 26)

Conclusion

The human primary organoid culture model provides a simple, robust, and functional intestinal assay for compound inhibitory potency testing. The total organoid swelling easily quantitates fluid transport across the intestinal epithelium, mimicking the *in vivo* tissue. This assay platform will be important for preclinical development of drugs targeting pathogen-induced secretory diarrhea as shown here for compounds targeting cholera toxin.

Experimental Section

Human Rectal Biopsies

Rectal biopsies were collected from a human subject after informed consent and approved by the local Ethics Committee.

Generating and Culturing Organoids

Organoids were generated, and biobanked, slightly differently as previously described.(6) After washing with PBS, crypts were isolated from the biopsies, via incubation in 10 mM EDTA for 60–90 min at 4 °C at a rocking platform. Crypts were collected, centrifuged, and supernatant removed. Crypts pellet was taken up in 40% Matrigel (Corning, diluted in culture medium), and droplets of crypts suspension were plated onto 24-well plates. After solidification of the Matrigel (±10 min, 37 °C), droplets were immersed in culture medium (advanced DMEM/F12 supplemented with HEPES, GlutaMAX, penicillin, streptomycin, N-2, B-27, mEGF (Life Technologies), N-acetylcysteine, nicotinamide, SB202190 (Sigma), A83-01 (Tocris), and 50% Wnt3a-, 20% Rspo-1-, and 10% Noggin-conditioned media). In 7 days, crypts grew out into full grown organoids, which were passaged via mechanical disruption weekly. Medium was refreshed every 2–3 days, and organoids were passaged at least two times before assays were performed.

Cholera Toxin and Inhibitors

Cholera toxin from Vibrio cholerae (Sigma) was used to stimulate organoid fluid secretion. Cholera toxin inhibitors were preincubated for 4 h with cholera toxin prior to organoid stimulation. The (multivalent) structures of the inhibitors are based on GM1os, and monovalent free galactose serves as a reference compound.(19)

Monovalent Inhibitor 3

A solution of GM1os-β-NAc-propargyl (Elicityl, Grenoble) (8.3 mg, 7.7 µmol), 11-azido-3,6,9-trioxaundecanol (3.4 mg, 15.5 µmol), $CuSO_4 \cdot 5H_2O$ (1.9 mg, 7.7 µmol), and sodium ascorbate (3.1 mg, 15.5 µmol) in H_2O/DMF (1/1, v/v, 2 mL) was heated under microwave irradiation at 80 °C for 20 min. The reaction mixture was treated with ion-exchange resin Cuprisorb, concentrated, and subjected to preparative HPLC purification (gradient of 5% MeCN and 0.1% TFA in H_2O to 5% H_2O and 0.1% TFA in MeCN). The product was obtained after lyophilization as a colorless glass (4 mg, 40%). Purity >95% determined by HPLC. Selected 1H NMR (500 MHz, D_2O) δ: 7.93 (s, 1H, CHtriazole), 5.14 (d, J = 8 Hz, 1H, H-1, Glc), 4.78 (H-1, GalNAc), 4.64 (m, 2H-NCH2Ctriazole), 4.58 (m, 2H-NtriazoleCH2), 4.56–4.50 (m, 2H, H-1, Gal(V), H-1, Gal(II)), 4.18–4.09 (m, 3H), 4.03 (m, 1H, H-2, GalNAc), 3.86 (m, 1H, H-9a, NeuAc), 3.37 (m, 1H), 2.65 (m, 1H, H-3eq, NeuAc), 2.25 (s, 3H, Glc-NC(O)CH3), 2.03 (s, 3H, NHC(O)CH3), 2.00 (s, 3H, NHC(O)CH3), 1.92 (t, 1H, J = 12 Hz, H-3ax, NeuAc). 13C NMR (126 MHz, D_2O) δ (obtained from HSQC spectrum): 125.47 (CHtriazole), 105.37 (C-1, Gal(II)), 103.20 (C-1, Gal(V)), 103.14 (C-1, GalNAc), 87.50 (C-1, Glc), 80.97, 78.62, 77.79, 77.45, 75.52, 75.22, 75.00, 74.98, 74.84, 73.72, 73.17, 72.93, 72.34 (CH_2CH_2OH), 71.31, 70.66, 70.44, 70.23 (OCH_2CH_2O), 69.42 (NCH_2CH_2O), 69.34, 69.24, 68.67, 68.55, 63.46 (C-9, NeuAc), 63.46 (C-9, NeuAc), 61.13 (C-CH_2CH_2OH), 61.60, 60.87, 60.71 (4 × C-6, GalNac, Gal, Glc), 52.26 (C-5, NeuAc), 51.82 (C-2, GalNAc), 50.68 (NtriazoleCH2), 37.60 (C-3, NeuAc), 37.00 (NCH_2Ctriazole), 23.26 (NHC(O)CH3), 22.73 (NHC(O)CH3), 21.86 (Glc-NC(O)CH3). HRMS (Q-TOF) m/z calcd for $[M - H]^-$ 1295.5001, found 1295.4981.

Bivalent Inhibitor 4

A solution of GM1os-β-NAc-propargyl (Elicityl, Grenoble) (8.2 mg, 7.6 µmol), 1,4-diazido-1,4-deoxy-2,3,6-tri-O-acetyl glucose(27) (1 mg, 2.8 µmol), $CuSO_4 \cdot 5H_2O$ (1.9 mg, 7.6 µmol), and sodium ascorbate (3 mg, 15.2 µmol) in H_2O/DMF (1/1, v/v, 2 mL) was heated under microwave irradiation at 80 °C for 20 min. The reaction mixture was treated with ion-exchange resin Cuprisorb, concentrated, and subjected to preparative HPLC purification (gradient of 5% MeCN and 0.1% TFA in H_2O to 5% H_2O and 0.1% TFA in MeCN). The product was obtained after lyophilization as a white fluffy compound (3.2 mg, 45%). Purity >95% determined by HPLC. Selected 1H NMR (500 MHz, D_2O) δ: 8.19 (s, 1H, CHtriazole), 8.08 (s, 1H, CHtriazole), 6.34 (d, J = 10 Hz, 1H, H-1, Glc'), 5.95 (m, 1H, H-3, Glc'), 5.72 (m, 1H, H-2, Glc'), 5.26 (m, 1H, H-4, Glc'), 5.14 (m, 2H, H-1, Glc), 4.58–4.51 (m, 4H, H-1, Gal(V), H-1, Gal(II)), 4.04 (m, 2H, H-2, GalNAc), 3.38 (m, 2H), 2.66 (m, 2H, H-3eq, NeuAc), 2.25 (s, 6H, Glc-NC(O)CH3), 2.06 (s, 3H, OC(O)CH3), 2.02 (s, 6H, NHC(O)CH3), 2.01 (s, 6H, NHC(O)CH3), 1.94–1.89 (m, 8H, H-3ax, NeuAc, 2 × OC(O)CH3). 13C NMR (126 MHz, D_2O) δ (obtained from HSQC spectrum): 125.78 (CHtriazole), 124.51 (CHtriazole), 105.37 (C-1, Gal(II)), 103.24 (C-1, Gal(V)), 103.10 (C-1, GalNAc), 87.41 (C-1, Glc), 85.61 (C-1, Glc'), 80.90, 78.65, 77.59, 77.46, 75.52, 75.38, 75.06, 75.02, 74.81, 74.79 (C-5, Glc'), 73.74, 73.15, 72.79 (C-3, Glc'), 72.75, 71.32, 71.31 (C-2, Glc'), 70.63, 70.61, 69.23, 69.17, 68.68, 68.54, 63.50 (C-9, NeuAc), 62.50 (C-6, Glc'), 61.64, 60.94, 60.77 (4 × C-6, GalNac, Gal, Glc), 59.90 (C-4, Glc'), 52.27 (C-5, NeuAc), 51.86 (C-2, GalNAc), 37.71 (C-3, NeuAc), 36.89 (NCH_2Ctriazole), 36.88 (NCH_2Ctriazole), 23.22 (NHC(O)CH3), 22.74 (NHC(O)CH3), 21.80 (Glc-NC(O)CH3), 20.64, 20.19 (3 × C-OC(O)CH3). HRMS (Q-TOF) m/z calcd for $[M - 2H]^{2-}$ 1254.4322, found 1254.4335.

Organoid Swelling Assay

Measuring CFTR function in intestinal organoids was performed slightly different as previously described.(6) Organoids cultured for 7 days were mechanically disrupted and reseeded into flat-bottom 96-well plates in 40% Matrigel and culture medium. Plates were incubated overnight at 37 °C, 5% CO2. The next day, cholera toxin was incubated with cholera toxin inhibitors for 4 h at rt prior to the organoid stimulation. Organoids were stained with calcein AM (Invitrogen), 1 h prior to the stimulation. Organoids were stimulated with the mix of cholera toxin (0.01 µg/mL) and inhibitors (titration) for 4 h and additionally with forskolin (0.1 µM, Sigma) for some conditions for another hour. Swelling of organoids was monitored in time using the Zeiss LSM 710 confocal microscope (images every 15 min during cholera stimulation, every 10 min during forskolin stimulation). Organoid area increase was analyzed using Volocity, and calculations were done with GraphPad Prism 6.

Conflict of interest

The authors declare the following competing financial interest(s): J.M.B. is inventor on a patent application related to these findings (PCT/IB2012/057497).

Acknowledgments

We thank Dr. H. R. de Jonge (Erasmus MC, Rotterdam) for carefully reading the manuscript. This research is funded by the Dutch Cystic Fibrosis Foundation (NCFS), ZonMW, and Wilhelmina Children's Hospital (WKZ) Research Fund. This research is supported by the Dutch Technology Foundation STW, Applied Science Division of NWO, and the Technology Program of the Ministry of Economic Affairs and by COST action CM1102 MultiGlycoNano. None of the supporters played a role in the study design, collection, analysis, or interpretation of data.

References

1. Sigman, M.; Luchette, F. A. Cholera: Something Old, Something New Surg. Infect. 2012, 13, 216– 222 DOI: 10.1089/sur.2012.127

2. Petri, W. A.; Miller, M.; Binder, H. J.; Levine, M. M.; Dillingham, R.; Guerrant, R. L. Enteric Infections, Diarrhea, and Their Impact on Function and Development J. Clin. Invest. 2008, 118, 1277– 1290 DOI: 10.1172/JCI34005 [Crossref], [PubMed], [CAS]OpenURL UTRECHT UNIV

3. Cholera Factsheet No. 107; WHO: Geneva, July 2015; www.who.int/mediacentre/factsheets/fs107/en (accessed June 15, 2016)

4. Kabir, S. Critical Analysis of Compositions and Protective Efficacies of Oral Killed Cholera Vaccines Clin. Vaccine Immunol. 2014, 21, 1195– 1205 DOI: 10.1128/CVI.00378-14

5. Laboratory Methods for the Diagnosis of Vibrio Cholera; Centers for Diseaes Control and Prevention: Atlanta, 2014; http://www.cdc.gov/cholera/laboratory.html (accessed June 15, 2016)

6. Dekkers, J. F.; Wiegerinck, C. L.; de Jonge, H. R.; Bronsveld, I.; Janssens, H. M.; de Winter-de Groot, K. M.; Brandsma, A. M.; de Jong, N. W. M.; Bijvelds, M. J. C.; Scholte, B. J.; Nieuwenhuis, E. E. S.; van den Brink, S.; Clevers, H.; van der Ent, C. K.; Middendorp, S.; Beekman, J. M. A Functional CFTR Assay Using Primary Cystic Fibrosis Intestinal Organoids Nat. Med. 2013, 19, 939– 945 DOI: 10.1038/nm.3201

7. Sato, T.; Clevers, H. Growing Self-Organizing Mini-Guts from a Single Intestinal Stem Cell: Mechanism and Applications Science 2013, 340, 1190– 1194 DOI: 10.1126/science.1234852

8. Bijvelds, M. J. C.; Loos, M.; Bronsveld, I.; Hellemans, A.; Bongartz, J.-P.; Ver Donck, L.; Cox, E.; De Jonge, H. R.; Schuurkes, J. A. J.; De Maeyer, J. H. Inhibition of Heat-Stable Toxin-Induced Intestinal Salt and Water Secretion by a Novel Class of Guanylyl Cyclase C Inhibitors J. Infect. Dis. 2015, 212, 1806– 1815 DOI: 10.1093/infdis/jiv300

9. Cheshev, P.; Morelli, L.; Marchesi, M.; Podlipnik, Č.; Bergström, M.; Bernardi, A. Synthesis and Affinity Evaluation of a Small Library of Bidentate Cholera Toxin Ligands: Towards Nonhydrolyzable Ganglioside Mimics Chem. - Eur. J. 2010, 16, 1951– 1967 DOI: 10.1002/chem.200902469

10. Branson, T. R.; Turnbull, W. B. Bacterial Toxin Inhibitors Based on Multivalent Scaffolds Chem. Soc. Rev. 2013, 42, 4613– 4622 DOI: 10.1039/C2CS35430F

11. Zuilhof, H. Fighting Cholera One-on-One: The Development and E Ffi Cacy of Multivalent Cholera-Toxin-Binding Molecules Acc. Chem. Res. 2016, 49, 274– 285 DOI: 10.1021/acs.accounts.5b00480

12. Wittmann, V.; Pieters, R. J. Bridging Lectin Binding Sites by Multivalent Carbohydrates Chem. Soc. Rev. 2013, 42, 4492– 4503 DOI: 10.1039/c3cs60089k

13. Tran, H.-A.; Kitov, P. I.; Paszkiewicz, E.; Sadowska, J. M.; Bundle, D. R. Multifunctional Multivalency: A Focused Library of Polymeric Cholera Toxin Antagonists Org. Biomol. Chem. 2011, 9, 3658– 3671 DOI: 10.1039/c0ob01089h

14. Stoll, B. J.; Holmgren, J.; Bardhan, P. K.; Huq, I.; Greenough, W. B., III; Fredman, P.; Svennerholm, L. Binding Of Intaluminal Toxin in Cholera: Trial Of GM1 Ganglioside Charcoal Lancet 1980, 316, 888– 891 DOI: 10.1016/S0140-6736(80)92049-8

15. Pukin, A. V.; Branderhorst, H. M.; Sisu, C.; Weijers, C. C. A. G. M.; Gilbert, M.; Liskamp, R. M. J.; Visser, G. M.; Zuilhof, H.; Pieters, R. J. Strong Inhibition of Cholera Toxin by Multivalent GM1 Derivatives ChemBioChem 2007, 8, 1500– 1503 DOI: 10.1002/cbic.200700266

16. Sisu, C.; Baron, A. J.; Branderhorst, H. M.; Connell, S. D.; Weijers, C. C. A. G. M.; de Vries, R.; Hayes, E. D.; Pukin, A. V.; Gilbert, M.; Pieters, R. J.; Zuilhof, H.; Visser, G. M.; Turnbull, W. B. The Influence of Ligand Valency on Aggregation Mechanisms for Inhibiting Bacterial Toxins ChemBioChem 2009, 10, 329– 337 DOI: 10.1002/cbic.200800550

17. Garcia-Hartjes, J.; Bernardi, S.; Weijers, C. A. G. M.; Wennekes, T.; Gilbert, M.; Sansone, F.; Casnati, A.; Zuilhof, H. Picomolar Inhibition of Cholera Toxin by a Pentavalent Ganglioside GM1os-calix[5]arene Org. Biomol. Chem. 2013, 11, 4340– 4349 DOI: 10.1039/C3OB40515J

18. Branson, T. R.; McAllister, T. E.; Garcia-Hartjes, J.; Fascione, M. a; Ross, J. F.; Warriner, S. L.; Wennekes, T.; Zuilhof, H.; Turnbull, W. B. A Protein-Based Pentavalent Inhibitor of the Cholera Toxin B-Subunit Angew. Chem., Int. Ed. 2014, 53, 8323– 8327 DOI: 10.1002/anie.201404397

19. Fu, O.; Pukin, A. V.; van Ufford, H. C. Q.; Branson, T. R.; Thies-Weesie, D. M. E.; Turnbull, W. B.; Visser, G. M.; Pieters, R. J. Tetra- versus Pentavalent Inhibitors of Cholera Toxin ChemistryOpen 2015, 4, 471– 477 DOI: 10.1002/open.201500006

20. Unpublished Results.

21. Cantu, L.; Del Favero, E.; Brocca, P.; Corti, M. Multilevel Structuring of Ganglioside-Containing Aggregates: From Simple Micelles to Complex Biomimetic Membranes Adv. Colloid Interface Sci. 2014, 205, 177– 186 DOI: 10.1016/j.cis.2013.10.016

22. Schengrund, C. L.; Ringler, N. J. Binding of Vibrio Cholera Toxin and the Heat-Labile Enterotoxin of Escherichia Coli to G(M1), Derivatives of G(M1), and Nonlipid Oligosaccharide Polyvalent Ligands J. Biol. Chem. 1989, 264, 13233– 13237

23. Pickens, J. C.; Mitchell, D. D.; Liu, J.; Tan, X.; Zhang, Z.; Verlinde, C. L. M. J.; Hol, W. G. J.; Fan, E. Nonspanning Bivalent Ligands as Improved Surface Receptor Binding Inhibitors of the Cholera Toxin B Pentamer Chem. Biol. 2004, 11, 1205–1215 DOI: 10.1016/j.chembiol.2004.06.008

24. Branderhorst, H. M.; Liskamp, R. M. J.; Visser, G. M.; Pieters, R. J. Strong Inhibition of Cholera Toxin Binding by Galactose Dendrimers Chem. Commun. 2007, 5043– 5045 DOI: 10.1039/b711070g

25. Turnbull, P. C. B.; Lee, J. V.; Miliotis, M. D.; Still, C. S.; Isaacson, M.; Ahmad, Q. S. *In Vitro* and *In Vivo* Cholera Toxin Production by Classical and El Tor Isolates of Vibrio Cholerae J. Clin. Microbiol. 1985, 21, 884– 890

26. Mroz, M. S.; Keating, N.; Ward, J. B.; Sarker, R.; Amu, S.; Aviello, G.; Donowitz, M.; Fallon, P. G.; Keely, S. J. Farnesoid X Receptor Agonists Attenuate Colonic Epithelial Secretory Function and Prevent Experimental Diarrhoea *in Vivo* Gut 2014, 63, 808– 817 DOI: 10.1136/gutjnl-2013-305088

27. Pertici, F.; de Mol, N. J.; Kemmink, J.; Pieters, R. J. Optimizing Divalent Inhibitors of Pseudomonas Aeruginosa Lectin Leca by Using a Rigid Spacer Chem. - Eur. J. 2013, 19, 16923– 16927 DOI: 10.1002/chem.201303463

Associated content

Synthetic scheme of compounds 3 and 4

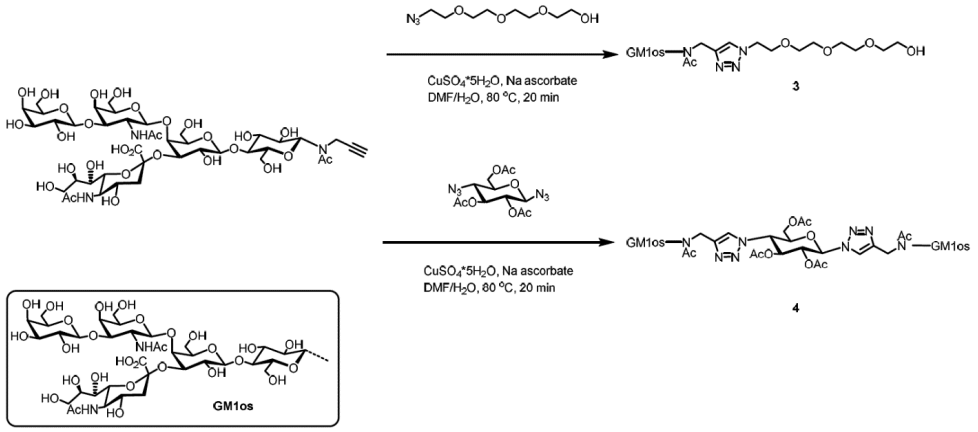

NMR spectra of compounds 3 and 4

^{1}H NMR Spectrum of the monovalent inhibitor **3** (500 MHz, D_2O)

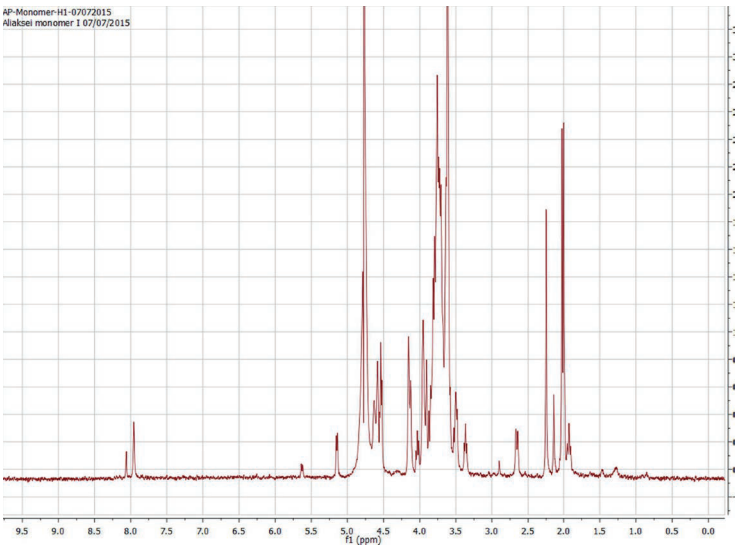

^{1}H NMR Spectrum of the bivalent inhibitor **4** (500 MHz, D_2O)

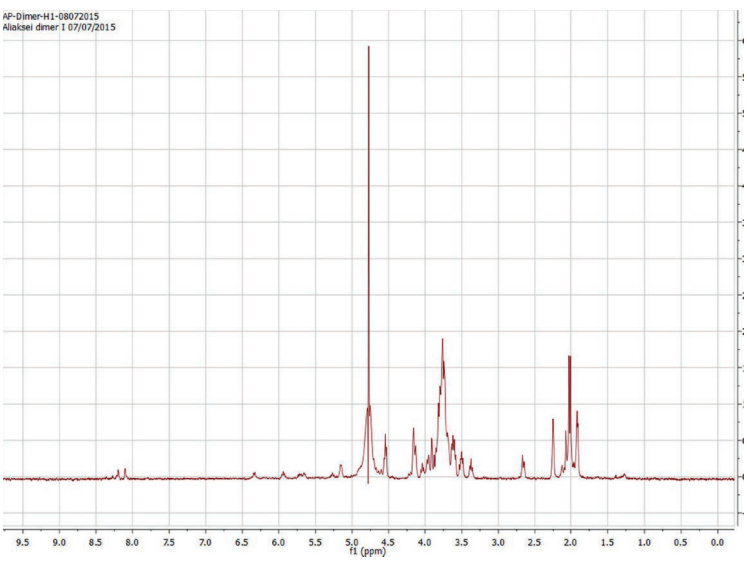

HSQC NMR Spectrum of the monovalent inhibitor **3** (500 MHz, D_2O)

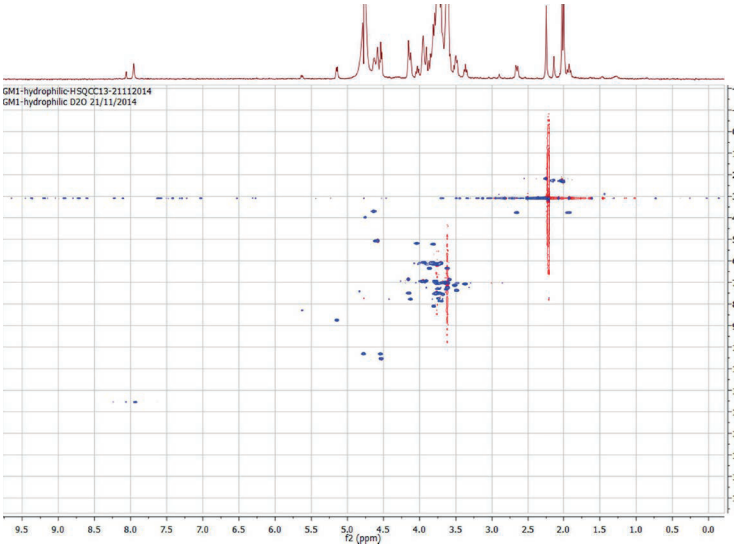

HSQC NMR Spectrum of the bivalent inhibitor **4** (500 MHz, D_2O)

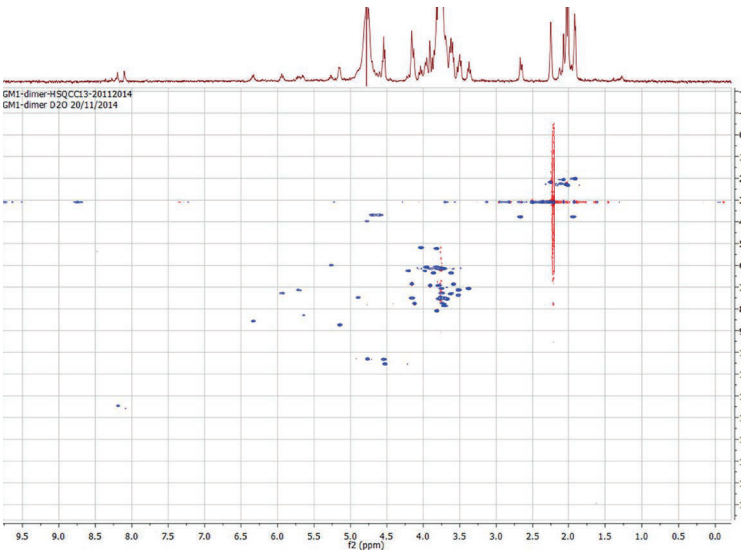

Functional characterization of cholera toxin inhibitors using human intestinal organoids

7

CHAPTER 8

General discussion

In 2018, organoid cultures won the 'method of the year 2017' from Nature Methods, recognizing organoids as potential model system for human biology, disease and precision medicine [1]. In this thesis, we also explored the possibilities of organoid culture technology for human disease modeling, focusing on ion transport studies using intestinal organoid-derived 3D and 2D models. Moreover, we also developed airway organoid cultures that facilitate long-term *in vitro* expansion of primary airway tissue and airway disease modeling. Altogether, our proof-of-concept studies demonstrate that the ion transport phenotypes in intestinal and airway organoids recapitulate essential characteristics of cystic fibrosis (CF) disease and response to treatment. The studies therefore highlight that these novel culture approaches will be instrumental to study human ion transport diseases, as well as the treatment thereof in a more precise or even personalized manner.

Intestinal organoids for preclinical CFTR modulator development

CFTR-restoring therapies have revolutionized CF treatment, but are clinically effective for a minority of patients [2,3]. The large *in vivo* treatment effects have sparked a larger drug development effort aiming to achieve highly effective treatment for the majority of subjects, mainly by targeting the p.Phe508del mutation. Functional studies in primary CF airway cells in Ussing chambers are the dominant tool to select potential drugs with clinical efficacy [4,5]. How do intestinal organoids fit in?

Current preclinical intestinal organoid models vary in sensitivity for CFTR activity, which helps to study the many different CFTR variants and CFTR modulators thereof [6–9]. We here developed more sensitive read-outs to measure very low levels of CFTR function. The lowest levels of CFTR activation can be observed with the assay in which we measure forskolin-induced lumen, right before organoid swelling is induced. This forskolin-induced lumen area increase detected induction of premature termination codon read-through by G418 and thus small levels of functional CFTR protein (Chapter 2), which was not detected by conventional forskolin-induced swelling (FIS). The forskolin-induced lumen area increase assay was already rapidly saturated as p.Phe508del-directed treatment in organoids with a single F508del allele was almost as high as the effect in F508del homozygous organoids. Whereas the forskolin-induced lumen area increase assay has value to detect minor changes in CFTR function by modulators, the translational properties towards the *in vivo* effect appears to be limited since CFTR function levels beyond the ceiling of this assay are needed, as concluded from *in vitro-in vivo* relation studies with the FIS. In this thesis, we used FIS to select and initiate *in vivo* studies with salbutamol, and to study salbutamol concentration in patient's plasma after treatment (Chapter 3). The FIS data, showing no (PTC-124) or marginal (salbutamol in plasma) *in vitro* response, appeared instructive for the lack or limited clinical efficacy *in vivo* [10]. Collectively, it appears that FIS currently has the best track record for predicting *in vivo* therapeutic response, albeit that FIS cannot measure CFTR function over the full range.

Also unpublished data support the predictive capacity of intestinal organoids for *in vivo* therapeutic response of CFTR protein modulators. To determine whether intestinal organoids could predict individual clinical outcome, we compared the organoid responses with the clinical outcomes of 24 individuals with various *CFTR* mutations and CFTR modulator treatments. Intestinal organoid swelling correlated significantly with *in vivo* clinical parameters, showing strong specificity and selectivity of this assay to predict clinical outcome (manuscript in submission by G. Berkers).

Thus, for the next generation CFTR modulators by Vertex Pharmaceuticals, Galapagos, Flatley Discovery Lab, Reata Pharmaceuticals and others that target nearly complete CFTR proteins with conformational defects, we think that intestinal organoid swelling assays can be used, dependent on the efficaciousness of the preclinical treatments. The highly sensitive readouts can be used to identify modulators of CFTR function, but modulators only affecting forskolin-induced luminal swelling will likely not be clinically efficacious due to too low efficacy.

Intestinal organoids and other CFTR-targeting drugs

Might the predictive capacity of intestinal organoids for *in vivo* therapeutic effect of CFTR modulators be translated to other therapeutic approaches, or should we remain cautious when testing drugs with distinct mode-of-actions?

Current CFTR modulators are shown or assumed to exert their function by direct binding to the mutant CFTR protein [11–13]. Additional next generation CFTR-targeting drugs are being developed with a broad scope of mode-of-actions that primarily aim to rescue (airway) CFTR via targeting biological pathways that control CFTR proteostasis [14]. A promising approach is the amplifier, which increases the amount of CFTR protein, resulting in enlarged substrate availability for correctors and potentiators [15,16]. Amplifier PTI-428 is currently in development for CF by Proteostasis Therapeutics and recently received Breakthrough Therapy Designation by the Food and Drug Administration (FDA) (www.proteostasis.com). Another drug category contains plasma membrane stabilizers that anchor CFTR in the plasma membrane, and could therefore improve protein stability and decrease protein degradation [16], but none are currently in clinical development. With PTC-124 no longer in development for premature termination codon mutations, additional approaches are being tested like compounds based on synthetic derived aminoglycosides with reduced side-effects as compared to the parental aminoglycosides [17,18], PTC-124 derivatives [19,20], and the herbal compound escin [21]. In addition, new genetic therapies are being developed like suppressor transfer RNAs to correct nonsense mutations by ReCode Therapeutics [22]; antisense oligonucleotides to insert the missing bases to correct the mRNA [23,24], like QR-010 which is in clinical development by ProQR and; enhancers to prevent endosomal trapping of these oligonucleotides [25].

In our work, we demonstrated that intestinal organoids could predict the negative outcomes of another class of drugs that regulate CFTR function (premature termination codon drugs, Chapter 2) as indicated by the lack of *in vitro* and *in vivo* efficacy of PTC-124 [10,26]. This suggests that shared biological features exists between the intestinal cells and airway cells that allow the study of drugs that do not target the CFTR protein directly, but underlying mechanisms that are present both in airway and intestinal epithelium. Therefore, the efficacy and potency of amplifiers and plasma stabilizers could likely also be determined using intestinal organoids. However, airway and intestinal cells are intrinsically different, and this may impact the efficacy of different treatments, and therefore the translation of intestinal organoids outcomes toward rescue of airway CFTR. For instance, intestinal organoids replicate faster, have differences in protein homeostasis, and high CFTR expression. Potentially, the pathway that is targeted by CFTR amplifiers is already biologically active in intestinal organoids, and thus has low potency to be stimulated further using drug candidates.

Gene therapy approaches have been developed since *CFTR* was cloned [27], with the size of the gene and the delivery to the lungs as major challenges. Various vectors and delivery systems have been explored, but unfortunately no successful therapy has been realized until now [8]. Still, non-viral gene delivery seemed to improve lung function in a phase 2b clinical trial [28]. More potent vectors and delivery systems need to be developed [27,28], and the need for intermittent treatment schemes does not bring complete cure. Repairing the CFTR defect *ex vivo* in patient's own cells also holds promise for future gene therapies, as shown with primary intestinal organoids using the CRISPR/Cas9 method [29]. Despite all these efforts, gene therapy remains difficult to develop, also with regards to CF being a multi-organ disease [29].

In summary, new CFTR therapies are currently in development with various mode-of-actions. Findings from this thesis indicate that intestinal organoids might be valuable to determine efficacies of drugs which indirectly increase CFTR function. Organoid responses of these drugs cannot directly be compared with CFTR modulators, because of the indirect mechanisms. Still, the additive values of these drugs might be studied using this assay.

Intestinal organoids to repurpose drugs for CF

Organoids also facilitate non-CF drug screening with the aim to repurpose clinically available drugs for CF treatment. Such approaches may not yield the most effective drugs, but are useful when drug development is economically challenging, e.g. for rare diseases. Our studies in chapter 3 provided a first example how organoids can be used for such an approach. In order to develop a screening approach using intestinal organoids, with limited capacity, we used a hypothesis-driven approach to identify the most effective cAMP-modifying drugs. We selected potential drugs, but also eligible patient groups, as the cAMP agonists were only effective in organoids from people with some CFTR residual function. Some but limited efficacy was observed in nasal potential differences after *in vivo* treatment.

Moreover, drug concentrations reached in plasma were also limited and the actual concentrations in the tissue are likely even lower. We obtained relevant scientific results with this proof-of-concept study, but it did not lead to significant treatment effects. However, some patients did feel better after salbutamol treatment and continued to use this drug on a daily basis. The paper mainly showed that the drug repurposing approach may be useful, but that compounds also need to be selected based on pharmacokinetic properties and potential side effects, and that *in vivo* studies in small patient cohorts with rare mutations are quickly underpowered.

The initial study has now been followed up by a much larger repurposing effort for people in the Netherlands with rare *CFTR* mutations. Intestinal organoids of >170 patients are currently being screened for 1,400 FDA approved drugs and clinically available CFTR modulators. The aim is to identify people with rare mutations that may benefit from clinically available CFTR modulators, but also to identify other drugs that might induce or lower CFTR function through various mechanisms. These other drugs may be independently developed into new treatments as standalone or add-on therapy for CFTR modulators, but may also be used to deselect treatments for CF patients due to their inhibiting activity on CFTR. In the process of hit validation, known pharmacokinetic properties and side effects will be taken along, before initiating N=1 studies to determine *in vivo* efficacy. These studies indicate the strength of stem cell models for individualized drug screen efforts.

Intestinal organoids for personalized CF therapy

One of the big advantages that intestinal organoids offer over other human primary cell culture approaches is the robustness by which individual tissue can now be cultured on the long-term and stored in biobanks. This facilitates the development of personalized drug testing (e.g. the testing of 1,400 FDA approved drugs as described above) and selection of the most effective treatments on an individual basis using a laboratory test, similar to how microbiologists grow micro-organisms for the selection of effective antibiotics. Currently, there are only a limited amount of CFTR modulators for CF on the market to mix and match, but this may change in the future when new drugs are developed as expected from the current densely filled drug development pipeline (www.cff.org). Compared to current *CFTR* genotype-based approaches, the use of living cells integrate both individual *CFTR* genetic variability and additional *CFTR* gene modifiers into a single functional response that might better identify responding and non-responding individuals.

An additional step to personalize treatment might be achieved through personalized dosing. We demonstrated proof-of-concept in Chapter 3 that intestinal organoid outcomes in plasma are related to clinical outcomes, but these observations were not studied at the individual level. Whereas drug levels might also be directly measured by analytical chemistry, the use of organoids to quantitate individual circulating drug levels may be beneficial as the functional impact is directly measured [30]. Such a functional measurement may further integrate binding of drugs to plasma factors such as albumin, or the impact of metabolites or other circulating factors. However, it also adds biological variation and technical difficulties and may therefore be difficult for e.g. CFTR correctors that require long-term incubation of plasma with organoids.

Ultimately, a complete personalized approach where drugs are mixed and matched based on the organoid response appears appealing, but this remains highly challenging in clinical practice. Several aspects need to be taken into account when we are heading for such approach. First, with the development of more effective treatments, the identification of non-responding subjects will becoming less relevant. Secondly, when treatments are so effective that even the low responders will gain CFTR function levels in the range of healthy control CFTR function, a personalized drug test might become irrelevant. Also, despite many drugs are being developed, it is unclear whether such drugs will become available as single or combination preparations. Additional complexity may arise from differences in pharmacokinetic properties and drug-drug interactions, as is already observed for ivacaftor and lumacaftor combination treatment [31,32]. Moreover, the preclinical testing does not incorporate differences in pharmacokinetic parameters, and *in vivo* CF disease is also driven by environmental factors that are not incorporated in the cell culture model. This means that these cultures only partially recapitulate the *in vivo* situation and can only partially predict the *in vivo* response [33]. Lastly, it is still unclear to what extend the intestinal rectal organoids represent the CFTR function in the airways, which remain the primary target for CF treatment.

Clearly, additional longitudinal studies are needed to determine whether CFTR function measurements in intestinal organoids can predict progression of CF lung disease and response to treatment [34]. Also, studies are currently ongoing to demonstrate the value of organoid-based selection over

CFTR genotype-based selection in individuals with identical *CFTR* genotypes such as homozygous p.Phe508del [7]. This may show that organoids have additional value over current *CFTR* genotype-based approaches to identify responders and non-responders to CFTR modulator treatment, and might further pave the road to a personalized approach using organoids.

Intestinal organoids for ultra-rare and unknown *CFTR* mutations

One obvious application, where currently *CFTR* genotyping is insufficient, is for very rare and/or uncharacterized *CFTR* genotypes. Organoids may be used to select people with ultra-rare *CFTR* genotypes for available drugs. In the Netherlands, this approach currently has led to treatment and reimbursement for approximately 10 subjects with rare *CFTR* mutations, and discussions are ongoing to further implement this strategy for an anticipated ~100-150 additional patients. They currently do not have access to CFTR modulator treatment although their intestinal organoids do respond and they will likely benefit. In the recently enrolled project HIT-CF Europe, intestinal organoids of 500 people with very rare *CFTR* mutations across Europe will be screened for three investigational drugs from different companies, followed by clinical trials. This project provides the opportunity to speed up the development process of three investigational drugs and thus also potential treatment for people with ultra-rare *CFTR* mutations. Also, conversations with regulatory authorities are initiated to include the first living biomarker into reimbursement programs. A personalized approach to stratify only individuals with rare and unknown *CFTR* mutations for treatment will likely remain highly relevant in the future therapeutic landscape.

Need for additional models

While this intestinal organoid model has great potential for CF disease modeling, it also has limitations. First, more data is needed to determine how accurate *in vitro* measurements can capture *in vivo* phenotypes, since current validations remain at the proof-of-concept level. Second, the 3D organization leads to cell stretching and sometimes bursting of organoid structures upon fluid secretion which limit the dynamic range of the organoid assay, and leads potentially also to the co-activation of other stretch-dependent ion channels, which can lead to misinterpretation of the CFTR activity. Furthermore, the inside-out 3D morphology, that is critical for the swelling assay, makes it difficult to target the apical side of organoids and to measure the apical fluids directly [7]. Whereas with micro-injection of the luminal membrane the luminal compartment can be directly stimulated [35], this is a complex and lengthy procedure which limits the throughput of measurements. Lastly, CFTR function in the intestine likely only partially reflects CFTR function in the airways. The representative cell culture models are expected to be most reflective for their tissue of origin, and therefore observations in intestinal cells may not be translated to airway cells and vice versa.

Intestinal organoid-derived monolayers

The monolayer protocol that we developed to study electrophysiological properties of intestinal epithelium complements CFTR function measurements in rectal biopsies and intestinal organoids (Chapter 4). We adapted our protocol to generate intestinal organoid-derived 2D monolayers from the group of T.S. Stappenbeck [36,3]. Using these monolayers, we now can directly study CFTR-mediated

ion transport using a cell resource that has beneficial expansion and storage capacities as compared to other primary epithelial cells that are normally used for electrophysiological assays. With the Multi Transepithelial Current Clamp (MTECC), we could distinguish wild type from CF and even severe CF from mild CF, indicating that the monolayer culture approach and MTECC system recapitulate features of *in vivo* CF disease. The 24-well MTECC platform and the short culture protocol both facilitate the generation of large datasets that will help to better understand ion transport characteristics in intestinal epithelium in the context of CF and other diseases.

The intestinal organoid-derived monolayers can be used to study ion transport properties of different epithelial cells, as we demonstrated by induction of differentiation of monolayers (Chapter 4). cAMP is the main but not exclusive activator of CFTR [38,39], which was also indicated by our findings with differentiated monolayers. Increased concentrations of intracellular calcium mediated apical chloride secretion, but which ion channels are involved in this pathway is mainly unknown [38]. Calcium-activated channels were shown to be expressed in various human enteroids [40], but in rectal organoids, we found that TMEM16A is not functionally present (Chapter 5&6). Also, carbachol-induced swelling was not increased in differentiated organoids, while in differentiated *CFTR* class I monolayers carbachol induced ion transport, indicating calcium-dependent chloride secretion (Chapter 4). This implies that morphology differences between the 3D and 2D cultures are important for ion channel properties, since all other conditions were equal between these cultures.

To further confirm and explore our findings, improved regulation of epithelial differentiation would be highly useful. Progress in controlled differentiation studies is already being made using mouse intestinal organoids. It was shown that epigenetically active compounds drive epithelial differentiation towards goblet cells in mouse intestinal organoids [41]. It was also recently suggested that nicotine and muscarine receptors play a role in epithelial cell differentiation of mouse intestinal organoids [42]. Moreover, mouse organoids derived from small intestine biopsies were directed to differentiate into absorptive cells, secretory goblet cells or Paneth cells by Pearce et al[43], and characterized by varying tight junction properties, affecting the paracellular ion transport pathway. These studies advance our understanding of the different subsets of cells in the complex multicellular epithelial environments. An important next step would be to translate these findings to human organoid models and to study their roles in human pathophysiology.

We found in this thesis that the intestinal organoid-derived monolayers were less sensitive in measuring CFTR function than both intestinal and airway organoid swelling assays (Chapter 4&5). Therefore, the intestinal monolayer model holds potential to measure very potent drugs like the upcoming triple CFTR modulator combinations, which might be underestimated by conventional FIS due to compensatory mechanisms upon cell stretching and organoid bursting. With monolayers, carriers could not be discriminated from wild type cultures, suggesting that the electrophysiological measurements in monolayers may need further optimization to enable discrimination between high CFTR function levels. One approach to modify the monolayer assay is by selective permeabilization of the basolateral membrane, using chemicals such as nystatin, to specifically study ion transport across the apical membrane. Since basolateral chloride loading is not rate-limiting under such conditions, it might be a useful assay to directly measure CFTR function and CFTR modulator efficacy.

We found that fluid secretion of intestinal organoids did not fully correlate with ion transport measurements in monolayers (Chapter 4), while both were cultured with identical culture media. In fact, organoid fluid transport appeared to be a better discriminator between *CFTR* genotypes than direct ion transport measurements in monolayers. It might be that patient-specific or culture-specific biological or technical factors play a role in the gap between fluid secretion and ion transport, but this needs to be further studied.

Intestinal organoid applications beyond CF

We showed that intestinal organoid swelling can be used to measure the effect of cholera toxins on chloride secretion (Chapter 7), indicating that the organoid model might be applicable to study other diarrheal diseases caused by infections with e.g. rotavirus and Escherichia coli [40]. Also, our proof-of-concept study indicated that the intestinal organoids could be useful to measure the efficacy of agents that prevent epithelial infection. It was previously shown that the human organoids-based intestinal monolayer protocol could be used for host-pathogen interactions [37], and was recently applied to study cellular infection by human adenovirus [44], and damage caused by non-steroidal anti-inflammatory drugs [45]. In summary, these findings indicate that the intestinal organoid and monolayer models hold great potential for the study of various gastrointestinal mechanisms in health and disease.

Human primary airway organoid cultures

The protocol we described here (Chapter 5) provides a significant step forward by facilitating the long-term culture of human adult airway stem cells. These airway organoids express the epithelial stem cell marker LGR5 and proposed lung stem cell marker LGR6, suggesting presence of stem cells [46]. Long-term culture is facilitated by the endogenous production of Wnt3A, and by supplementing the culture medium with growth factors FGF7 and FGF10, as well as other essential factors that are commonly shared with other organoid culture protocols such as epidermal growth factor, R-spondin and Noggin [47]. The 3D composition of the airway organoid cultures appear to recapitulate the *in vivo* epithelial situation, as indicated by a pseudostratified architecture and the presence of all major epithelial cell subsets in the conducting airways such as basal, ciliated, goblet and club cells. This sustainable *in vitro* resource of cells will likely play an important starting point for the development of new models of human airway diseases, analogous to what we have observed for the intestinal organoid cultures.

Airway organoid swelling

Our findings showed that airway organoids can discriminate between severe *CFTR* genotypes and milder ones, while the swelling of airway organoids was slower compared to intestinal organoids upon stimulation with forskolin (Chapter 5). One explanation might be that CFTR is less abundant in the airways, resulting in lower responses to cAMP inducers. Also, it might be a physical swelling limitation due to the multi-layered, pseudostratified composition of the airway organoids. Still, the characterization of swell responses in these cultures remains limited when compared to intestinal cells. With airway organoids, increased technical variation was observed when quantitating swelling, requiring quadruple conditions within one experiment. A large variety in organoid size, and presumably also cell composition within one culture, may contribute to this. Subsequently, the average increase in organoid size per well

varies when different proportions of organoid structures are present in the cultures. Since the complete broncho-alveolar biopsy or cell suspension is used to generate organoids, this results in mixed and sample-specific cell populations. Clonally growing the cultures greatly reduced the organoid size and swelling variation. Isolating beforehand e.g. the LGR5/LGR6+ population might reduce the culture variation. However, something similar to intestinal crypt isolation would be better, considering the importance of the stem cell niche for cell survival [9,48]. Also, inhibition of FIS varied between the cultures, indicating that cell composition varies between donors. Altogether, our findings indicate that the airway organoid swelling assay might be useful to study CFTR, but further assay development is needed, since the outcomes are partially dependent on the starting material.

In this thesis we show that, besides CFTR, also other fluid driving ion channels can be functionally studied using human primary airway organoids. Functional presence of calcium-dependent ion channels was indicated by TMEM16A activator-induced airway organoid swelling which exceeded FIS in CF organoids. This model facilitated a direct comparison of CFTR modulators and an activator of calcium-activated chloride channels, indicating the bypass potential of TMEM16A [49,50]. However, the therapeutic potential is currently still challenging. Systemically activating TMEM16A would induce epithelial mucus secretion, but would also increase airway smooth muscle contraction [51], requiring local targeting. Also, TMEM16A activation functionally induced tumorigenesis [52]. Using our airway organoid model, other alternative ion channels with different mode-of-actions might be identified. To conclude, human primary airway organoids are a valuable additive model to further explore the bypass potential of alternative ion channels.

It is currently unknown how airway organoid swelling and CFTR function measurements relate to the intestinal organoid model, and which model can better translate outcomes to *in vivo* phenotypes. Despite it is the primary tissue of choice, assay and culture performance may be limiting translation (including heterogeneity of the airways, assay variability, assay stability upon long-term passaging, etc.). Therefore, we are currently studying CFTR function and response to CFTR modulators in both airway and intestinal organoids derived from individuals with CF and non-CF volunteers, and how that correlates with the *in vivo* CF phenotypes.

Other airway organoid assays for CF

The 2D culturing of primary airway cells, the main preclinical model for CF drug screens, is limited in expansion capabilities and requires lengthy culture protocols for obtaining pseudo-stratified, highly differentiated epithelium [53]. Preliminary studies from our lab indicate that electrophysiological measurements of CFTR-mediated ion transport in organoid-based ALI cultures yield comparable data as compared to common ALI cultures using difficult to expand airway basal cells (unpublished data from G.D. Amatngalim). This indicates that this method of culturing airway adult stem cells is versatile, similar to intestinal organoids. Also, expanding airway basal cells might be improved using airway organoid cultures.

An important next step is to generate organoids from various locations in the airways to further unravel the heterogeneity of the airways. Stem cell and other cell populations vary along the airways and are not fully characterized yet [54–57], as well as the CFTR expression [58]. For the upper airways, primary nasal tissue-

derived organoids and ALI cultures are being established in our lab and by others (unpublished data from G.D. Amatngalim) [59]. The main advantage of obtaining human adult stem cells via nasal brushings, instead of broncho-alveolar lavages or biopsies, is the reduced burden for the subject. Whether CFTR function measurements in nasal cell-derived cultures are representative for the airways remains to be determined.

Both airway surface liquid (ASL) maintenance and cilia beating are important for airway mucociliary clearance and are reduced in CF [38,60]. The process of ASL maintenance in the lower airways is less studied compared to the upper airways. [38] Directly targeting ASL restoration was not effective enough to halt *in vivo* lung function decline [61], thus regulating ASL preferably would go via CFTR or e.g. SLC26A9 [49]. The role of these ion channels in ASL homeostasis might be studied using our airway organoids model. Reduced ASL subsequently impairs cilia beating, leading to reduced capabilities of the airways to remove pathogens [62,63]. Cilia beating and resulting mucus circulation is visible in the airway organoids we described (Chapter 5), indicating that these cultures might be used to develop a novel assay to monitor cilia beating and mucociliary clearance together with the effect of e.g. CFTR modulators.

In this thesis we focused on epithelial fluid secretion, but submucosal glands (underlying the airway epithelium) also highly contribute to this process [38]. It is known that reduced detachment of mucus strands from the submucosal ducts contribute to impaired mucociliary clearance in CF [64,65]. Moreover, high CFTR expression cells are found in the submucosal gland tissue [66]. Co-culture systems with airway surface epithelial cells and submucosal glands are needed, allowing the combined study of fluids and mucus, and the efficacy of CFTR modulators and mucolytics thereof. To conclude, human primary airway organoids hold various potentials to develop new airway models, including assays which focus on mucus secretion and mucociliary clearance.

Future perspectives of epithelial organoids

The ease by which human's own cells can now be cultured *in vitro* using current stem cell culture technologies causes a paradigm shift, leading to the establishment of primary human cell collections representing health and disease. Here, we show that intestinal and airway adult stem cell cultures can be used to develop new preclinical models, and that these models are useful for disease modeling, drug repurposing and determining drug efficacy.

However, the cultures are generated from adult epithelial cells and lack the presence of additional cell types and tissue architecture. Using these technologies to improve the development of more complex human *in vitro* models would provide a big step forward to study organ-level complexity. One example is the organ-on-a-chip model, where multiple cell types can be spatially organized and co-cultured on solid supports with controlled perfusion of nutrients and liquids using a microfluidics perfusing system. [67] Also, on-a-chip cultures have an open lumen with an accessible apical side. [68] These complex culture models will not be useful for personalized treatment screens, but can be used to study interactions of various cell types. It was recently published that primary human small intestine epithelial cells did interact with underlying endothelial cells, and better recapitulated the duodenum function than the organoids from which the organ-on-a-chip cultures were derived. [68] Other combinations published are intestinal epithelial cells with immune cells, to study bacterial invasion [69] or communication between

intestine and liver during inflammation [70]; and liver-skin cells combination, supplemented with endothelial cells to mimic human vasculature [71]. For primary human airway cells, the first organ-on-a-chip model was described in 2016 [72], where mucociliary bronchiolar epithelial cells and endothelial cells were combined, recapitulating disease specific features of human primary cells from subjects with COPD or asthma. Therefore, organ-on-a-chip models might provide a platform to unravel current contradictory theories including whether CF induces the susceptibility to inflammation and what the underlying cause is of impaired mucociliary clearance [27].

This thesis shows how new technologies are leading to next generation culture models for advanced disease modeling and drug development. These new culture models have high individual success rates and facilitate long-term *in vitro* expansion of patient-derived cells. Future applications will help to further utilize the opportunities of these cultures for disease modeling, and improving drug development and personalized therapy.

References

1. Editors. Method of the Year 2017: Organoids. *Nat Methods*. 2018;15:1. http://dx.doi.org/10.1038/nmeth.4575.
2. Ramsey B, Davies JC, McElvaney N, et al. A CFTR Potentiator in Patients with Cystic Fibrosis and the G551D Mutation. 2011;365(18):1663-1672.
3. Wainwright CE, Elborn JS, Ramsey BW, et al. Lumacaftor-Ivacaftor in Patients with Cystic Fibrosis Homozygous for Phe508del CFTR. *N Engl J Med*. 2015:1-12. doi:10.1056/NEJMoa1409547.
4. Van Goor F, Hadida S, Grootenhuis PDJ, et al. Correction of the F508del-CFTR protein processing defect in vitro by the investigational drug VX-809. *Proc Natl Acad Sci U S A*. 2011;108(46):18843-18848. doi:10.1073/pnas.1105787108.
5. Van Goor F, Hadida S, Grootenhuis PDJ, et al. Rescue of CF airway epithelial cell function in vitro by a CFTR potentiator, VX-770. *Proc Natl Acad Sci U S A*. 2009;106(44):18825-18830. doi:10.1073/pnas.0904709106.
6. The Clinical and Functional TRanslation of CFTR. http://cftr2.org. Accessed September 8, 2017.
7. Dekkers JF, Berkers G, Kruisselbrink E, et al. Characterizing responses to CFTR-modulating drugs using rectal organoids derived from subjects with cystic fibrosis. *Sci Transl Med*. 2016;8(344):13. doi:10.1126/scitranslmed.aad8278.
8. Bell SC, De Boeck K, Amaral MD. New pharmacological approaches for cystic fibrosis: Promises, progress, pitfalls. *Pharmacol Ther*. 2015;(145):19-34. doi:10.1016/j.pharmthera.2014.06.005.
9. Dekkers JF, Wiegerinck CL, de Jonge HR, et al. A functional CFTR assay using primary cystic fibrosis intestinal organoids. *Nat Med*. 2013;19(7):939-945. doi:10.1038/nm.3201.
10. Kerem E, Konstan MW, De Boeck K, et al. Ataluren for the treatment of nonsense-mutation cystic fibrosis: a randomised, double-blind, placebo-controlled phase 3 trial. *Lancet Respir Med*. 2014;2(7):539-547. doi:10.1016/S2213-2600(14)70100-6.
11. Okiyoneda T, Veit G, Dekkers JF, et al. Mechanism-based corrector combination restores ΔF508-CFTR folding and function. *Nat Chem Biol*. 2013;9(7):444-454. doi:10.1038/nchembio.1253.
12. Farinha CM, King-Underwood J, Sousa M, et al. Revertants, Low Temperature, and Correctors Reveal the Mechanism of F508del-CFTR Rescue by VX-809 and Suggest Multiple Agents for Full Correction. *Chem Biol*. 2013;20(7):943-955. doi:10.1016/J.CHEMBIOL.2013.06.004.
13. Eckford PDW, Li C, Ramjeesingh M, Bear CE. Cystic fibrosis transmembrane conductance regulator (CFTR) potentiator VX-770 (ivacaftor) opens the defective channel gate of mutant CFTR in a phosphorylation-dependent but ATP-independent manner. *J Biol Chem*. 2012;287(44):36639-36649. doi:10.1074/jbc.M112.393637.
14. Amaral MD, Balch WE. Hallmarks of therapeutic management of the cystic fibrosis functional landscape. *J Cyst Fibros*. 2015;14(6):687-699. doi:10.1016/j.jcf.2015.09.006.
15. Molinski S V, Ahmadi S, Ip W, et al. Orkambi® and amplifier co-therapy improves function from a rareCFTRmutation in gene-edited cells and patient tissue. *EMBO Mol Med*. 2017;9(9):1224-1243. doi:10.15252/emmm.201607137.
16. De Boeck K, Davies JC. Where are we with transformational therapies for patients with cystic fibrosis? *Curr Opin Pharmacol*. 2017;34:70-75. doi:10.1016/j.coph.2017.09.005.
17. Rowe SM, Sloane P, Tang LP, et al. Suppression of CFTR premature termination codons and rescue of CFTR protein and function by the synthetic aminoglycoside NB54. *J Mol Med (Berl)*. 2011;89(11):1149-1161. doi:10.1007/s00109-011-0787-6.
18. Xue X, Mutyam V, Tang L, et al. Synthetic Aminoglycosides Efficiently Suppress CFTR Nonsense Mutations and are Enhanced by Ivacaftor. *Am J Respir Cell Mol Biol*. November 2013. doi:10.1165/rcmb.2013-0282OC.
19. Pibiri I, Lentini L, Melfi R, et al. Enhancement of premature stop codon readthrough in the CFTR gene by Ataluren (PTC124) derivatives. *Eur J Med Chem*. 2015;101:236-244. doi:10.1016/J.EJMECH.2015.06.038.
20. Pibiri I, Lentini L, Tutone M, Melfi R, Pace A, Di Leonardo A. Exploring the readthrough of nonsense mutations by non-acidic Ataluren analogues selected by ligand-based virtual screening. *Eur J Med Chem*. 2016;122:429-435. doi:10.1016/J.EJMECH.2016.06.048.
21. Mutyam V, Du M, Xue X, et al. Discovery of clinically approved agents that promote suppression of cystic fibrosis transmembrane conductance regulator nonsense mutations. *Am J Respir Crit Care Med*. 2016;194(9):1092-1103. doi:10.1164/rccm.201601-0154OC.
22. Hagemeijer MC, Siegwart DJ, Strug LJ, et al. Translational research to enable personalized treatment of cystic fibrosis. *J Cyst Fibros*. 2017;17(2):S46-S51. doi:10.1016/j.jcf.2017.10.017.

23. Montiel-Gonzalez MF, Vallecillo-Viejo I, Yudowski GA, Rosenthal JJC. Correction of mutations within the cystic fibrosis transmembrane conductance regulator by site-directed RNA editing. *Proc Natl Acad Sci*. 2013;110(45):18285-18290. doi:10.1073/pnas.1306243110.
24. Igreja S, Clarke LA, Botelho HM, Marques L, Amaral MD. Correction of a Cystic Fibrosis Splicing Mutation by Antisense Oligonucleotides. *Hum Mutat*. 2016;37(2):209-215. doi:10.1002/humu.22931.
25. Wang L, Ariyarathna Y, Ming X, et al. A Novel Family of Small Molecules that Enhance the Intracellular Delivery and Pharmacological Effectiveness of Antisense and Splice Switching Oligonucleotides. *ACS Chem Biol*. 2017;12(8):1999-2007. doi:10.1021/acschembio.7b00242.
26. McElroy SP, Nomura T, Torrie LS, et al. A lack of premature termination codon read-through efficacy of PTC124 (Ataluren) in a diverse array of reporter assays. *PLoS Biol*. 2013;11(6):e1001593. doi:10.1371/journal.pbio.1001593.
27. Elborn JS. Cystic fibrosis. *Lancet*. 2016;388(10059):2519-2531. doi:10.1016/S0140-6736(16)00576-6.
28. Alton EWFW, Armstrong DK, Ashby D, et al. Repeated nebulisation of non-viral CFTR gene therapy in patients with cystic fibrosis: a randomised, double-blind, placebo-controlled, phase 2b trial. *Lancet Respir Med*. 2015;3(9):684-691. doi:10.1016/S2213-2600(15)00245-3.
29. Schwank G, Koo B-K, Sasselli V, et al. Functional repair of CFTR by CRISPR/Cas9 in intestinal stem cell organoids of cystic fibrosis patients. *Cell Stem Cell*. 2013;13(6):653-658. doi:10.1016/j.stem.2013.11.002.
30. Dekkers R, Vijftigschild LAW, Vonk AM, et al. A bioassay using intestinal organoids to measure CFTR modulators in human plasma. *J Cyst Fibros*. 2015;14(2):178-181. doi:10.1016/j.jcf.2014.10.007.
31. Veit G, Avramescu RG, Perdomo D, et al. Some gating potentiators, including VX-770, diminish ΔF508-CFTR functional expression. *Sci Transl Med*. 2014;6(246):246ra97. doi:10.1126/scitranslmed.3008889.
32. Cholon DM, Quinney NL, Fulcher ML, et al. Potentiator ivacaftor abrogates pharmacological correction of ΔF508 CFTR in cystic fibrosis. *Sci Transl Med*. 2014;6(246):246ra96. doi:10.1126/scitranslmed.3008680.
33. Ikpa PT, Bijvelds MJC, de Jonge HR. Cystic fibrosis: Toward personalized therapies. *Int J Biochem Cell Biol*. February 2014. doi:10.1016/j.biocel.2014.02.008.
34. Dekkers JF, van der Ent CK, Beekman JM. Novel opportunities for CFTR-targeting drug development using organoids. *Rare Dis (Austin, Tex)*. 2013;1:e27112. doi:10.4161/rdis.27112.
35. de Lau W, Kujala P, Schneeberger K, et al. Peyer's patch M cells derived from Lgr5(+) stem cells require SpiB and are induced by RankL in cultured "miniguts". *Mol Cell Biol*. 2012;32(18):3639-3647. doi:10.1128/MCB.00434-12.
36. Moon C, VanDussen KL, Miyoshi H, Stappenbeck TS. Development of a primary mouse intestinal epithelial cell monolayer culture system to evaluate factors that modulate IgA transcytosis. *Mucosal Immunol*. 2014;7(4):818-828. doi:10.1038/mi.2013.98.
37. VanDussen KL, Marinshaw JM, Shaikh N, et al. Development of an enhanced human gastrointestinal epithelial culture system to facilitate patient-based assays. *Gut*. July 2014. doi:10.1136/gutjnl-2013-306651.
38. Frizzell RA, Hanrahan JW. Physiology of epithelial chloride and fluid secretion. *Cold Spring Harb Perspect Med*. 2012;2(6):a009563. doi:10.1101/cshperspect.a009563.
39. Bijvelds MJC, Loos M, Bronsveld I, et al. Inhibition of Heat-Stable Toxin–Induced Intestinal Salt and Water Secretion by a Novel Class of Guanylyl Cyclase C Inhibitors. *J Infect Dis*. 2015:jiv300. doi:10.1093/infdis/jiv300.
40. Kovbasnjuk O, Zachos NC, In J, et al. Human enteroids : preclinical models of non-infl ammatory diarrhea. 2013;4(Suppl 1):1-4.
41. Cao L, Kuratnik A, Xu W, et al. Development of intestinal organoids as tissue surrogates: Cell composition and the Epigenetic control of differentiation. *Mol Carcinog*. 2015;54(3):189-202. doi:10.1002/mc.22089.
42. Takahashi T, Shiraishi A, Murata J. The Coordinated Activities of nAChR and Wnt Signaling Regulate Intestinal Stem Cell Function in Mice. *Int J Mol Sci*. 2018;19(3):738. doi:10.3390/ijms19030738.
43. Pearce SC, Al-Jawadi A, Kishida K, et al. Marked differences in tight junction composition and macromolecular permeability among different intestinal cell types. *BMC Biol*. 2018;16(1):19. doi:10.1186/s12915-018-0481-z.
44. Holly MK, Smith JG. Adenovirus infection of human enteroids reveals interferon sensitivity and preferential infection of goblet cells. *J Virol*. February 2018:JVI.00250-18. doi:10.1128/JVI.00250-18.
45. Bhatt AP, Gunasekara DB, Speer J, et al. Nonsteroidal Anti-Inflammatory Drug-Induced Leaky Gut Modeled Using Polarized Monolayers of Primary Human Intestinal Epithelial Cells. *ACS Infect Dis*. 2018;4(1):46-52. doi:10.1021/acsinfecdis.7b00139.

46. Joo-Hyeon Lee A, Tammela T, Hofree M, et al. Anatomically and Functionally Distinct Lung Mesenchymal Populations Marked by Lgr5 and Lgr6 In Brief Heterogeneous mesenchymal cell populations in the lung play a central role in epithelial maintenance and alveolar differentiation. Anatomically and Functionally Distinct Lung Mesenchymal Populations Marked by Lgr5 and Lgr6. *Cell*. 2017;170. doi:10.1016/j.cell.2017.07.028.

47. Sato T, Stange DE, Ferrante M, et al. Long-term expansion of epithelial organoids from human colon, adenoma, adenocarcinoma, and Barrett's epithelium. *Gastroenterology*. 2011;141(5):1762-1772. doi:10.1053/j.gastro.2011.07.050.

48. Sato T, Clevers H. Growing self-organizing mini-guts from a single intestinal stem cell: mechanism and applications. *Science*. 2013;340(6137):1190-1194. doi:10.1126/science.1234852.

49. Mall M a., Galietta LJ V. Targeting ion channels in cystic fibrosis. *J Cyst Fibros*. 2015;14(5):561-570. doi:10.1016/j.jcf.2015.06.002.

50. Sondo E, Caci E, Galietta LJ V. The TMEM16A chloride channel as an alternative therapeutic target in cystic fibrosis. *Int J Biochem Cell Biol*. 2014;52:73-76. doi:10.1016/j.biocel.2014.03.022.

51. Huang F, Zhang H, Wu M, et al. Calcium-activated chloride channel TMEM16A modulates mucin secretion and airway smooth muscle contraction. *Proc Natl Acad Sci U S A*. 2012;109(40):16354-16359.

52. Duvvuri U, Shiwarski DJ, Xiao D, et al. TMEM16A induces MAPK and contributes directly to tumorigenesis and cancer progression. *Cancer Res*. 2012;72(13):3270-3281. doi:10.1158/0008-5472.CAN-12-0475-T.

53. Fulcher ML, Randell SH. Human Nasal and Tracheo-Bronchial Respiratory Epithelial Cell Culture. 2013;945:109-121. doi:10.1007/978-1-62703-125-7.

54. Jacob A, Morley M, Hawkins F, et al. Differentiation of Human Pluripotent Stem Cells into Functional Lung Alveolar Epithelial Cells. *Cell Stem Cell*. 2017;21(4):472-488.e10. doi:10.1016/j.stem.2017.08.014.

55. Yamamoto Y, Gotoh S, Korogi Y, et al. Long-term expansion of alveolar stem cells derived from human iPS cells in organoids. *Nat Methods*. 2017;14(11):1097-1106. doi:10.1038/nmeth.4448.

56. Rock JR, Onaitis MW, Rawlins EL, et al. Basal cells as stem cells of the mouse trachea and human airway epithelium. *Proc Natl Acad Sci U S A*. 2009;106(31):12771-12775.

57. Rock JR, Randell SH, Hogan BLM. Airway basal stem cells: a perspective on their roles in epithelial homeostasis and remodeling. *Dis Model Mech*. 2010;3(9-10):545-556. doi:10.1242/dmm.006031.

58. Jiang Q, Engelhardt JF. Cellular heterogeneity of CFTR expression and function in the lung: implications for gene therapy of cystic fibrosis. *Eur J Hum Genet*. 1998;6:12-31. https://www.nature.com/articles/5200158.pdf. Accessed March 20, 2018.

59. Guimbellot JS, Leach JM, Chaudhry IG, et al. Nasospheroids permit measurements of CFTR-dependent fluid transport. *JCI Insight*. 2017;2(22). doi:10.1172/JCI.INSIGHT.95734.

60. Stanke F. The Contribution of the Airway Epithelial Cell to Host Defense. 2015;2015.

61. Muhlebach MS, Clancy JP, Heltshe SL, et al. Biomarkers for cystic fibrosis drug development. *J Cyst Fibros*. 2016;15(6):714-723. doi:10.1016/j.jcf.2016.10.009.

62. Proesmans M, Vermeulen F, De Boeck K. What's new in cystic fibrosis? From treating symptoms to correction of the basic defect. *Eur J Pediatr*. 2008;167(8):839-849. doi:10.1007/s00431-008-0693-2.

63. Matsui H, Grubb BR, Tarran R, et al. Evidence for periciliary liquid layer depletion, not abnormal ion composition, in the pathogenesis of cystic fibrosis airways disease. *Cell*. 1998;95(7):1005-1015. doi:10.1016/S0092-8674(00)81724-9.

64. Stoltz DA, Meyerholz DK, Welsh MJ. Origins of Cystic Fibrosis Lung Disease. *N Engl J Med*. 2015;372(4):351-362. doi:10.1056/NEJMra1300109.

65. Hoegger MJ, Fischer AJ, McMenimen JD, et al. Cystic fibrosis. Impaired mucus detachment disrupts mucociliary transport in a piglet model of cystic fibrosis. *Science*. 2014;345(6198):818-822. doi:10.1126/science.1255825.

66. Engelhardt JF, Yankaskas JR, Ernst SA, et al. Submucosal glands are the predominant site of CFTR expression in the human bronchus. *Nat Genet*. 1992;2(3):240-248. doi:10.1038/ng1192-240.

67. Hiemstra PS, Grootaers G, van der Does AM, Krul CAM, Kooter IM. Human lung epithelial cell cultures for analysis of inhaled toxicants: Lessons learned and future directions. *Toxicol Vitr*. 2018;47:137-146. doi:10.1016/J.TIV.2017.11.005.

68. Kasendra M, Tovaglieri A, Sontheimer-Phelps A, et al. Development of a primary human Small Intestine-on-a-Chip using biopsy-derived organoids. *Sci Rep*. 2018;8(1):2871. doi:10.1038/s41598-018-21201-7.

69. Kim HJ, Li H, Collins JJ, Ingber DE. Contributions of microbiome and mechanical deformation to intestinal bacterial overgrowth and inflammation in a human gut-on-a-chip. *Proc Natl Acad Sci U S A*. 2016;113(1):E7-15. doi:10.1073/pnas.1522193112.

70. Chen WLK, Edington C, Suter E, et al. Integrated gut/liver microphysiological systems elucidates inflammatory inter-tissue crosstalk. *Biotechnol Bioeng*. 2017;114(11):2648-2659. doi:10.1002/bit.26370.

71. Maschmeyer I, Hasenberg T, Jaenicke A, et al. Chip-based human liver–intestine and liver–skin co-cultures – A first step toward systemic repeated dose substance testing in vitro. *Eur J Pharm Biopharm*. 2015;95:77-87. doi:10.1016/J.EJPB.2015.03.002.

72. Benam KH, Villenave R, Lucchesi C, et al. Small airway-on-a-chip enables analysis of human lung inflammation and drug responses in vitro. *Nat Methods*. 2016;13(2):151-157. doi:10.1038/nmeth.3697.

Addenda

ADDENDUM

In dit proefschrift beschrijven we nieuwe modellen om de ziektes taaislijmziekte (cystic fibrosis, CF) en cholera te bestuderen in het laboratorium. We gebruikten het model van de darmorganoïden (verder minidarmpjes genoemd) die worden gemaakt uit stamcellen van mensen, met en zonder CF. Hiermee hebben we verschillende typen medicijnen getest en hier vanuit ook andere laboratoriummodellen ontwikkeld, zoals minilongetjes. Hier beschrijf ik in gemakkelijk Nederlands de onderdelen uit dit proefschrift.

In het kort wat er in dit proefschrift staat

In hoofdstuk 2 laten we zien dat minidarmpjes te gebruiken zijn voor het testen van medicijnen voor CF, die niet het CFTR-eiwit verbeteren, maar de voorloper CFTR-mRNA. In hoofdstuk 3 gebruiken we minidarmpjes om medicijnen te screenen waarvan er één ook iets bleek te doen in mensen. Ook gebruikten we de minidarmpjes om een nieuw laboratoriummodel te maken waarmee we direct chloortransport kunnen meten in cellen van mensen (hoofdstuk 4). In hoofdstuk 5 beschrijven we hoe menselijke minilongetjes kunnen worden gekweekt uit longcellen en dat deze kunnen worden gebruikt als model voor CF en ook andere ziektes. We laten ook zien dat we met behulp van minidarmpjes en minilongetjes gevonden hebben dat CFTR werd geactiveerd door een stof die dat helemaal niet zou moeten doen, zie hoofdstuk 6. In hoofdstuk 7 passen we minidarmpjes toe om te meten hoe goed cholera remmers werken. Dit proefschrift wordt afgesloten met een discussie over alle resultaten (hoofdstuk 8). De resultaten per hoofdstuk worden hieronder in meer detail beschreven, maar eerst even iets meer over het 'waarom' van dit onderzoek.

Waarom wordt dit onderzoek met cellen gedaan om CF te onderzoeken?

Onze lichamen worden fysiek beschermd voor de omgeving door een laag van cellen, epitheelcellen geheten. Het bekendste type van deze cellen is de huid. Ons spijsverteringskanaal zit aan de binnenkant van ons lichaam, maar staat ook in contact met de buitenwereld. Ook daar bevindt zich een soort huid van epitheelcellen, ter bescherming van organen zoals longen en darmen. De epitheelcellen zijn essentieel voor het goed functioneren van diverse organen, want ze regelen het transport van belangrijke stoffen in en uit de cellen. In de wand van de cellen zitten namelijk kanalen die bepalen wat er wel en niet doorheen komt, een soort deuren dus. Bij CF is dit transport chronisch ontregeld, bij een cholera infectie is dat tijdelijk.

In dit proefschrift focussen we met name op taaislijmziekte (verder CF genoemd), dat een erfelijke ziekte is en leidt tot een verstoring in het CFTR-eiwit, of CFTR in het kort. CFTR is een kanaal in epitheelcellen en transporteert met name chloor van binnen naar buiten. Als chloor naar buiten wordt getransporteerd, wordt er op die plek ook water aangetrokken. Op die manier zorgt CFTR voor een goede laag slijm in de holtes van onder andere de longen en de darmen, waardoor de longen goed bacteriën kunnen uitdrijven en de darmen het eten verteren.

Bij CF wordt CFTR door DNA-fouten helemaal niet aangemaakt, of veel minder, of gaat CFTR niet vaak genoeg open om chloor door te laten. De balans in chloor- en watertransport is verstoord, waardoor de slijmlaag in organen te dik of taai wordt. Het gevolg is onder andere dat in de longen bacteriën minder goed kunnen worden weggehoest, wat weer leidt tot infecties, ontstekingen en uiteindelijk verlittekening. Bij mensen met CF gaat de functie van meerdere organen in de loop van de tijd achteruit

(zie figuur 1 in hoofdstuk 1), maar de meeste mensen overlijden omdat de longen niet meer kunnen functioneren. De gemiddelde levensverwachting is lager dan 50 jaar.

Wat weten we nog niet over CF en medicijnen?

Het doel in de zorg voor mensen met CF is om de achteruitgang van de organen zo goed mogelijk te remmen. Tegenwoordig zijn er medicijnen die CF heel gericht behandelen door CFTR te verbeteren. Er worden ook steeds betere medicijnen ontwikkeld, en de verwachting is dat CF straks een chronische aandoening zal zijn, in plaats van de levensverkortende ziekte die het nu nog is. Dat is goed nieuws natuurlijk! Maar toch is daarmee niet alles gezegd.

Er zijn een aantal lastige kwesties. De eerste is dat er meer dan 2000 verschillende DNA-fouten van CFTR bekend zijn, en er dus veel versies van CF zijn. Van veel DNA-fouten is nog niet bekend wat de gevolgen in de cel en voor de patiënt dan zijn. De nieuwe medicijnen verbeteren specifieke fouten van CFTR, en zijn daardoor niet voor iedereen geschikt. Daarnaast zien we dat mensen met dezelfde versie van CF anders kunnen reageren op hetzelfde geneesmiddel. We weten niet precies waardoor dat komt.

In het laboratorium zoomen we in op de cel of zelfs alleen op CFTR. Maar CFTR werkt niet alleen, er zijn nog meer kanalen die bijvoorbeeld ook chloor transporteren, of juist andere ionen, zoals natrium. Die zouden misschien de verstoorde balans door CFTR een beetje kunnen corrigeren. Wat behandeling van en onderzoek naar CF ook lastig maakt is dat we weten dat CFTR anders werkt in darmen dan bijvoorbeeld in de longen, maar het is nog niet helemaal duidelijk wat precies de verschillen zijn, en de gevolgen. Onderzoeken tussen verschillende laboratoria spreken elkaar soms ook tegen.

Waar het op neer komt is dat de werking van medicijnen verschilt per mens, per versie van CF, en per orgaan. Om daar meer inzicht in te krijgen en uiteindelijk de behandeling van mensen met CF te verbeteren, zijn er meerdere manieren van onderzoek nodig.

Waarom gaat dit proefschrift over minidarmpjes?

De veelgebruikte CF-modellen in het laboratorium maken gebruik van menselijke cellen die lastig te verkrijgen zijn (longcellen bijvoorbeeld) en daarna niet lang in leven kunnen worden gehouden. Dat is jammer, omdat we inmiddels weten dat CF varieert tussen mensen, en om te ontrafelen hoe dat komt zijn cellen van patiënten essentieel. Na één experiment weten we helaas niet alles, maar meerdere keren longcellen afnemen bij iemand is ook niet wenselijk.

Gelukkig is er de afgelopen jaren veel bereikt om de menselijke stamcellen te vinden in het lichaam van volgroeide mensen (dus niet embryo's). Een paar jaar geleden heeft een onderzoeksgroep uit Nederland een model ontwikkeld om menselijke stamcellen uit de darm 'oneindig' in leven te houden. Deze stamcellen kunnen ook ingevroren worden om later opnieuw te gebruiken voor onderzoek. Uit deze stamcellen worden 3D minidarmpjes (intestinale of darmorganoïden) gemaakt, die veel lijken op de echte darm. Door eenmalig een stukje darmweefsel af te nemen (dat doet geen pijn), is het mogelijk om heel veel onderzoeken te doen.

Ons laboratorium heeft met deze minidarmpjes een model voor CF ontwikkeld: als we CFTR in deze minidarmpjes stimuleren, dan wordt er chloor naar de binnenkant van de 3D minidarmpjes

getransporteerd, en dat trekt water aan, net als in het lichaam. Daardoor gaan de minidarmpjes opzwellen, afhankelijk van hoe goed CFTR het doet. In minidarmpjes van mensen met een ernstige versie van CF gebeurt er vrijwel niks, terwijl er bij 'gezonde' minidarmpjes veel zwelling is. CFTR kan worden gestimuleerd door boodschappers in de cel die laten weten dat er chloor naar buiten moet. In het laboratorium kunnen wij deze boodschappers bij de minidarmpjes doen om dit proces na te bootsen. De zwelling van de minidarmpjes laat dan zien hoe goed CFTR het doet. De relatieve verandering in grootte kunnen we kwantitatief vaststellen. Daarnaast is het model ook heel gevoelig om kleine verschillen op te pikken. We kunnen daardoor de verschillende versies van CF onderscheiden, verschil meten tussen mensen met dezelfde versie van CF, onbekende versies van CF plaatsen en ook testen hoe goed medicijnen CFTR verbeteren. Want ook dat kunnen we nabootsen in het laboratorium. We hebben zelfs aanwijzingen dat de resultaten in minidarmpjes voorspellend zijn voor het effect van medicijnen in mensen. Dat laatste is heel handig, want daardoor kunnen we allerlei medicijnen testen zonder dat de patiënt daar allerlei onderzoeken voor hoeft te ondergaan.

De minidarmpjes zijn dus een goed model om CF op een persoonlijk niveau te bestuderen, en nieuwe medicijnen te testen. Maar er zijn natuurlijk ook nadelen, bijvoorbeeld dat de zwelling van minidarmpjes een gevolg is van het chloortransport door CFTR. Om echt te begrijpen hoe chloortransport werkt, of verstoord is, is het handiger om het chloortransport te kunnen meten. Daarnaast zijn minidarmpjes waarschijnlijk niet heel goed voorspellend voor bijvoorbeeld de longen, omdat het verschillende organen zijn met andere functies. We wilden daarom nieuwe modellen ontwikkelen, op basis van deze minidarmpjes, om deze nadelen te verhelpen. We hebben een aantal eerste stappen gemaakt en dat laten we zien in dit proefschrift met als titel 'het toepassen van menselijke organoïden voor ion transport studies'. Met ion transport bedoelen we in dit geval met name de werking van het CFTR-eiwit als chloorkanaal.

Hoofdstuk 2, minidarmpjes kunnen bevestigen welke medicijnen niet goed genoeg werken

Ons lab had eerder al laten zien dat met minidarmpjes kan worden getest hoe goed medicijnen CFTR verbeteren. In **hoofdstuk 2** laten we zien dat ze ook te gebruiken zijn om medicijnen te testen die het CFTR-mRNA zouden verbeteren, de voorloper van het CFTR-eiwit, het uiteindelijke chloorkanaal. Ongeveer 12% van de mensen met CF heeft namelijk een DNA-fout in CFTR waarbij vervolgens het CFTR-mRNA zo afwijkt dat er geen chloorkanaal wordt gemaakt. Er was een geneesmiddel in ontwikkeling dat wat tegenviel in de studies in mensen. Wij zagen geen enkel effect met dit gmiddel in de minidarmpjes, terwijl we wel zagen dat een ander middel het mRNA van CFTR kon verbeteren. Helaas is dat andere middel niet te gebruiken in mensen in verband met toxiciteit. Het middel dat CFTR niet verbeterde in minidarmpjes is inmiddels niet meer in ontwikkeling. De minidarmpjes blijken dus ook van waarde te zijn om te bepalen welke medicijnen waarschijnlijk niet effectief genoeg zijn voor mensen. Ook zijn er betere, effectievere medicijnen nodig om het mRNA van CFTR te verbeteren, want die zijn er nu niet.

Hoofdstuk 3, medicijnen voor andere ziektes inzetten voor CF

We kunnen meerdere geneesmiddelen tegelijk testen in minidarmpjes. We hebben in **hoofdstuk 3** de eerste screening gedaan met 61 medicijnen die CFTR activeren. CFTR wordt namelijk actief als boodschappers in de cel dat aangeven. Er zijn medicijnen die deze boodschappers vaker op pad sturen,

en daarmee ook CFTR meer actief maken. Het idee is dat als CFTR al vrij goed is (bij een milde versie van CF), of wordt verbeterd met een ander medicijn, een activator dit effect kan versterken. De medicijnen die CFTR het beste activeerden, zijn medicijnen die de luchtwegen kunnen verwijden, bijvoorbeeld voor mensen met astma of COPD. Met één van die medicijnen, salbutamol, hebben we een kleine studie in mensen met CF gedaan, en we zagen een kleine verbetering in chloortransport gemeten in de neus. We hebben bloed afgenomen tijdens de studie, voor en na geneesmiddelgebruik. We hebben dat bloed bij de minidarmpjes gedaan om te meten of CFTR ook zo werd geactiveerd. Dat was het geval, maar heel minimaal, net als het kleine effect bij de mensen eigenlijk. Dit is het eerste bewijs dat de minidarmpjes kunnen worden gebruikt als screen én voor het testen van medicijnen die CFTR activeren.

Hoofdstuk 4, chloortransport meten met menselijke stamcellen uit de darm

Zwelling van minidarmpjes is een gevolg van het chloortransport door CFTR. Er is ook een manier om het chloortransport zelf, direct, te meten, door middel van het meten van elektrische stroompjes (elektrofysiologie). Voor CF wordt dat gedaan in darmbiopten en longcellen, welke maar kort in leven te houden zijn buiten het menselijk lichaam. Om chloortransport te kunnen meten met minidarmpjes moet je eerst de minidarmpjes plat maken. Onderzoekers hadden al eerder beschreven hoe je platte minidarmpjes kan groeien. Wij hebben dat protocol iets aangepast en laten als eerste zien dat je daarmee chloortransport kan meten door die cellen heen (**hoofdstuk 4**). Ook laten we zien dat dit model onderscheid maakt tussen ernstig CF, iets minder ernstig CF en niet-CF. We hebben de resultaten van dit nieuwe model vergeleken met de resultaten uit chloormetingen met biopten en zwellingexperimenten met minidarmpjes van dezelfde patiënten. De uitkomsten waren heel erg vergelijkbaar, wat aangeeft dat dit model bruikbaar is om chloortransport te meten in minidarmpjes in plaats van de lastiger te groeien en bewaren darmbiopten of longcellen.

Hoofdstuk 5, van minidarmpjes naar minilongetjes

Het model van de minidarmpjes is een basis gebleken voor andere miniorgaantjes, het is nu ook mogelijk om minilevertjes te laten groeien, of mini-alvleesklieren. En, zoals eerder gezegd, de minidarmpjes vormen een heel mooi model om CFTR en CF te bestuderen. Maar met name in de longen werkt CFTR samen met meerdere kanalen. In het veld is daarom al lang vraag naar minilongetjes, gemaakt uit menselijke stamcellen. Er wordt al heel lang onderzoek gedaan om de stamcellen van de longen te vinden, en pas de laatste jaren zit er schot in de zaak. Daarnaast is het een lastigere en vervelende ingreep om longcellen bij iemand af te nemen. Het Hubrecht heeft, in samenwerking met ons, een protocol ontwikkeld om minilongetjes te maken uit longcellen (zie **hoofdstuk 5**). Deze groeien ook in 3D, en de manier waarop de cellen groeien lijkt daardoor op de cellen in de mens. We laten zien dat we ook hiermee verschil in CFTR-activatie kunnen meten, tussen minilongetjes van mensen met en zonder CF. We zien ook dat in CF minilongetjes er dikker slijm aanwezig is. Daarnaast hebben we aanwijzingen dat er in de minilongetjes ook chloortransport kan plaatsvinden via een ander kanaal. Dat betekent dat minilongetjes best goed lijken op de longen in de mens én dat we hiermee ook andere kanalen kunnen bestuderen die in minidarmpjes en de darmen van de mens niet aanwezig lijken te zijn.

Hoofdstuk 6 en 7, ongewenste activatie van CFTR

In laboratoriumonderzoek met verschillende kanalen is het belangrijk om deze te kunnen activeren en remmen, om iets te kunnen zeggen over de rol van de kanalen in de cel. Dat kan je onder andere doen

met chemische verbindingen of stoffen. Helaas is de werking van deze stoffen niet altijd even 'schoon' of selectief. In **hoofdstuk 6** laten we zien dat minidarmpjes en minilongetjes waardevol zijn om te testen of stoffen een bijeffect hebben op de CFTR-functie. Het bleek namelijk dat een remmer van een ander chloorkanaal juist CFTR activeerde. Dat maakt nogal uit voor resultaten van andere onderzoeken, waar niet naar CFTR werd gekeken, maar de activatie ervan wel de andere kanalen zou kunnen beïnvloeden.

CF wordt gekarakteriseerd door minder tot geen CFTR-functie. De resulterende diarree bij cholera is juist het gevolg van te veel activiteit van CFTR. We hebben in **hoofdstuk 7** laten zien dat deze hyperactivatie van CFTR door cholera te meten is in minidarmpjes en dat nieuwe potentiële cholera remmers ook kunnen worden getest. Het is de eerste keer dat zulke remmers in een menselijk stamcelmodel zijn gemeten. Deze resultaten kunnen er misschien voor zorgen dat er minder dierproeven nodig zijn om potentiële medicijnen te testen.

Hoofdstuk 8, toekomstperspectief voor minidarmpjes en minilongetjes

Voor mensen met CF worden er nu diverse nieuwe medicijnen ontwikkeld, soms wel drie-in-één, die heel goed CFTR lijken te kunnen verbeteren. Deze therapieën zijn bedoeld voor mensen met de meest voorkomende DNA-fout van CFTR: F508del. Zo'n 90% van de mensen met CF heeft deze versie, dus de toekomst is best veelbelovend. We denken dan ook dat geïndividualiseerd behandeling voor deze mensen niet nodig is. De resterende groep mensen heeft hele zeldzame DNA-fouten in CFTR, vaak zelfs met onbekende impact. Het zal dus nodig zijn om met minidarmpjes van deze mensen een behandeling op maat te bepalen. Er loopt nu een Europees project (HIT CF Europe) voor mensen met zulke versies van CF. Op minidarmpjes van zo'n 500 mensen worden drie medicijnen getest die nu nog in ontwikkeling zijn. Als er positief effect wordt gemeten in de minidarmpjes, dan worden ze ook getest in de mensen zelf.

Voor minilongetjes is dit allemaal nog niet aan de orde. Ze kunnen wel handig zijn om bijvoorbeeld een model te maken om trilhaarfunctie te meten. Bij mensen met CF werken de trilharen in de longen minder goed, door het taaie slijm. De huidige laboratoriumtesten gebruiken de longcellen die lastig te groeien en te onderhouden zijn. Daarnaast hebben we laten zien dat minilongetjes ook heel handig zijn voor onderzoek naar andere longziekten zoals het verkoudheidsvirus RSV of longkanker.

Minidarmpjes en minilongetjes lijken dus bruikbaar om CF op een persoonlijk level te bestuderen, CFTR-functie te bepalen en het effect van medicijnen te meten. In het menselijk lichaam bestaan organen echter uit meer dan alleen epitheelcellen. Om de complexiteit van een compleet orgaan te bestuderen, is er dus een model nodig dat meerdere typen cellen combineert, omdat alle cellen met elkaar in interactie zijn. Er wordt nu veel onderzoek gedaan naar zogeheten organen-op-een-chip, en de stamcelmodellen in dit proefschrift beschreven kunnen hierbij van pas komen. Zo'n model zou misschien kunnen verklaren of bijvoorbeeld mensen met CF vatbaarder zijn voor ontstekingen of dat er juist intrinsiek geen verschillen zijn met mensen zonder CF.

Kortom, in dit proefschrift wordt duidelijk hoe recente stamceltechnologieën kunnen leiden tot nieuwe laboratoriummodellen die ziektes beter representeren en medicijnontwikkeling verbeteren.

A

ADDENDUM

Op voorkant van dit proefschrift staat enkel mijn naam vermeld, maar dit werk en de vorming van mijzelf zijn de afgelopen jaren natuurlijk beïnvloed door de omgang met diverse mensen.

Kors, mijn promotor, ontzettend bedankt dat je mij deze functie hebt gegund. Ik heb veel respect voor de manier waarop jij leiding geeft, overzicht houdt, en daarin jezelf blijft. Jij bent voor mij een voorbeeld in de manier waarop jij je persoonlijke levensovertuiging zichtbaar maakt in je werk. Ook je nuchterheid kan ik erg waarderen, 'accept all changes'.

Jeffrey, of eigenlijk Jeff, ik heb het heel erg naar mijn zin gehad bij jou in het team. Je bent een toffe, maffe co-promotor, boordevol wilde plannen mét een doel. Ik heb veel geleerd van je en ik ben blij dat je altijd tijd maakt als dat echt nodig is, werkinhoudelijk of juist niet. En misschien dat ik ooit nog eens leer schrijven zoals jij.

Beste leden van de beoordelingscommissie, beste opponenten; geachte prof. dr. R.H.J. Houwen, prof. dr. I. Braakman, prof. dr. L.J. Bont, prof. dr. N.M. Wulffraat, prof. dr. H. Tiddens, dr. H.R. de Jonge en dr. V. Gulmans. Hartelijk dank voor de functie die jullie hebben ingenomen.

Lieve collega's van team Beekman, ik mis jullie, hoor. Evelien en Annelot, jullie vormen de vaste factor. Eerst gebroederlijk naast elkaar, nu elk een eigen verantwoordelijkheid in het steeds groter groeiende team. Evelien, jouw punctualiteit is van het hoogste niveau, héél erg bedankt voor al je werk achter de schermen. Annelot, binnen en buiten het werk is het een waar genoegen met je om te gaan; bijna de trein naar Parijs missen of weer een 'knipfestival' met natuurlijk curry. Florijn en Lodewijk, Marne en Gimano, fijn om met jullie te mogen samenwerken aan diverse projecten, en bedankt voor de gezelligheid op het lab! Hugo, ook jij hebt uiteindelijk een plek in dit team gevonden, dank je wel voor al je praktische inzet en natuurlijk de bewerking van app-foto's binnen een minuut. Eyleen, eerst was je een hele fijne masterstudent, later werden we collega's (heel leuk!) en nu ben je ook nog mijn paranimf. Ik vind het super leuk om zo'n leuk mens als jou te kennen en ik hoop dat we contact zullen blijven houden. Succes in de komende jaren van je traject! Gitte en Peter, jullie vormen de brug tussen kliniek en lab. Gitte, je werkt hard, en bent tegelijkertijd ook altijd gezellig en in voor iets geks, jij komt er wel! Peter, tof dat jij je eigen plan trekt, ook nu in Australië! Sylvia en Jesse, we hebben niet lang samengewerkt maar jullie zijn een aanwinst voor het team en ik vond het leuk jullie te leren kennen. En dank aan alle studenten die tijdelijk hebben meegelopen met dit team waar je maar net bij moet passen. ORGANOIDS ECHT COOL!

Lieve mensen van de afdeling Kinderlongziekten/allergologie, bedankt voor alle inkijkjes in de zorg voor mensen met taaislijmziekte. Helaas is de afstand tussen jullie en het lab best groot geworden. Ik vond het daarom heel leuk en leerzaam om een jaar lang één dag in de week bij jullie te kunnen zitten. Margot en Sabine, dank jullie wel voor al jullie hulp bij de klinische studies en onderzoeksprotocollen. Karin, Sylvia, Cora, Marit, Hetty, Judith, Valesca, Rolien, Hannah en Hannah, bedankt voor de gezellige (lunch)momenten. Bert, bedankt dat ik op jouw plek mocht werken. De korte intermezzo's en ook de hardloopsessies bij Willem waren altijd goed. Myriam, wat ben je toch een lief mens met een heel groot hart. Het is altijd fijn om jou te zien, dank je wel voor het altijd klaar staan en het vele werk dat je verricht.

Dank aan de (kinder)longartsen, onderzoekers en alle anderen die zich inzetten voor mensen met CF. In het bijzonder wil ik Hugo de Jonge bedanken voor het altijd behulpzaam zijn bij lastige elektrofysiologische kwesties. Het is een waar genoegen om jou te kennen. Ook de mensen met CF wil ik bedanken, voor hun inzet voor de wetenschap.

Oud-afdelingcollega's van het Laboratory of Translational Immunology (LTI) en met name de kamer '..degekste' (met Emmerik, Alsya, Gerdien, Michiel, Hilde, Eveline, Kim, Ananja, Kerstin en Kirsten), bedankt voor de gezellige tijd! Michiel, ik was vanaf het begin onder de indruk van je kritische én behulpzame houding, en nog steeds. Gelukkig zijn we regelmatig blijven koffiedrinken. Het LTI liet ook een gezamenlijke muzikale hobby verschijnen: bedankt Erik, Michiel, Kevin, Shamir en Judith voor de band 'Erik en de Hackers', met als toppunt het optreden in de Efteling tijdens de NVVI 2014. Ik vond het geweldig en mis het stiekem nog wel eens. Regenerative Medicine Centre, bedankt voor de 'nieuwe' start die we kregen met heel fijne faciliteiten. Mede PhD-studenten van Regenerative Medicine School, onder andere bedankt voor de leuke PhD dagen. Sarah, dank je wel voor je inzet voor de RM School en voor alle aangesloten PhD studenten.

Leuke, huidige collega's bij de NCFS: dank jullie wel dat ik nu deel uit mag maken van een heel ander veld binnen taaislijmziekte, ik leer veel van jullie op allerlei vlakken. Jacquelien, dank je wel voor de ruimte die je hebt gegeven om dit project goed af te ronden, en dat ik bij de NCFS mocht komen werken. Vincent, je bent een hele leuke collega (wat ik van tevoren al wel wist natuurlijk), en het is fijn om samen de 'onderzoekssectie' te vormen. Mirjam en Anouk, bedankt voor jullie inbreng voor de Nederlandse samenvatting van dit proefschrift.

Roland Pieters, bedankt voor de samenwerking voor het cholera toxine project. Bas Ponsioen, dank je wel voor je enthousiasme en inzet, ik vind het jammer dat het TMEM16A project met 'de gekke inhibitor' (nog) niet is afgerond met een publicatie. Hettie Janssens, bedankt dat je onze gezamenlijke artikelen altijd kritisch hebt gelezen. Norman, it was very nice to collaborate with you on the airway organoids, during my whole PhD period. Thank you for your enormous amount of work and many good ideas, resulting in a very nice paper in this thesis.

Er is natuurlijk ook een leven naast werk, hierbij wil ik dan ook al mijn vrienden bedanken voor alle leuke vakanties, weekenden, feestjes, etc. Lieve bitterbalvrienden Judith, Joanne, Melanie, Linda en Nathanje, dank jullie wel voor alle mentale steun, die VrijMiBo houden we er maar in. Thirza, wie had gedacht dat onze binding de studententijd zou overleven? Ik vind het gezellig met je, altijd goed om een avond samen te spenderen. Met een biertje natuurlijk. Elise, we zijn al heel lang bevriend, en ik hoop dat we dat nog lang zullen blijven! Mirjam, zo leuk om in diverse fases samen op te trekken. Dank je wel dat je mijn paranimf wilde zijn!

Lieve familie en schoonfamilie, ik heb het maar getroffen met jullie. Bij jullie kan ik gewoon 'Do(menique)' zijn, al betekent dat dus ook de betweterige, jongste telg van de familie, of bijdehante aanhang van de al bijdehante zoon/broer Peter. Pap, dank je wel voor de herinnering die je stuurde de dag voordat ik mocht bellen voor een promotiedatum ;) Mama, Wilma, Loes, Arina, Jeroen en Dieuwke, dank jullie wel voor al het oppassen op Janne op mijn 'mamadagen', anders was dit nooit op tijd afgekomen.

A

ADDENDUM

Janne, kleintje, jij kwam er in deze periode ook nog bij. Dank je wel voor het gemakkelijke en vrolijke moppie dat je bent en voor alle afleiding die jij geeft, want hoe belangrijk is werk nu eenmaal. Lieve Peter, jij bent de leukste. Dank je wel dat we samen een basis vormen en het goed hebben. Thuis, bij jou, is de plek om te ontspannen en te relativeren. Ik heb superveel zin in onze volgende pelgrimstocht.

Bovenal wil ik mijn dank betonen aan God. “Want in Hem leven wij, bewegen wij en zijn wij” (Handelingen 17:28a).

Domenique was born on October 25th 1988, in Tiel, the Netherlands. Following graduation in 2007 from pre-university secondary education at 'de Passie' in Utrecht, she started Pharmacy at Utrecht University. She continued with the research master Drug Innovation with internships at University Medical Center Utrecht and biotechnology company Genmab. During her internship at Genmab, she got in contact with dr. Jeffrey Beekman via her examiner dr. Jeanette Leusen. In September 2013 she started as a PhD student at his lab for the project called 'Personalized approaches to understand cystic fibrosis disease and therapy'. During this four-years-project, the focus shifted towards finding new applications of the intestinal organoid model for cystic fibrosis, established at Beekman's lab. The results of the project are described in this thesis. In January 2018, she continued her career at the Dutch Cystic Fibrosis Organization (NCFS) as staff member Registry and Quality of Care at the research section, with research communication as additional project. She currently lives in the small village Westbroek, next to Utrecht, with her husband Peter and one-year-old daughter Janne.